Faculty of Science
University of Technology Sydney, Australia

Modelling and surgical analysis of fracture repair of the facial skeleton using generic and patient matched finite element models

Richard Conway

October 2017

This dissertation is submitted for the degree of Doctor of Philosophy

CERTIFICATE OF ORIGINAL AUTHORSHIP

This thesis is the result of a research candidature conducted jointly with another University as part of a collaborative Doctoral degree. I certify that the work in this thesis has not previously been submitted for a degree nor has it been submitted as part of the requirements for a degree except as part of the collaborative doctoral degree and/or fully acknowledged within the text.

I also certify that the thesis has been written by me. Any help that I have received in my research work and preparation of the thesis itself has been acknowledged. In addition, I certify that all information sources and literature used are indicated in the thesis.

_____ _____

Richard Conway **Date**

ACKNOWLEDGEMENT

First and foremost, I express my gratitude to my supervisors, Professor Besim Ben-Nissan and Professor Bruce Milthorpe, for sharing their knowledge and passion for this subject during the research work, for contributing significantly to my professional growth and finally for their friendship.

Whilst this research thesis is novel, it draws from previous works to understand where finite element analysis began to where it is currently, as well as its limitations to date, particularly in the fields of medicine and dentistry. In particular, I have drawn extensively on the technical expertise of my academic colleagues so that I could provide my surgical expertise to produce this work. As such special acknowledgement goes to the following:

Dr Andrew Choi has been invaluable for his friendship, guidance and expertise in preparing this thesis. In particular, he helped me understand finite element models and assisted me in the technical aspects of preparing and interpreting generic finite element models used in this thesis, which was fundamental in completing the research.

Dr Valerio Taraschi helped immensely in all aspects of the preparation and interpretation of the patient specific model.

Professors Ben-Nissan and Milthorpe allowed me to understand the previous and current works of Drs Choi and Taraschi. In doing so, the foundations to produce this thesis were formed.

Mr Richie Mohan from Medical and Optical provided invaluable data relating to commercially available plating systems that were incorporated into this analysis.

I would like to thank my family for supporting me through this long process and providing invaluable encouragement. With all my heart, thank you Danya, Amelia and Charlotte.

Last but not least I would like to thank Lei Cameron who helped me in proofreading and formatting my thesis, as well as providing valuable insight into my preparation of this document.

PREFACE

As a surgeon working in the maxillofacial field I have always had a keen interest in trauma of the facial skeleton. As part of my contact at the University of Technology with Professor Ben-Nissan, Professor Milthorpe, Dr Choi and Dr Taraschi over the past 20 years I have had the honour of being involved in finite element based research. During this time, it became apparent that utilising this methodology to analyse both current fracture management and future directions of fracture management was a worthy ground for research as part of a doctorate of philosophy. To achieve this goal, I have been most fortunate to have the wealth of technical knowledge from my aforementioned university colleagues to draw upon and integrate into my surgical expertise.

The following dissertation presents my analysis as a surgeon of modelling and fracture repair of the facial skeleton, using generic and patient matched finite element models with technical support provided by those academic colleagues addressed in my acknowledgements.

I hope that those who read this thesis, whether scientists or clinicians or both, find it as interesting as I have.

TABLE OF CONTENTS

LIST OF FIGURES

Abstract

Chapter 1

Chapter 2

Chapter 3

Chapter 4

Chapter 5

Chapter 6

Chapter 7

Chapter 8

Chapter 9

Chapter 10

Appendix A

Appendix B

LIST OF TABLES

Chapter 1

Chapter 3

Chapter 4

Chapter 5

Chapter 6

Chapter 7

Chapter 8

Chapter 9

Appendix A

Appendix B

PUBLICATIONS ARISING FROM RESEARCH WORK

A.H. Choi, B. Ben-Nissan, R.C. Conway, & I.J. Macha (2104). *Advances in calcium phosphate nanocoatings and nanocomposites*. Advances in Calcium Phosphate Biomaterials, Springer Publishing, pp. 485-511.

A.H. Choi, B. Ben-Nissan, & R.C. Conway (2014). Finite Element Analysis (FEA) in Dentistry. In *Handbook of Oral Biomaterials*, J.P. Matinlinna (Ed.), Singapore: Pan Stanford Publishing, Ch. 17, pp. 535-576.

A.H. Choi, B. Ben-Nissan, & R.C. Conway (2005). Three‐dimensional modelling and finite element analysis of the human mandible during clenching. *Australian Dental Journal*, *50*(1), 42-48.

A.H. Choi, J.P. Matinlinna, R.C. Conway, & B. Ben-Nissan (2012). Application of Biomaterials and Finite Element Analysis (FEA) in Nanomedicine and Nanodentistry. In: Computational Finite Element Methods in Nanotechnology, S.M. Musa (Ed.), CRC Press-Taylor and Francis Group, USA, Ch. 11, pp. 373-399.

A.H. Choi, R.C. Conway, & B. Ben-Nissan (2004). Finite element analysis of ceramic dental implants incorporated into the human mandible, *Key Engineering Materials*, *254*, 707-712.

A.H. Choi, R.C. Conway, V. Taraschi, & B. Ben-Nissan (2014). Biomechanics and functional distortion of the human mandible, *Journal of Investigative and Clinical Dentistry*, *6*(4), 241-251.

A.H. Choi, B. Ben-Nissan, J.P. Matinlinna, & R.C. Conway (2013). Current perspectives: Calcium phosphate nanocoatings and nanocomposite coatings in dentistry. *Journal of Dental Research*, *92*(10), 853-859.

ABSTRACT

Surgical analysis of fracture repair of the facial skeleton using generic and patient matched finite element models

This thesis is aimed at finite element modelling of the fractured and repaired facial skeleton, specifically the mandible and surgical aspects that influence a rapid and complete recovery process without complications that otherwise lead to significant patient morbidity and sometimes mortality.

The mandible, as a site of specific investigation, was chosen due to the following factors. Firstly, as a prominent part of the facial skeleton, the mandible is a highly complex structure, being composed in its hard tissue elements by cancellous and cortical bone and the dental complex consisting of enamel, dentine and cementum. These hard tissue components house the associated soft tissues consisting of major nerves and blood vessels, fat and other connective tissues. Already one can see the complexity of the mandible but its unique anatomical character does not stop there as the entire structure articulates with the remainder of the facial skeleton via the temporomandibular joints.

The mandible is also unique because it is being commonly affected by all of the major disease classifications, being congenital, traumatic, neoplastic, infective, inflammatory and iatrogenic disease. As a consequence, clinicians ranging from dentists through to maxillofacial surgeons are often confronted with complex disease patterns that require complex reconstructive methods to restore form and function (Figure 0.1). At the terminus of reconstruction, these elements of form (cosmesis) and function (speech, facial expression, mastication, deglutition, taste and airway maintenance) are what our patients demand and should be entitled to expect from modern day surgical techniques.

The aim of this work is to look at the fractured mandible using finite element modelling and ascertain what provides the surgeon with the best results when performing

osteosynthesis of the fracture and hence lead to rapid, complete and complication free healing.

The models used in this thesis are based on a well established and validated model, initially taking its heritage from the works of Ben-Nissan in 1987, followed by Choi in 2005. In this thesis, it is termed the 'generic (GEN) model'. A second model is also used throughout this thesis, which is based on computed tomography scans of a human mandible, termed as the 'patient specific (PS) model'. With the GEN and PS models, various fracture fixation systems were designed and applied to both FE models and analysed for their efficacy. This brings to the study a unique attribute of comparing a GEN model with a PS model, thus allowing multiple fracture fixation systems to be analysed. In doing so, a better correlation is provided with the pathophysiology and mechanics of trauma as it occurs in vivo.

The results of this study show that most importantly we have been able to produce a valid models that closely mirrors trauma and its repair as occurring in real life, not just as it appears in laboratory analysis.

Not only are the models valid, but equally important, they are predictably reproducible. Specifically, the PS model could be applied in PS scenarios to allow a customised design of surgery that best suits the individual in question.

In the analysis, we studied various plate shapes ranging from traditional linear plates to mesh pattern fixation plates. We also looked at various plate material ranging from titanium alloy (Ti-6Al-4V) to zirconia (ZrO_2) and polylactic acid (PLA) and also in various dimensions.

With the analysis of these variants we found that whilst there were variations in performance between the various designs, they all performed equal to the physical parameters required for fracture fixation and subsequent repair. Across all variants of fixation methods, one significant factor is that the fractured ends of the bone are applied as closely as possible but not compressed.

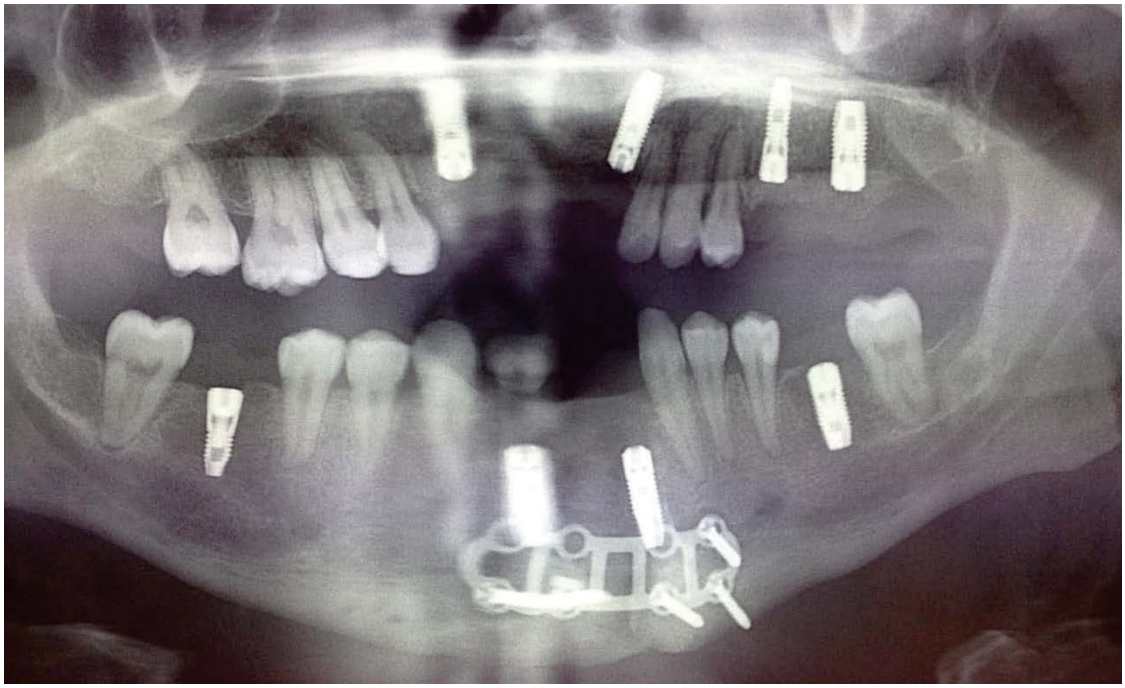

Figure 0.1 Facial skeleton affected by congenitally associated tooth absence and neoplasia, requiring complex reconstruction with dental implants, grafting and fixation plate

The final product of this work is a reproducible valid model where production, performance and results represent a dialectic improvement over past mandibular models and which reproduces the most realistic scenario of constraints and forces during functional movements.

With further improvements, such as patient specific bone mineral density and the use of dedicated software for the manipulation of the computed tomography data, this model is destined to become a functional tool for clinical diagnosis and treatment in maxillofacial surgery and dentistry.

ABBREVIATIONS

CBCT	cone beam computed tomography
CT	computed tomographic
EMG	electromyogram
FEA	finite element analysis
FEM	finite element model
FS	fracture segment
GEN	generic
IEMG	integrated electromyogram
IP	isolated plate
MRI	magnetic resonance image
PLA	polylactic acid
PS	patient specific
Ti	titanium
Ti-6Al-4V	titanium alloy
TMJ	temporomandibular joint
ZrO_2	zirconium oxide (also known as zirconia)

CHAPTER 1:
INTRODUCTION

The aim and purpose of this research is to produce a valid and reproducible finite element model (FEM) of the mandible derived from real patient CT scan data, utilising the patient specific (PS) model to analyse fracture repair and healing using various fixation devices alongside similar analysis using a GEN model.

1.1 Approach

In order to introduce the foundations for this thesis it is important to understand trauma. To do so, the following areas are covered: (i) history and understanding of trauma as it applies to current clinical practice; (ii) mandibular fractures and their surgical management; (iii) rapid repair and recovery from facial fractures; (iv) limitations of current fracture management; and (v) specific difficulties with the fractured edentulous mandible.

1.2 History and the understanding of trauma as it contributes to our current practice

Since records have been kept, and I am sure well before this, all biological creations, including man, have been the subject of trauma. The perpetrators of trauma have changed and evolved with time as initially natural events, which violently shaped our planet were probably the most likely cause of trauma. Events such as volcanic activity, earthquake or flood must have inflicted immense trauma to those creatures living at the time.

As time passed and evolution progressed, the planet became more populated and diverse with animals now having much more personal interaction than previously. Inevitably such interaction leads to violent clashes, either accidentally or intentionally, and unfortunately whilst natural events still account for considerable physical trauma, personal interaction particularly among people have produced a significant additional source of trauma and its increasing association with drug intake, such as alcohol and methamphetamine use, is a point of much concern.

More recent local history in Australia has shown that death and injury from trauma such as falls and tribal conflict was an integral part of Australian Aboriginal life prior to European settlement (Berndt, 1994).

With European colonisation in 1788, traumatic injury was the most common cause of death, however, with advances in trauma prevention management, particularly accelerated around periods of military conflict (Kirkup, 2003), trauma has now dropped to become the fourth most common cause of death in Australia (Henley, 2009) with oncology, heart attack and stroke leading the way. Despite this improvement, trauma remains the leading cause of death in women and men under the age of 45 years in Australia (Australian institute of Health and Welfare, 2003).

Table 1.1 shows the incidence of the major external causes of all trauma in Australia over 2012-2013. Falls, other unintentional causes (e.g. sport), transport crashes, intentional self harm and assaults account for the majority.

Table 1.1 Major external cause groups for injury cases, by sex, Australia, 2012-2013 (Australian institute of Health and Welfare)

	Males		Females		Persons	
External cause	**Number**	**%**	**Number**	**%**	**Number**	**%**
Unintentional injuries						
Transport crashes	36,877	14.7	17,728	9.0	54,606	12.2
Drowning and submersion	362	0.1	182	0.1	544	0.1
Poisoning, pharmaceuticals	3,612	1.4	3,664	1.9	7,276	1.6
Poisoning, other substances	1,251	0.5	699	0.4	1,950	0.4
Falls	77,857	31.1	100,920	51.4	178,780	40.0
Thermal causes	3,800	1.5	2,057	1.0	5,857	1.3
Other unintentional causes	98,431	39.3	44,347	22.6	142,780	32.0
Intentional injuries						
Intentional self-harm	9,759	3.9	17,340	8.8	27,100	6.1
Assault	14,769	5.9	6,365	3.2	21,134	4.7
Undetermined intent	2,558	1.0	2,104	1.1	4,662	1.0
Other or missing	1,164	0.5	827	0.4	1,991	0.5
Total	**250,440**	**100**	**196,233**	**100**	**446,680**	**100**

Table 1.2 shows the trend in these external injury causes from 1999 to 2013. Interestingly, whilst many categories have either fallen or remained static, those that have shown significant increases are lead by falls, followed by other unintentional causes (primarily sports) and intentional self harm.

The increase in falls can be explained by an aging population, however, the worrying trend in sports related and intentional self harm is not as readily explained.

Assaults, which seem to occupy a great deal of attention from the media, shows no change as the causation of trauma in general, but of concern is that assault is the leading cause of facial trauma.

Table 1.2 Trends in age standardised rates of injury cases by type of external cause, Australia, 1999-2000 to 2012-2013 (Australian Institute of Health and Welfare, 2015)

External cause	Trend	Per cent change per year	Per cent of all injuries 2012–13
Unintentional injuries			
Transport crashes	↔	**	12.2
Drowning and submersion	↓	1.2*	0.1
Poisoning, pharmaceuticals	↓	4.1*	1.6
Poisoning, other substances	↓	3.6*	0.4
Falls	↑	2.4*	40.0
Thermal causes	↔	**	1.3
Other unintentional causes	↑	1.6*	32.0
Intentional injuries			
Intentional self-harm	↑	0.4*	6.1
Assault	↔	**	4.7

* Average per cent change per year differed from zero to a statistically significant extent ($p<0.05$).

** Average percent change per year was small (<0.1%) and did not differ significantly from zero ($p\geq0.05$).

Note: Rates for 2012–13 were not used when calculating per cent change per year due to the narrowing of Victorian policy on admissions (see Box 1.3).

The financial cost burden that injury has on economic consumption is documented in different ways depending on the mechanism of injury. Road injury costs include property damage, long-term disability costs and insurance administration costs in a full-cost model. Work-related injury costing models include time off work, lost production, equipment damage, compensation and insurance administration. Traumatic injury accounts for a significant number of hospital admissions which results in a considerable portion of trauma related expenditure. Outside these areas, the cost of injury data is limited, making comparisons difficult.

In 2004-05, injury accounted for A$3.4 billion of allocated health expenditure in Australia, an increase of 22% since 2001, the greatest proportion of which was spent during hospital admissions. The management of trauma, including facial injury, often requires extended hospitalisation. The mean length of stay in hospital correlates well with the cost of associated treatment, as illustrated in Figure 1.1 for age groups up to 85+ experiencing external trauma. In 2008-09, Australia-wide, trauma was responsible for the second highest cause of hospital admissions expenditure, following cardiovascular disease. The majority of admissions were reported for the public hospital sector (Curtis, 2012).

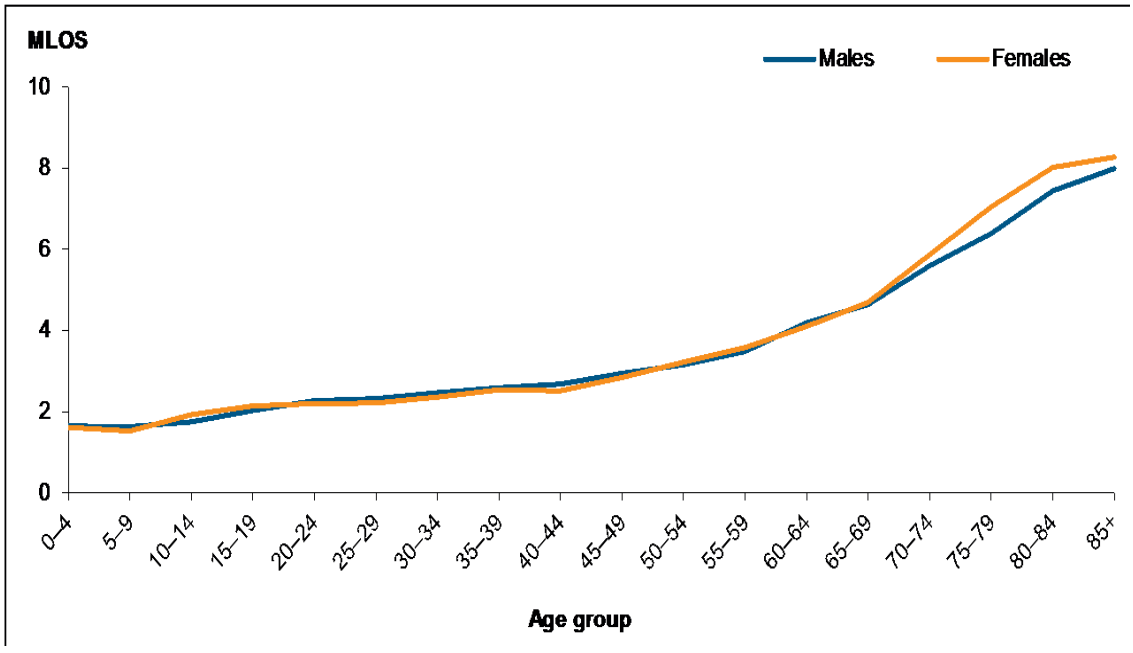

Figure 1.1 Mean length of stay in days for injury by age and sex, Australia, 2012-13 (Australian Institute of Health and Welfare)

Human cost as a result of traumatic injury is vast, ranging from extensive recovery periods, long-standing disabilities and loss of life. For those who do not survive traumatic injury, there is a net loss of their contribution to society (WHO, 2007). On average, each fatal injury before the age of 75 years results in the loss of 32 years of potential life, compared with nine years for cancer and five years for cardiovascular disease (Kriesfeld, 2004). Injuries were responsible for 7.0% of the total burden of disease and injury in Australia in 2003, equating to 185,050 years of healthy life lost due to premature death or disability (Begg, 2007). The subsequent grief and loss experienced by families and significant others have caused an impact on their mental health, and leads to secondary healthcare costs, loss of productivity and subsequent economic burden.

For those who survive traumatic injury, recovery periods and long-term disabilities result in a reduced economic contribution and/or long-term economic liability imposed on health and social systems. Post-traumatic stress disorder (PTSD) and cognitive changes as a result of traumatic brain injury have been recognised as a significant cause of psychological impairment in response to injury. Some studies reported an incidence of up to 51% of patients who had sustained traumatic injuries meeting diagnostic criteria for PTSD (Starr, 2004). Yet, psychological consequences such as PTSD are currently neglected in the burden of injury calculations (Haagsma, 2010). While there is little evidence for the efficacy of early debriefing on post-traumatic injury, there is some evidence that early cognitive behavioural therapy may lessen the psychological impact of injury and help prevent progression towards PTSD (Bisson, 2004).

Whilst facial trauma in general terms follows the parameters for causation of general trauma, there are slight nuances with regard to facial trauma compared with general trauma. The most common causes of facial fractures for hospital admissions in 2007 were assaults (37%), falls (25%) and motor vehicle collisions (MVCs) (12%). Assaults contrast heavily, accounting for the causation of 4.7% overall trauma compared with 37% for facial trauma (Allareddy, 2011). In certain locations and communities within Australia, the incidence of assault causing mandibular fractures is as high as 74% (Oderdan, 2007). It is thought that in these cases, drugs and alcohol play a significant role as the precursor to interpersonal violence.

Specifically discussing facial fractures, the flowchart shown in Figure 1.2 shows where facial trauma lies within the spectrum of body regions. Figure 1.2 serves to highlight the close relationship between head, face, neck and brain, and how there is often an interplay with facial trauma and other closely anatomically related regions that can complicate management significantly.

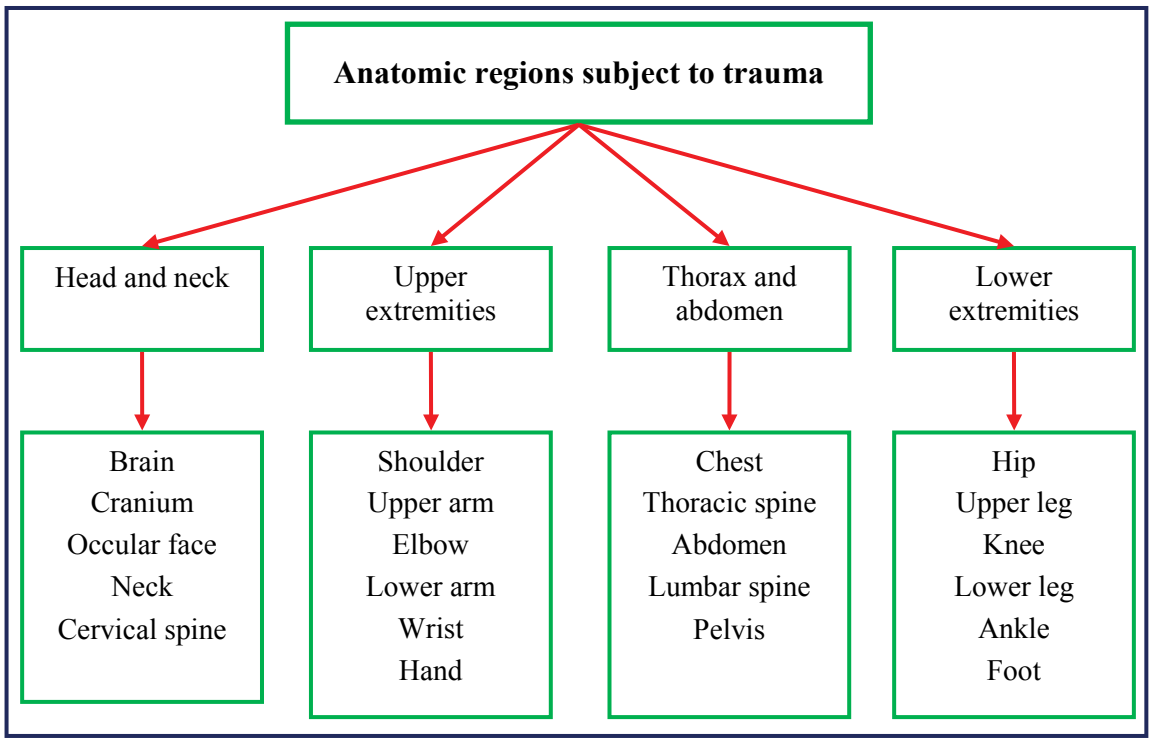

Figure 1.2 Flowchart of trauma by anatomical region that shows where facial trauma lies within the spectrum

The anatomical region affected by trauma depends on the type of trauma being experienced with the mechanism broadly split into penetrating and blunt trauma. The position of the body in relation to the blunt and or penetrating force also plays a role.

Blunt trauma accounts for 89% of trauma with the head/face, thorax and limbs being most commonly affected. Penetrating trauma accounted for 6.3% of injuries with thorax and abdomen most frequently affected, with burns at 4.7% accounting for the remainder. Of the anatomical regions head injury with concomitant, facial trauma shows the highest mortality (Cameron, 1995).

In monetary terms, whilst not derived from Australian data, Table 1.3 shows the cost per admission to provide management of various facial fractures ranging from US$88,442 for maxillary fractures to US$49,892 for mandibular fractures. These figures would be comparable to Australian figures given the identical methods of management in Australia versus the USA and comparable health economy.

Table 1.3 Cost in US$ for hospitalisation to repair various facial fractures (Allareddy)

		Hospitalization Charges ($)		Length of Stay (Days)	
Type of Facial Fracture Reduction	*N* (%)	Mean	Standard error	Mean	Standard error
Reduction in facial fracture, not otherwise specified	34 (0.2)	$65 131	1810	5.82	0.24
Closed reduction in malar and zygomatic fracture	48 (0.2)	$34 136	2233	3.98	0.34
Open reduction in malar and zygomatic fracture	2499 (11.8)	$56 661	4699	4.90	0.34
Closed reduction in maxillary fracture	202 (1.0)	$32 696	3736	3.61	0.46
Open reduction in maxillary fracture	1477 (7.0)	$88 442	7851	7.84	0.72
Closed reduction of mandibular fracture	2578 (12.1)	$26 035	2046	2.53	0.13
Open reduction in mandibular fracture	11 097 (52.2)	$49 892	3914	4.15	0.21
Open reduction in alveolar fracture	130 (0.6)	$45 171	6074	3.72	0.52
Other closed reduction in facial fracture	52 (0.2)	$32 351	3233	2.89	0.26
Other open reduction in facial fracture	3127 (14.7)	$54 091	3872	5.00	0.34

Of the bones involved in the facial skeleton, Figure 1.3 and Figure 1.4 show the incidence of injury (fracture) to these bones and the incidence of those that require surgery to repair. Whilst mandibular fractures rank second behind nasal bone fractures, mandibular fractures are twice as likely to require surgical repair than any other facial bone fracture (VandeGriend, 2015).

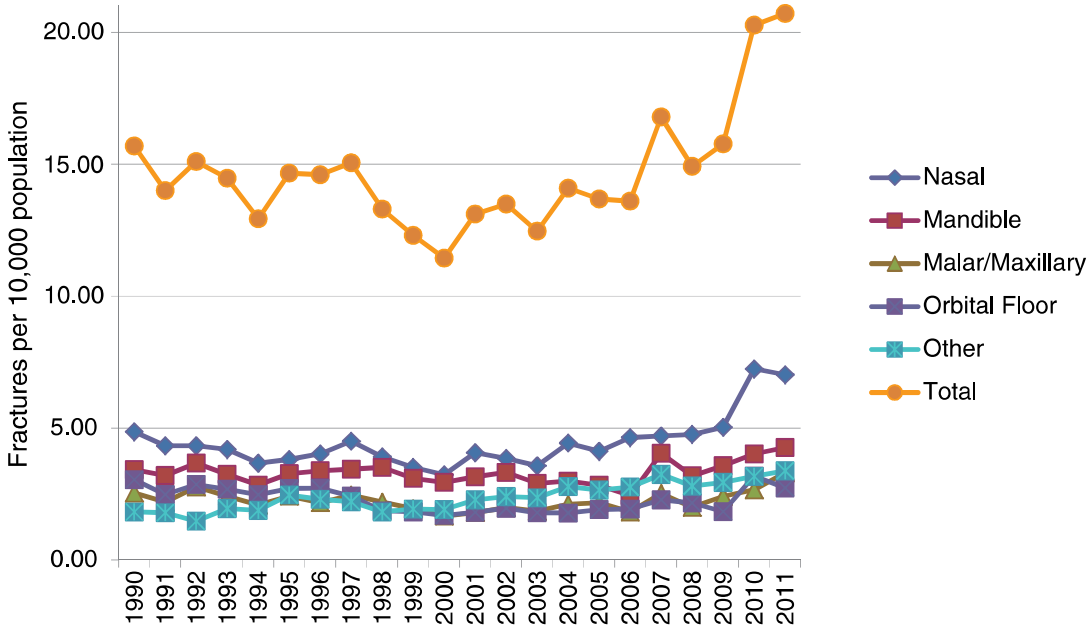

Figure 1.3 Incidence of facial bone fractures (VandeGriend, 2015)

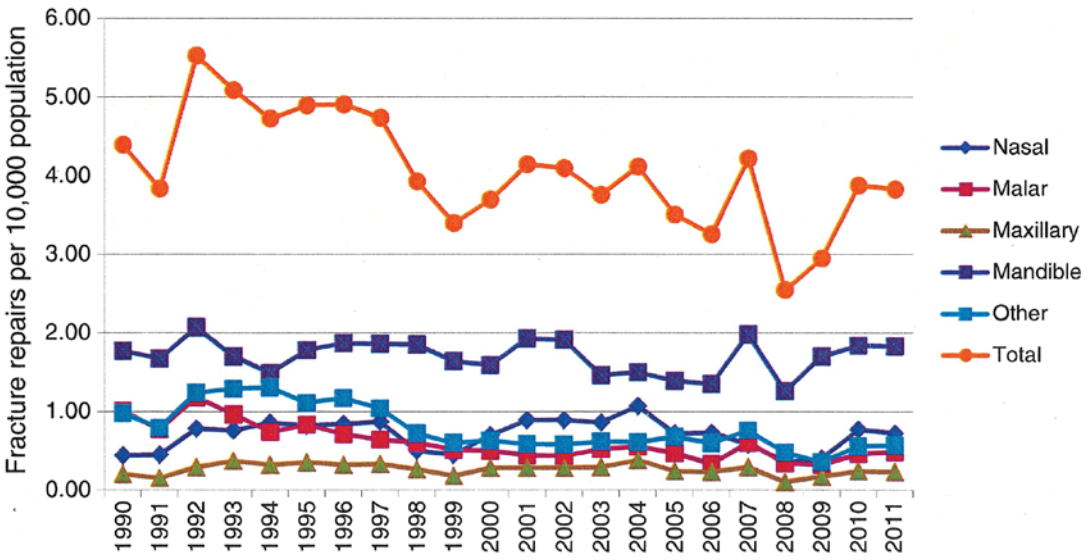

Figure 1.4 Facial bone fractures requiring surgical repair (VandeGriend, 2015)

The relevance of this is that if the treatment of traumatic injuries to the mandible can be improved, then given its high incidence and particularly those that require surgical repair, this would have a significant impact on the provision of health, not only to the individual but also to the entire community.

1.3 Fracture of the mandible and surgical aspects

The mandible is a prominent and easily accessible bone, but unfortunately it is commonly involved in trauma that results in fracture. The leading cause of mandibular fractures is interpersonal violence followed by sporting injury, motor vehicle collision, falls, pathologic and iatrogenic.

With the advent of improved vehicle design and road safety, motor vehicle injury, which previously was number one has now regressed to the third most common cause of mandibular fractures. Unfortunately, as has been widely advertised in the general media, interpersonal violence remains a major problem. The peak incidence of mandibular fractures occurs in males between 20 and 28 years of age with females of the same age showing a ten-fold decreased incidence compared with males.

Children and the elderly are less likely to suffer a fractured mandible, however, have idiosyncrasies that complicate management. For example, children are still in their growth phases and fractures of the mandible are often incomplete (greenstick) and may involve growth centres (condylar processes) and unerupted developing deciduous and adult dentition. The elderly similarly pose management difficulties due to possible general health comorbidities and more specifically relating to the mandibular osteoporosis either in isolation or combined with tooth loss as mandibular atrophy.

The most commonly involved sites of mandibular fracture in descending order are the parasymphysis equal with the angle (junction between horizontal and vertical ramus), condyle, body of horizontal ramus, symphysis and coronoid. The explanation for this is a combination of anatomy and trauma biomechanics. For example, the parasymphysis just to the right or left of the mandibular centre line is the most likely area of direct blunt trauma impact in assaults and sporting accidents. It is also the anatomical site of the mental foramen and canine teeth with a long root structure compared with adjacent teeth. For these two reasons, the mandible is structurally less robust at the parasymphysis. The same reasons apply to the angle of the mandible but in this site the anatomical idiosyncrasy is the wisdom tooth which is commonly unerupted and hence a site of less structural integrity.

Modern management of mandibular fractures essentially revolves around the degree of fracture displacement and stability (termed ‘favourable’ and ‘unfavourable’). For example, if a fractured mandibular angle is undisplaced and unlikely to be dislodged further by muscle pull and or function, it is termed a ‘favourable’ fracture and would be treated in the first instance conservatively. This would consist of soft diet for four to six weeks (possibly longer in the elderly), antibiotics (if a risk of infection), analgesia and regular clinical and radiographic assessment. If unsuccessful, interventional management would be undertaken.

Where conservative management has failed or the fracture is initially displaced, or due to muscle pull and/or function likely to be displaced (termed an ‘unfavourable’ fracture), then surgical intervention combining fracture reduction and fixation is mandated. In today’s practice, this would involve open reduction and internal fixation of the fracture with one of a variety of osteosynthesis plates that are commercially available.

Historically before the advent of modern internal fixation with plates, other techniques were used. Wiring of the maxilla and mandible together for six to eight weeks with intermaxillary fixation was common (Figure 1.5). The patient, however, was considerably debilitated during this period and airway compromise was a significant risk factor for this technique in the immediate postoperative phase.

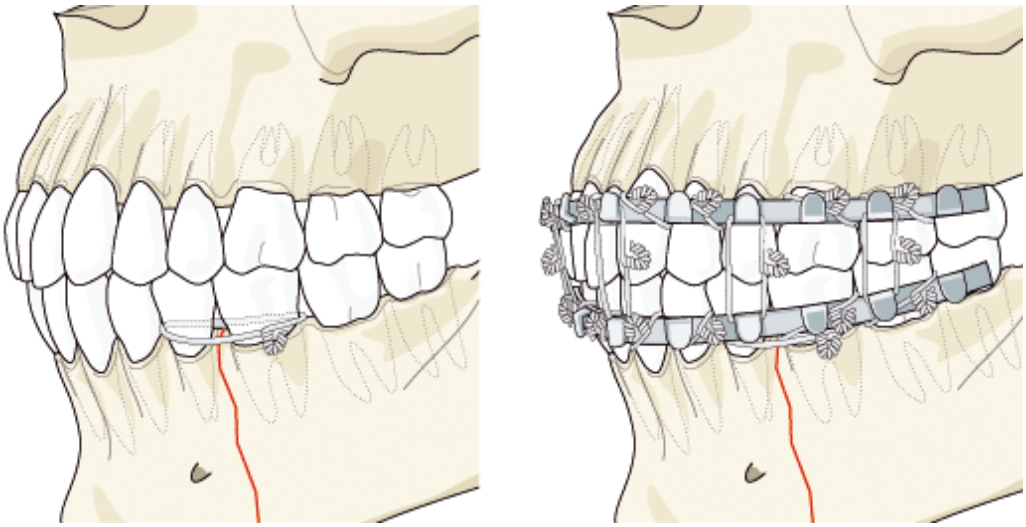

Figure 1.5 Intermaxillary wire fixation (modified, courtesy of AO Foundation)

Historical methods included fracture fixation with cortical wires or intramedullary pins, use of cast dental splints and external fixation devices (Figure 1.6). As can be seen, these methods had significant potential morbidities and were far from ideal.

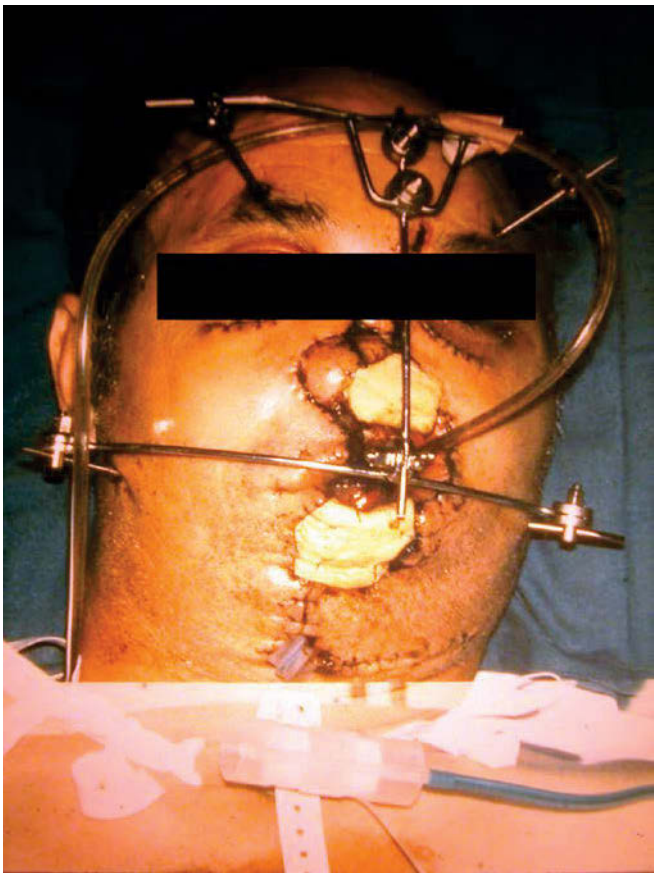

Figure 1.6 External fixators used in managing facial trauma from gunshot wound

Current internal fixation with osteosynthesis plates and screws has been a significant step forward over these historical methods but even so, are still plagued by difficulties (Ellis 1996). One of these is hardware failure either not being able to withstand mandibular functional forces allowing continued fracture displacement (Figure 1.7) and mobility and in its worst case, catastrophic implant failure via fracture of the implant itself (Figure 1.8).

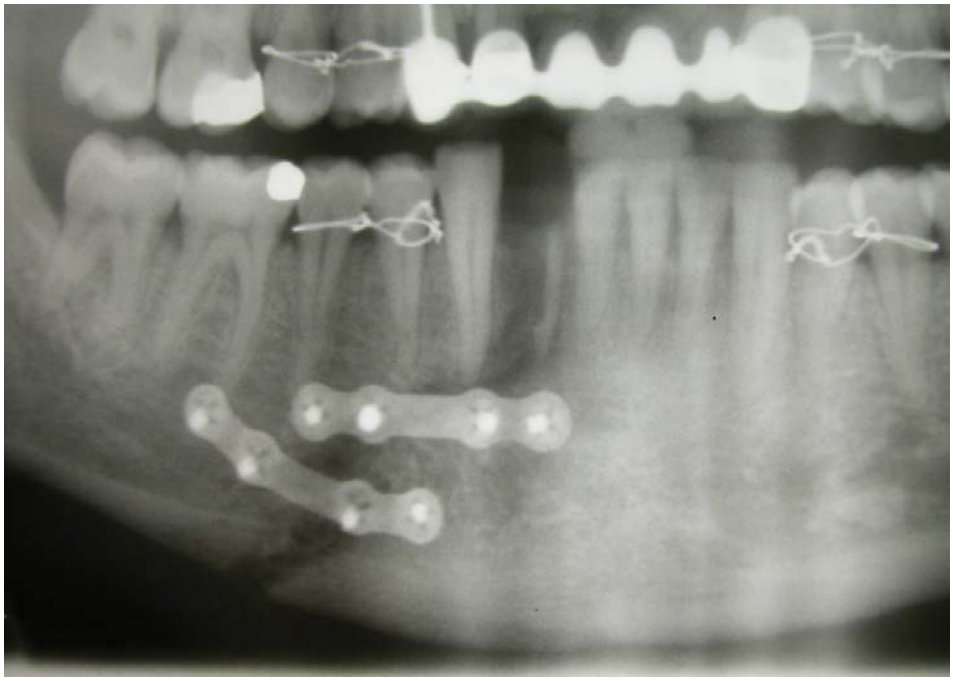

Figure 1.7 **Inadequate fracture apposition and fixation leading to persistent fracture displacement and delayed healing**

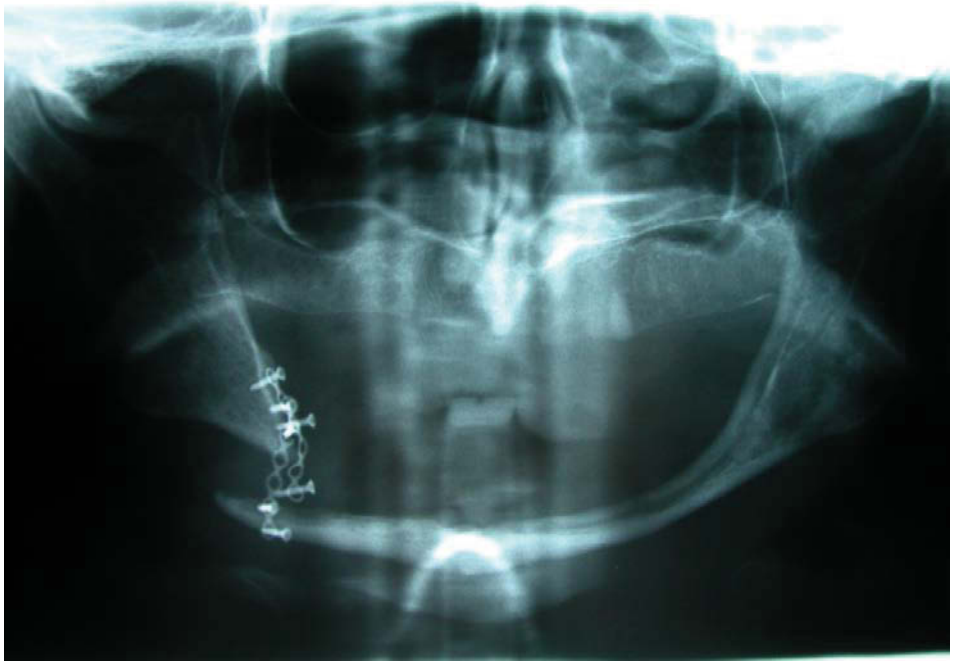

Figure 1.8 **Inadequate fracture fixation leading to implant failure resulting in fracture non-union in an elderly female with osteoporosis and an atrophic mandible**

Even with the best osteosynthesis techniques available today, the design of these fracture fixation systems and their method of use still rely on generic data dating back to bite force analysis and mandibular stress line models produced by Champy and others in the 1970s. Patient idiosyncrasies, such as anatomical variances, state of dentition, bone density and detailed data available from modern CT studies are generally not taken into account.

The surgical aim of this research is therefore to develop the best method of computational fracture analysis, not based on generic data, but specifically customised to each individual patient, followed by analyse for that individual and identifying the optimal fixation implant design and appropriate surgical method.

1.4 Rapid repair and recovery from facial fractures

Rapid repair of any fracture and an associated speedy, uncomplicated recovery is obviously important and requires discussion in more detail.

Firstly, rapid repair benefits the patient in pain relief and fast restoration of function. As it pertains to the facial skeleton, it is important to understand the functions of the facial skeleton so that we can understand why this concept of rapid repair is so important.

The facial skeleton acts as the scaffold and functional support for five major facial, head and neck functions: (i) facial expression; (ii) speech production; (iii) mastication; (iv) deglutition; and (v) airway maintenance.

1. ***Facial expression*** is seemingly not initially thought of as a primary function compared with speech or chewing. However, it is critically important to a person's non-verbal expression and psychological health. It has been extensively proven that facial expression is intrinsically associated with a person's mood. For example, pleasure versus pain and depression versus euphoria. Some might think that if one is in pain, then a depressed mood and associated characteristic facial expression will follow, but with facial fractures, the resultant inability to perform normally subconscious facial expression in oneself can lead to depression. In this aspect, the facial skeleton is unlike any other part of the skeletal anatomy. In

fact, the Queensland Institute of Medical Research is currently conducting research into the relationship between the ability to perform facial expression and the development of mental ill health in its role as a possible diagnostic tool for mental disease.

2. ***Speech production*** involves a highly developed and complex set of neural pathways that control breathing and lung function, along with vocal cord tension and tongue and mouth posture to produce sound as a distinct and understandable vocabulary. Koshy (2010) in his comprehensive article entitled 'Pearls of mandibular trauma management' recognised the significantly deleterious effect of facial, particularly mandibular trauma has on speech. He discussed that not only does the initial trauma impact speech but management of the fracture can also significantly impact speech with issues such as post-operative swelling and the use of intermaxillary fixation (wiring the jaws together, Figure 1.abc).

3. ***Mastication*** is the process of chewing food. It involves food being manipulated around the oral cavity by the lips, cheeks, teeth and tongue. Such manipulation positions the food between appropriate teeth to begin the dissection into manageable sizes with the incisor, canine and premolar teeth, and then crushing and grinding with the premolar and molar teeth.

   In order to process the food, the bite force needs to be developed by the muscles of mastication and distributed through the maxilla and mandible and their inherent teeth. Bite forces in healthy middle-aged humans averages 520N for males and 340N for females, however, maximal forces have produced up to the high 700s. To properly harness this force, the facial skeleton must be intact, otherwise diet must be considerably modified to liquids only or possibly purees or a soft diet depending on the extent of the injury. Whilst acceptable for short periods, prolonged malnutrition begins to negatively impact, not only the general body systems, but significantly impairs healing and causes the individual to be susceptible to infection, which again would deleteriously affect healing.

4. ***Deglutition*** is defined as the process that makes something pass from the mouth to the pharynx and into the oesophagus while shutting the epiglottis. Swallowing is an important part of eating and drinking. If the process fails and material (such as food or fluid) goes through the trachea, then choking or pulmonary aspiration can occur. In the human body, the automatic temporary closing of the epiglottis is controlled by the swallowing reflex. The mandible acts in an integral fashion in swallowing. For example, the tongue, which is suspended from the mandible by way of musculature such as the mylohyoid, acts to initially push the food bolus from the mouth into the pharynx where pharyngeal constrictors are again partly supported by the mandible and act to propel the bolus from the pharynx into the oesophagus. It can easily be imagined that if the mandible is affected by pathology, such as a fracture, then the associated musculature, as outlined above, will be debilitated and uncoordinated in the function of swallowing. Such an issue easily leads to the inability to swallow and subsequent starvation or improper swallowing leading to potentially disastrous aspiration (entry of food into the trachea and lung).

5. ***Airway maintenance***, as we can already see from the discussion, directly above airway protection relies on proper deglutition and an intact facial skeleton (mandible) to do so. The lower facial skeleton also works harmoniously with the middle facial skeleton to allow respiration to occur unimpeded. Whilst quiet breathing often only involves the nasal passages, more rigorous breathing usually involves the oral cavity and stabilisation of these structures to resist the negative pressure developed by the lungs on inspiration.

Rapid fracture repair as a basic principle is the same for all bones of the skeleton. The process is predictable as long as certain parameters are met. A fractured or broken bone undergoes repair through four stages (Figure 1.9).

1. ***Hematoma formation:*** With trauma associated with a fracture, not only does the bone break, but associated tissues, in particular the blood vessels, are also disrupted. This initially produces bleeding, followed by the clotting process to form a haematoma at the fracture site. This haematoma formation at the fracture

site is the first step in fracture healing as cytokines contained within the clotted blood direct the surrounding tissue to begin the process of bone healing. In stark contrast, avascular or poorly vascularised bone, when fractured poorly or completely, fails to heal.

2. ***Bone generation:*** Within days of a fracture, cytokines contained within the haematoma encourage new blood vessels to grow. The process is coordinated between osteoclasts to clear dead unviable bone tissue and osteoblasts to produce new immature cartilaginous bone at the fracture site. Fibroblasts are also recruited by the cytokines to produce collagen fibres that are associated with new bone formation. The new bone being formed at this stage is referred to as 'fibrocartilaginous callous'.

3. ***Bony callous formation:*** As days turn into weeks the initial fibrocartilaginous callous is slowly converted into calcified tissue, and is now referred to as 'bony callous' containing spongy bone. At this point, the fracture starts to achieve some structural integrity but this phase in a healthy adult still takes two to three months to progress. This process of laying down calcified bone along a fibrocartilaginous scaffold is termed 'endochondral bone formation'.

4. ***Bone remodelling:*** After two to three months, the immature newly formed spongy bone is gradually converted to compact bone by a continuing interaction between osteoclasts and osteoblasts called 'bony remodelling'. This stage of the process can take months or years to be fully complete, therefore, it is important to return the fractured bone to its structural integrity prior to the fracture occurring. Only at this point has full fracture repair occurred.

These four stages of fracture healing in a fit middle-aged individual routinely takes 12 weeks.

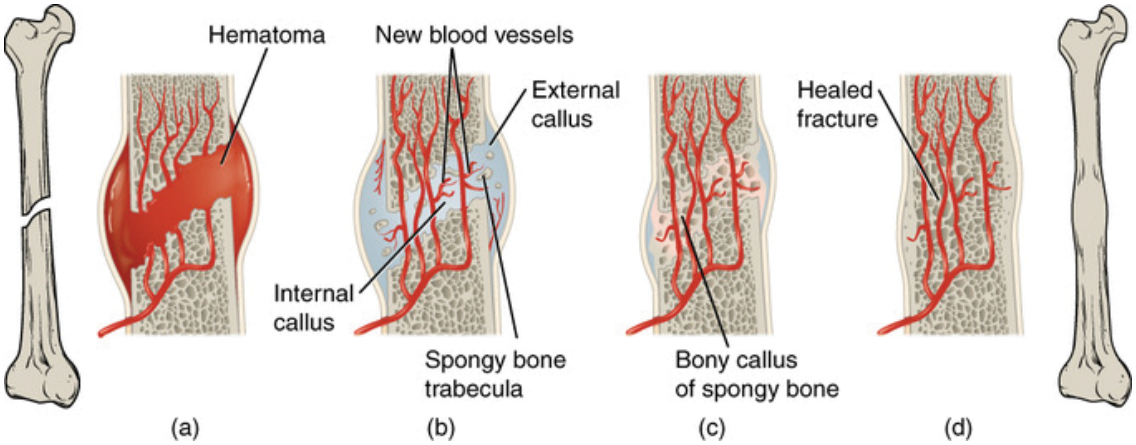

Figure 1.9 Four stages of fracture healing: (a) haematoma formation; (b) bone regeneration; (c) bony callous formation; and (d) bone remodelling (courtesy of Boundless)

The parameters required for the above representation of uncomplicated fracture healing to occur include the following.

1. Well vascularised tissue is the key to fracture healing. Without an intact blood supply, haematoma formation cannot occur. As Simpson (2006) eloquently demonstrated, bone morphogenetic proteins, transforming growth factor beta, insulin-like growth factor, fibroblast growth factor, platelet-derived growth factor and vascular endothelial growth factor are all present during normal healing of fractures.

2. In addition, the individual's overall health is an important factor. Whilst not necessarily blocking fracture healing entirely, comorbidities such as infection, diabetes or nutritional deficiencies can significantly negatively impact on the healing process, resulting in prolonged or incomplete fracture repair.

Fracture reduction and immobilisation is very important because the continuity defect that has occurred as a result of the fracture must be firstly obturated with haematoma, then the primary and secondary callous followed by mature bone. In particular, at the haematoma and callous stages, these biologic materials are extremely fragile and easily prone to disruption if excessive fracture mobility and instability continue, however, some controlled fracture micromotion (as discussed later) is of benefit to fracture

healing. This thesis concentrates specifically on fracture reduction and fixation utilising various fixation hardware. Whilst not dwelling on any specific hardware at this point, a description of reduction and fixation, as well as its importance is worth addressing further. For centuries, it has been well recognized that the closer the two fractured ends of bone can be brought back together, the less fracture healing is required. Indeed, if fracture ends are not in contact and a discontinuity (gap) defect occurs, then fracture healing may not occur at all and a non-union develops where bone healing the fracture site soft fibrotic tissue fills the continuity defect instead. This is obviously not desirable as the function of the bone is permanently disrupted and suboptimal. Schmitz and Hollinger (1985) suggested that as little as 5.0mm as a continuity defect in a mandibular fracture either completely or severely impairs fracture healing with bone.

Figure 1.10 shows a mandibular fracture 16 weeks post-injury and the initial attempt to fix the fracture with hardware. What is interesting is that despite having fixation hardware in situ, the gap discontinuity is approximately 5.0mm and bone union has not occurred.

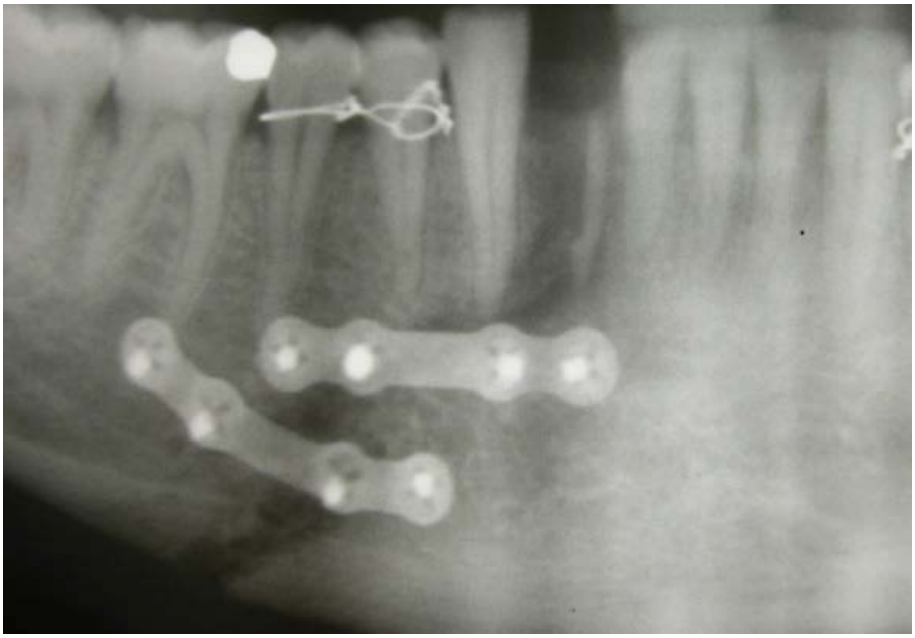

Figure 1.10 Gap discontinuity in repaired fractured mandible despite immobilisation facture healing not occurring

Fracture immobilisation can either be done externally in the form of plaster casts or other forms of splinting (external fixators, Figure 1.6). This method is usually confined to a non-displaced fracture that can be easily reduced into position and can be kept in the reduced position by limiting function until fracture healing occurs. In many cases, this is not possible and/or desirable. Under these circumstances, open reduction and internal fixation is employed. Internal fixation can be produced with screws, wires, pins, plates and screws. The latter method is the form most often employed in facial fracture fixation.

Of debate regarding this technique is: How much immobilisation is required? Furthermore, is movement controlled by the fixation hardware actually beneficial to healing? That is, is some fixation too rigid? From the research, a point of aim has been established that some micromovements allowed by flexible fracture fixation hardware is beneficial to the completeness and speed of fracture repair. A balance between interfragmentary micromovement and macromovement determines whether the vascular in-growth will be stimulated or broken down (Alpert, 1998). For successful treatment, the osteosynthesis device must provide adequate stability, which controls the interfragmentary movements without necessarily preventing it completely. Interfragmentary micromovement is reported to help fracture healing by stimulating external callus formation (Marsh, Ghanem & Alpert, 1998, 1999, 2011). In discussing the results of this thesis in Chapters 8 and 9, we will focus on movement and the variations as allowed by the hardware systems that were tested.

1.5 Rigid versus semi-rigid fixation, micromovement and stress shielding

In rigid fixation, the plate or fixation system assumes 100% of the functional loads and allows no movement at the fracture site. This is also termed ‘load bearing fixation’. Alternately, in semi-rigid (flexible) fixation systems, the fixation and bone share the functional loads almost equally. This is sometimes also termed load sharing fixation and in this scenario micromovement is allowed and is actually beneficial to healing. The significance of this comes to light when we talk about stress shielding.

In stress shielding, if a rigid, load bearing fixation system is applied across a fracture then a disuse osteoporosis can occur, producing suboptimal healing (Kennady 1989). In 2010, Liu looked at mandibular fractures and bone density. Bone density was measured pre-operatively, then at intervals of up to six months post-operatively. Liu found a drop in bone density over this time and attributed this to stress shielding with rigid fixation which then indicated that the fixation system should be removed, thus necessitating a second procedure.

In contrast with semi-rigid load sharing fixation a small amount of movement is acceptable and promotes ideal anatomical healing. In this scenario, the plate can remain in situ and does not need to be removed because it acts symbiotically with the mandibular biomechanics.

In this thesis, all of the fixation systems were designed to be semi-rigid (flexible), that is, load sharing, allowing micromovement with the adjacent bone. In the presentation of data and discussion, data for distortion will be presented.

1.6 Limitations of current fracture management

In the preceding sections of Chapter 1, we covered the interplay between fracture management, requirements for healing to occur and idiosyncrasies that make the mandible and facial skeleton unique compared to the rest of the human skeleton. This now allows us to discuss in more detail where current fracture management has progressed to and moreover where this research will have a role in future development and improvement in fracture management.

The current gold standard for the management of mandibular fractures is open reduction and internal fixation with titanium (Ti) osteosynthesis miniplates. As Uthoff (2006) summarised, metal plates for internal fixation of fractures have been used for over 100 years. Although initial shortcomings, such as corrosion and insufficient strength have been overcome, more recent designs have not solved all the problems. Such problems include the plate contact interfering with cortical surface perfusion, stress shielding and difficulty in adapting (bending) plates to properly match the patient's morphology. Therefore, further research is needed to develop a plate that accelerates fracture healing

while not interfering with bone physiology. To a significant degree, this research helps to further this endeavour.

Plating of fractures began in 1895 when Lane introduced a metal plate for use in internal fixation. His plate was eventually abandoned owing to problems with corrosion (Figure 1.11).

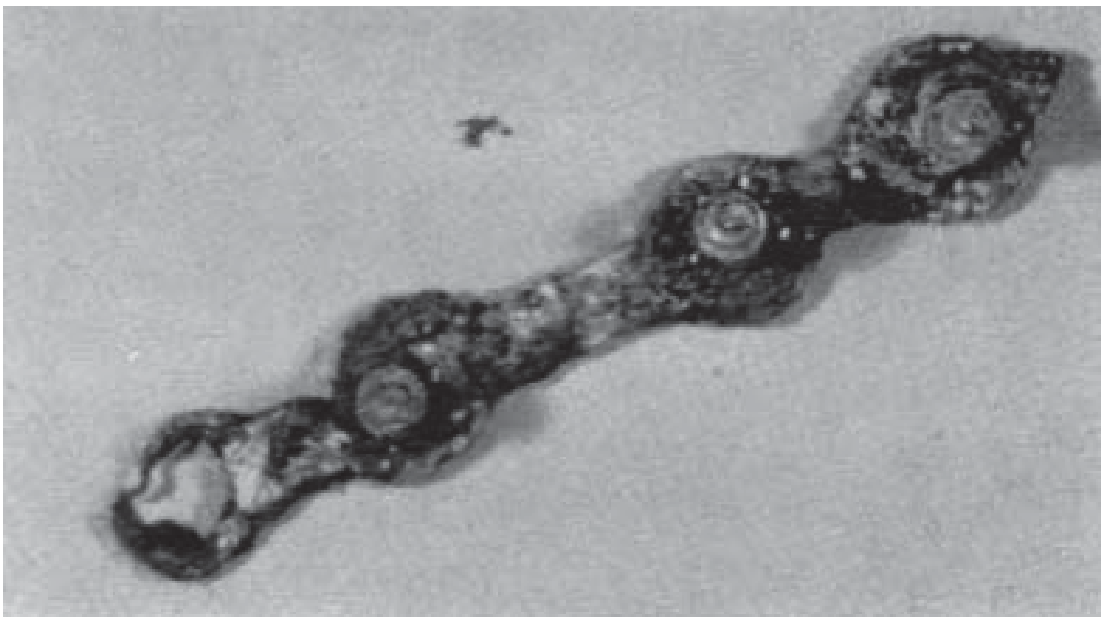

From Bechtol CO, Fergusson AB, Laing PE. (1959). *Metals and Engineering in Bone and Joint Surgery*. Baltimore: Williams Wilkins.

Figure 1.11 Lane's metal plate introduced in 1895 but abandoned due to corrosion

Although Lane's plate corroded, what I find most interesting is the design and morphology of the plate. His plate shows a four hole linear plate that is retained by mono cortical screws. For comparison, shown in Figure 1.12 is a contemporary design that is almost identical to Lane's design of 1895.

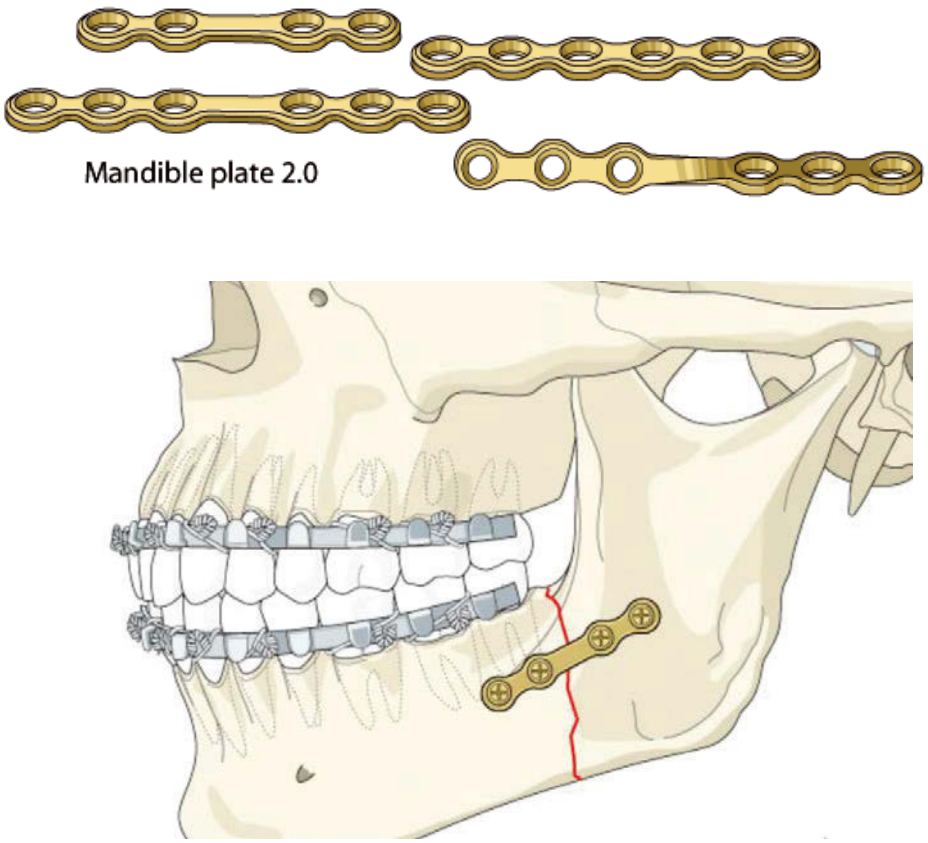

An example of contemporary four screw hole Ti miniplates and various other configurations available specifically designed for the management of mandibular trauma and beneath one such plate in situ (courtesy AO Foundation).

Figure 1.12 Example of contemporary four screw hole Ti miniplates

Rigid internal fixation was initially used in the oral and maxillofacial region in the late 1970s. Since the works of Michelet et al. (1973) and later Champy et al. (1978), miniplate osteosynthesis has become an important fixation method in maxillofacial and craniofacial surgery.

The metallurgy of these contemporary plates based on the works of Champy (1978), Michalet (1973) and Luhr (1985) in comparison with Lane's design, has certainly improved. The current alloy in use is Ti-6Al-4V which has excellent corrosion resistance in the human tissue fluid but is prone to difficulties in shaping which can introduce early fatigue, and if continued in vivo due to excessive fracture site mobility, can lead to failure.

Azevedo (2003) described this as the action of a corrosion fatigue related mechanism and indicated that the breakage of the miniplate was caused by mechanical instability of the fracture reduction. This process is begun when the plate has to be manipulated to fit to the contour of the fracture site and is a significant source of hardware failure which according to Choi (2005) and Mommaerts (2005) is 7% to 8.6% of cases based on clinical studies.

Figure 1.13 shows a plate design similar to that used by Azevedo (2003) in his study where the plate typically fails due to corrosion fatigue.

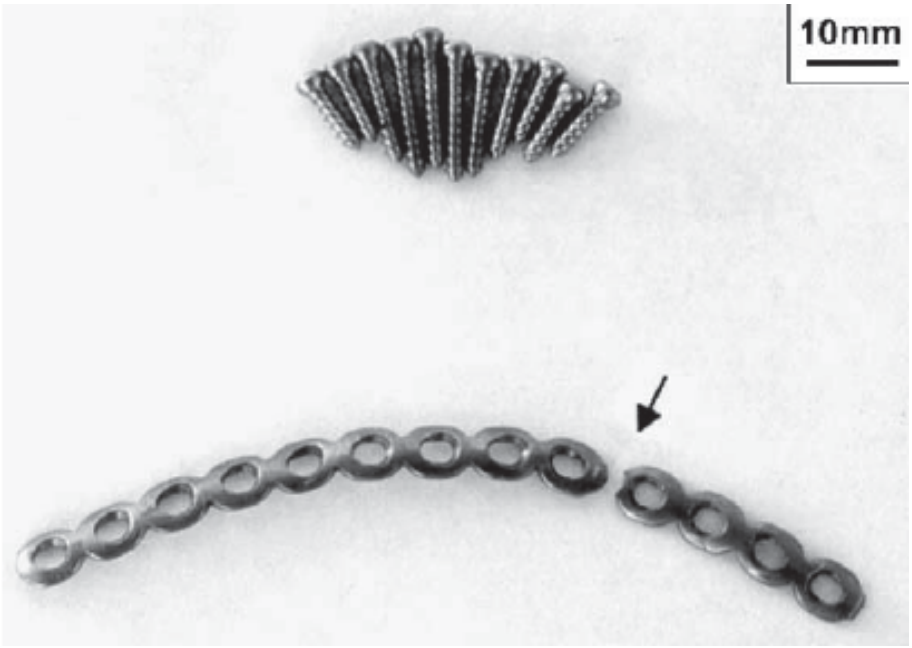

Figure 1.13 Failed commercially pure Ti plate for osteosynthesis (Azevedo, 2003)

The findings of Azevedo (2003) also correlate well with Sugiura (2009) who showed that in a four hole Ti miniplate held in situ with four mono cortical screws, the concentration of von Mises stress was highest at the bridge of material between the screw holes (Figure 1.14). This location corresponded to where Azevedo (2003) found the plates were most likely to fail (Figure 1.15).

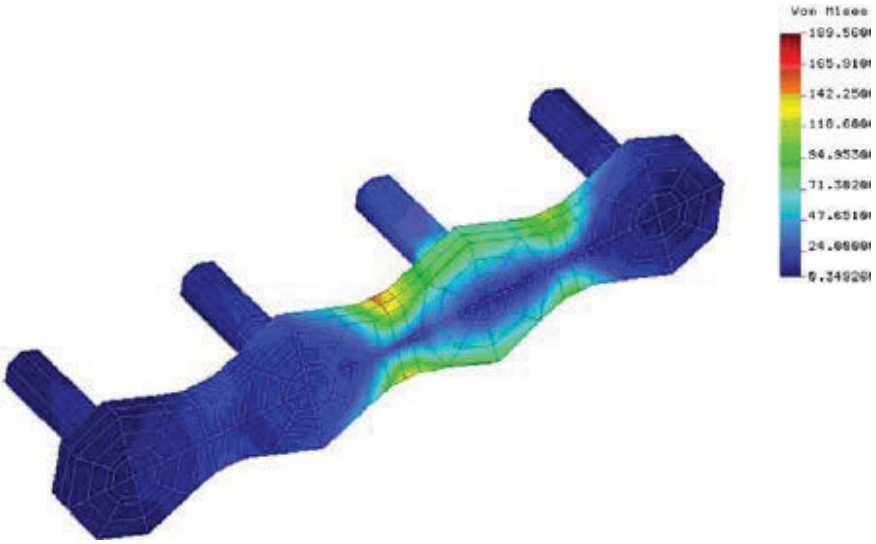

Figure 1.14 FEM of four hole miniplate showing the location of highest von Mises stress (Sugiura, 2009)

This evidence of FEM analysis from Sugiura (2009) and clinical correlation from Azevedo (2003) points to the conclusion that failure of a Ti plate is initiated at the time of plate bending to allow it to fit the patient, as displayed in Figure 1.13). If continued, stress occurs in vivo, resulting in plate failure. Figure 1.13 shows the typical instruments used to manipulate the plates prior to insertion and potentially introducing early fatigue.

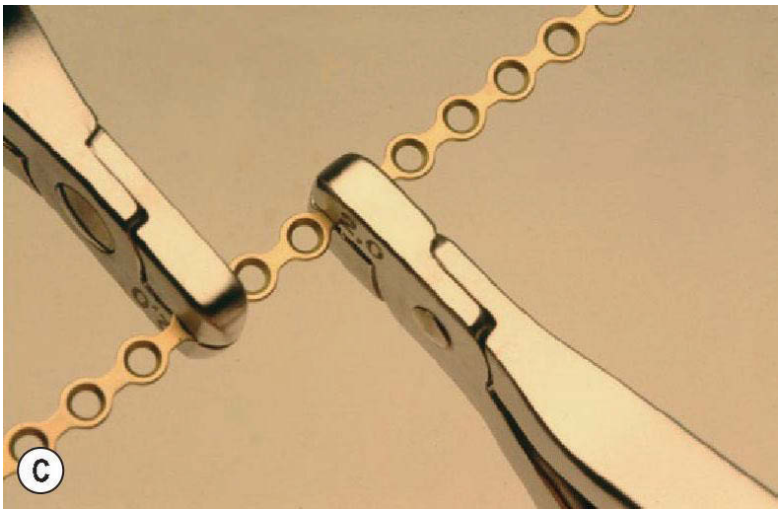

Plate benders being applied to manipulate and shape a Ti plate prior to insertion onto the fracture site. Plate benders are applied and produce material distortion at the site where plate failure is most likely to occur (courtesy of AO Foundation).

Figure 1.15 Plate benders used to manipulate a generic non-patient specific plate

From this, we see a fixation system that is specifically designed, manufactured and tested for the individual, as this thesis suggest, is significantly better than an off-the-shelf generic plate that requires much alteration for a satisfactory fit. In doing so compromises structural integrity and predisposes to hardware failure.

1.7 Specific difficulties with the fractured edentulous mandible

Since the earliest discussion on the management of facial bone fractures, the edentulous mandible and especially the atrophic fracture, have been recognized as posing additional significant difficulties in management. The mandible as a process of aging and tooth loss undergoes atrophy. This presentation is common for people aged in their 70s and 80s as the elderly have often lost many teeth, resulting in an extremely thin mandible that is weak and prone to fracture. The difficulty this poses in management is a combination of biological and biomechanical conditions that are unfavourable for fracture fixation and bone healing (Novelli, 2012).

Although atrophic mandibular fractures only account for a small percentage of facial fractures according to Marciani (2001) the frequency of these fractures is considered to be less than 1% of all facial fractures. Biologic compromise exists primarily due to systemic disease that is common in the elderly. For example, vascular disease would compromise the necessary blood supply that is critical to fracture healing.

Biomechanical compromise exists primarily due to the thin nature of the mandibular bone and its resultant susceptibility to fractures, even with minor trauma. To this aspect, Luhr (1996) developed a classification of the atrophic mandible based on its dimension and resultant biomechanical integrity, which is widely used (Table 1.4 & Figure 1.16).

Table 1.4 Luhr's classification for fractures of the edentulous atrophic mandible

Class of atrophy	Mandible height at fracture site (mm)
I	16–20
II	11–15
III	<10

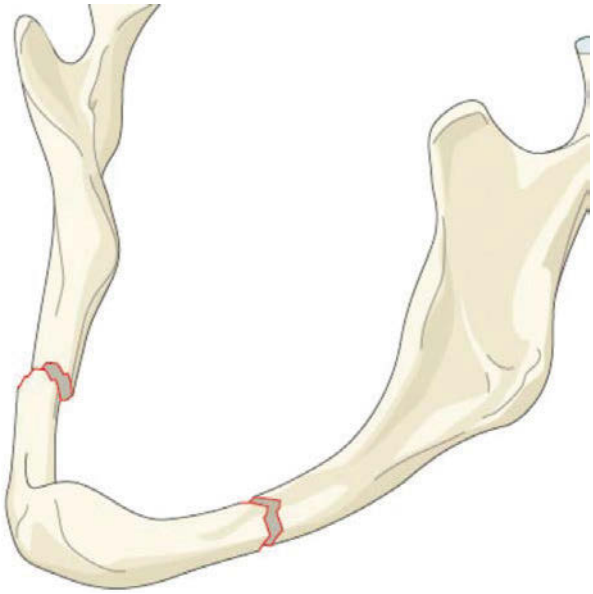

Figure 1.16 Diagram showing Luhr Class III atrophy and a common clinical presentation of bilateral fractures (courtesy of AO Foundation)

This thesis looks at the edentulous mandible as a model and its response to fracture repair, but does not concentrate on the severely atrophic Class III mandible as Class I and Class II fractures for which we have modelled, accounting for the majority of fractures in the atrophic mandible. However, separate research into a specific model to investigate Class III fractures is warranted, but outside the scope of this thesis.

1.8 Anticipation of research and its application

As presented in the following chapters, this research produces three main outputs:

1. A FEM of a Class I (Luhr 1996) edentulous mandible also termed as the 'generic (GEN) model'.

2. A PS model of a Class I (Luhr 1996) edentulous mandible using morphological and density data from a computed tomographic scan.

3. The design of a fracture in each model and then applying various biodegradable and permanent plates to repair these fractures. Analysis involve stresses and deformations generated within the plates and within the mandibular bone.

These models use a biomechanically correct complete set of muscle forces in equilibrium with the condyle reaction and advanced material properties, as well as an accurate mapping of cancellous and cortical bone.

In **Chapter 2,** the relevant anatomy and biomechanics of the mandible is presented, along with a calculation of the stresses and distortions of the mandible during functional movements. These calculations validate the consistency of the predictions of the developed FEM with previously published models.

In **Chapter 3**, the general principles used in the preparation of a biomechanically correct FEM of the human mandible are described and discussed.

Chapter 4 produces the first output of the thesis, that is the modelling of a generic edentulous human mandible.

Chapter 5 produces the second output of a PS model**.** This work represents an innovative FEM of the human mandible.

Chapter 6 addresses the nucleus of this thesis, that is, mandibular and fracture repair modelling. It critically begins to form the data required to formulate the hypothesis that answers the questions raised in the surgical analysis.

Chapter 7 covers the third output of fracture and repair modelling method.

Chapter 8 presents the mandibular fracture and repair modelling results of both the GEN model and PS model.

Chapter 9 provides a summary and conclusions.

Chapter 10 proposes future works to be undertaken.

CHAPTER 2:
ANATOMY AND BIOMECHANICS OF THE MANDIBLE

2.1 Anatomy of the mandible

The mandible is suspended below the maxilla by muscles, ligaments and other soft tissues. It is a unique bone in the human skeleton having the following properties:

1. It forms via intramembranous ossification.

2. The mandible is not connected to the base of the skull via fixed rigid bone sutures but by the bilateral temporomandibular joints.

3. It plays a key role in mastication, deglutition, speech, airway maintenance and facial cosmetic profile.

4. It commonly requires reconstruction with the mandible accounting for close to 50% of facial fractures.

Anatomically, it is composed of two vertical components, vertical ramii, joining at obtuse angles to the horizontal body of the mandible, which via its superior margin, the alveolar bone supports the teeth. With tooth loss due to dental pathology and/or the aging process, the alveolar bone resorbs leaving an atrophic mandible, as discussed in Chapter 1.

The inferior margin of the horizontal ramus (composed of more dense cortical bone than the alveolus) meets the posterior margin of the vertical ramus in an area that is called ‘angle of the mandible’ (Figure 2.1).

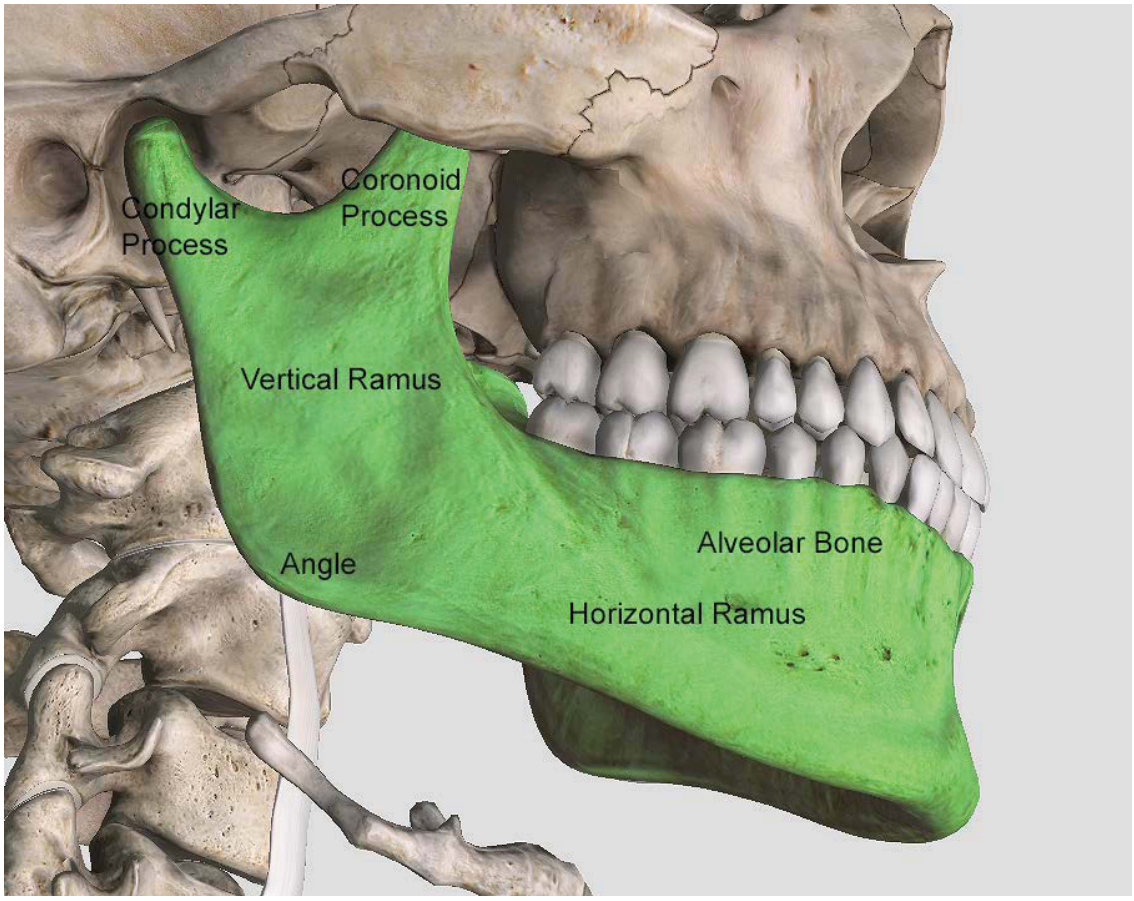

Figure 2.1 Showing the vertical ramus joining with the horizontal ramus at the angle of the mandible and alveolar bone at the superior aspect of the horizontal ramus housing the dentition (diagram constructed using 3D4MEDICAL software)

2.1.1 Major muscles of mastication

The angle of the mandible provides attachment to the masseter muscle on its lateral aspect and the medial pterygoid on its medial aspect and both of these muscle form the powerful pterygo-masseteric sling, as seen in Figure 2.2 along with the masseter in isolation.

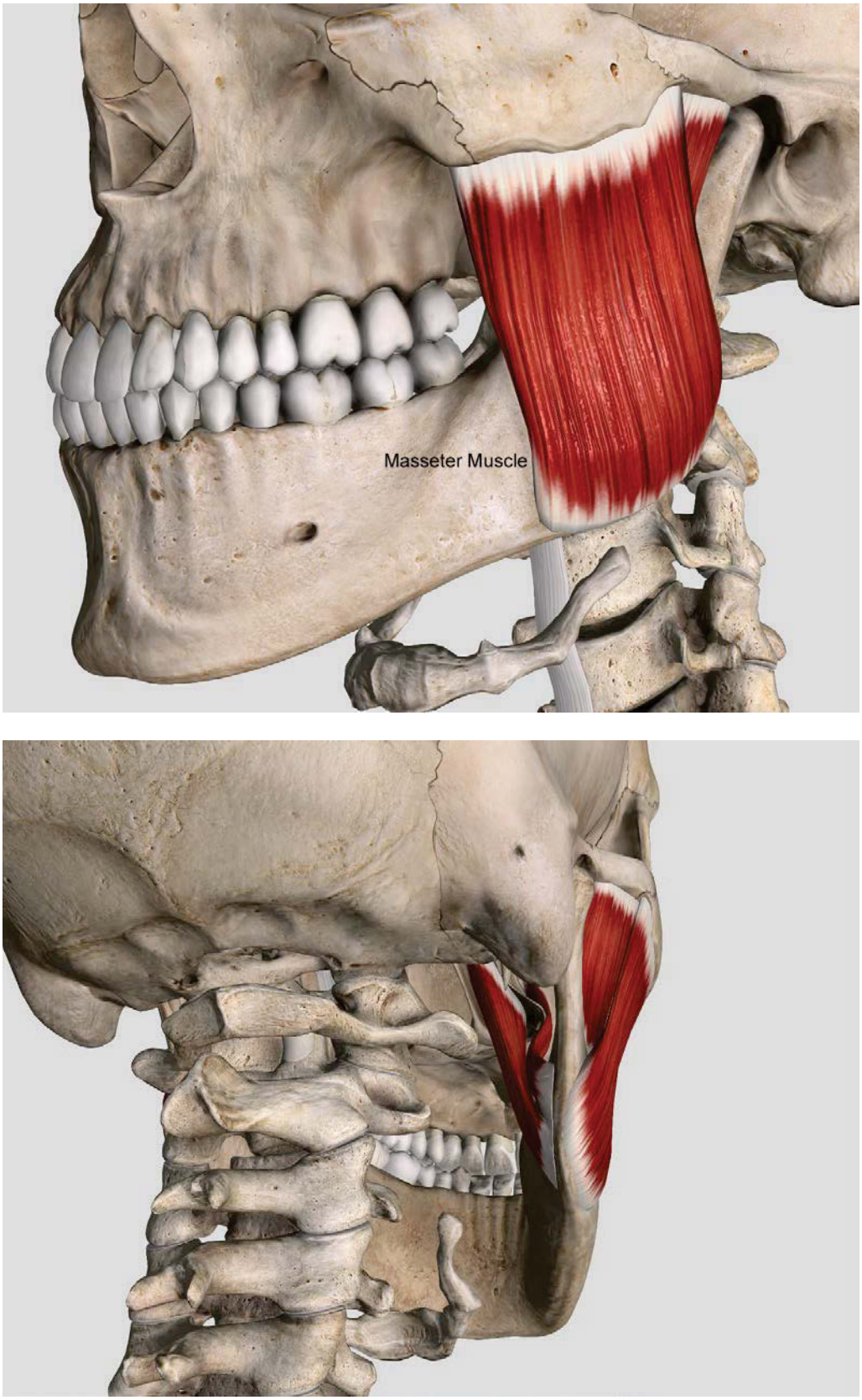

Figure 2.2 **Showing the masseter in isolation above and its combination with the medial pterygoid muscle to form the pterygo-masseteric sling (diagram constructed using 3D4MEDICAL software)**

The coronoid process on the anterosuperior aspect of the vertical ramus carries attachment of the temporalis muscle (Figures 2.3 & 2.4).

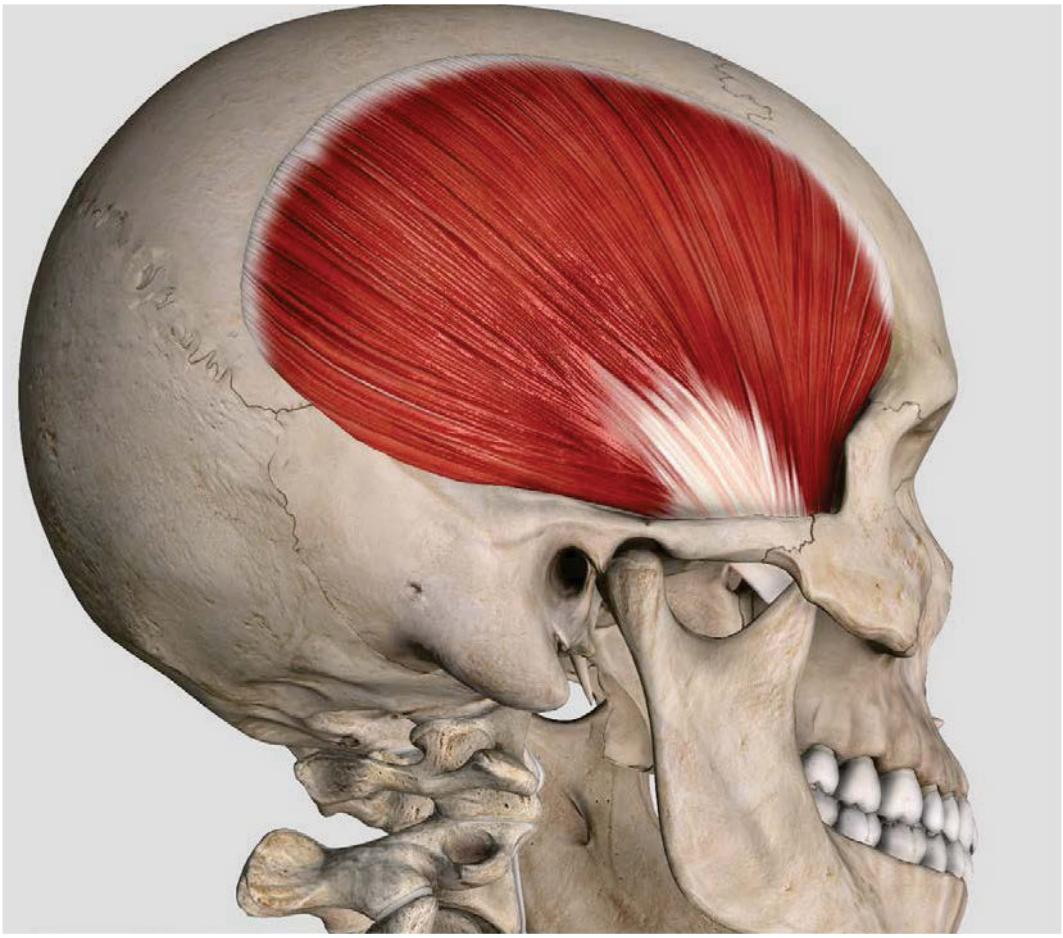

Figure 2.3 Temporalis muscle (diagram constructed using 3D4MEDICAL software)

The above musculature is considered to be the primary muscles of mastication. The temporalis, masseter and medial pterygoid are muscles of some bulk and are thought to provide the power for mastication.

2.1.2 Accessory muscles of mastication

The main accessory muscles of mastication are considered to be the lateral pterygoid, digastric and geniohyoid muscles. These muscles are not involved in the powerful closing action of chewing as are the temporalis, masseter and medial pterygoid.

Rather, accessory muscles are involved in mandibular opening, mandibular protrusion and coordination of the condylar process and articular disc on jaw opening. We will look at each muscle in turn and discuss their role.

On the posterior superior aspect of the vertical ramus sits the condylar process that carries an attachment for the lateral pterygoid, as illustrated in Figure 2.4.

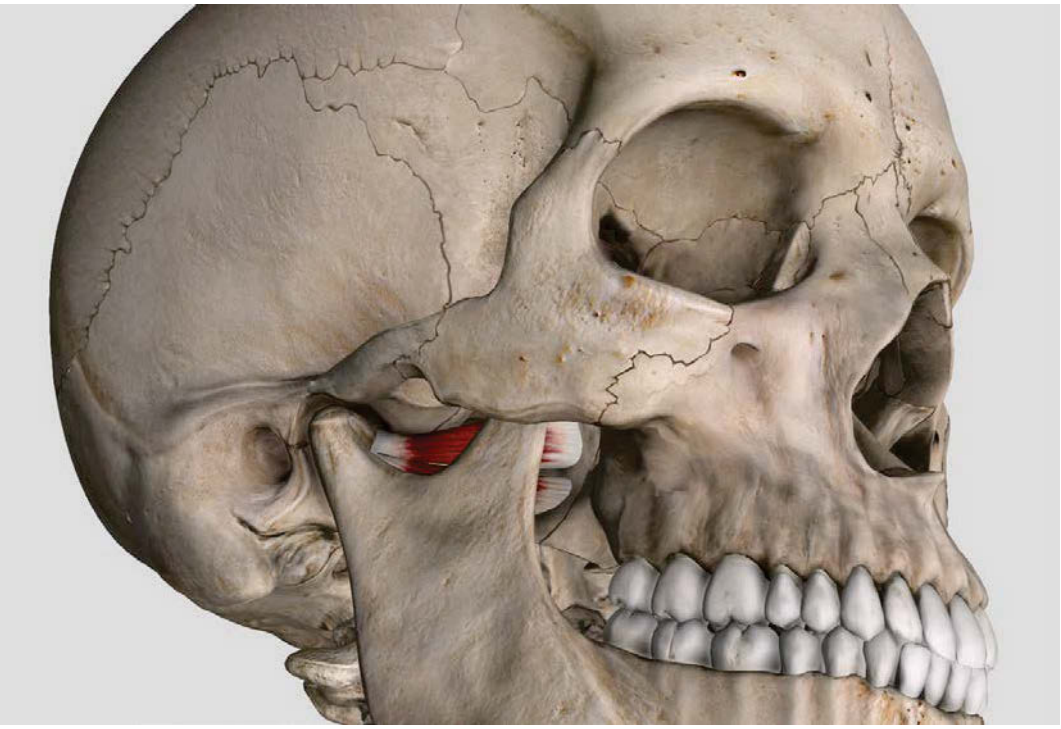

Figure 2.4 Lateral pterygoid muscle (diagram constructed using 3D4MEDICAL software)

The lateral pterygoid is thought to function as guidance for the anterior translation of the condylar head upon opening, as well as positioning of the articular disc (to be discussed later in the thesis). It also plays a role in jaw protrusion.

The digastric muscle origin and insertion is shown in Figure 2.5. Again, similar to the lateral pterygoid muscle, it is a relatively delicate muscle and not thought to be a primary muscle of mastication like the temporalis, masseter and medial pterygoid. However, it is unique in that it is a depressor of the mandible in its chewing cycle, that is, it helps to open the jaw whereas other muscles of mastication are elevators that help to close the jaw in its chewing cycle.

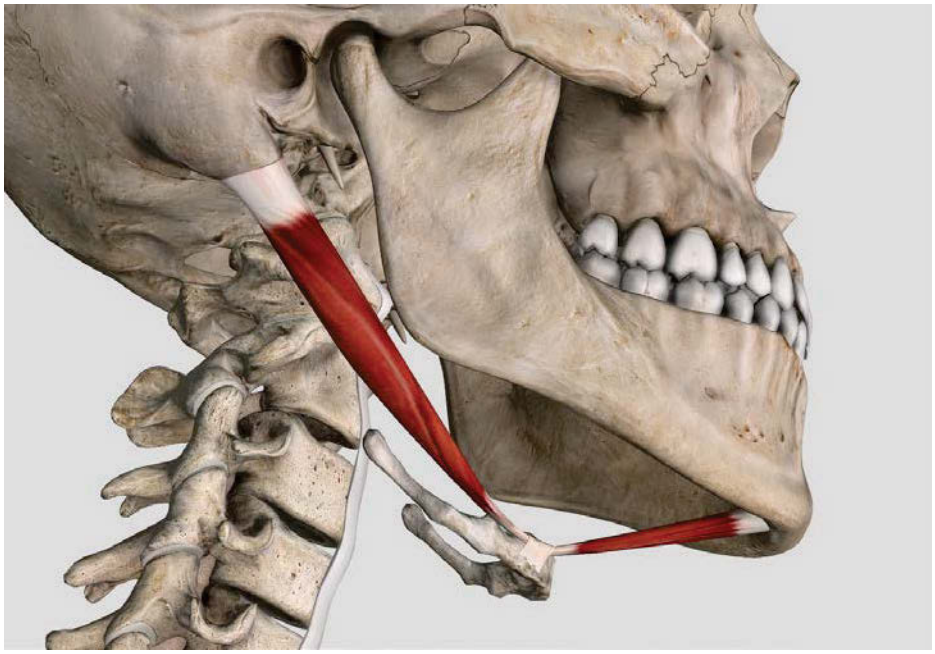

Figure 2.5 Digastric muscle is a depressor of the mandible in the chewing cycle (diagram constructed using 3D4MEDICAL software)

The geniohyoid also plays a small role in jaw depression during mastication with its origin and insertion being shown in Figure 2.6

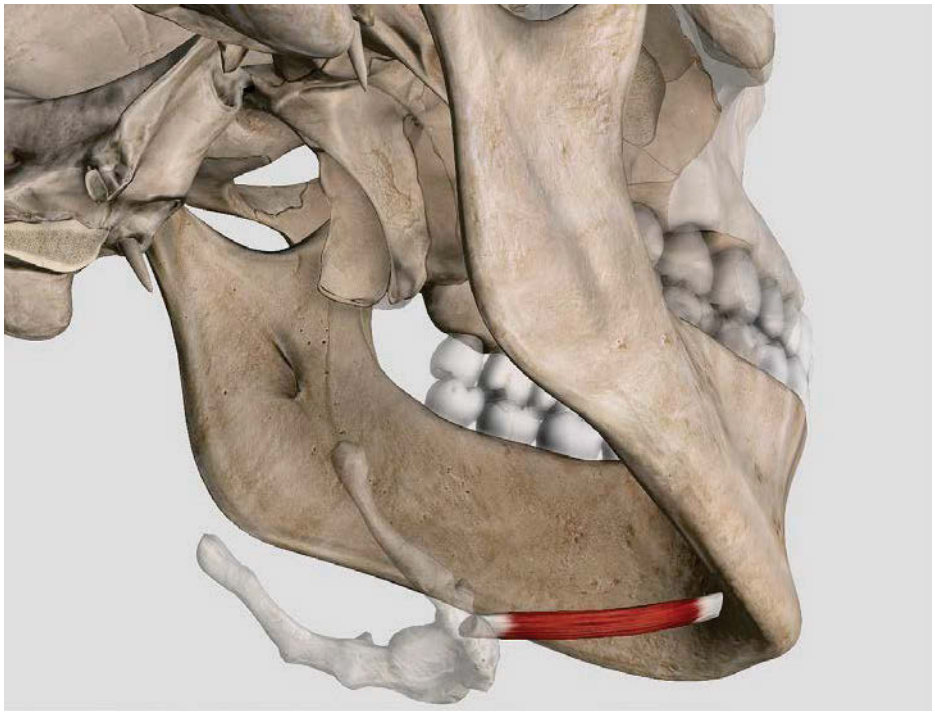

Figure 2.6 Geniohyoid muscle is a depressor of the mandible in the chewing cycle (diagram constructed using 3D4MEDICAL software)

2.1.3 The temporomandibular joint complex

On the posterosuperior aspect of the vertical ramus sits the condylar process that articulates with the glenoid fossa. The glenoid fossa is part of the temporal bone of the skull (Figure 2.7).

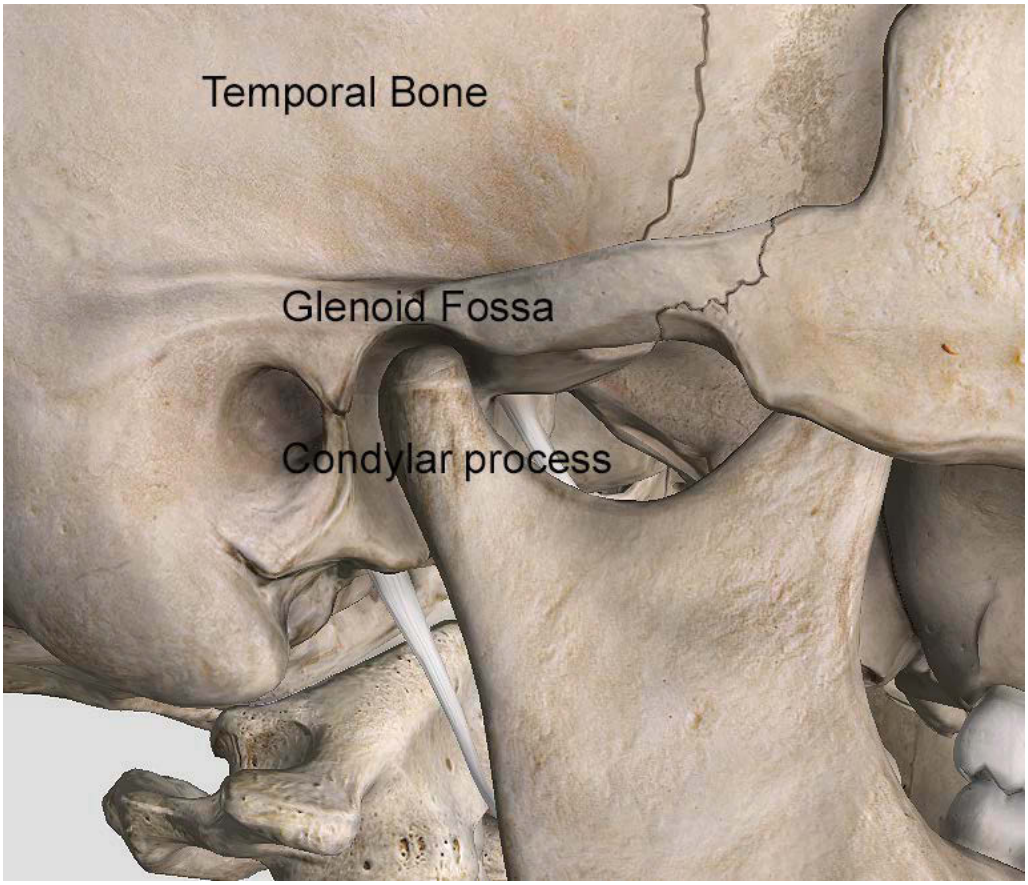

Figure 2.7 Bony components of the temporomandibular joint (diagram constructed using 3D4MEDICAL software)

A cartilaginous articular disc separates the articular surfaces which are covered by articular cartilage. The joint complex is lined by a synovial membrane that produces synovial fluid and the entire complex is contained within the articular capsule. This unique synovial joint is called the temporomandibular joint (TMJ) (Figure 2.8). It is also interesting to note in Figure 2.8 that the lateral pterygoid has two heads, one of which directly inserts into the articular disc. As mentioned, this muscle whilst being a muscle of mastication is thought to be more involved with the coordination of the movement of

the condylar head and articular disc in function in contrast to the temporalis, masseter and medial pterygoid.

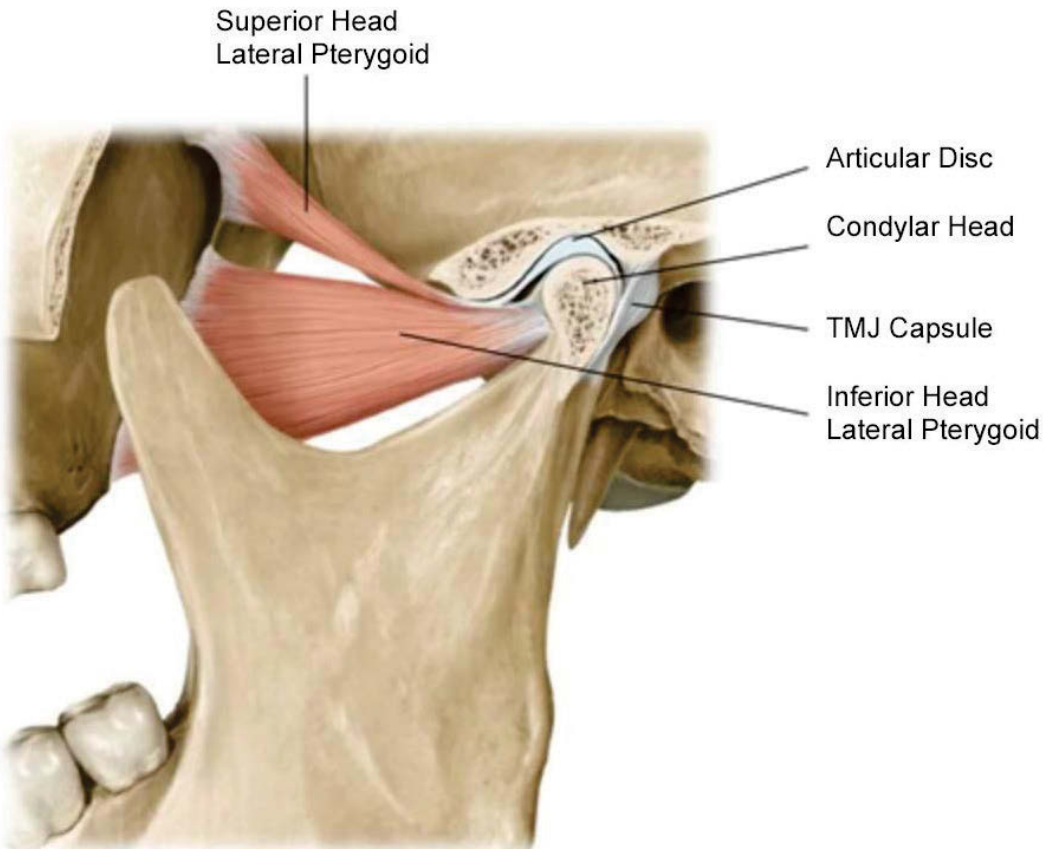

Figure 2.8 Soft tissue component of the temporomandibular joint (Netter Atlas of Human Anatomy)

These closing or clenching muscles are far stronger than the musculature that opens the mandible, such as the lateral pterygoid, digastric and geniohyoid. The medial pterygoid, combined with action from the digastrics, is also responsible for protrusion of the mandible.

Whilst not being scientifically new, it is important to understand the relevant anatomy as it applies to this thesis since all of the anatomical aspects are accounted for in model development which is crucial to this research. Specifically, this thesis concentrates on two major issues regarding the biomechanics of the mandible: (i) reaction forces acting on the condyles during functional mandibular movements; and (ii) muscles insertion topology, which takes into account an area rather than a single point, and the muscle

intensity determination. These two aspects, together with an integrated CT scan and PS approach, significantly contribute to make the proposed model unique compared to previously published models.

2.2 Biomechanics of the mandible

The most frequently used biomechanical analogy for the mandible has been the Class III lever (Figure 2.9) in which the condyle acts as a fulcrum, the masticatory muscles as applied force, and the bite pressure as resistance (Smith, 1978).

For mechanical equilibrium, the Class III lever requires the bite force to be less than the applied force so that the masticatory 'machine' would have a mechanical advantage equal to less than one.

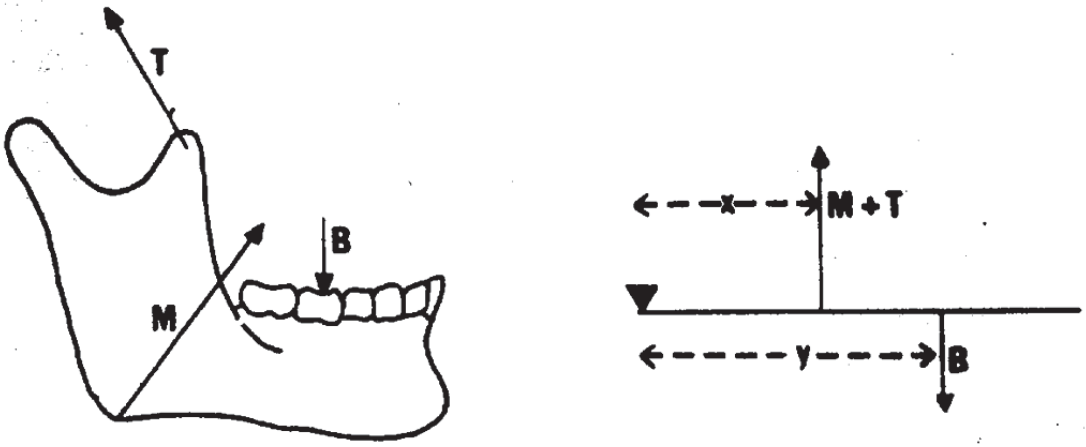

Figure 2.9 Mandible as a Class III lever (Smith, 1978)

Other researchers have argued that the condyle and articular fossa are simply not structured to withstand the large resultant forces required by the model and hence in vivo, the system does not represent a Class III lever (Robinson, 1946; Roberts & Tattersall, 1974). The Class III lever model has also been criticised because it does not consider the centre of mandibular rotation (Grant, 1973; Roberts & Tattersall, 1974).

Roberts and Tattersall (1974) were also concerned with whether there is force at the condyle, rather than with the mechanism of force generation. Roberts (1974) suggested

that since the masseter, temporalis and bite force vectors can form a closed triangle, there is no additional reaction force at the condyle. In their argument, a vector with its length equal to the force magnitude represents each force. Since accurate data on the direction of three forces, and certainly on the magnitude of two muscle forces are completely unknown, a triangle of these forces in equilibrium is entirely hypothetical. Roberts and Tattersall (1974) stated that their analysis rests on the basic assumptions that no significant force is expended at the TMJ during elevation of the mandible and this would be consistent with the architectural structure of the joint system.

Parrington (1934) has suggested that external forces on the mandible during mastication could be analysed by considering the mandible to be a stationary beam. Furthermore, several works (Badoux, 1966; Bock, 1966; Bock & Kummer, 1968; Hylander, 1977) have examined the internal stresses and strains of mastication on the mandible with this approach.

Stern (1974) pointed out that calculating moments about the instantaneous centre of rotation, the centre of the mandibular condyle, the centre of the chin or any other point in space give the same information about the amount of force that is being applied to the dentition, since under conditions of equilibrium, the moments about any point equal zero.

Hylander (1975) suggested that although analysing the mammalian jaws solely in the lateral projection is probably appropriate for incisor or bilateral molar biting, such an analysis is incomplete for unilateral biting. This is because the projected bite point is never actually located in the mid-sagittal plane. Therefore, it is useful to analyse the human mandible in the frontal projection.

According to Hylander (1979), the contralateral mandibular condyle could have a large compressive reaction force acting across it during both unilateral mastication and molar biting, while lower levels of compressive stress act across the ipsilateral condyle during mastication. In some instances during unilateral molar biting, the ipsilateral condyle might even be free of stress, or there may be tensile stress acting across it.

Widening or narrowing of the dental arches may not, as Hylander (1975, 1984) has suggested, change the total magnitude of force at the condyles, but only the proportion borne by each condyle. The nature of muscle positions in the sagittal plane dictates that condylar forces will occur.

2.2.1 Non-lever action hypotheses

As an alternate hypothesis to the Class III lever model of the mandible, various workers have suggested either directly or indirectly that there is little or no reactive force at either mandibular condyle.

Wilson (1920) was one of the first investigators to disagree with the lever action notion of human jaw mechanics, arguing that because the resultant force of the temporalis, masseter and medial pterygoid muscles lie perpendicular to the occlusal plane, there can be no reaction force at the mandibular condyle; and thus it is incorrect to view the human mandible as a lever.

Robinson (1946) was another worker who advanced a non-lever theory of jaw mechanics but he took a slightly different approach than Wilson. According to Robinson, the resultant adductor muscle force passes through the first molar tooth. Assuming that the resultant force has been correctly determined, biting on the first molar in this projection would indeed result in a non-lever action of the mandible, that is, the resultant muscle force would be transmitted directly through the teeth, again leaving the bilateral joint complexes relatively stress-free from bite force.

Frank (1950) also suggested non-lever action of the mandible. His arguments were based on a radiographic analysis of the human mandibular condyle. In each of the radiographs, he noted that the condyle was never in direct contact with the articular eminence. He concluded that the condyle was not functioning as a fulcrum and therefore the mandible could not function as a lever.

Another worker to suggest non-lever action in the human mandible is Gingerich (1971) who stated that during biting, the jaw is functionally a link between the adductor muscle

force and the bite force rather than a lever. Tattersall (1973) also suggested that the mandible does not function as a lever during chewing or biting.

In this thesis, the mandibular biomechanics are modelled on the hypothesis that the mandible acts as a modified Class III lever.

2.3 Biomechanics of mandibular movement

The masticatory system is the functional unit of the body primarily responsible for a variety of functions. The primary functions, however, could be considered to be mastication, speech and swallowing. The system is made up of bones, connective tissue including ligaments and cartilage, muscles, nerves, blood vessels and most uniquely, teeth.

2.3.1 Biomechanics of the Temporomandibular Joint

The TMJ is a compound joint. Its structure and function can be divided into two distinct systems:

1. ***Rotational system:*** The articular disc composed of cartilage is tightly bound to the condyle by discal ligaments. This system constitutes the lower joint space (Figure 2.10). The only physiological movement that can occur between these surfaces is rotation of the disc on the articular surface of the condyle. Therefore, the condyle-disc complex is the joint system responsible for rotational movement in the TMJ.

2. ***Translational system:*** Since the disc is not tightly attached to the articular fossa, free sliding movement can occur between these surfaces in the superior cavity. This movement occurs as a result of the mandible being positioned forward (translation). Translation therefore occurs in the superior joint cavity (Figure 2.11) between the superior surface of the articular disc and the mandibular fossa. Figure 2.11 also illustrates the resultant functional difference between TMJ rotation and translation, as well as illustrates that whilst rotation can occur in isolation, translation cannot and always has a slight degree of associated rotation accompanying it.

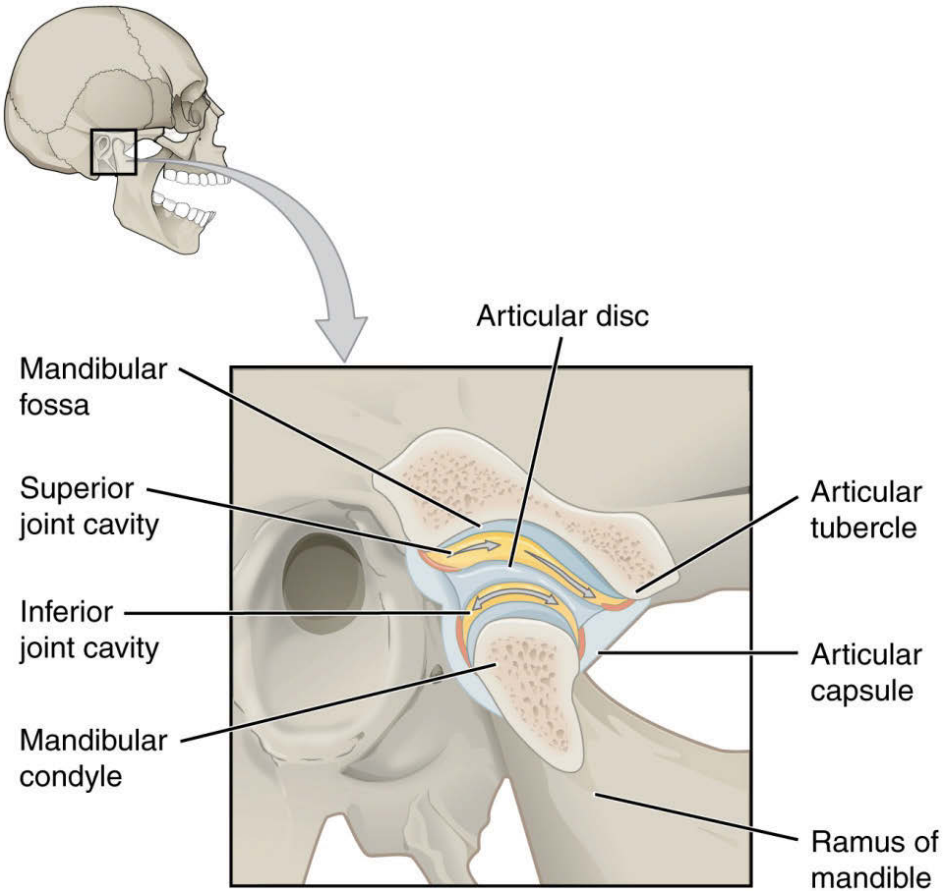

The arrows in each joint space indicate that in the superior joint cavity only translation occurs and in the inferior joint space only rotation occurs.

Figure 2.10 Demonstrates the inferior joint cavity and superior joint cavity (Lumen, Anatomy of Selected Synovial Joints)

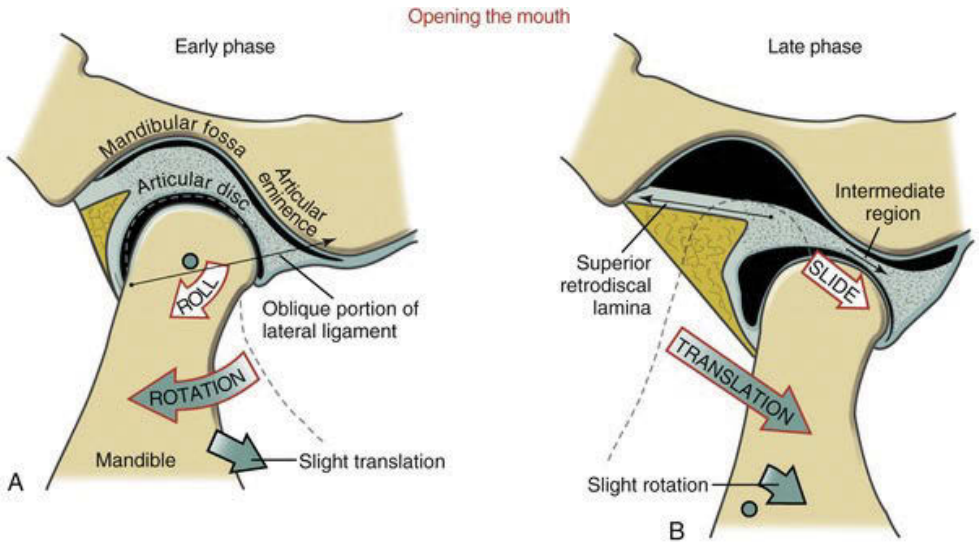

Figure 2.11 Illustrates temporomandibular rotation and translation (Neumann, 2016)

As muscle activity increases, the condyle is forced strongly against the disc and the disc against the fossa, resulting in an increase in interarticular pressure of these joint structures. In the absence of interarticular pressure, the articular surfaces will separate and the joint will technically dislocate. The width of the articular disc space varies with interarticular pressure. When pressure is low, as in the closed rest position, the disc space widens. When pressure is high, as during clenching of the teeth, the disc space narrows.

2.3.2 Mastication biomechanical analysis

Mastication is defined as the act of chewing food. It is a complex function that utilises the muscles, teeth and periodontal supportive structures, as well as lips, cheeks, tongue, palate and salivary glands.

2.3.3 The chewing stroke

Each opening and closing of the mandible represents a chewing stroke. The complete chewing stroke has a movement pattern described as tear shaped (Figure 2.12). It can be divided into an opening phase and a closing phase. The closing movement has been further subdivided into the crushing phase and grinding phase.

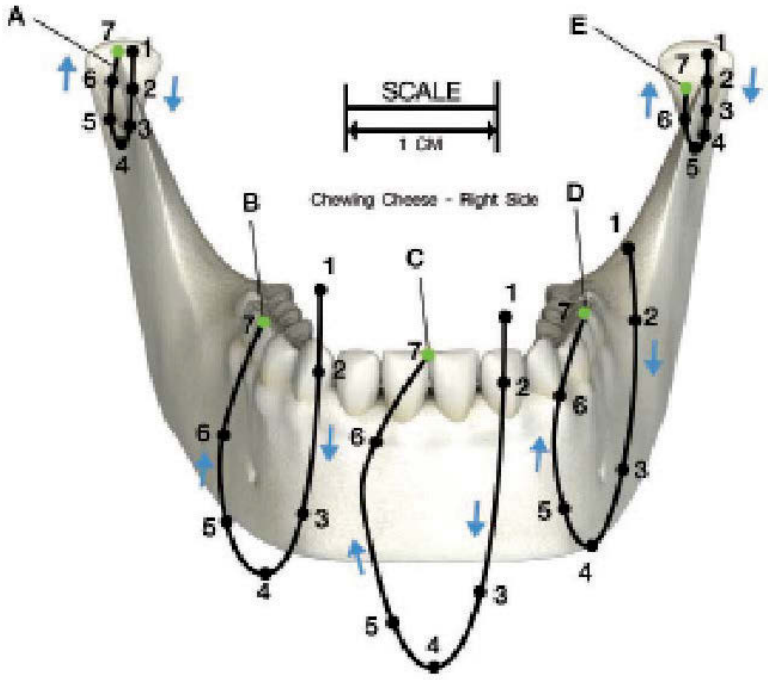

Figure 2.12 The chewing stroke (Croll, 2017)

When the mandible is traced in the frontal plane during a single chewing stroke, the following sequence occurs:

1. In the opening phase, it drops downward to a point where the incisal edges of the teeth are about 16-18mm apart (Hildebrand, 1931). The first phase of closure traps the food between the teeth, called the 'crushing phase'.

2. As the mandible continues to close, the mass of food is trapped between the teeth. This begins the grinding phase of the closure stroke.

3. During the grinding phase, the mandible is guided by the occlusal surfaces of the teeth back to the intercuspal position, which causes cuspal inclines of the teeth to pass across each other, permitting shearing and grinding of the mass of food.

2.3.4 Tooth contacts during mastication

When food is initially introduced into the mouth, few contacts occur. As the mass is broken down, the frequency of tooth contacts increases. In the final stages of mastication just prior to swallowing, contacts occur during every stroke (Adams, 1964). Two types of contact have been identified:

1. ***Gliding,*** which occurs as cuspal inclines pass by each other during the opening and grinding phases of mastication.

2. ***Single,*** which occurs in the maximum intercuspal position (Glickman, 1969).

The average length of time for tooth contact during mastication is 194msec (Suit, 1975). It is apparent that these contacts influence or even dictate the initial opening and final grinding phase of the chewing stroke. During mastication, the quality and quantity of tooth contacts constantly relay information back to the central nervous system regarding the character of the chewing stroke. This feedback mechanism allows for alteration in the chewing stroke, according to the particular food being chewed.

2.3.5 Forces of mastication

The maximum biting force that can be applied to the teeth varies from individual to individual. Brekhus et al. (1941) reported that female maximum biting loads range from 35kg to 44kg whereas male biting loads vary from 53kg to 64kg. The maximum biting force appears to increase with age up to adolescence (Garner et al., 1973; Worner, 1944). It has also been demonstrated that individuals can increase their maximum biting force over time with practice and exercise (Brekhus, 1941; Worner, 1939, 1944).

Howell et al. (1948) reported that the range of maximum force applied to the first molar was 41kg to 90kg whereas the maximum force applied to the central incisors was 13kg to 23kg. During chewing, the greatest amount of force is placed on the first molar region. With tougher foods, chewing occurs predominantly on the first molar and second premolar area (Brudevold, 1951).

2.4 Mandibular movement

Mandibular movement occurs as a complex series of interrelated three-dimensional rotational and translational activities. Mandibular movement is limited by the ligaments and articular surfaces of the TMJ, as well as the morphology and alignment of the teeth.

The masticatory muscles combine in various patterns to execute the different movements of the mandible. It is especially important to realise that one muscle may act synergistically with different muscles at different times. In no one instant does a muscle act as an independent unit; instead the musculature acts in groups of various sizes according to the function being performed.

The most important muscles that affect movements of the mandible can be divided into three major groups:

1. ***Elevators*** – the temporalis, masseter, and medial pterygoid muscles;
2. ***Depressors*** – the digastrics primarily and to lesser degree the lateral pterygoid and hyoid musculature
3. ***Protractors*** – the lateral pterygoid muscles.

2.4.1 Mandibular rest position

It is commonly assumed that the mandible is maintained in a fairly constant position in relation to the maxilla when a person is relaxed, and that the maintenance of this position is the function of a postural control mechanism that produces a low level of activity in the elevator muscles to oppose the effects of gravity (Posselt, 1962).

If the elevator muscles are engaged in actively maintaining the position of the mandible against gravity in the rest position, it should be possible to record EMG activity from them. There have been reports of low levels of activity in the masseter, temporalis, lateral pterygoid and suprahyoid muscles at rest (Carlsoo, 1952, 1958; Kawamura et al., 1967; Lehr et al., 1971; Lund et al., 1970). Furthermore, there are changes in the activity of these muscles when the body is tilted, suggesting that the resting activity may be adjusted according to gravitational effects (Lund et al., 1970).

2.4.2 Opening movement

During simple opening and closing mandibular movements, the mandible rotates around a frontal axis that passes approximately through the centres of two condyles while the axis itself progresses in space (Gibbs et al., 1969).

Moyers (1950), in his EMG analysis of temporomandibular movements, postulated that the opening movement is caused by a combined action of the lateral pterygoid and digastric muscles. If this movement occurs without resistance, the depressors act without any great force.

According to Sicher and Du Brul (1975) and Hylander (1975), in the opening movement of the jaw the condyles rotate against the discs around a transverse axis as they slide downward and forward along the posterior slope of the articular eminence. The movement is effected by an initial activity of the lateral pterygoid, which first fixes the condyles firmly against the posterior slope of the eminence. This is immediately followed by contraction of the digastric muscles and sustained activity of both muscle pairs acting as a force-couple. This motion affects all other muscles anchored to the mandible, but it also has a receding influence on muscles more peripheral to the central

action. Thus, the elevators of the jaw must lengthen (pay-out) to act as mild balancers to ensure smoothness of performance.

2.4.3 Protrusive mandibular movement

A protrusive mandibular movement occurs when the mandible moves forward from the centric occlusion position. Any area of a tooth that contacts an opposing tooth during protrusive movement is considered to be protrusive contact (Figure 2.13).

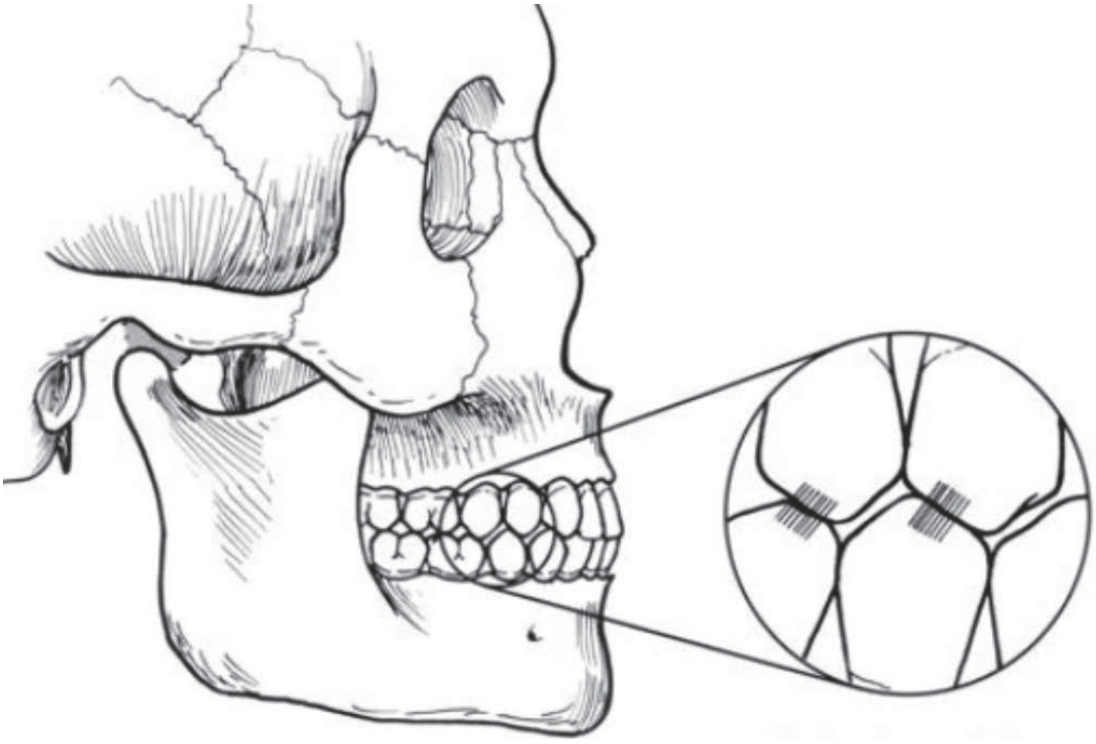

Figure 2.13 Protrusive mandibular movement showing occlusal contacts (Okeson, 1985)

Moyers (1950), Woelfel et al. (1960) and Moller (1966) showed that a forward thrust of the mandible is the result of contraction of the inferior head of the lateral pterygoid muscles and holding action of the masseter and medial pterygoid muscle. The temporalis muscle is not active during this movement, and the depressors are only active to a minor degree.

2.4.4 Laterotrusive mandibular movement

During a lateral mandibular movement, the right and left mandibular posterior teeth move across their opposing teeth in different directions (Figure 2.14).

If the mandible moves laterally to the left (Figure. 2.14), the left mandibular posterior teeth will move laterally across their opposing teeth. However, the right mandibular posterior teeth will move medially across their opposing teeth. The potential contact areas for these teeth are in different locations and are therefore designated by different names.

According to Sicher and Du Brul (1975), in the lateral movement one condyle and disc slide downward, medially and forward along the articular eminence while the other rotates laterally around a vertical axis. The lateral pterygoid muscle, inserted on the inwardly thrust medial pole of the condyle, pulls inward and forward in the horizontal plane. The horizontal fibres of the temporalis muscle inserted at the posterior tip of the coronoid process pull outward and backward. These muscles, operating as a force-couple, contribute to the torque of the rotating condyle necessary to effect chewing on this side.

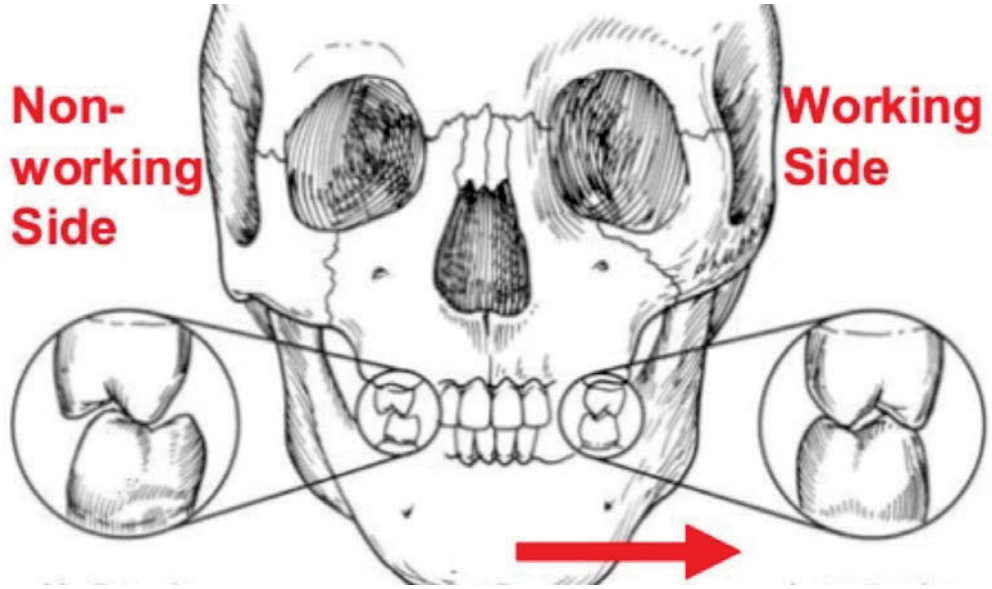

Figure 2.14 Left laterotrusive movement (Okeson, 1985)

2.4.5 Retrusive mandibular movement

A retrusive movement occurs when the mandible shifts posteriorly from a centric occlusion. During a retrusive movement, the mandibular buccal cusps move distally across the occlusal surface of their opposing maxillary teeth (Figure 2.15). Retrusive contacts occur on the reverse inclines of the protrusive contacts since the movement is exactly opposite.

In the retracting movement, the middle and posterior fibres of the temporalis muscle combine forces with the depressors, while the remaining elevators exhibit varying amounts of activity (Woelfel et al., 1960).

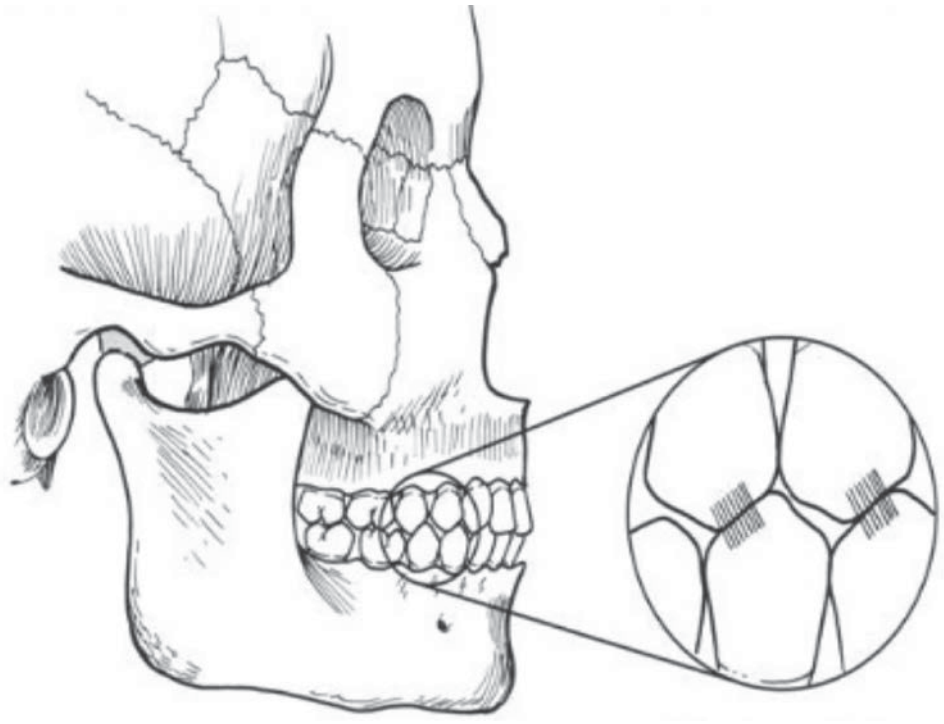

Figure 2.15 Retrusive mandibular movement showing occlusal contacts (Okeson, 1985)

2.4.6 Closing movement

The elevators of the mandible execute the closing movement, which returns the jaw to the rest or occlusal position. If the mouth is opened to its maximal extent, the timing of the activation and relaxation of the different parts of these muscles is important for proper closure.

2.5 Biomechanics and anatomy of the edentulous mandible

So far in Chapter 2 we have looked at the biomechanics of the dentate maxilla, mandible and TMJ complex. The edentulous complex, however, displays significantly different anatomy and biomechanics, which we will cover in the following sections.

2.5.1 Anatomy of the edentulous mandible

The anatomy of the edentulous mandible holds true to the description given in Section 2.1, however, differs in three significant areas.

2.5.1.1 Lack of teeth

By definition, the edentulous mandible lacks all teeth. This in itself is significant as we have discussed in its implication on biomechanics and function but also has flow on affects to such areas as lower facial height. Whilst the absolute average decrease in lower facial height between the dentate versus the edentulous individual is difficult to determine (due to different resting points between individuals), it is agreed that significant decrease does occur with the loss of teeth (Morais, 2015).

2.5.1.2 Loss of alveolar bone

With the loss of teeth, the investing alveolar bone is often resected at the time of tooth removal to help facilitate the extraction or once the tooth is gone, undergoes atrophy which occurs predictably due to the fundamental principles of bone physiology. That is the adaptation of bone mass and bone structure to the levels and frequencies of strain. The reduction of the alveolar ridge dimensions after tooth extraction is a natural consequence of tooth loss and an alteration in the level and frequency of strain which ultimately results in atrophy (Hansson, 2012). The loss of this alveolar bone leads to a mandible that consists only of basal bone. The diminished volume of bone left produces a reduction in the strength of the mandible.

2.5.1.3 Alteration in mandibular blood supply

The blood supply of the dentate mandible comes from the endosteal supply of the inferior alveolar artery as illustrated in Figure 2.16.

The controversy, however, surrounds what occurs in the edentulous atrophic mandible. Bradley (1975) used angiography to document that the inferior alveolar artery provided inconsistent supply to the atrophic mandible. As such, he felt that the primary blood supply in the atrophic mandible arises from the periosteum.

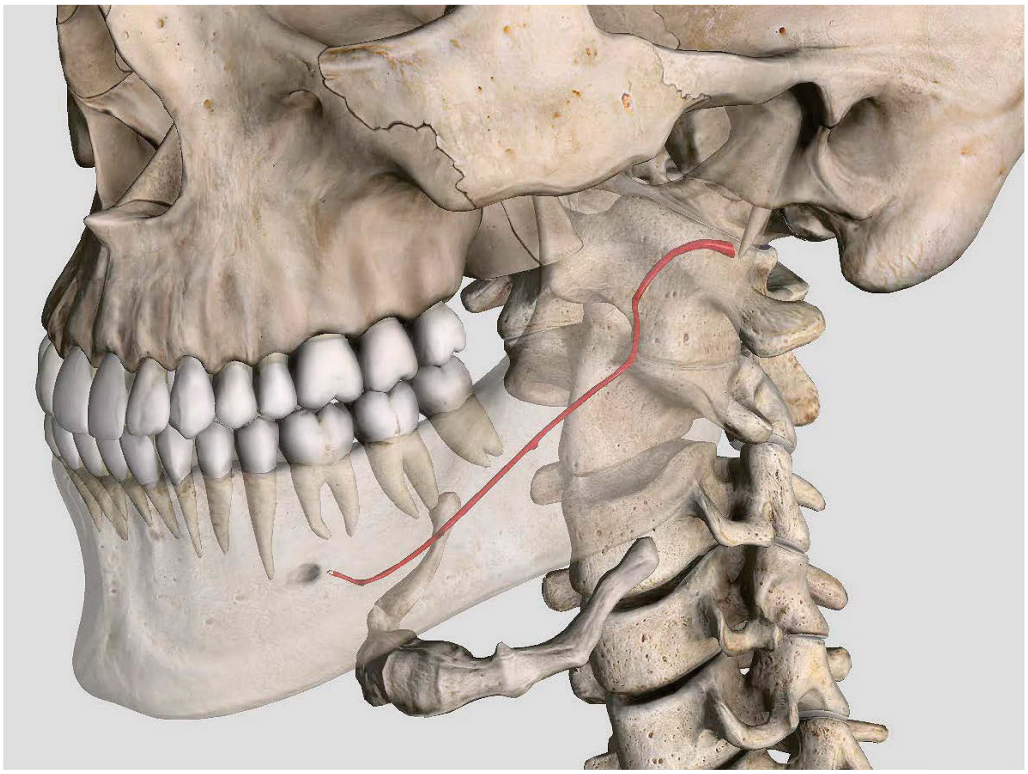

Figure 2.16 Inferior alveolar artery which provides the dentate mandible with blood supply (diagram constructed using 3D4MEDICAL software)

This observation has produced two issues regarding fixation of a fractured edentulous mandible. Firstly, it is agreed that the periosteal blood is not as consistent and plentiful as the endosteal blood supply of the dentate mandible. This can have a profound effect on healing post-fracture and places even more importance on the fixation system and its efficacy. Secondly, it has raised debate over what method of surgical access is best for the fractured edentulous mandible. In the past, some have advocated a supraperiosteal approach in order to preserve the periosteal blood supply as much as possible, but many authors in recent years have advocated open reduction of atrophic mandible fractures as superior to closed techniques, because open reduction provides direct visualisation and semi rigid fixation provides the stability required for fracture healing. In addition, these

same studies have shown that a supraperiosteal dissection provides no significant advantage in healing compared with subperiosteal dissection. However, limitation of subperiosteal dissection is recommended. This has a direct bearing on the design of the plate to be used in that it must be structurally sufficient to perform its role of fracture fixation and immobilisation but not overly engineered and so bulky that unnecessary dissection is required to allow the plate to be fitted. As such, much of the research in this thesis reviews the edentulous model and determines the size, material and configuration of plating system for optimal results.

2.5.2 Edentulous bite force

It has been well recognised that without teeth the bite force that an individual can produce is significantly reduced. Howell (1948) and Brekhus (1941) showed that bite force at the first molar site in dentate patients varies from 35kg to 90kg. In comparison, Tripathi (2014) demonstrated that an edentulous individual using dentures produces a mean force of only 4.43kg at the first molar site.

The reasons behind this significant difference are multi factorial but are primarily the result of the following factors.

1. The periodontal surface area available for biting in a fully dentate individual has a mean value of 75cm^2 (Hujoel, 1994). Whereas the mucosal surface area used to support dentures is much less with the average available area to support a mandibular denture being 14cm^2 and 24cm^2 in the maxilla (Zarb, 2012).

2. The tissue consistency of teeth and supporting periodontal ligaments is designed to resist greater forces than the delicate oral mucosa. This is well demonstrated by Jainkittivong (2010) who showed that 45% of denture wearers have oral mucosal lesions of which traumatic ulcers accounted for the majority.

2.5.3 Edentulous chewing stroke

As covered in this thesis, the chewing stroke of a dentate individual is a combination of joint rotation and translation that produces an elliptical shaped cycle at the dentition. In comparison, the edentulous individual wearing a full denture shows an overall longer

period of mastication, a greater number of chewing cycles per period of mastication and a tendency to adopt more rotational movement than translation as this better stabilises the dentures during function (Jemt, 1981; Slagter et al., 1993, 1992b; Veyrune et al., 2007; Mishellany-Dutour et al., 2008).

CHAPTER 3:
FINITE ELEMENT MODEL OF THE HUMAN MANDIBLE

3.1 What is a finite element model?

A finite element model (FEM) is a numerical procedure for analysing structures and continua where the analysis would be too complicated to be solved satisfactorily by classical analytical methods.

Finite element analysis (FEA) solves a complex problem by redefining it as the summation of solutions of a series of interrelated simpler problems. This requires subdivision of a complex geometry like the human mandible into a suitable set of smaller 'elements' of 'finite' dimensions, which form the 'mesh' model of the investigated structure when combined (Choi, 2005).

For a FEM to be able to predict stresses and strain in bone under certain loading conditions, it needs to be properly and accurately constructed. Its construction, particularly involving the complexities of the mandible, must take into account its anatomical and biomechanical nuances. To this end, we have now established a good understanding of the anatomy involved and its relation to function in Chapters 1 and 2. We have also discussed the surgical aspects of fracture care in general and specifically as they relate to the mandible. Both of these points are very important to appreciate since this thesis not only looks at the biomechanics of a mandibular model but uniquely relates it directly back to the surgical and clinical scenario.

Once a comprehensive and accurate model is constructed it can be applied to quantify the stresses around; in this case, fixation systems. In order for it to be accurate, the model must account for the overall mandible structure as flexible and therefore calculate its stiffness across several iterations. For this reason, modelling the internal structure of the mandible with different bone structures and geometries becomes a necessary requirement for a correct biomechanical simulation of the mandible's behaviour. In creating a model of a human mandible that can be used in a realistic simulation using FEM, the shape of the bone needs to be reverse-engineered from a living subject or a

cadaver, as we have done by using PS CT derived data. Only in this way can the intricate and asymmetrical morphology of the mandibular bone can be truly modelled in three dimensions.

3.2 Complexity of exterior shape and interior structure of the mandible

Modelling the human bone has been subject of extensive research in dentistry and in particular in maxillofacial surgery. The morphology of the human bone presents different complexities in comparison to other parts of the human body.

Although the external morphology of the mandible (cortical bone component) can be classified into several configurations such as a U-configuration (undercut), a P-configuration (parallel) or C-configuration (convex), depending on the shape of the alveolar ridge, it becomes a new challenge to model the internal structure, that is, the cancellous bone component of the mandible (Nickening, 2015).

A computed tomographic (CT) scan however is one option for inspecting the internal bone structure in vivo. Other modalities available are plain radiographs such as an Orthopantomograph^{TM} or magnetic resonance image (MRI). The advantage of a CT scan over plain radiographs is that with sagittal and coronal reconstructions, CT scans can depict all the portions of the mandible in three planes. Its advantage clinically over plain radiology and MRI is that CT scanning is the best method for detecting subtle or questionable fractures (Soule, 2015). CT scanning can also better elucidate hard-to-see fractures through the thin cortex of a pathologic lesion. From the perspective of constructing a PS FEM, a CT scan was chosen to provide the data because it had the best combination of clinical application to investigate fractures, obtain a full map of the mandibular topology, provide the ability to use a three-dimensional scan and segment raw images from the scanned volume to reverse-engineer the shape of the internal components of the bone.

At a microscopic level, bone is composed of a matrix of cylinders (osteons) forming a Haversian system. Nomura (2003) described these osteons to be oriented universally parallel to the anteroposterior axis of the mandible except as they approached the

condylar and coronoid process they branched into other axes. The cells of bone, osteocytes, consist of layers laminated between the osteons. The osteocytes produce calcium phosphate from which osteons are composed.

On a larger scale, bone occurs in two forms. When less densely packed, the macroscopic structure can be considered cancellous bone in comparison to cortical bone which is tightly packed. The most obvious difference between these two types of bone is their relative densities or volume fractions of solids. Bone with a volume fraction of solids less than 70% is classified as cancellous or trabecular; bone with a volume fraction of solids greater than 70% is classified as compact or cortical (Choi, 2013).

Regarding the nature of cancellous (trabecular) bone, the mandibular cancellous pattern can vary from being sparse to mixed dense plus sparse, or dense. Furthermore, the transition from cancellous to intercancellous spaces and the size and number of these spaces are highly subject-specific (Jonasson, 2014). The distribution of trabeculae, which has been found to affect the strength of the bone, is highly variable and is dependent on the sex of the individual (Figure 3.1), age, nutrition, lifestyle and the presence of disease, such as osteoporosis. In addition to variations between individuals, there is a variation within one individual over time based on their physiologic health at any specific point.

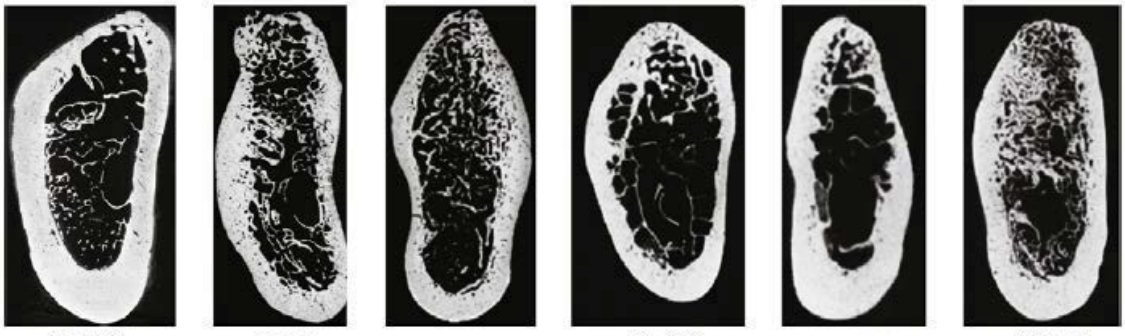

For each bone sample, the bone volume fracture is reported, together with the sex (F: female; M: male) and the age of the patients (Marcian, 2014).

Figure 3.1 Morphologically different bone samples acquired from female and male mandibles

Models of cancellous bone have been used to investigate the interface between implantable devices and the bone tissue. In a study that used micro-CT to model the architecture of the trabeculae around a series of osseointegrated implants, Marcian (2014) found that the strain distribution is primarily dependent on the shape of the bone and morphology of the cancellous bone. Whilst these studies are of value, due to their limited scale and high subject-specificity, they are not suitable to accurately predict overall biomechanical behaviour to the extent required for this thesis.

3.3 Influence of the morphological complexity on the modelling

Whether trabeculae are modelled as separate entities (Marcian 2014) or part of a larger more encompassing model, their topology is always complex and therefore affects the performance and capacity of the simulation. Differing from structural studies in engineering simulations, the geometry of the bone in this thesis is reversed engineered from natural mandibular shapes through a high number of local mathematical approximations of the physical surfaces. Small details in the bone geometry require a higher number of mathematical data approximating its morphology, resulting in a simplified mesh of finite elements used for the FEM. As a consequence, over the last 30 years, modelling biological structures using FEA has progressed along with the increased computing power of personal computers. To balance the complexity of the topological structures, FEA researchers were forced to use a number of approximations in the pre-processing stage.

In this work regarding the construction of a FEM, the aim is to construct a functional model with PS properties from CT data and loading conditions while accurately reflecting the internal morphology and composition of the mandible, as well as to compare the PS model alongside a highly detailed GEN model derived from the previous works of Ben-Nissan and Choi. In doing so, approximations were eliminated as much as possible, hence, creating a model for analysis that related back with validity to the investigation of our clinical scenario, the assessment of mandibular fracture management.

Analyses in this thesis were carried out, firstly for a natural intact mandible, followed by an analysis of a model consisting of a mandibular fracture with stress calculations after various systems of repair.

3.4 Cortical bone property variations

Most experimental tests conducted to measure the elastic modulus in cortical bone have used relatively long sections of machined femoral bone. Early research by Reilly and Burstein (1974) estimated that studies measured Young's modulus for dry cortical bone in the range of 6MPa to 28MPa. Values obtained from a variety of researchers are summarised in Table 3.1.

Table 3.1 Summary of various Young's modulus values for dry cortical bone

Author	Method	GPa
Reilly, 1974	Tension	11.4-19.3
	Compression	14.7-19.7
Reilly and Burnstein, 1975	Tension	15.6-18.3
McCalden, 1993	Tension	9-21
Kaneko, 2003	Tension	19.3-26.3
	Compression	20.4-26.4
Currey, 2004	Tension	16.7
Bayraktar, 2004	Tension	11-24

Although no significant differences between tensile and compressive experimental setups have been reported for E (Reilly et al., 1974; Kaneko et al., 2003), it has been shown that cortical bone is stronger in compression then in tension, as outlined in Table 3.2.

Table 3.2 Mechanical properties measured for femoral cortical bone by different studies

Author	Method	Yield Stess MPa	UTS MPa
Reilly and Burnstein, 1975	Tension		129
	Compression		193
Kaneko, 2003	Tension	84	96
	Compression	153	162

Currey (2004) found that cortical bone with higher Young's modulus also has higher tensile yield stress, while its yield strain did not vary with Young's modulus. These results indicate how bone yields at a particular strain rather than a particular stress.

Another cause of variation in the measured mechanical properties of the cortical bone is the age and sex of the subject, as described by Carter and Spengler (1978), Keaveny and Hayes (1993), Burnstein and others (1976), and McCalden and others. (1993). Results relative to these last studies are reported in Table 3.3.

Table 3.3 Relation between mechanical properties of the cortical bone and subjects showing comparison of different studies

Author	Subject Age	E GPA	UTS MPA	Ultimate Strain %
McCalden 1993	45		107	2.8
	85		82	1.5
Burnstein 1976	40-49	17.7	139	3.0
	80-89	15.6	120	2.4

3.5 Cancellous bone property variations

The mechanical properties of cancellous bone are highly dependent on the direction of loading, showing significant differences when the applied force is aligned with the osteonal axis. This behaviour has been accurately observed by Cody et al. (1996) whose results for elastic modulus and ultimate tensile stress are summarised in Table 3.4.

It must be noted that the stiffness of the cancellous bone can be measured at a microscopic scale or 'tissue level' by using single trabeculae as specimens or at a larger scale where a portion of bone containing several trabeculae is tested (Brown et al., 2010). In the first case nanoindentation and acoustic microscopy methods should be used to assess bone elasticity (Jirousek, 2012).

In a two-dimensional FEM of the mandible focused on bone-implant interfaces, elaborated by Guan et al. (2009), it was shown how influential the assumptions made on the thickness of the cortical bone, and the cortical and cancellous bone ratios are.

Table 3.4 Cody's results (1996) for range of femoral cancellous bone mechanical properties

Location	Property	Orientation	Mean	SD
Neck	E	A-P	193	159
	E	M-L	176	126
	E	I-S	194	153
	UTS	A-P	4.29	3.7
	UTS	M-L	3.72	2.36
	UTS	I-S	5.81	4.5
Head	E	A-P	202	211
	E	M-L	161	135
	E	I-S	210	162
	UTS	A-P	4.14	3.73
	UTS	M-L	3.59	3.42
	UTS	I-S	6.47	5.37

Values are in MPa; AP: anteroposterior direction; ML: medial-lateral direction; IS: inferior-superior direction.

Using average standard values for Young's modulus of two bone types (respectively *E cortical* = 13GPa and *E cancellous* = 7GPa), Guan (2009) found that as the thickness used to model the cortical bone decreased, the ability of the cortical bone to support the load also decreased and therefore the magnitude of the stresses in the cancellous bone increased. From the viewpoint of engineering design, this was obvious and expected. This also has notable ramifications where the management of fractures in the edentulous and/or atrophic mandible is concerned. Whilst muscle forces and bite force through such bone may be decreased, the bone structure to resist such force is also diminished. This behaviour is explained in Figure 3.2 which summarises the findings of Guan's research work.

The contribution from Guan's research supports the attention given to the approximations made in this work to segment and separate the cortical from the trabecular bone (Figure 3.2). Hence, it is clear that to accurately represent the cortical and cancellous bone components of the mandible (two-bone model) in a FEM will produce a realistic model that will be advanced over currently available models. Such an

approach is one of several unique features to this research. The modelling approach is visually explained in Figure 3.2. The plots in Figure 3.2 report the equivalent von Mises stress variation on the bone interface respectively at the implant proximal and longitudinal surfaces. Each curve is associated to a specific set of load application. Distances in longitudinal (VV) and radial direction (HH) from the implant head are reported in the horizontal axis.

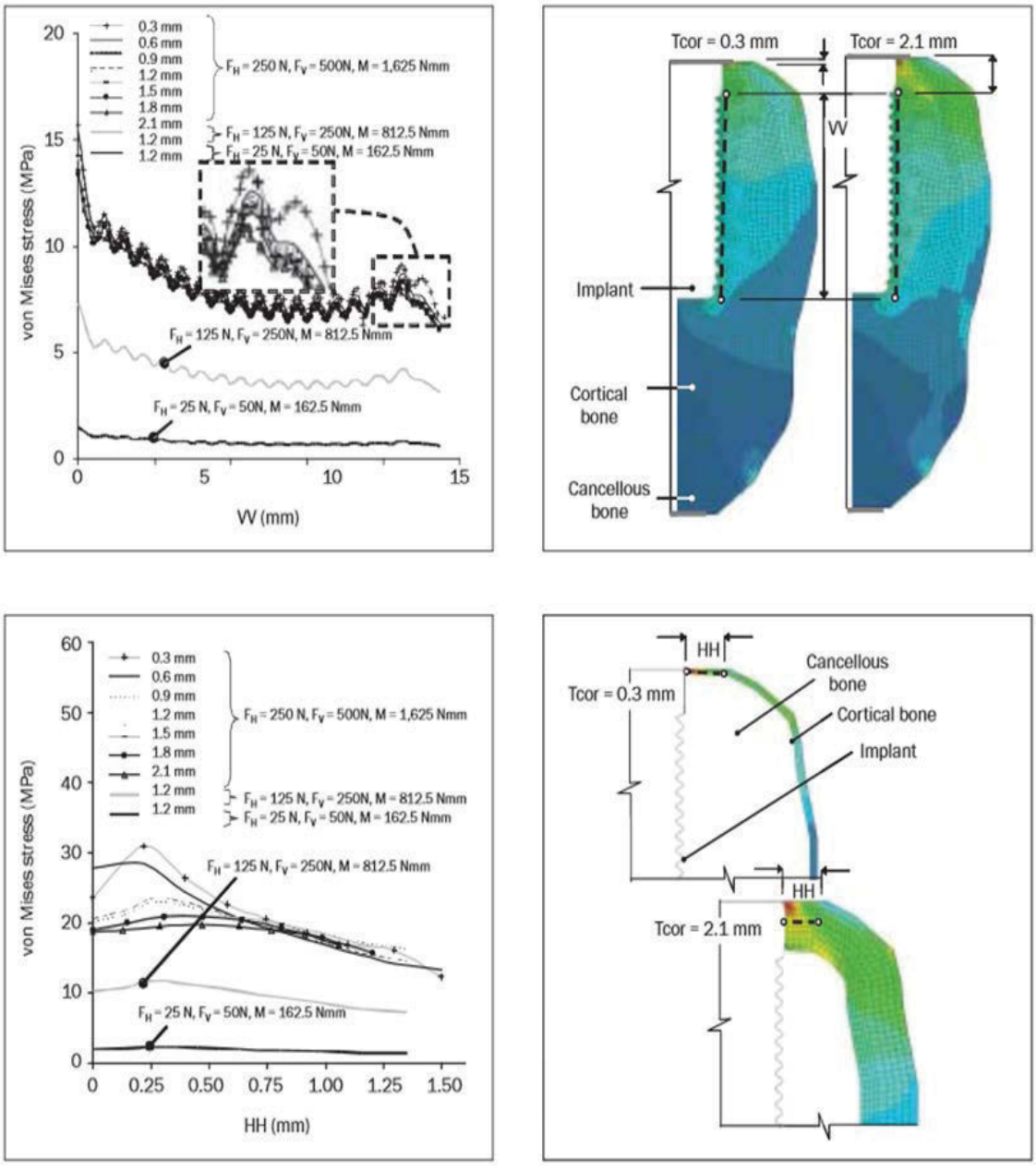

Figure 3.2 Stress profiles along bone-implant interface with varying thickness assigned to the cortical bone (Guan et al., 2009)

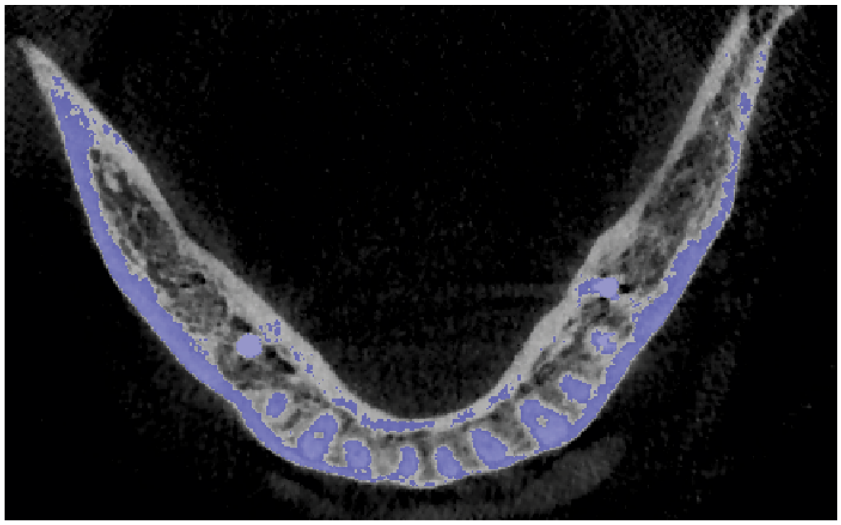

Figure 3.3 Example of segmentation using a 'threshold' function (modified from Taraschi, 2016)

Figure 3.3 shows how separation between the cortical and cancellous bone is detectable by plotting variation in CT numbers that correlate to density. In this case example CT numbers above a certain threshold value are coloured in violet.

3.6 Interface between bone types

Through an accurate segmentation of the mandibular bone from CT scan data, denser areas (cortical bone) can be identified separately to less dense regions that contain primarily trabecular bone but also fatty marrow, haemopoetic marrow, blood vessels, and nerves (Figure 3.4). However, unavoidable inaccuracies do occur due to estimations of segmentation. This occurs due to the limited power of segmentation editing software or the variable resolution of CT scanners in identifying the boundary between cortical and cancellous bone. As can be seen in Figure 3.3, whilst the corticocancellous segmentation has occurred, it is not complete with areas of segmentation being unidentified by the software. Additional inaccuracies can come from artefacts produced in a scan due to metallic restorations (Figure 3.5), dental implants or previously placed Ti fixation plates, patient movement during the scan or the preferential deflection of low energy tissues (Lewis et al., 2013). In addition, it has been reported that artefacts can be created in the region to be segmented due to x-ray beam 'hardening effects' (Schuller et al., 2015).

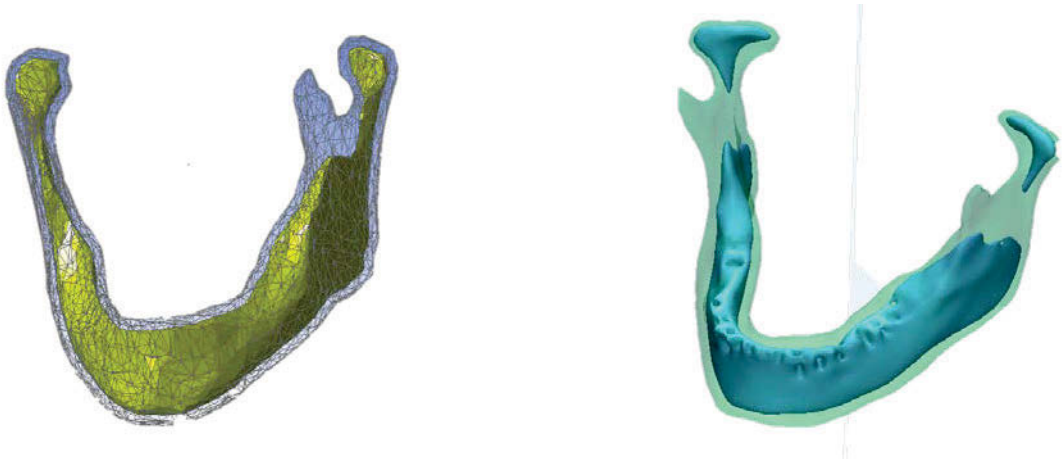

Figure 3.4 Examples of cortical-cancellous bone model approximation prepared in Amira and visualised in ANSYS software (modified from Taraschi, 2016)

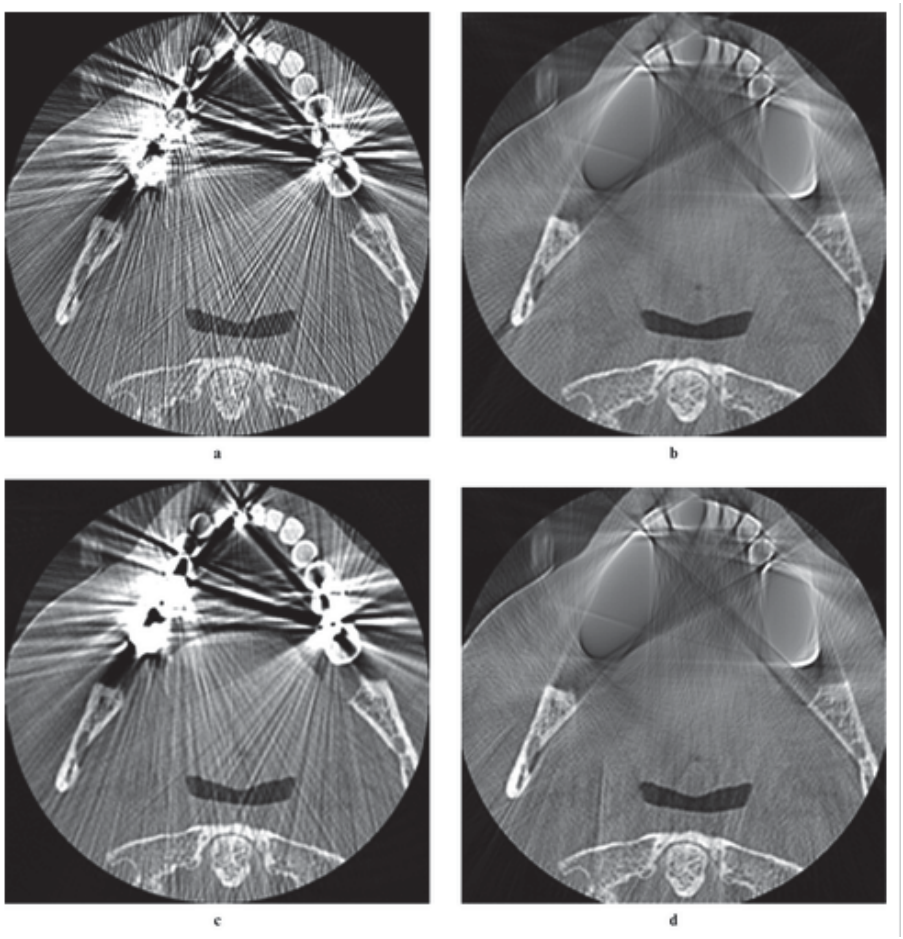

Artefact reduction methods do exist (Tohnak, 2011), however, such artefact reduction would render the cortical and cancellous segmentation difficult, as illustrated above and adversely affect it's transposition to a FEM.

Figure 3.5 Significant artefact from metallic restorations in a mandibular CT scan (Tohnak, 2011)

The majority of mandibular models found in literature to date reverse engineer the human jaw using solid models: one for the cortical bone and another one for the trabecular bone based on femoral bone modelling proposed in the 1980s (Ben-Nissan, 1987: Kitagawa, 2005; Li, 2009; Barao, 2009; Bujitar, 2010; Qian, 2009; Ding, 2009; Okumura, 2010).

3.7 Choice of material properties

Mechanical properties were obtained from previously published values and all materials were assumed to be uniform, linear and isotropic to facilitate a comparison with earlier models (Ben-Nissan, 1987; Choi et al., 2005, 2014). Additional information on the material properties used will be given in later chapters where specific FEMs will be analysed and discussed, however, Table 3.5 shows a summary of the values used for cortical and cancellous bone.

Table 3.5 Summary of material property values used in this thesis for cortical and cancellous bone

Bone	Young's modulus (GPa)	Poisson's ratio
Cortical	17.2	0.30
Cancellous	1.29	0.30

3.8 Biomechanical considerations

Muscle forces have been assigned according to Ben-Nissan's study (1987) on a biomechanically correct load set for clenching and opening movements of the mandible. In contrast to previously published models, in this work all forces and loads were applied and distributed to surfaces corresponding to the anatomically correct muscle attachment areas. In previous models, muscle forces were specified vectors with a specific origin and insertion rather than area.

Where additional forces have been applied, they will be discussed in their relevant chapter according to the specific biomechanical scenario that the FEM of the mandible is being used to analyse.

In general, for the whole duration of the simulations, the mandible was considered in static equilibrium conditions using the reference system described in Table 3.6.

Table 3.6 Reference system used for the FEM

Axis	Description
X	Line joining the geometrical centres on the mandibular condyles
Y	Line perpendicular to the X axis and parallel to the occlusal plane
Z	Line perpendicular to the origins of the X and Y axis

CHAPTER 4:
FIRST OUTPUT – MODELLING OF AN AVERAGE EDENTULOUS HUMAN MANDIBLE

4.1 Introduction

The evolution of this model began prior to this research, dating back to its infancy when first developed by Professor Besim Ben-Nissan in 1982. The evolution undertaken by Ben-Nissan utilised a dry mandible that was cross-sectioned and digitised average to create the model and apply the properties and biomechanical forces under functional conditions. Early models used NASTRAN, PATRAN and STRAND FEA packages at different stages.

This model allowed easy manipulation and fracture modelling. However, to follow with the aim of this thesis, the model evolved further through using computed tomography scans to produce **patient specific (PS) mandibular models** with biomechanical data from Ben-Nissan's first work added and the results compared.

The final stage of this thesis was carried out by using different fracture fixation systems, looking at biodegradable and non-biodegradable materials, and comparing different material thicknesses at different lengths and configurations.

4.2 The first model

This phase was initiated to model an edentulous human mandible by using high order linear and three-dimensional solid elements. Finally, the model was utilised to analyse the functional distortion and stresses acting on the mandible during normal opening, protrusion and clenching, as well as with and without the insertion of a mandibular fracture.

The analysis was carried out in seven stages:

1. Modelling of the mandible using digitiser and computer-aided design software.

2. The development of CAD/Finite Element Analysis (FEA) modelling sequence.

3. Rationalisation of input data, incorporating mechanical properties and muscle forces acting on the mandible during opening, protrusion and clenching.

4. The muscle forces required to balance the external system were found and from these, joint forces were calculated.

5. FEA using the STRAND7 (G+D Computing Australia Pty Ltd) program.

6. Design, modelling and analysis of a mandibular fracture and its repair with a range of fracture fixation systems. Various modifications in the position and properties were implemented and stress strain behaviour analysed.

7. Analysis of distortion and stress acting on the mandible and plates during opening, protrusion and clenching using the STRAND7 FEA program.

4.3 Equipment used

4.3.1 STRAND7

STRAND7 is a general-purpose FEA system developed by G+D Computing Australia Pty Ltd. The system consists of pre-processing, post-processing and solution processing functionality. It provides a single consistent environment for the creation and analysis of FEMs and the extraction of results.

The non-linear solvers support geometric, material (including plasticity and large strain) and boundary non-linearity (that is, contact). This non-linearity can also be included as initial conditions in the natural frequency and buckling solvers.

The pre-processing environment includes a powerful set of tools for manipulating the geometry and elements directly, and simplifying the modelling of complex engineering structures. All element types can be fully rendered to aid in the visualisation of the model. The post-processing environment has been designed to allow easy extraction of the results, graphically on the screen in spreadsheet format and in printed report form.

4.3.2 Digitiser

Digitisation is a process by which graphic material in the form of designs, tracings, layouts and patterns can be converted into sets of x-y coordinates. Summagraphic I.D. (Logic Group, Texas, USA), with a built-in microprocessor providing the computing capability, was used for digitising the cross-sections of the mandible.

4.3.3 Earlier models

Earlier models included a dry human mandible to define the geometry of the model. The mandible was cast in a polyester resin, including a guide pin, which was positioned along the alveolar ridge. The mandible was then cross-sectioned vertically into 28 sections using an Isomet low speed diamond blade cutter to minimise the loss of bone (Figures 4.1 & 4.2). The cortical bone outlines, cancellous bone layers and reference points were traced onto drawing paper for one half of the symmetric structure. These outlines were then digitised by using the Summagraphic ID digitiser and specifically developed data producing sequence.

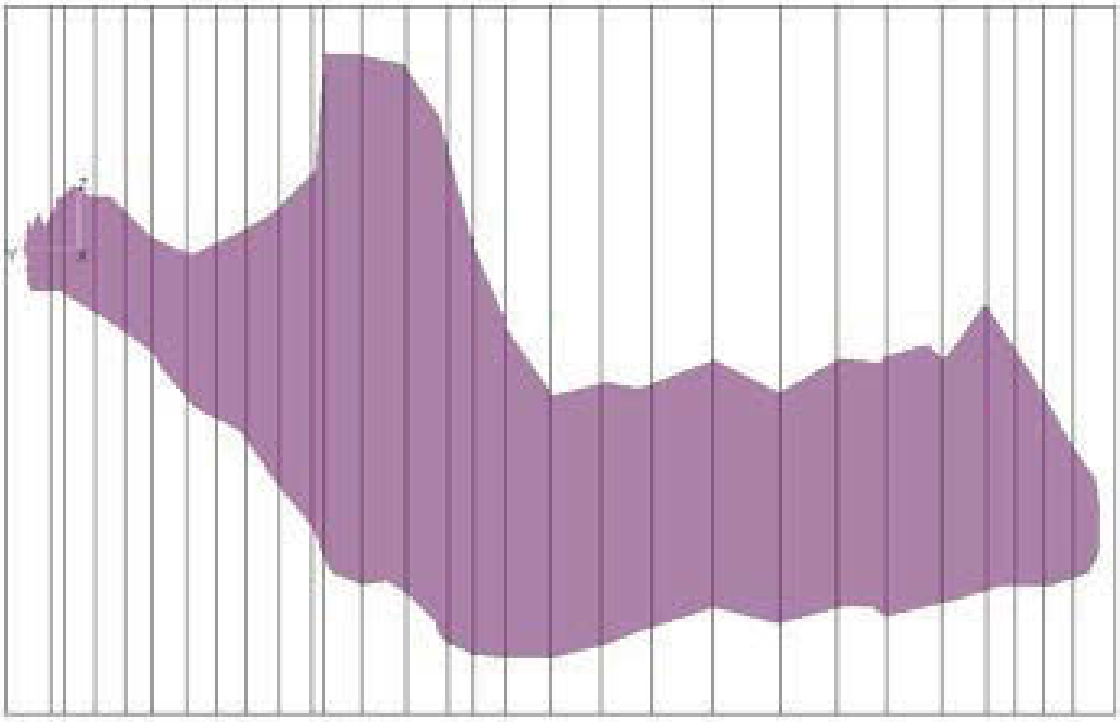

Figure 4.1 A typical cross-section of the human mandible showing 28 vertical sections (modified from Ben-Nissan et al., 1987)

Each cross-section of the bone was divided into five sections with the outer four representing cortical bone and the inner one representing cancellous bone (Figure 4.2).

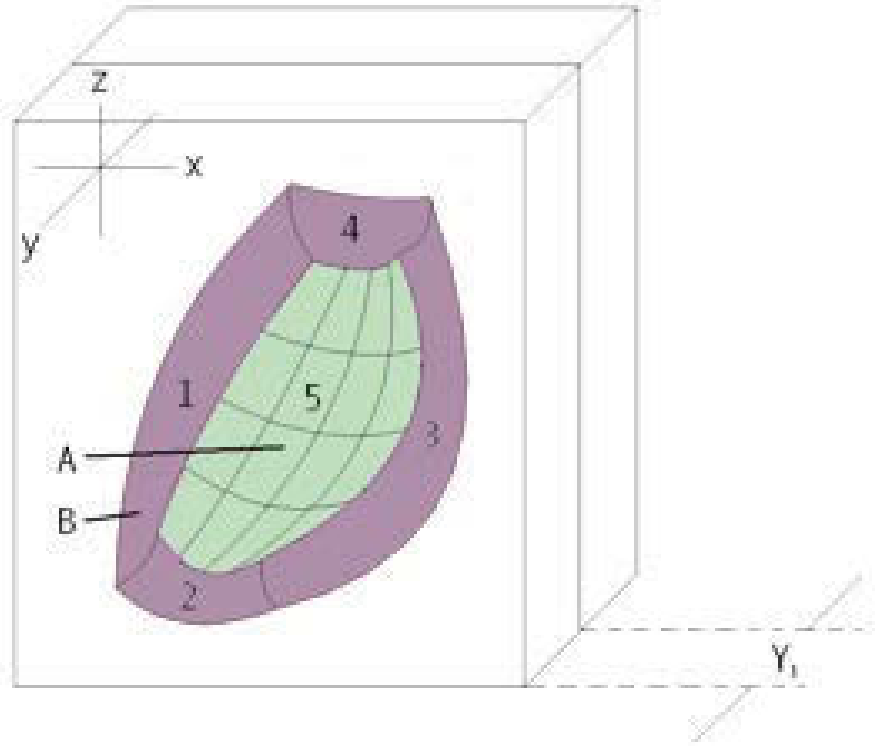

(A) cancellous bone; (B) cortical bone

Figure 4.2 Element divisions (modified from Ben-Nissan et al., 1987)

To model this composite, a number sequencing method was developed to match the finite element input data sequence (Figure 4.3). The way in which the sequencing method works is by picking a number of nodal points on each mandible cross-section and numbering them consecutively. For example, numbers 1 to 8 represent the cortical bone outline and numbers 13 to 20 represent the interface between cortical and cancellous bone to allow brick element mid-point arrangement. The first element single face – measured by a single cross-section – contained nodal numbers 1, 2, 3, 9, 10, 13, 14 and 15. Digitising starts with the origin designated 0 and each point after that digitised as 1-8; then 9-12 and finally 13-20. The same digitising sequence was applied to the second cross-sectional plane and a subroutine was written to join these planes to generate the first five elements, four at the sides and one at the centre (Figure 4.4). The

first four were assigned properties relating to the cortical bone and the centre element relating to the cancellous bone mechanical properties.

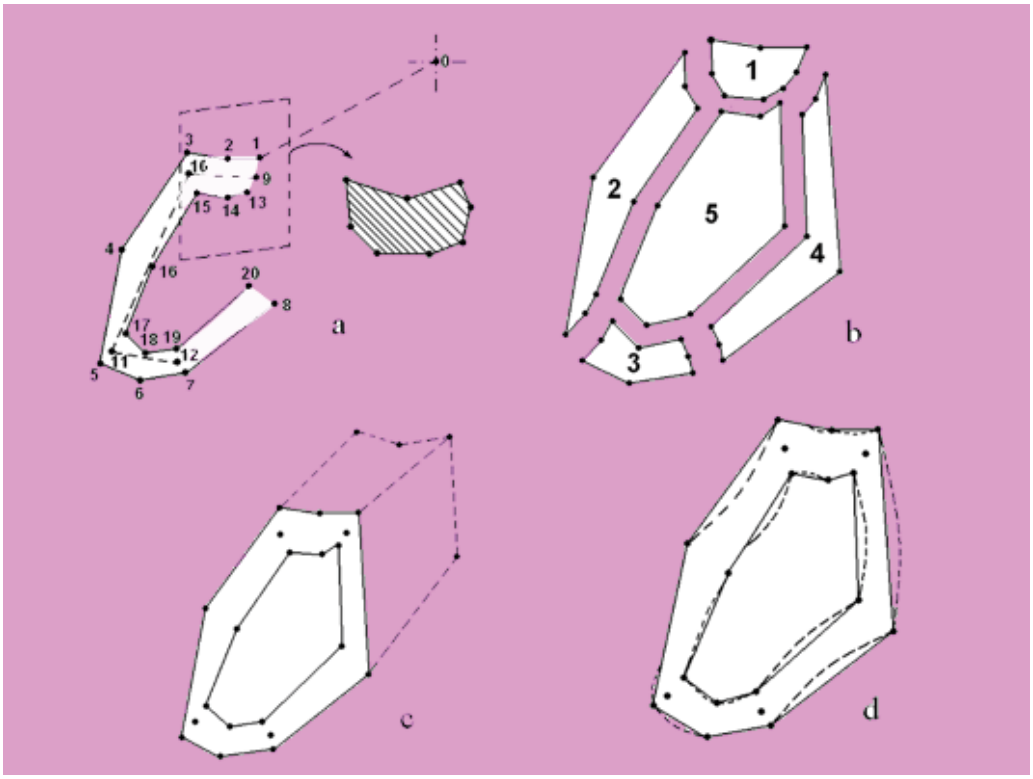

(a) Digitizing sequence and wire frame diagram. (b) Generation of surface planes of the brick elements where numbers 1 to 4 represent cortical bone and number 5 represents cancellous bone. (c) Element perimeter and midsize nodes on cross-section. (d) Element perimeter superimposed on real cross-section.

Figure 4.3 Nodal point generation using digitizer (modified from Ben-Nissan et al., 1987)

During the first stage modelling, the direction of number sequencing is very important. The wrong sequence can change the inputted data and final analysis of the preceding finite element work. Once the two-dimensional model is completed, the cross-sections can be joined using the known thickness (y) values obtained during the cross-sectioning of the mandible (Figure 4.4). A small subroutine was utilised during the joining process (Figure 4.5).

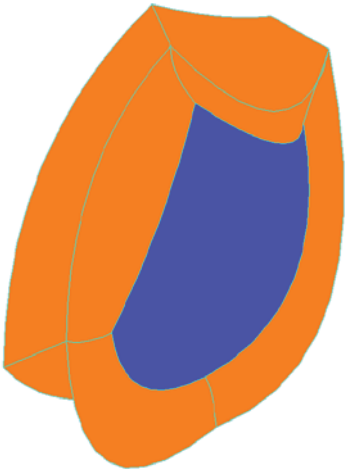

Figure 4.4 A typical cross-section of the mandible generated from nodal points (produced in STRAND7 modified from Choi et al., 2005)

The three-dimensional model (Figures 4.5 & 4.6) was completed using the Palette CAD-Database software (Palette Systems Ltd Australia) and once obvious geometric faults were identified and corrected, general coordinate data was generated. This generated data could then be compared with the bulk mandibular measurements. If coordinate data were satisfactory, they could be sent to STRAND7 for analysis.

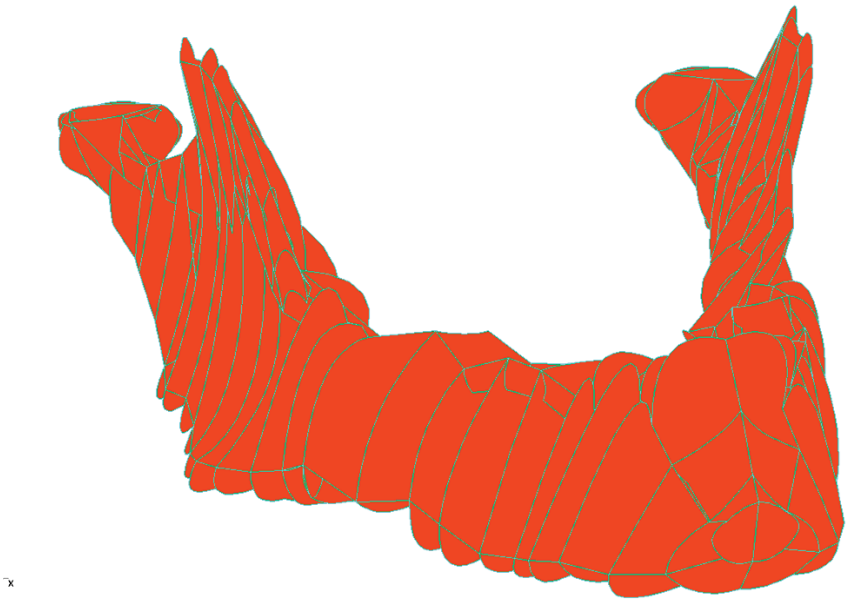

Figure 4.5 Finite element model of the human mandible (produced in STRAND7 modified from Choi et al., 2005)

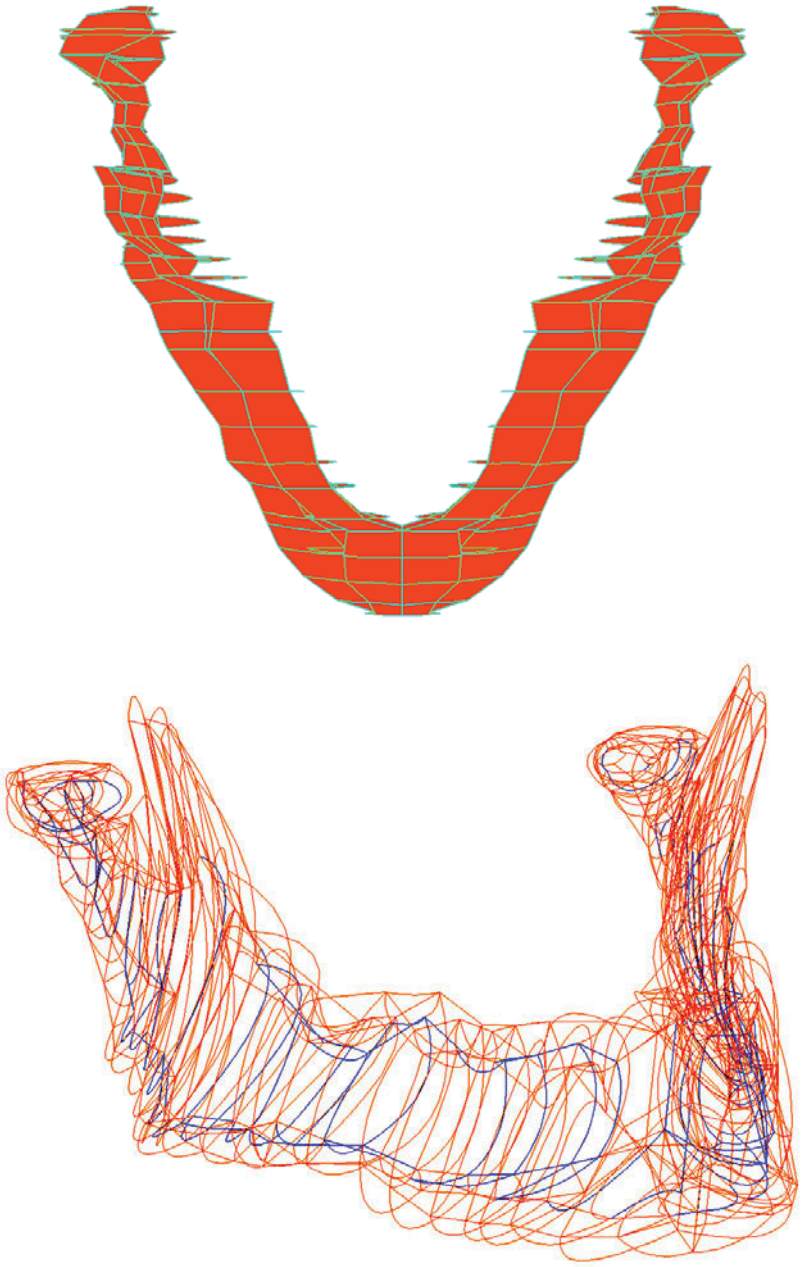

Figure 4.6 Finite element and wire frame mandibular models: The cortical bone outline is represented in orange and the cancellous bone inner layer is represented in blue (produced in STRAND7 modified from Choi et al., 2005)

In this model, materials were idealised as homogeneous, isotropic and linearly elastic. The complete model consisted of 258 brick elements and 1,635 nodes. Material properties for cortical and cancellous bones were selected from various investigators, as discussed in Chapter 3.

Restraints are used to define the boundary conditions of a model for structural analysis. They specify displacement conditions for individual nodes. A feature of the FEA is that the reference plane for deformation must be defined to remove possible rigid body motion. For this analysis, three nodes on the symmetry plane were fixed in space by the use of spring elements (Figure 4.7). Reactions of those points were shown to be zero so that restraining these parts had no effect on the stress distribution. It is important to note that the model is completely free to deform, removing the approximation caused by over-restraining in the previously published models.

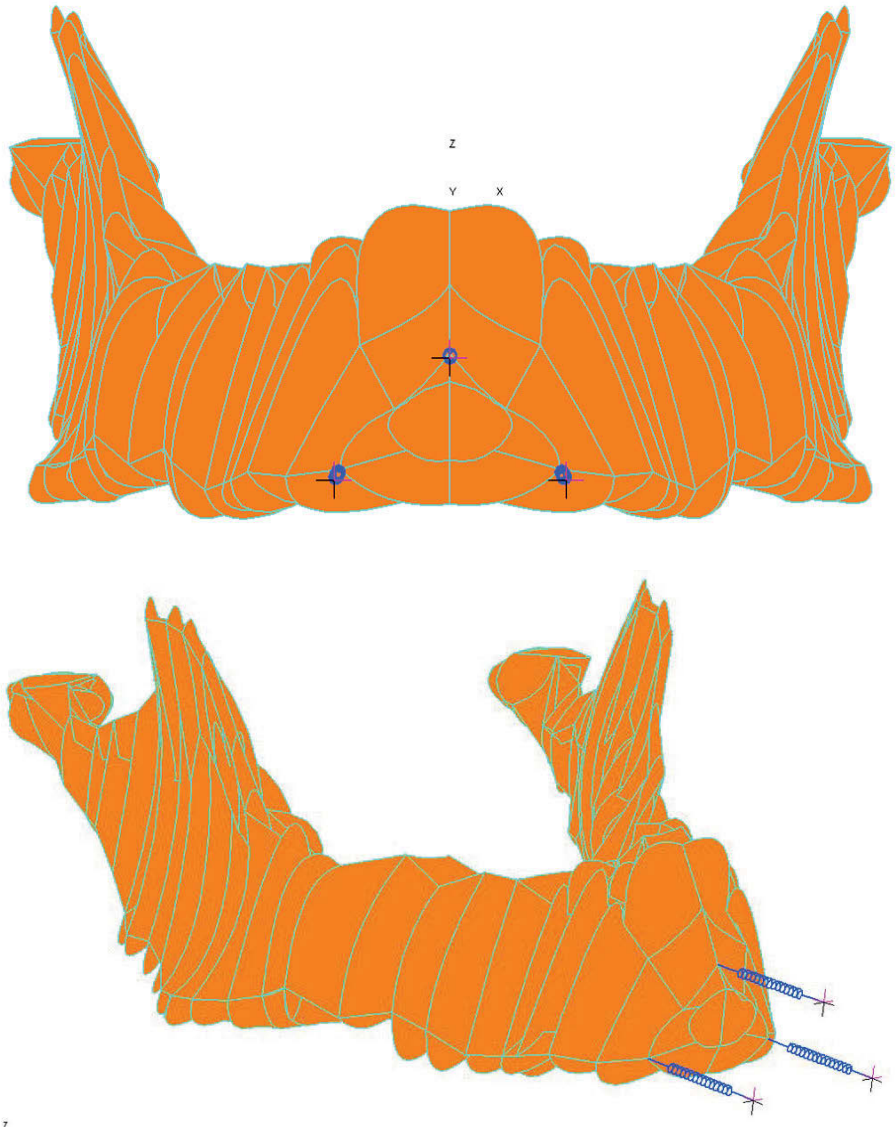

Figure 4.7 **Frontal and lateral views of the finite element model of the human mandible, showing restraining spring elements (produced in STRAND7 modified from Choi et al., 2005)**

4.4 Forces acting on the mandible

Earlier mandibular models, mostly two dimensional or partial, incorporated some muscle forces for consideration in analysis, but not all. In addition, the direction of the bite force and direction and magnitude of muscle forces were largely unknown and estimated at best. In most cases, the mandible was assumed to be made of an homogeneous and isotropic rigid material with a uniform cross-section with all loads and reactions applied in the same plane. This was a gross oversimplification of the true structure and biomechanical function of the mandible and produced results from analyses that were in harmony with the oversimplification.

In more realistic models and in this current work, the muscle forces considered in this model for analysis were derived from the works of Mainland and Hiltz (1934), Barbenel (1972), Schumacher (1961) and Pruim et al. (1980). All forces were assumed to be symmetrical with respect to the mid-line and to have an equal magnitude on the right and left side of the mandible. The forces exerted by contracting muscles were represented by vectors. Similar assumptions were made by the number of other workers (Paul, 1966; Morrison, 1967; Paulson, 1973). These assumptions are reasonably true when the muscle is homogeneous and acts as a whole. Later models incorporated in this current work used distributed muscle forces inserted over an area rather than at singular points.

In earlier models, the direction of these vectors were defined by the connecting lines between the centre of the origins and insertions of the muscles. Descriptions of these areas of attachments were derived from the anatomical literature (Schumacher, 1961; Mainland & Hiltz, 1934; Sicher & Du Brul, 1975; Hawthorne, 1969; Hylander, 1978) and three-dimensional observations and measurements on different skulls.

The force a muscle can exert is not only determined by physiological parameters (level of neuronal activation, speed of contraction, muscle length and muscle type) but also by anatomical parameters, such as the total cross-section of all muscle fibres, the so-called physiological cross-section. Measured physiological cross-sectional areas and published data available (Schumacher, 1961; Pruim et al., 1980) were used to determine the forces of the various muscles (Table 4.1).

Table 4.1 Physiological cross-sectional area (cm^2) of the facial muscles

Muscles	Schumacher (1961)	Pruim et al. (1980)	This investigation
Medial Pterygoid	1.97	5.3*	2.0
Masseter	3.02		3.0
Temporalis	3.81	4.2**	3.8
Openers	-----	1.0***	1.4
Lateral Pterygoid	1.83	2.1	1.8

* Includes medial pterygoid and masseter

** Includes anterior and posterior temporalis

*** Only digastric was measured

In this study, the physiological cross-sectional areas of various facial muscles were based primarily on the work by Schumacher (1961). The value of maximum muscle tension Γ, which directly relates to the maximum force exerted by a muscle to its physiological cross-sectional area, is shown in Table 4.2.

Table 4.2 Average maximum muscle tension (Γ) in N/m^2

Investigators	Γ (N/m^2)
Fick, 1904	1.0×10^6
Morris, 1948	0.9×10^6
Carlsoo, 1952, 1958	1.1×10^6
Hettinger, 1961	0.4×10^6
Ikai, Fukunaga, 1968	0.7×10^6
Pruim, 1980	1.4×10^6
This Work	1.47×10^6

Two methods have been used to estimate the magnitude of muscle forces. Various workers (Carlsoo, 1952; Gysi, 1921; Mainland & Hiltz, 1934; Pruim et al., 1980; Schumacher, 1961) have attempted to estimate the force generated by each muscle from the total cross-sectional area of the muscle. In the second method (Barbenel, 1974; Pruim et al., 1978, 1980), the integrated electromyogram (IEMG) from each muscle was used as an estimate of muscle force (Table 4.3).

Table 4.3 Averaged calculated maximum muscle forces (N) in each single muscle group and related standard deviations

Muscle	Carlsoo (1952)	Schumacher (1961)	Pruim (1980)	Osborn (1985)	This investigation
Medial Pterygoid	299±46	190	639±176**	254	190
Masseter	614±107	340		450	340
Ant. Temporalis	519±102	420*	362±65	264	528*
Post. Temporalis	305±102		197±26	323	
Openers	-----	-----	115±40	107	155
Lateral Pterygoid	525	175	378±106	382	378

* Anterior Temporalis + Posterior Temporalis

** Medial Pterygoid + Masseter

The bite force was assumed to be around 700 to 800 N according to Pruim et al. (1978, 1980).

In this study, magnitudes of the averaged calculated maximum muscle forces are determined by the physiological cross-sectional area based on the work of Ben-Nissan (1987) of the facial muscles (Table 4.4).

Table 4.4 Calculated muscle, joint reaction and bite force magnitudes (N) acting on the mandible during clenching (Ben-Nissan, 1987)

Muscles	F_x	F_y	F_z	F_{total}
Masseter	141.9	-53.6	304.3	340.0
Temporalis Anterior	50.6	102.9	238.1	264.3
Temporalis Posterior	50.6	102.9	238.1	264.3
Medial Pterygoid	-82.9	-29.7	170.0	191.4
Lateral Pterygoid	-215.4	-307.6	-43.2	378.0
Joint Reaction Force	0.0	63.8	-467.6	471.9
Bite Force (2nd premolar)	0.0	33.33	-244	246.3
Bite Force (1st molar)	0.0	21.31	-156	157.4
Openers	0.0	133.2	-79.3	155.0
Masseter*	-141.9	-53.6	304.3	340.0
Temporalis* Anterior	-50.6	102.9	238.1	264.3
Temporalis* Posterior	-50.6	102.9	238.1	264.3
Medial Pterygoid*	82.9	-29.7	170.0	191.4
Lateral Pterygoid*	215.4	-307.6	-43.2	378.0
Joint Reaction Force*	0.0	63.8	-467.6	471.9
Bite Force (2nd premolar)*	0.0	33.33	-244	246.3
Bite Force (1st molar)*	0.0	21.31	-156	157.4

* Forces applied on the right side of the mandible model

For the FEM to be valid, the applied forces must be in equilibrium so that reactions at the restrained nodes in Figure 4.8 will be zero. It was therefore necessary to define physical conditions during the various mandibular movements of clenching, opening and protrusion to reduce the complex force system to a form that allows of valid loads for the FEM. In addition to the information in Table 4.3, Figure 4.8 describes the muscle force direction of action for temporalis, masseter, medial pterygoid, lateral pterygoid and anterior digastric muscles.

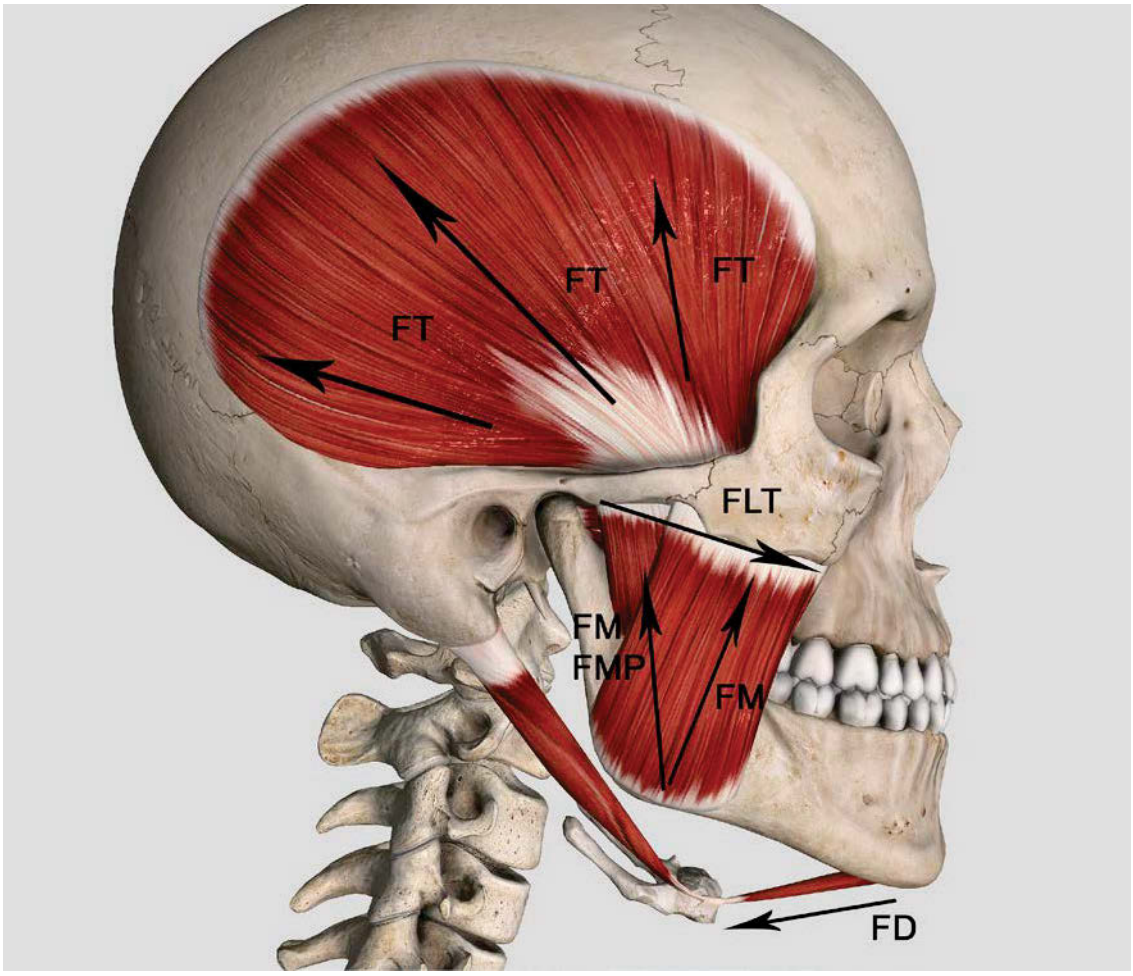

FT = Temporalis (anterior, middle and posterior bellies); FM = Masseter (superficial and deep bellies); FMP = Medial pterygoid; FLT = Lateral pterygoid; FD = Anterior digastric, geniohyoid and mylohyoid

Figure 4.8 Lateral projection of muscle force directions (diagram constructed using 3D4MEDICAL software)

4.4.1 Clenching

When analysing bite forces during clenching without a food bolus, the mandible may be considered to be in static equilibrium so that the sum of forces on it (represented in Table 4.3 and Figure 4.8) and the sum of torques generated by forces about an arbitrary but fixed point in space are zero.

According to Wood (1986), the medial pterygoid muscle activity during an intercuspal clench appears to contribute to the force generated between the teeth. The lateral components of masseter on temporal muscles that are also active during clenching must also be taken into account. Any resulting distortions of the mandible and interocclusal forces represent the combined action of several major muscle groups acting in concert. From this and his own work, Ben-Nissan (1987) produced Table 4.4, showing the calculated forces acting on the mandible during clenching. This is also represented diagrammatically in Figures 4.9 and 4.10.

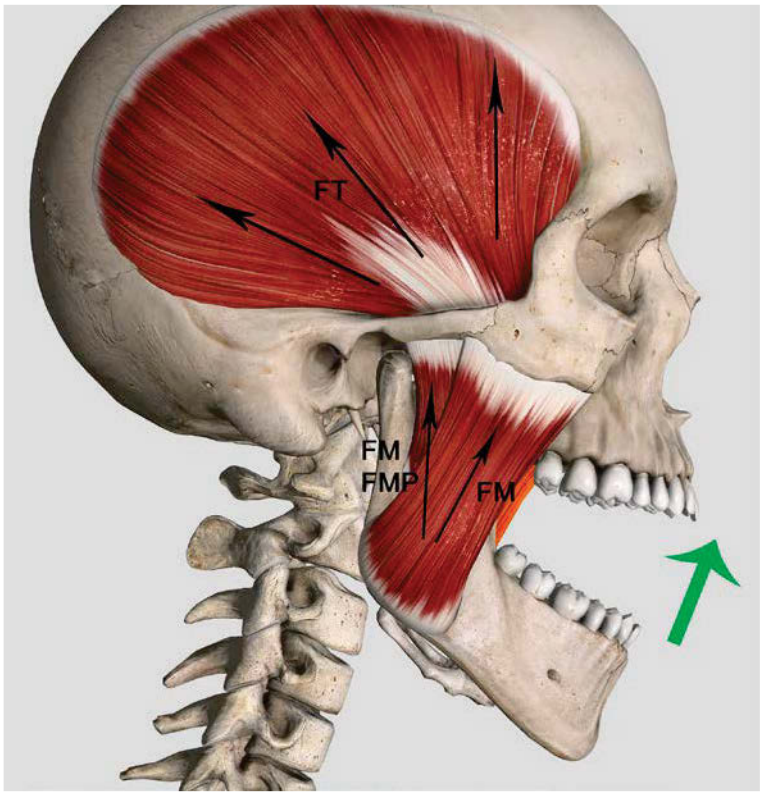

FT = Anterior, middle and posterior bellies of temporalis; FM = Superficial and deep bellies of masseter; FMP = Medial pterygoid

Figure 4.9 Diagrammatic representation of direction of muscle pull during clenching (diagram constructed using 3D4MEDICAL software)

For this thesis, the clenching bite force was directed at an angle of approximately 85° to an averaged occlusal plane. Each bite force was equally divided between two teeth, the second premolar and first molar bilaterally thereby replicating Pruim et al.'s (1980) simulation.

During clenching, all muscles were assumed to be active. Calculated muscle forces were taken from the values in Table 4.4. The reaction forces were assumed to be acting at the centre of the condyles and are displayed in Figure 4.10.

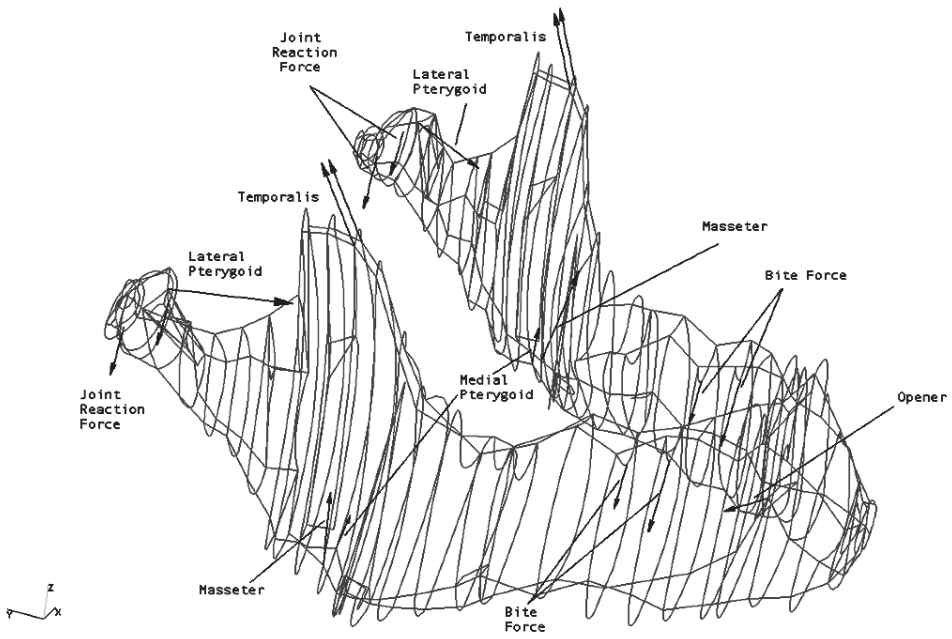

Figure 4.10 Applied muscle, joint reaction and bite forces and coordinate system during clenching (modified from Choi, 2004)

4.4.2 Opening

At its simplest, the jaw is opened by a moment couple consisting of the anterior bellies of the digastric, the lower heads of the lateral pterygoids and the geniohyoid (Figure 4.11). If adductor muscles 'pay out' their length while maintaining 'tension', the condyle will remain in contact with the articulator eminence until, and if, it passes over the eminence.

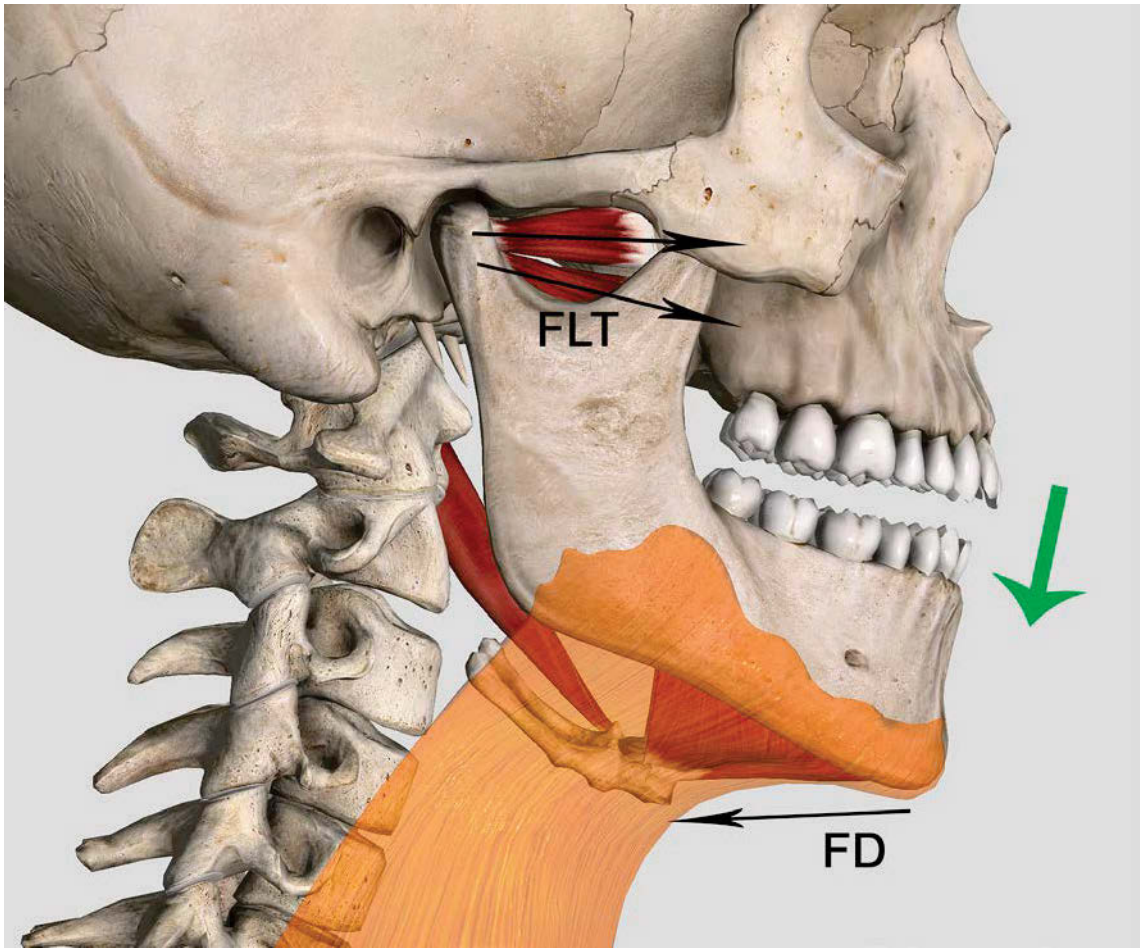

FLT = Lateral pterygoid; FD = Anterior digastric, geniohyoid and mylohyoid

Figure 4.11 Diagram of interplay between FD and FLT to produce moment arm and opening of the mandible (constructed using 3D4MEDICAL software)

During wide opening, masseters and medial pterygoid muscles were assumed to 'pay out' their length and guide the opening movements (Figures 4.11 & 4.12). Lateral pterygoid and opener muscles were utilised as main depressors (Moyer, 1950; Jarabak, 1957; Carlsoo, 1958; Munro & Basmajian, 1971; Lehr et al., 1971). Opener muscle forces were postulated according to published physiological cross-sectional area values, which included digastrics, mylohyoid and geniohyoid muscles.

The ratio of masseter to medial pterygoid muscle forces was assumed to be 2:1 (Carlsoo, 1952; Schumacher, 1961). The physiological cross-sectional area ratios of various workers were used to postulate the force magnitudes of the various muscles (Table 4.5).

During wide opening, due to the right angle created by the masseter and medial pterygoid muscles, the horizontal (y-axis) force components $F_{masseter}$ and $F_{medial\ pterygoid}$ can be assumed to be zero or very close to zero. By reducing these components, we can obtain the equilibrium by calculating the rest of the components of these two unknown muscles. These assumptions are based on cephalometric measurements and electromyographic studies. All opener muscles are assumed to be active at all time, that is, no antagonistic muscle action.

Antagonistic muscle action is assumed to occur only for short periods of the opening cycle where activity in one muscle group declines as activity in another group increases. Such antagonistic action cannot be gauged from the equilibrium equations and as yet there is no reliable method of measuring muscle force directly under conditions of contraction where muscle tension, length and velocity of shortening are changing.

Calculated values of the forces acting on the mandible during opening are given in Table 4.5.

Table 4.5 Calculated muscle and joint reaction force magnitudes (N) acting on the mandible during opening (Ben-Nissan, 1987)

Muscles	**F_x**	**F_y**	**F_z**	**F_{total}**
Masseter	44.7	0.0	121.2	129.1
Medial Pterygoid	-24.5	0.0	60.6	65.3
Lateral Pterygoid	-197.2	-281.6	156.1	377.6
Joint Reaction Force	0.0	213.0	-300.3	368.6
Openers	0.0	135.6	-75.1	155.0
Masseter*	-44.7	0.0	121.2	129.1
Medial Pterygoid*	-24.5	0.0	60.6	65.3
Lateral Pterygoid*	197.2	-281.6	156.1	377.6
Joint Reaction Force*	0.0	213.0	-300.3	368.6

* Forces applied on the right side of the mandible model

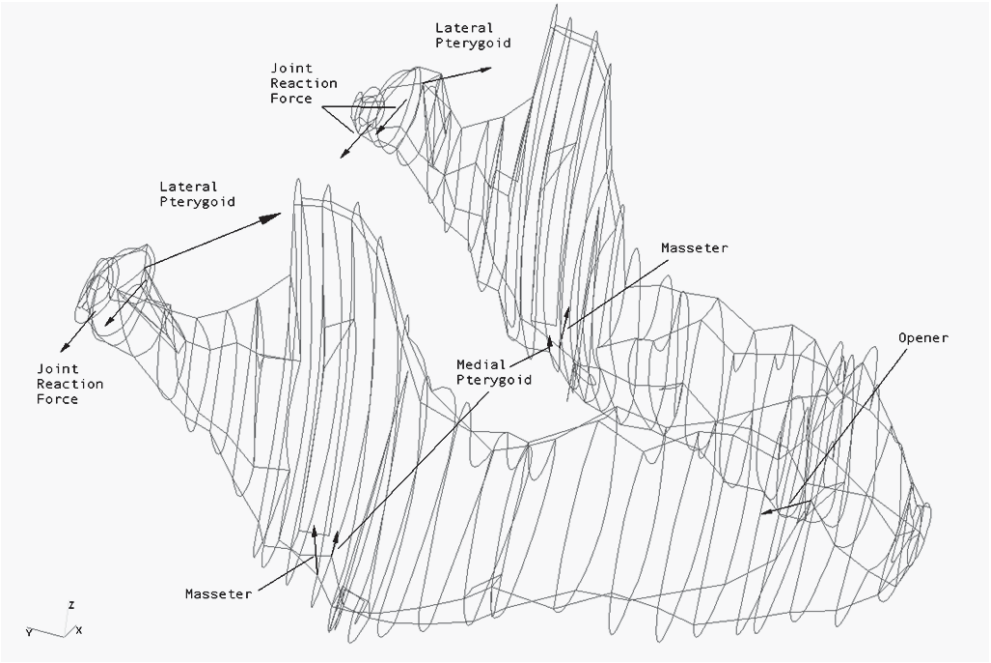

Figure 4.12 Applied muscle and joint reaction forces and coordinate system during opening (modified from Choi, 2005)

4.4.3 Protrusion

During the protraction of the mandible without occlusal contact, the masseter was assumed to be silent while the medial pterygoid and, to a lesser extent, the lateral pterygoid was the only active elevator guiding the movement (Moyers, 1950; Carlsoo, 1952) (Figures 4.13 & 4.14). The digastric (openers) muscle does not contribute to the elevation of the mandible. Again, the horizontal component of the medial pterygoid was zero, and other components were calculated accordingly (Table 4.6).

Table 4.6 Calculated muscle and joint reaction force magnitudes (N) acting on the mandible during protrusion (Ben-Nissan, 1987)

Muscles	F_x	F_y	F_z	F_{total}
Medial Pterygoid	-74.4	0.0	181.8	196.4
Lateral Pterygoid	-197.2	-281.6	156.1	377.5
Joint Reaction Force	0.0	213.8	-300.3	368.6
Openers	0.0	135.6	-75.1	155.0
Medial Pterygoid*	74.4	0.0	181.8	196.4
Lateral Pterygoid*	197.2	-281.6	156.1	377.5
Joint Reaction Force*	0.0	213.8	-300.3	368.6

* Forces applied on the right side of the mandible model

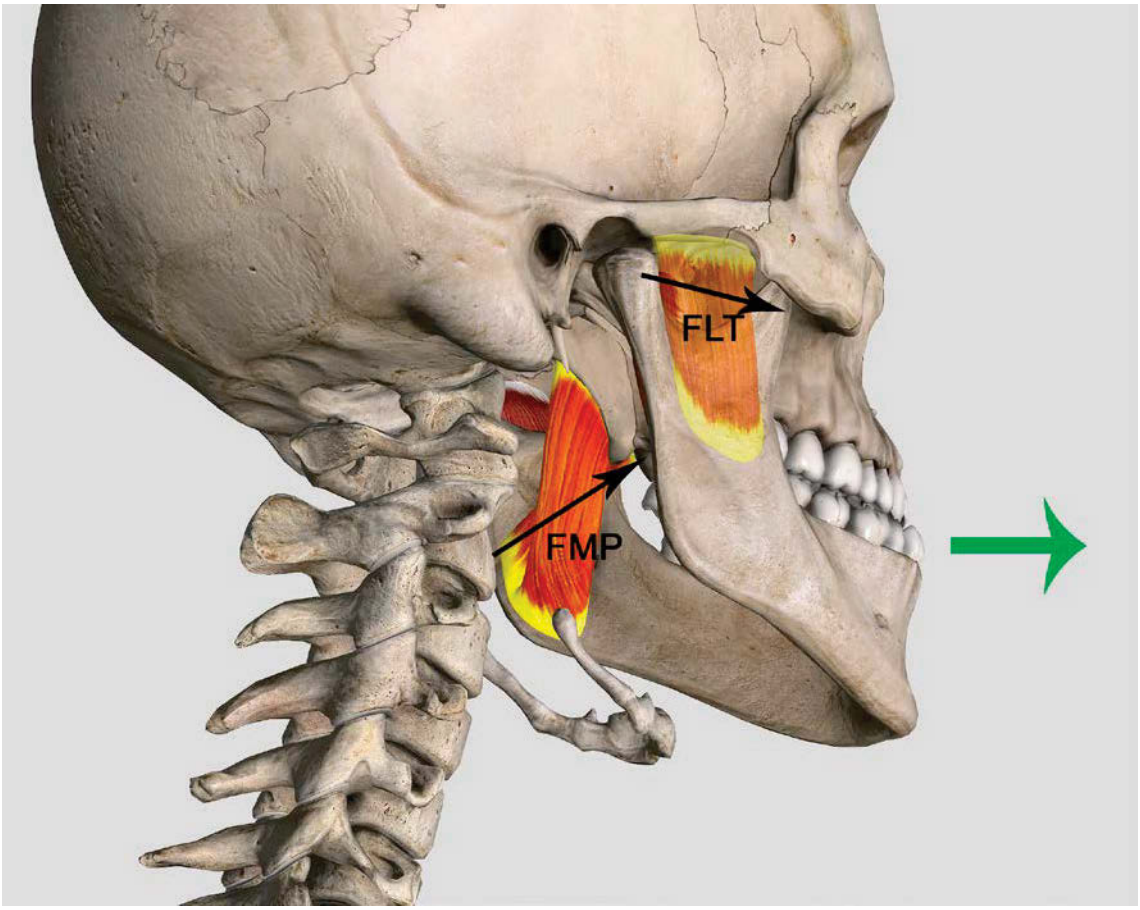

FLT = Lateral pterygoid; FMP = Medial pterygoid

Figure 4.13 Diagram of interplay between FMP and FLT to produce gliding and protrusion of the mandible (constructed using 3D4MEDICAL software)

Baragar and Osborn (1984) assumed that the temporomandibular ligament is active during wide open and protrusion movements. During these movements, the temporomandibular ligament might be helping, on the guidance and degree of opening of the elevator muscles. Some of the force could be distributed to this ligament during these movements. According to geometrical data, the angle of the temporomandibular ligament to the condyle centre is similar or very close to the angle of the masseter or medial pterygoid to the condyle centre during wide open and protrusion movements.

These assumptions might not drastically change the final results during flexion but are more realistic.

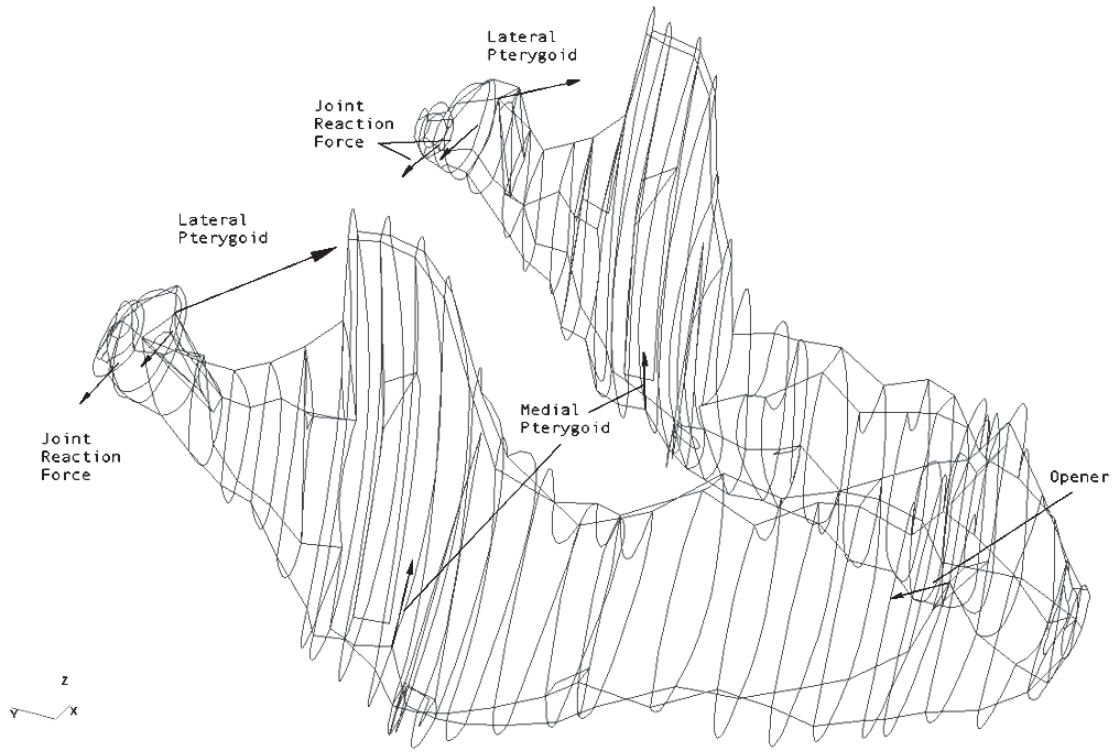

Figure 4.14 Applied muscle and joint reaction forces and coordinate system during protrusion (modified from Choi, 2005)

4.5 Summary

A dry human mandible, judged by visual inspection to be normal, has been used to define the geometry of the model. The mandible was then cross-sectioned vertically into 28 sections. Each cross-section of the bone was divided into five sections, the outer four representing the cortical bone and the inner one the cancellous bone. The complete model consisted of 258 brick elements and 1,635 nodes. Material properties for cortical bone and cancellous bone were taken from previously published values. For this analysis, three nodes on the symmetry plane were fixed in space by the use of spring elements. The muscle forces considered in this analysis were selected from various investigators. The model was analysed under non-linear static conditions using the STRAND7 FEA package.

Three types of functional movements were analysed: (i) clenching; (ii) opening; and (iii) protrusion. During clenching, all muscles were assumed to be active. The reaction forces were assumed to be acting at the centre of the condyles. During wide opening,

the masseters and medial pterygoid muscles were assumed to guide the opening movements, and the lateral pterygoid and opener muscles were utilised as main depressors. During the protraction of the mandible, the masseter was assumed to be silent while the medial pterygoid was the only active elevator guiding the movement.

CHAPTER 5:
SECOND OUTPUT – PATIENT SPECIFIC MODELLING

This chapter presents the next progression in the production of an innovative finite element model (FEM) of the human mandible and the validation of a mandibular fracture system for clinical analysis and discussion on potential clinical applications to benefit patients.

The model is derived on a computed tomography (CT) scan of the jaw performed on a living subject. The CT scan was chosen to provide the building blocks of data due to its inherent accuracy in describing bony anatomy, ease of access being available through most radiology practices or hospitals and the relatively low cost to produce the data required. By utilising patient CT data, innovative attributes of being PS is given to the study.

However, not only must the model be PS, it must also be biomechanically valid in order to produce realistic scenarios of constraints and forces during functional movements, and also to have relevance to reflect accurately these scenarios as they occur in vivo. By fulfilling our research aims through advanced modelling and clinically relevant applications, such as PS material mapping of bone mineral densities and the generation of dedicated software for the developed technology with further refinement, this approach to modelling can become a functional tool readily available to the clinician and researcher to aid in clinical diagnosis treatment planning and prosthetic design and manufacture, not only planning in oral and maxillofacial surgery, but broadly across all aspects of healthcare provision. Most importantly, however, the availability of such technology will ultimately benefit our patients.

Figure 5.1 illustrates the pathway from initial presentation of the patient through CT, input of mechanical properties and density data into the solid model and FEA, followed by distortion and stress analysis and finally, surgical analysis.

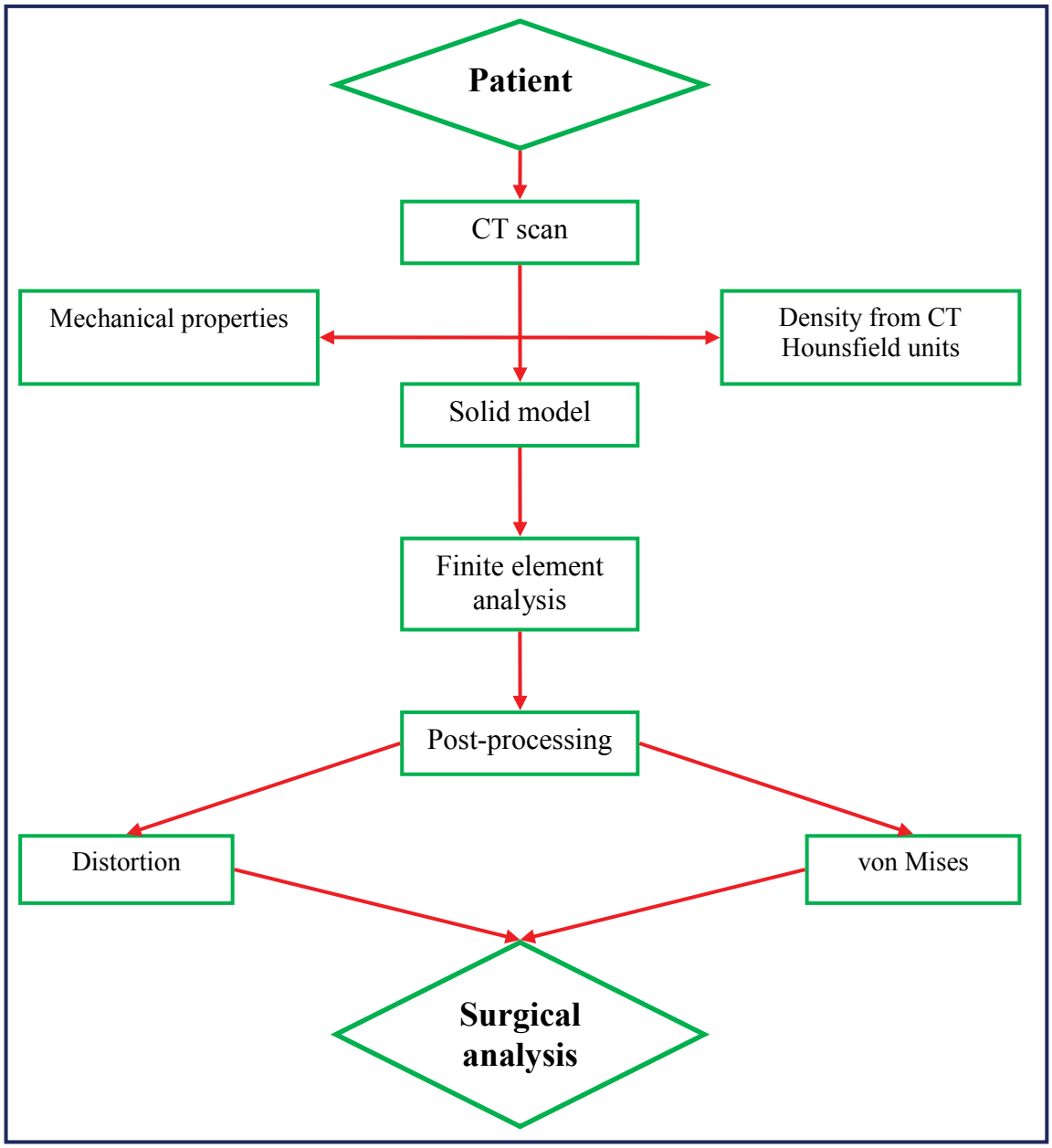

Figure 5.1 Process in conducting surgical analysis of a patient specific finite element model

5.1 Mandibular model

Mandibular modelling and finite element analysis (FEA) with biomechanical considerations goes back to the early 1980s although earlier biomechanical considerations were initiated in the 19th century.

A number of investigators, namely, Barbanel (1975), Throckmorton (1985), Pruim (1980), Hylander (1985), Knoll (1977), Ben-Nissan (1987), Hart (1992) and Choi (2005) have reported that there is a broad range of fundamental questions regarding the biomechanics of the mandible which need to be investigated. For example: How do strain and stress changes in the mandibular bone respond to the loss of teeth? What is the comparison between the biomechanical function of the dentate mandible versus the edentulous mandible? (as discussed in previous chapters). How is the biomechanical function of the mandible affected by prosthetic devices, such as osseointegrated implants or fracture fixation systems?

To describe the biomechanical movements observed, there has been more than one approach to the problem of characterising a morphologically correct musculoskeletal representation of the mandible and associated muscles. One approach developed by Ben-Nissan and described in Chapter 4 overcame many of the problems presented in modelling. A common limiting factor to all the approaches has been that, to date, stress is not easily, directly and accurately measurable within the mandible by any in vivo means, as we shall discuss immediately.

5.2 Biomechanical Approach and FEA

Prior to finite element modelling, several methods were developed to explore the biomechanical behaviour of the mandible. Hylander (1975) used a free-body analysis, followed by the use of photo elastic resin for modelling mandibular stresses (Lehman, 1968; Ralph & Caputo, 1975; Standlee, 1977; Mongini, 1979). More recently, holographic interferometry (Hussein & Rabie, 2015) and an empirical assessment of stress distribution through in vivo and in vitro strain gauge studies have been investigated.

However, whilst in vivo strain gauges can give accurate localised measurements on the surface of a structure, strain cannot be measured at internal locations (Hylander, 1984). Moreover, the choice of surface locations to analyse with the strain gauge is restricted due to potential interference from muscle attachments.

Photo elastic models require the use of a transparent resin model of the structure to be analysed. In particular, as described earlier, the mandibular biomechanical system is extremely complex and such a simple resin model does not accurately reproduce true biomechanical properties (Caputo & Standlee, 1987).

Again, due to the complexity of the mandibular biomechanical system, analytical solutions in general are unviable because of the complexity involved, incomplete knowledge of the mechanical properties of the tissues, and complex time-dependent loading and boundary conditions. Unfortunately until recently, despite previous excellent contributions from previous workers, FEM fell under the same banner and even contemporary models lacked patient specificity.

Ferre and Knoell (1977) and Choi et al. (2005) eloquently summed up the problems in FEA-based stress analyses of a mandible by including gross simplifications that involved mandibular geometry, material properties and incorrect boundary conditions, such as fixed supports. In addition, analyses were two-dimensional representations (Haskell 1986). Therefore, accurate solutions for strain distribution in a biomechanically complete mandibular model were not entirely and satisfactorily established using early modelling techniques.

For this reason, accurate anatomical design as provided by CT data is essential for three-dimensional finite element modelling and analysis so that such technology can take its rightful position as a valid analytical tool that can confidently be correlated back to clinical application.

5.3 FEM models and differentiation criteria: Materials, restraints Hounsfield units and data acquisition

The modelling of accurate anatomy, appropriate loading, musculature, load distribution, functional movements, material properties and realistic supports for a mandibular model represents the evolution path of FEMs. We have already covered much of this territory in previous chapters but we will revisit some areas and build upon key areas as they pertain to the aims of this thesis.

The assumptions that differentiate models from one another include material compositions, structural properties, load application topology and choice of restraints. These are required for the relevant mathematical simulations to converge for regional or for full mandible analysis and finally computational capacity to run the simulations.

The focus for the assignment of material properties relates to the fact that the mandibular bone is principally made of two types of bones: (i) cortical; and (ii) cancellous, as described in Chapters 2 and 3, containing the mandibular canal for inferior alveolar nerves and vessels. Additional voids or medullary spaces do exist in the cancellous bone and these are primarily occupied by fatty marrow tissue (Futterling et al., 1998).

It has been observed that in musculoskeletal structures, similar to the human mandible, the type of bone and density changes strongly throughout the geometry. For this reason, averaging and assigning only one or two material properties throughout the entire model can lead to inaccurate results (Futterling et al., 1998).

For example, in a study on the rigidity of the mandible at three different stages of life, Bujtar (2010) observed how visco-elastic anisotropic features of the anatomy are rarely taken into account in predicting the behaviour of components of the facial skeleton when loading or trauma. Similarly observations made by Li (2009) noted how the lack of local information on material properties resulted in significant limitations in the realism of mandibular models.

If a two-bone approximation is used, two encapsulated solids represent the trabecular and cortical bone. The interaction between two solid entities creates issues with assigning boundary conditions. Comparing fixed bond, slip contact and non-linear contact interface boundary conditions, numerous finite element analyses have shown profound differences in resultant stress patterns.

In this work a linear isotropic approximation for the bone tissue is used, although its stiffness is determined locally through a correlation with the apparent density, as demonstrated from data collected from the CT scan. This choice is also due to the fact

that the biomechanical configuration is believed to have a higher influence on generated stresses and distortions during functional movements than the degree of anisotropy.

This is one of the features differentiating this work from other studies published in literature. The most common biomechanical scenarios used in mandibular simulations involve explicit bite forces and require the use of fixed supports around the bone for preventing rigid body movement. Other studies assign a vector load to a few muscles believed to be active during clenching and constrain the movement of the condyles to achieve static equilibrium. Nevertheless, as noted by Bujtar (2010), the lack of articulation-like contact in some of the simulations generated high stresses in the condyles jeopardising the realism of the FEM.

This study, in contrast, assumes that the mandible is free to move during functional movements and requires that a complete set of the current active muscles be in equilibrium with the reaction exerted in the temporomandibular joint.

In order to represent the complexity of the inner structure of the bone, Ben-Nissan (1987) developed the first anatomically correct three-dimensional model of the mandible for the analysis of functional distortions, as discussed in Chapter 4.

To reiterate, Ben-Nissan (1987) used models of the mandible cast in polyester resin and cross-sectioned in order to get cortical bone outlines, cancellous bone layers and reference points for structural symmetry. By assigning two specific Young's modulus for the cortical and trabecular bone, Ben-Nissan defined a continuous range of possible values of elastic modulus of the homogeneous linear isotropic bone model. He also designed an interpolation between the behaviour of a fully cortical mandible and a fully trabecular one. This allowed the results for distortion and stress/strain in a range of anatomically different mandibles under functional loading conditions, such as clench, opening and protrusion to be obtained.

Fixtures were only defined for three constraint points on three different directions at the symphysis where, in case of applied load, reaction forces would be null. Using an anatomically correct structure, appropriate measured musculature, insertion and origins

of muscles, three dimensional forces and, most importantly, appropriately constraining the model that is free to deform, Ben-Nissan's model was truly innovative at that time.

According to Choi (2004), the cortical and cancellous bone of the mandible can be considered to be transversely isotropic with a higher elastic modulus in the longitudinal direction and a lower elastic modulus in all transverse directions. In preventing any possible rigid body motion, Choi fixed three nodes in space in a symmetry plane perpendicular to the intercondylar axis by using spring elements.

Ben-Nissan's use of dry (cadaveric) mandibles for three-dimensional modelling represents a trend followed by other workers in his field.

Korioth et al. (1992) developed a three-dimensional model from the scan of a dry human mandible through computed tomography. More than his innovative non-destructive reproduction of the jaw morphology, Korioth's model considers the cancellous bone as trabecular bone without medullary spaces. In accordance with the constraints used, Korioth fixed the solid model at the labial and occlusal thirds of the right first lower molar.

Two models made in the early 1990s (Hart, 1992; Meijer, 1993) modelled the border of the cortical plate and assigned different material properties for cortical and cancellous bone. Hart's model also used computer tomography to scan a dry jaw. Similarly to Ben-Nissan (1987), Hart focused on the behaviour of the mandible during functional ordinary movements, such as biting and loading due to mastication, which provokes stresses in multiple regions. As Vollmer (2000) pointed out, Hart described the conformity between the calculated results and strain gauge investigations made by Hylander (1984) on a primate (Macaca Fascicularis) mandible.

Korioth et al. (1992) found that strains on a loaded in vitro mandible were in agreeance with the ones calculated by FEA on the same specimen. Vollmer (2000) and Al-Sukhun et al., (2005) based the validity of their own models on the same conformity. They both used computed tomography to scan dry mandibles and assigned material properties

according to the absorption values reported in the tomography results. These absorption values are termed by radiologists as Hounsfield units.

A Hounsfield unit represents the degree of radiodensity of a material. Water at standard temperature and pressure is assigned as having the radiodensity of zero Hounsfield units. Details of the determination of the Hounsfield units, their frequency and density distributions are given in Appendices A and B.

Table 5.1 characterises the Hounsfield units of various tissues that are encountered in using a CT scan to develop a PS mandibular FEM.

Table 5.1 Comparative values of Hounsfield units (Shetty et al., 2009; Choi et al., 2010)

Tissue type	Hounsfield units
Water	0
Air	-1000
Fat	-120 to -90
Blood	+30 to +45
Neural tissue	+20 to +45
Muscle	
+35 to +55	
Cartilage	-140 to -120
Cancellous bone	+700
Cortical bone	+3000
Dentine	+1000 to +1500
Enamel	
>+1500	
Titanium (Ti)	+2,921± 218

The data tabulated in Table 5.1 specifically relates to that of a medical grade computed tomography scanner but not to a cone beam computed tomography (CBCT) scan (De Vos et al., 2009). Whilst a full and comprehensive comparison of medical grade CT versus CBCT is outside the scope of this research, it is interesting to mention this disparity in data collected from medical grade CT scanners versus CBCT. Due to being

relatively inexpensive compared with the cost a medical grade CT scanner, CBCT machines have been installed in dental practices. However, for comprehensive information, a full medical grade CT scanner is necessary and has been used for this thesis.

Once a scale of Hounsfield units have been established and measured by the computed tomography, this data can be transformed into bone density values and then correlated with Young's modulus (Vollmer, 2000).

Vollmer (2000) and Al-Sukhun et al. (2005) also measured mandibular surface strain, using strain gauges and medial convergence, using a custom-fabricated linear variable differential transformer. Although using two different techniques for converting CT scan data to density values and therefore stiffness, both groups found a good correlation between the experimental results and FEM-based analysis outcomes.

The experimental apparatus set up by Vollmer was limited in detecting the three-dimensional orientation of the reaction on the condyles. This model lacked detailed knowledge of the material properties of cancellous bone and lacked certainty on how to realistically distribute the muscle loading. In addition, the boundary conditions on the condyles were also uncertain.

In diverging from these studies of Vollmer (2000) and Al-Sukhan et al. (2005), this present work proves that the topology of loads during functional movements is one of the variables that heavily affect the validity of the FEM.

5.4 FEA model: Biomechanical considerations

5.4.1 Material mapping

The cancellous bone is composed of plate-like bone partitions with bone marrow spaces of varying sizes and shapes, and contains the mandibular canal for the inferior alveolar vessels, nerves and other cavities.

The degree of anisotropy in the condyle increases from the superior to the inferior part, and the trabeculae are more aligned towards the mandibular neck (Giesen, 2000).

As stressed by Futterling (1998), in biomechanical structures like the human mandible, the type of bone and density are changing strongly throughout the geometry, thus averaging and assigning only one or two material properties can lead to inaccurate results. However, the bone mineral density and morphology is also subject-specific, since it varies with age and sex. For this reason, the model developed in this thesis takes into account the patient's original mandibular morphology and individual bone mineral density.

For a more comprehensive understanding of the specificity of our model, a brief overview on the main concepts involved in the FEA and modelling of the human mandible is needed.

Four important areas already covered in Chapters 1 to 4 are: (i) anatomy and biomechanics of the mandible; (ii) principles of FEA; (iii) morphology; and (iv) material properties of the mandible. We will now explain four additional areas: (i) load application; (ii) equilibria and the reaction force; (iii) reaction force positioning; and (iv) analysis application issues, whilst building on the earlier chapters.

5.4.2 Load application

One improvement introduced by the proposed model that contributes to more realistic results and accuracy in predicting stress and strain is the application of muscles forces on areas instead of single nodes. According to Vollmer (2000), there is uncertainty on how to realistically distribute the muscle loading and fix the boundary conditions at the condyle. Moreover, after recording experimental data with strain gauges, Vollmer proves that changing the location of biting forces significant changes in stress distribution and magnitude occurred near the condyles.

5.4.3 Equilibria and the reaction force

Early biomechanics workers suggested that there is no significant direct or indirect load acting on the temporomandibular joint (TMJ). The most interesting interpretations in this direction are the ones by Frank (1950) and Gingerich (1971). Frank based his arguments on a radiographic analysis, which showed that the condyle was never in direct contact with the articular eminence. Therefore, he concluded that the condyle was

not functioning as a fulcrum, causing the mandible to not function as a lever. Gingerich stated that during the biting action, the jaw is functionally a link between the adductor muscle force and the bite force rather than a lever.

Roberts and Tattersall (1974), in their simplified biomechanical model, stated that there is no significant force at the TMJ during elevation of the mandible since the masseter, temporalis and bite force vectors form a closed triangle.

It is now accepted that the mandibular biomechanical activity is comparable to a simplified Class III lever in which the condyle acts as a fulcrum, masticatory muscles act as applied force and the bite load act as resistance. The approach used in the present work agrees with the assumption that there is a reaction force acting on the condyles during clenching (Figure 5.2) and wide opening.

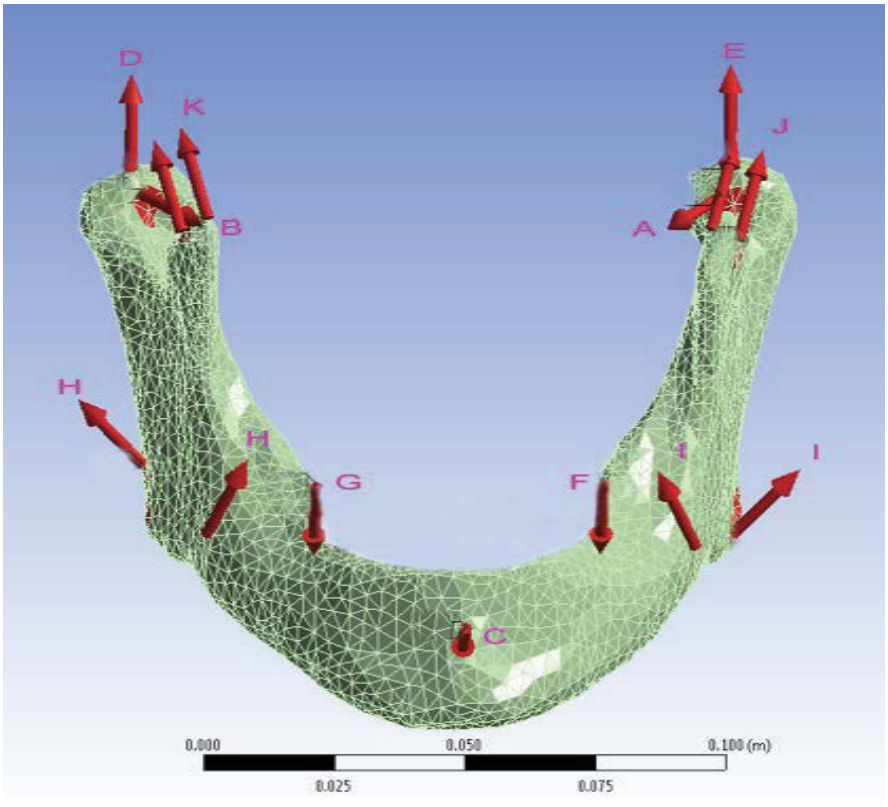

A & B: Left and right lateral pterygoid 378N, C: Openers 155N, D & E: Right and left joint reaction force 471N, F & G: Left and right bite force 113N, H & I: Right and left pterygo masseteric force 388N, J & K: Left and right temporalis force 199N.

Figure 5.2 Three-dimensional vector representation of loads applied during clenching including joint reactions forces (modified from Taraschi, 2016)

The intensity and direction of the three dimensional vector representing the reaction force in the simulation is calculated by balancing the equations for resulting force and momentum generated with respect to the intercondylar axis. Hence, calculation of the total joint reaction force requires the magnitude and direction of the bite force, magnitude and direction of each acting muscle and lengths of the moment arms of each muscle force.

Magnitude and direction of the bite force can be directly measured with force transducers (Hylander, 1978) while lengths of the moment arms can be generally estimated from lateral cephalograms. Therefore, it is evident that the quality of these results could depend on the estimation of the intensity of all muscle forces applied to our structure.

Two methods have been successfully used to estimate these forces: (i) the use of the integrated electromyogram (IEMG) chosen by Barbenel (1974) and Pruim (1978); and (ii) the hypothesis that each muscle generates a force proportional to its cross-sectional area (Crowningshield, 1978; Amis, 1980).

In this work, the author uses Ben-Nissan's (1987) calculations for vectors representing the muscle forces because it combines both of the approaches above. Ben-Nissan's calculated values also refer to the muscle forces estimated by Barbanel (1975), Throckmorton (1985) and Pruim (1980). The muscle force exerted during isometric contraction is directly proportional to the IEMG in a quantitative relation that takes into account, for calibration purposes, the maximum value of a single muscle recorded during an experimental session.

5.4.4 Reaction force positioning

Another issue to consider in a critical review of past biomechanical models is how the movement of the TMJ influences the location of condyle reaction forces. Since the articular disc is bound to the condyle by discal ligaments, the only physiological movement that can occur between these surfaces is a rotation of the disc on the articular surface of the condyle. Nevertheless, because the disk is not attached to the articular fossa, the former is able to slide on the condylar surface when the mandible is

protruded, as discussed previously. In this work, the dynamics of condyle reaction are investigated in order to determine the influence of positioning the reaction force vector on predictions on mandibular stress and strain.

Meijer (1993) experienced how applying the loads on a larger scale geometry determined a different biomechanical behaviour. Kavanagh (2008), whose model was also based on computed tomography scan data, used areas instead of nodes for load application. Nevertheless, he built a model exclusively for a resting position which had condyles unrealistically fully constrained at the top surface.

In this current study, the reaction force is distributed over the condylar surface rather than a single node and its components depend on the direction and magnitude of each muscle force component and functional loading. The necessity for reproducing a realistic model rests on a good level of detail of the scanned anatomical body, appropriate and realistic constraints and adequately placed musculature during common functional loadings of clenching, protrusion and opening of the mandible.

For this reason, the possibility to alter the area of application of condyle force reaction suits the actual complexity of the movements of the condyle during different functional movements. As Koolstra (2004) suggested, the deformations in the cartilaginous structures in joints are caused by the mutual displacements of the articulating body segments. Therefore, the areas on the condyle where major stress occurs are shifted during the functional movements, requiring attention on the reaction force position (Figure 5.3).

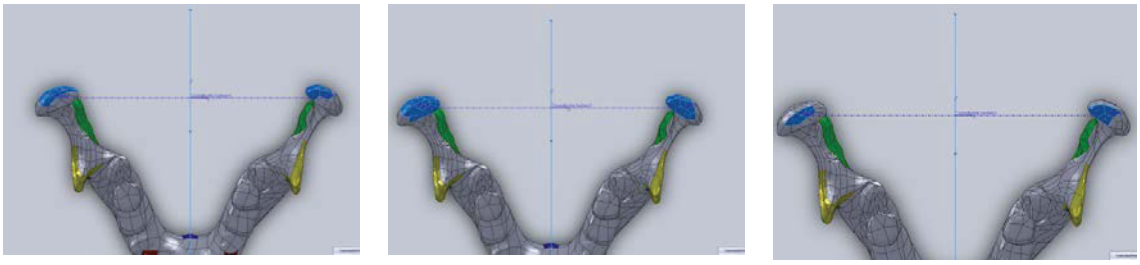

Figure 5.3 Variable area for reaction force application during clenching simulation (SolidWorks Educational Edition, c. 1195-2008, Dassault Systemes©)

5.4.5 Finite element analysis application

Finite element analysis (FEA), in principle, solves a complex problem by redefining it as the summation of solutions of a series of interrelated simpler problems. The complex geometry is decomposed into a set of 'finite' dimensions that form the 'meshed' model of the analysed object. Each finite element is limited by nodes, and knowing its internal strain function, one can write equilibrium equations corresponding to each degree of freedom of each node.

The analysis starts by dividing the complex body to be examined into finite simpler elements through a user-controlled mesh generation. In the case of a static structural analysis of a linear isotropic material to each element, a value for density, modulus of elasticity and Poisson's ratio is assigned.

Loads are applied at specific nodes or groups of nodes (area) that are constrained by setting certain nodal displacements to known values. At this point, the system is composed of many linear algebraic equations and many degrees of freedom are solved so that for each node a vector of displacement is calculated. The solution to the system of equations depends on boundary conditions imposed on the solid model

Finally, it is possible to calculate the element strain and stresses generated by the strain through an interpolation between nodes relative to the same element. All three-dimensional FEMs of the mandible require a meshed solid model input. As stated earlier, models were produced and used to interpolate digitalised sections of dry mandibles in order to reconstruct a solid body under the form of a CAD object readable by the finite element pre-processor.

The use of laser (Tsukrov et al., 2009) or CT scans on dry mandibles represented a significant improvement in determining a detailed morphology of the bone. Nevertheless, the real innovation, as pursued in this research, is the use of CT to scan the mandible from living subjects.

As Taddei (2004) suggested, it is well known that CT images can provide fairly accurate quantitative information on bone geometry since the attenuation coefficient of

bone tissue is much higher than the one of surrounding soft tissues, resulting in well contrasted edges.

Taking into account these aspects, this work improves on previous models for its approach regarding reaction forces acting on the condyles during functional movements and the muscles insertion topology, which takes into account areas rather than single nodes. Considering that these two aspects will be combined with a PS bone density mapping, that is, medical grade CT at a local level and then combined with clinically relevant applications, the author believes that the proposed model has the potential to become significant among published simulations on the mandible.

CHAPTER 6:
RESULTS AND DISCUSSION OF THE COMPARISON BETWEEN THE GENERIC MODEL AND PATIENT SPECIFIC MODEL

6.1 Introduction

Based on previously published models and data, von Mises stress and deformation was calculated for each developed model and compared to the literature for mandibular models. Firstly, a two-bone GEN model was analysed, followed by the PS model referred to in this chapter as MI and MII.

The justification for using von Mises stress for the comparison of validity is based on appropriate stress calculations in published medical models in both orthopaedic and maxillofacial applications.

In materials science and engineering, the von Mises yield criterion can also be expressed in terms of the von Mises stress or equivalent tensile stress. To further the discussion and its relevance to this thesis, a material is said to start yielding when the von Mises stress reaches a value known as yield strength. The von Mises stress is used to predict yielding of materials under complex loading from the results of uniaxial tensile tests. In this thesis, von Mises stress is used to give an indication of whether the various fracture fixation systems designed will fail under load, being primarily clenching.

The von Mises stress is calculated from six stress components normally present in homogeneous structures which can be defined as safe under load when the generated stress is less than the absolute value of the yield stress in tension or compression (tested during uniaxial loading).

Von Mises stress values are defined as the beginning of deformation for ductile materials, since failure occurs when von Mises stress values exceed the yield strength of a material. The von Mises stress is calculated from six stress components normally present in three-dimensional stress analysis of homogeneous structures. The structure is safe when the von Mises stress is less than or equal to the absolute value of the yield stress in tension or compression, as determined in a uniaxial tension of compression test on a sample of the same material.

$$\sigma_{\text{Von Mises}} = \frac{[(\sigma_{xx} - \sigma_{yy})^2 + (\sigma_{xx} - \sigma_{zz})^2 + (\sigma_{yy} - \sigma_{zz})^2 + 6(\sigma_{xy}{}^2 + \sigma_{xz}{}^2 + \sigma_{yz}{}^2)]^{\frac{1}{2}}}{\sqrt{2}}$$

From the von Mises stress equation it is evident that any value calculated by this would be positive, regardless of the sign of different stress components.

For evaluating the reliability of the simulation, this work was compared with models presenting the same biomechanical configurations. In 2005, Choi published the highest von Mises stresses observed in the mandible during clenching and wide opening (Table 6.1 & Figure 6.1) using the same load set of this work, which was firstly calculated from a cross-section of cadaver muscles from Ben-Nissan in 1987.

Table 6.1 Maximum von Mises stresses recorded during functional movements in Choi et al(2005)

	von Mises stress (MPa)	
	Cortical	**Cancellous**
Clenching	38.91	4.27
Opening	35.47	2.56
Protrusion	35.44	2.56

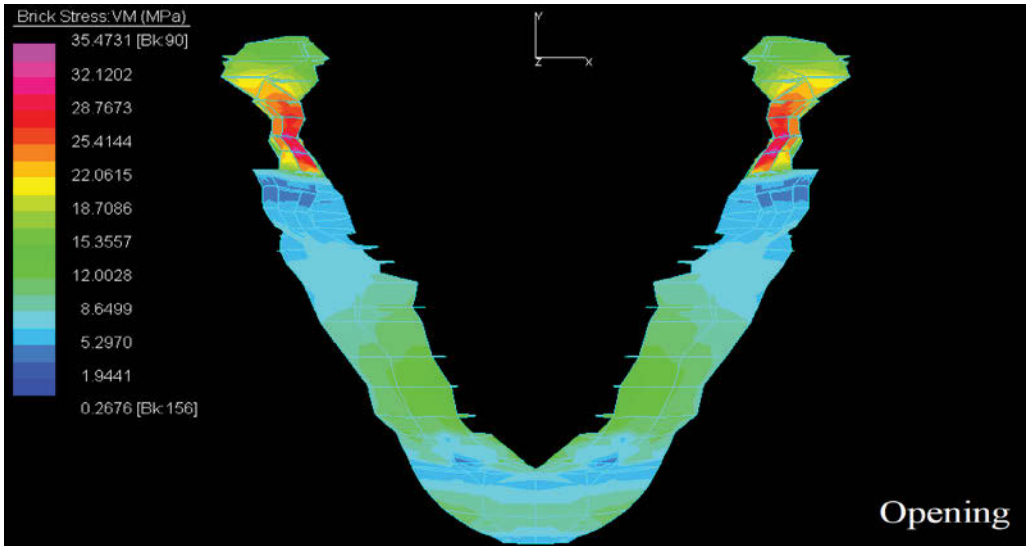

Figure 6.1 Representation of results obtained by Choi et al. (2005) for von Mises stresses

6.2 The generic model (MI)

The MI model developed results for mandibular distortion in the first and second molar region respectively. The results were obtained by probing the deformed model on a surface comparable to the dimension of a molar tooth (Figure 6.2).

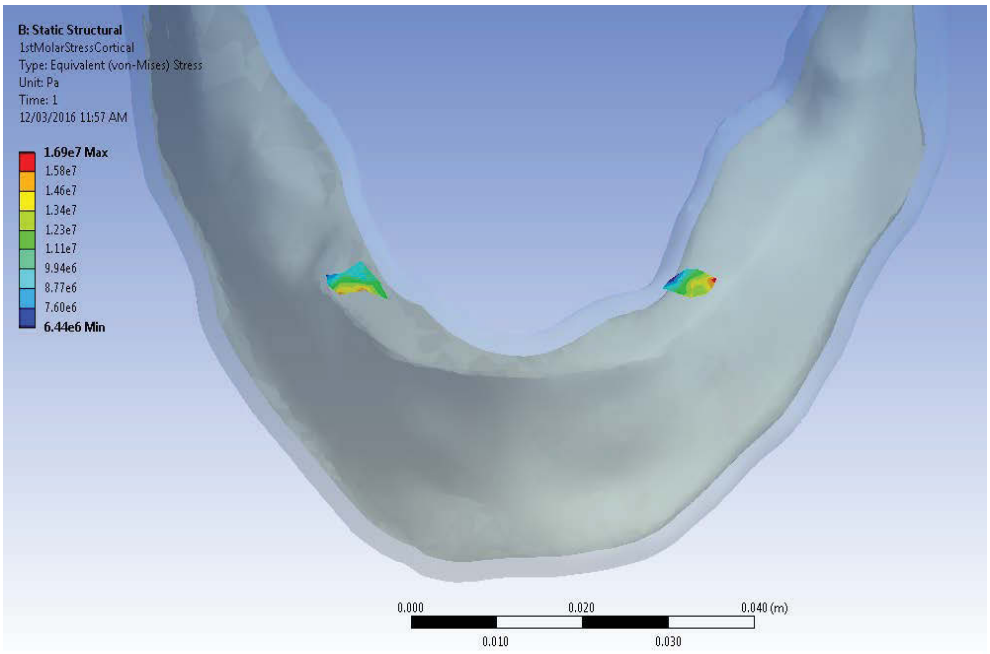

Figure 6.2 Probing of the equivalent stress in the molar region (modified from Taraschi, 2016)

Additional verification came from plotting the resulting stresses in bands clearly visible through the molar regions and normalised to the ranges of stresses observed in the areas of interest, as illustrated in Figure 6.3.

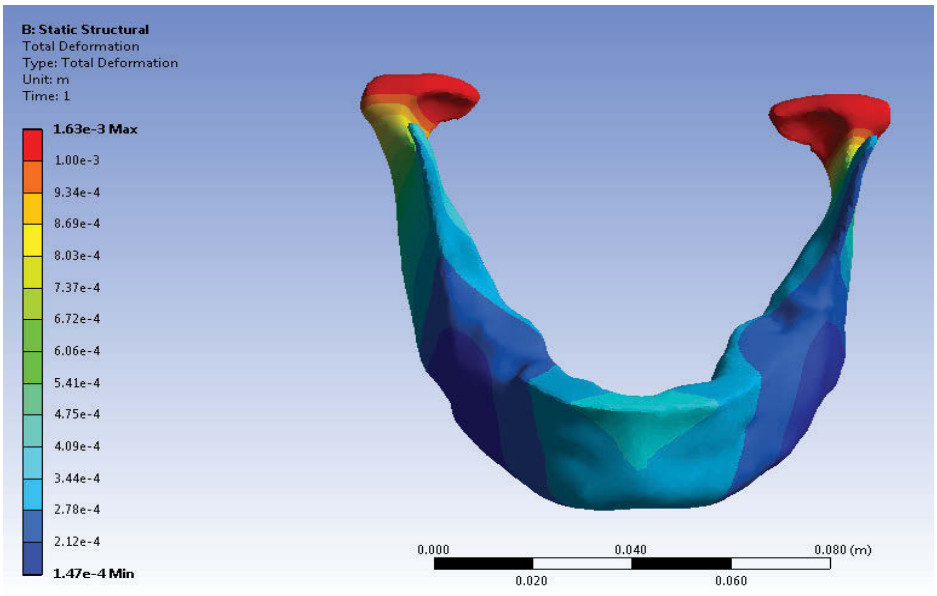

The deformation scale (visible on the left) has been normalised to promote discretisation of colours, and therefore distinct stress ranges in the molar regions.

Figure 6.3 Example of deformation colour bands for visualising the simulation results (modified from Taraschi, 2016)

A maximum deformation of 0.96mm during clenching was located on the left condyle (Figure 6.4) with maximum deformation being at the left condyle in opening (Figure 6.5). Whilst much higher than the fixation system deformation system results in Chapter 8, the results above correlate well with data previously published by Ben-Nissan, and serves to validate the model.

The deformation results for Ben-Nissan's model showed a maximum distortion of approximately 1.00mm deformation around the condyles. The same biomechanical load set was applied from Ben-Nissan's work with Young's modulus values of respectively 17.2GPa and 1.3GPa. A maximum distortion in the range of 0.32 to 0.35mm was found for the molar regions for clenching and between 0.30mm and 0.32mm for wide opening. These values match the experimentally and clinically measured values (Ben-Nissan, 1987).

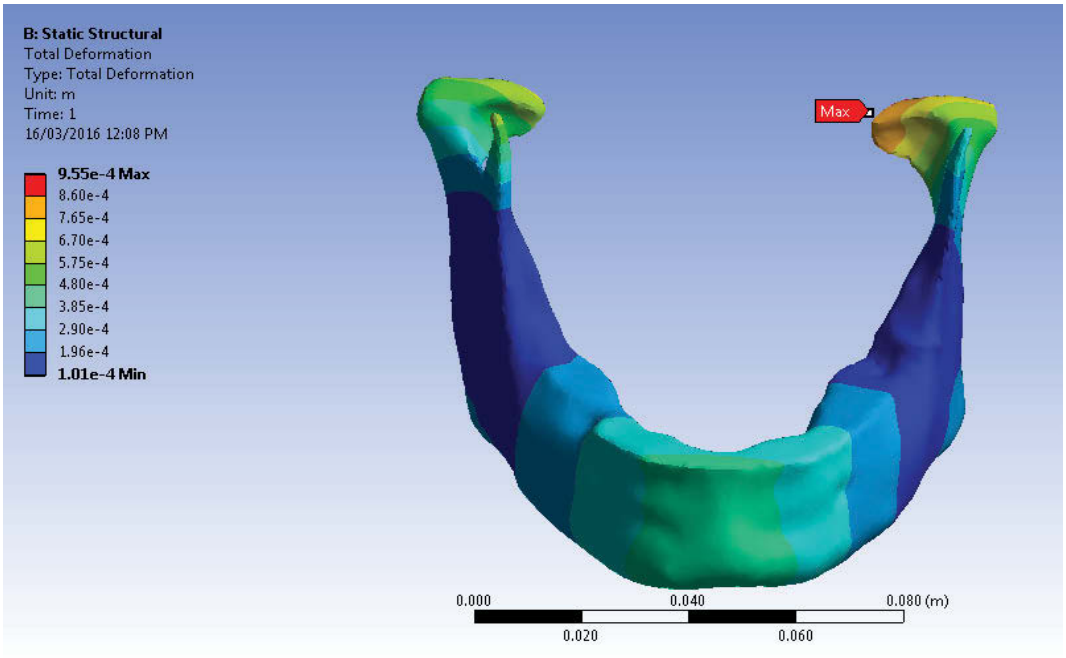

Maximum deformation is observed in the left condyle. The asymmetric deformation between the two condyles is due to the lack of symmetric morphology in the model.

Figure 6.4 Deformation during clenching (modified from Taraschi, 2016)

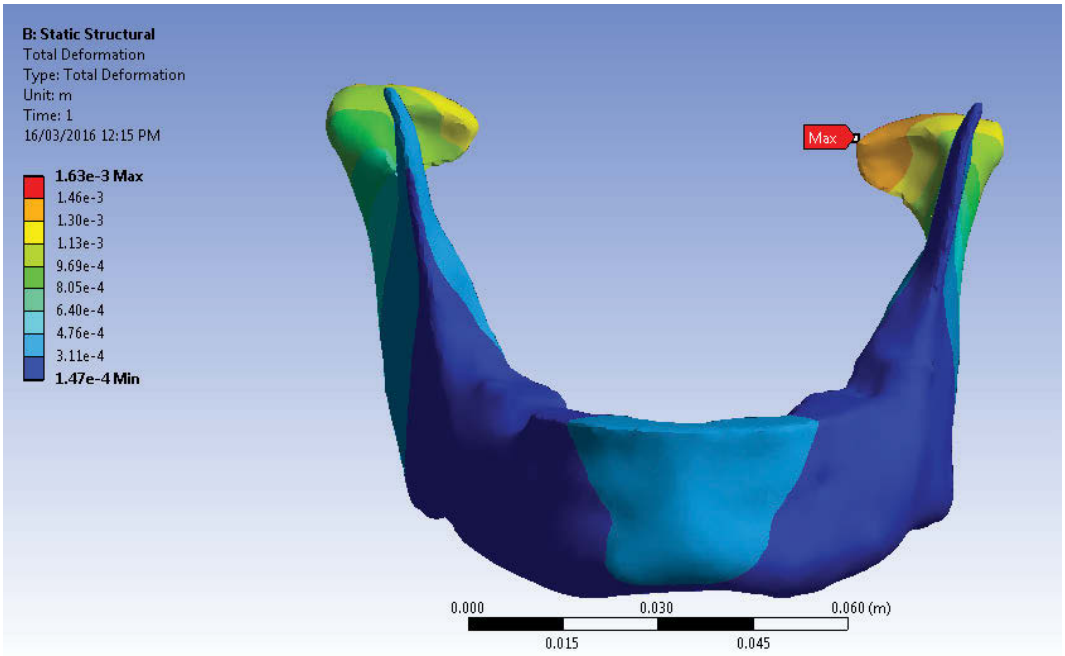

Maximum deformation is observed in the left condyle. The asymmetric deformation between the two condyles is due to the lack of symmetric morphology in the model.

Figure 6.5 Deformation during wide opening (modified from Taraschi, 2016)

As seen in Table 6.2, distortions obtained for the first and second molar regions are also aligned with other results recorded in literature for similar mandibular models.

Table 6.2 Results for maximum distortion in the first and second molar region during clenching and wide opening movement compared with previous investigations

		1st molar (mm)	2nd molar (mm)
MI	Clenching	0.35	0.32
	Wide opening	0.32	0.30
Kollner, 1978*	Wide opening	0.2	
Ben-Nissan, 1987	Clenching	0.3 – 0.4	0.32
	Wide opening	0.43	0.51
Gates & Nicholls, 1981*	Wide opening		0.31
Chen, 2000	Wide opening	0.44	

* measured

Maximum stress concentration for the presented model was registered in the right coronoid process. This behaviour is most likely due to the very thin section of the bone model which generates sharp features during meshing and is pertinent to the results for the PS model reported in Chapter 8.

To explain this anomaly in further detail, the MI and MII models are made of separate solids representing the cancellous bone inside an external shell representing the superficial cortical bone. For this reason, regions like the coronoid process result in very thin walls that are often difficult to mesh through an automatic mesh generator which is required to generate PS shapes. In comparison, models made using only one solid with averaged material properties are not exposed to these modelling singularities. The combination of thin walls and poor local mesh features creates unrealistic maximum equivalent stresses that must be interpreted and, if necessary, discarded (Figures 6.6 & 6.7). The understanding and interpretation of this in the data produced is of particular importance as this does occur with the results produced from the PS fracture plate data in Chapter 8 giving a spuriously high reading. With correct interpretation of this unrealistic maximal von Mises stress, the remaining data can be correctly interpreted and relied upon.

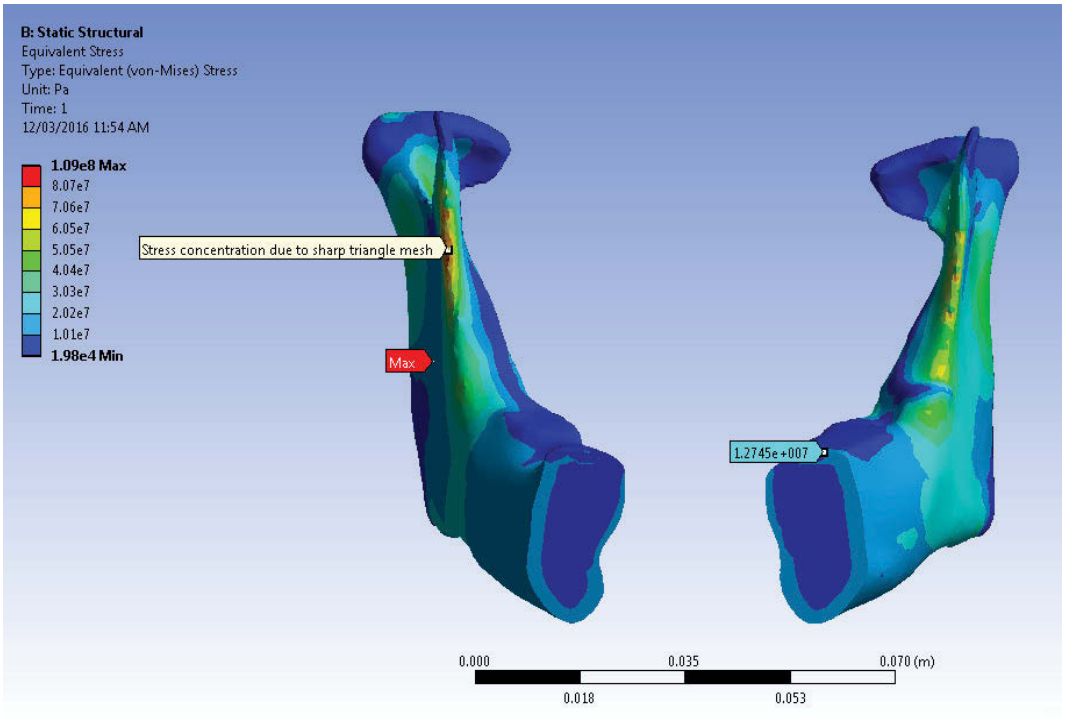

The section on the right coronoid process is erroneous, as explained in previous text, however, the value at the left premolar region is valid.

Figure 6.6 Erroneous von Mises stress maximum during clenching (modified from Taraschi, 2016)

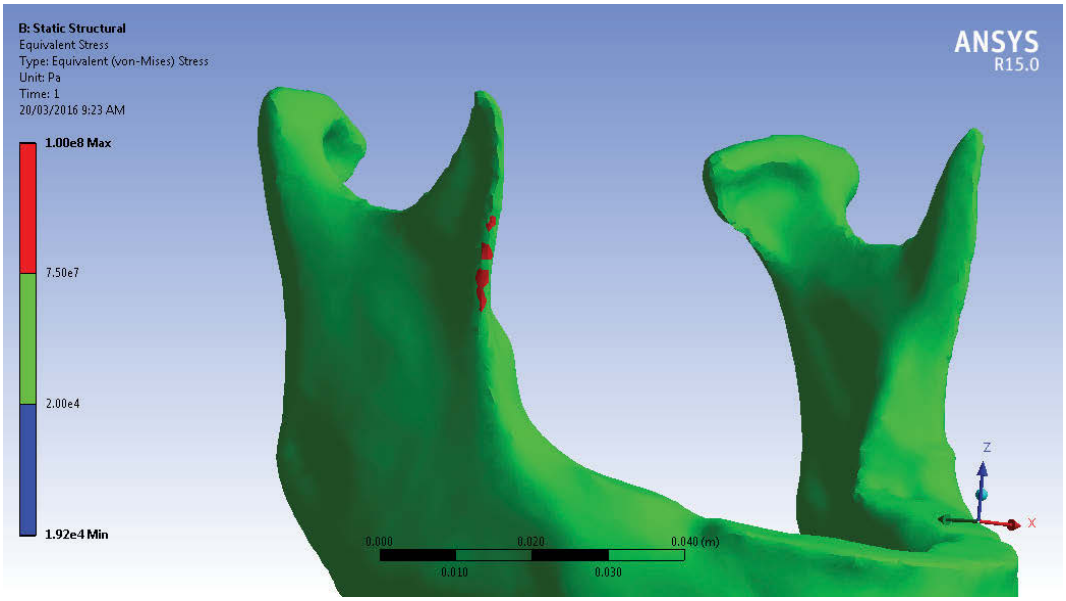

Again, stress concentration in the right coronoid process is erroneous due to the poor accuracy of the triangles in meshing thin areas.

Figure 6.7 Erroneous von Mises stress maximum during clenching (modified from Taraschi, 2016)

The simulations recorded erroneous maximum von Mises stresses of 75MPa during wide opening located on the left mandibular notch (thin wall) and 79MPa during clenching on the bony ridge of the right coronoid process.

In contrast, the results for the premolar regions show von Mises stresses between 23MPa and 25MPa for clenching and between 9MPa and 11MPa for wide opening, as reported in Table 6.3. These results are comparable with the ones obtained by Choi (2005) with a FEM based on a similar biomechanical configuration.

Table 6.3 Results for maximum von Mises stress in the first and second molar region during clenching and wide opening movement.

		1st molar region von Mises stress (MPa)	2nd molar region von Mises stress (MPa)
MI	Wide Opening	9.1	11.2
	Clenching	25.4	23.8
Choi (2013)	Wide Opening	10-12	9-11
	Clenching	16-18	13-15

These results align with stress and distortions found for a wet human mandible during bilateral clenching and wide opening functional movements. Similar to the studies of Ben-Nissan (1987), Gates and Nicholls (1981), Choi (2005) and Taraschi (2016), the author proposes that the model is valid and can be confidently used to analyse biomechanically the responses of the mandible to various fracture fixation systems. In particular, such simulation has grounds to realistically predict stresses and distortions at the surgical site for which such fixation systems would be utilised.

6.3 The patient specific model (MII)

For a CT scan generated model, results were obtained for mandibular distortion and stresses in respectively the premolar region by probing the deformed model on areas comparable to the dimension of a tooth as was also performed on the MI model. The results are shown in Table 6.4 and Table 6.5 where a comparison with the MI model is given.

Table 6.4 Results for mandibular deformation of the MII model during wide opening compared with values obtained in the MI model

Wide Opening – Deformation (mm)	2nd molar region	1st molar region	Max
MII	0.15-0.18	0.12-0.15	1.29
MI	0.30	0.32	1.63

Table 6.5 Results for mandibular deformation of the MII model during clenching compared with values obtained in the MI model

Clenching – Deformation (mm)	2nd molar region	1st molar region	Max
MII	0.12-0.15	0.09-0.12	1.00
MI	0.32	0.35	0.96

In order to better visualise stresses from the simulations in the premolar region, Figures 6.8 to 6.15 illustrate by colour bands the results obtained from varying perspectives. The premolar region is concentrated on since this will be the area for incorporation of the fracture in the model, as introduced in Chapter 7.

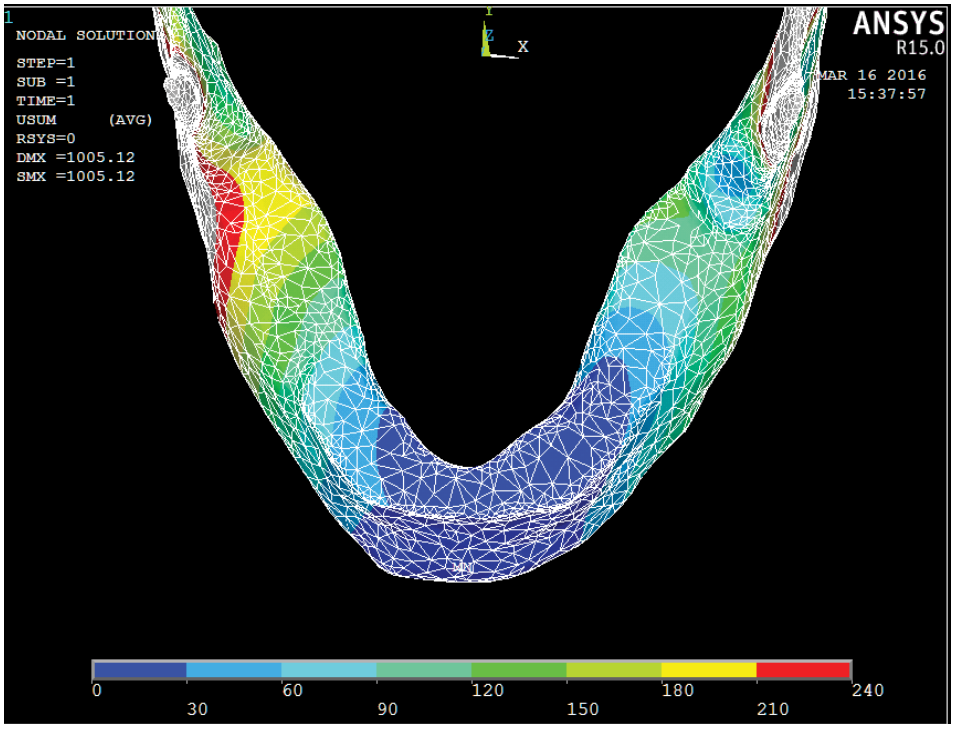

Figure 6.8 Colour bands corresponding to deformation during clenching (scalar values are in micrometers) (results post-processed with ANSYS APDL; modified from Taraschi, 2016)

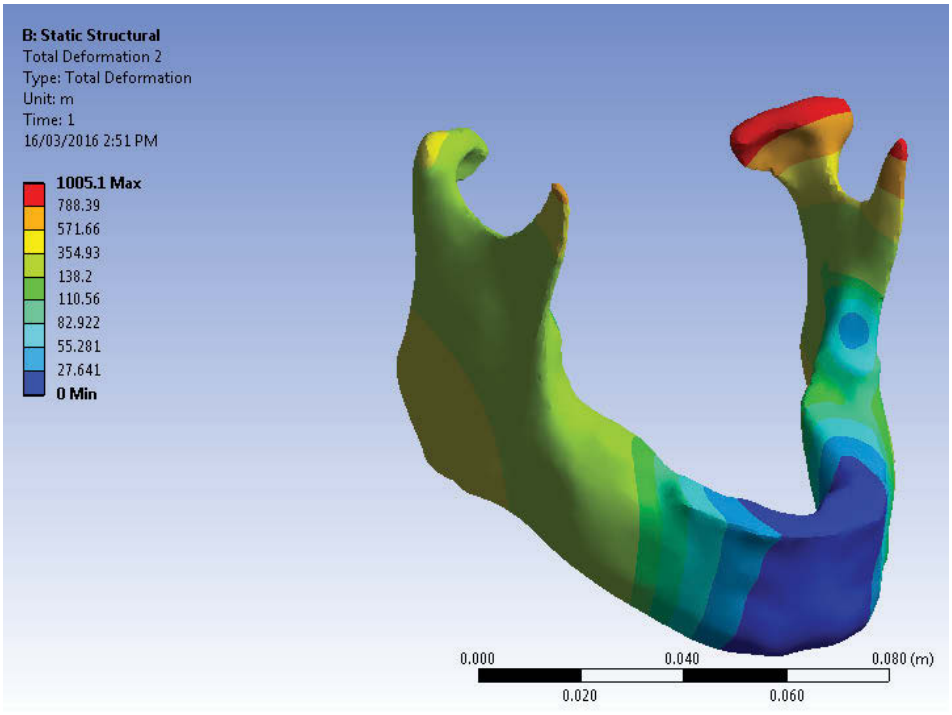

Figure 6.9 Results for deformation during clenching visualised in ANSYS Workbench Mechanical (modified from Taraschi, 2016)

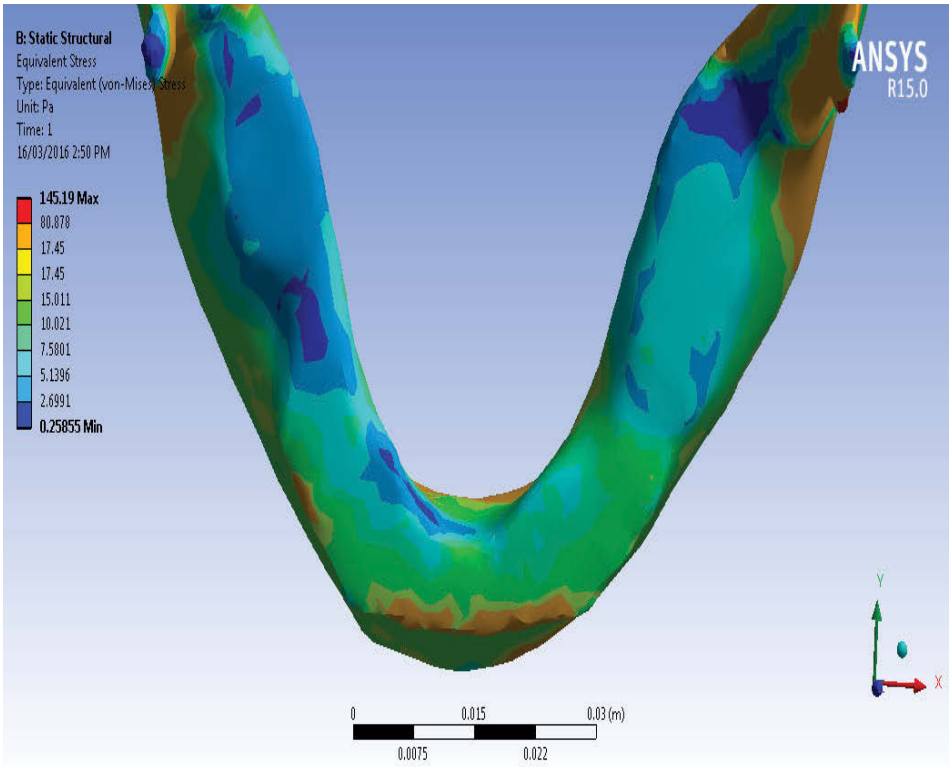

Figure 6.10 von Mises stress in premolar regions during clenching (units are MPa) (modified from Taraschi, 2016)

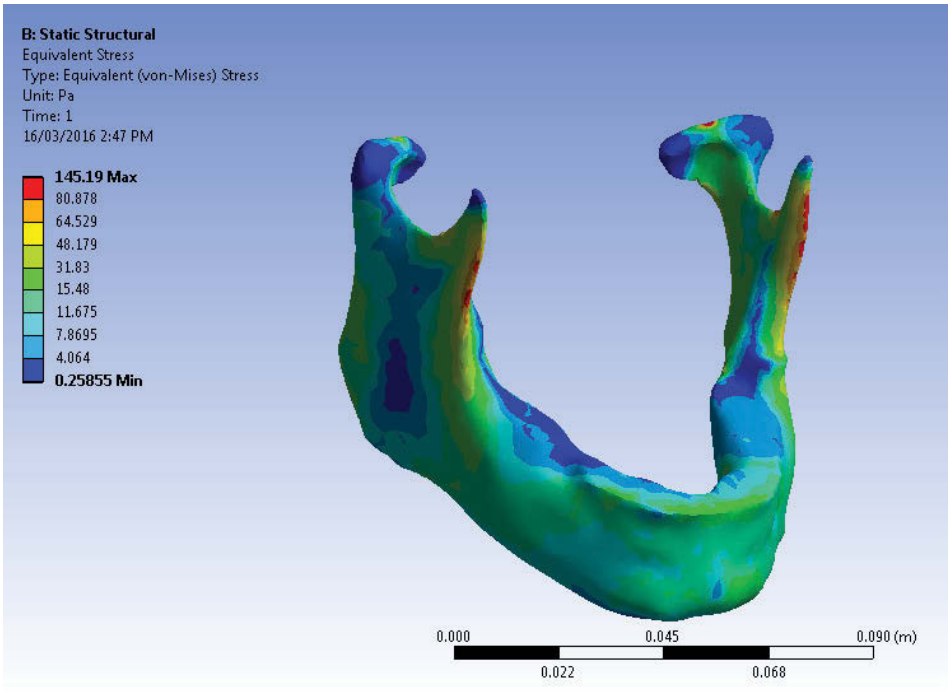

Figure 6.11 **von Mises stress during clenching showing higher stresses on the coronoid processes (units are MPa) (modified from Taraschi, 2016)**

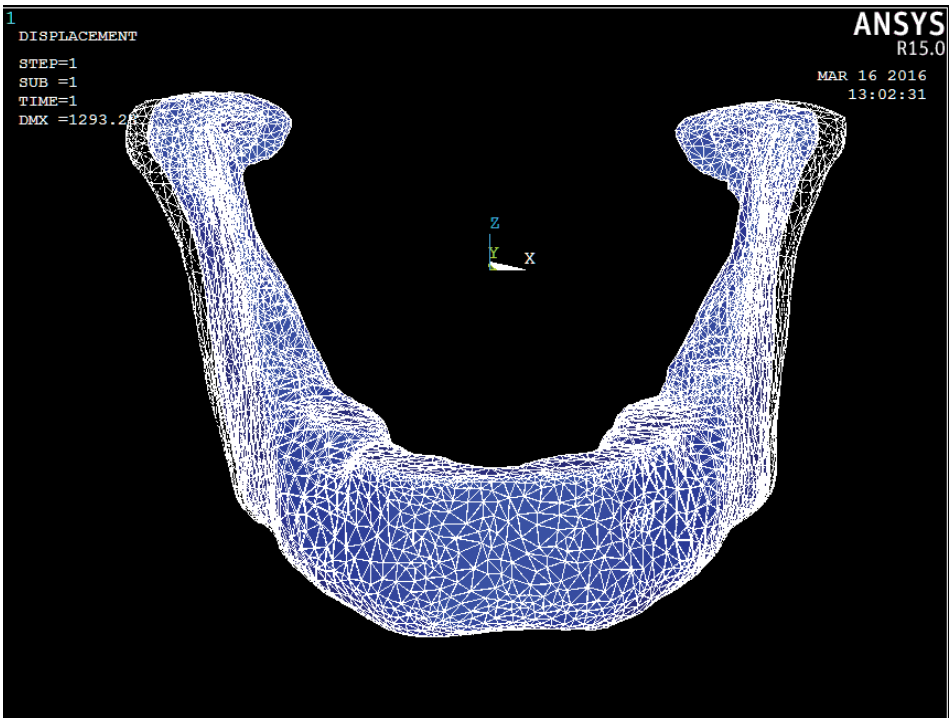

Figure 6.12 **Deformed shape (coloured blue) versus undeformed shape during wide opening movement (modified from Taraschi, 2016)**

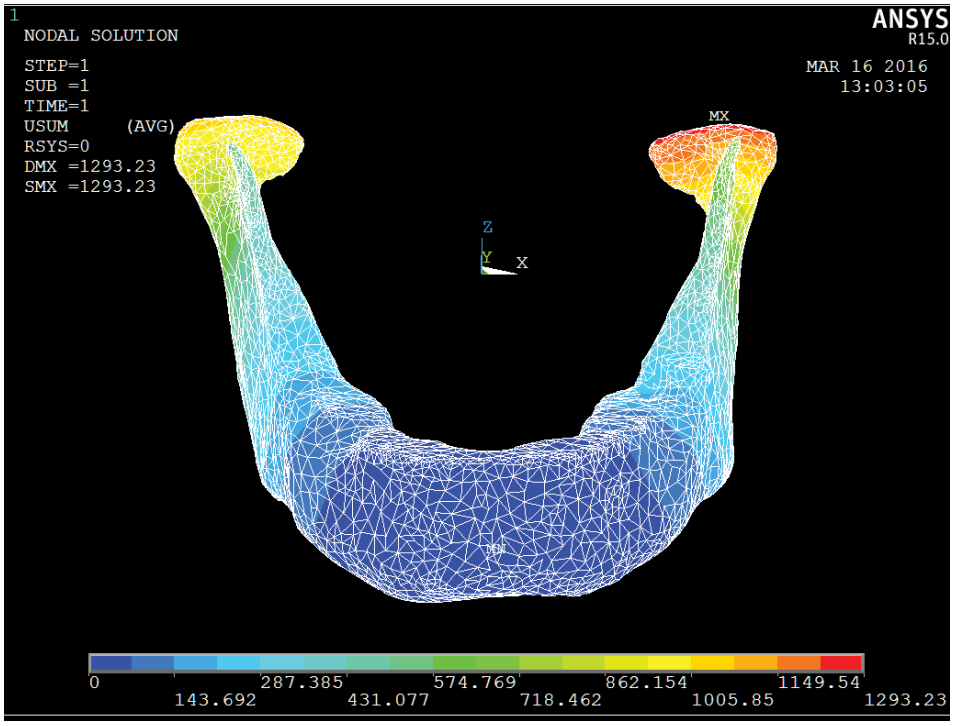

Figure 6.13 Mandibular distortion during wide opening movement (units are in Pa) (modified from Taraschi, 2016)

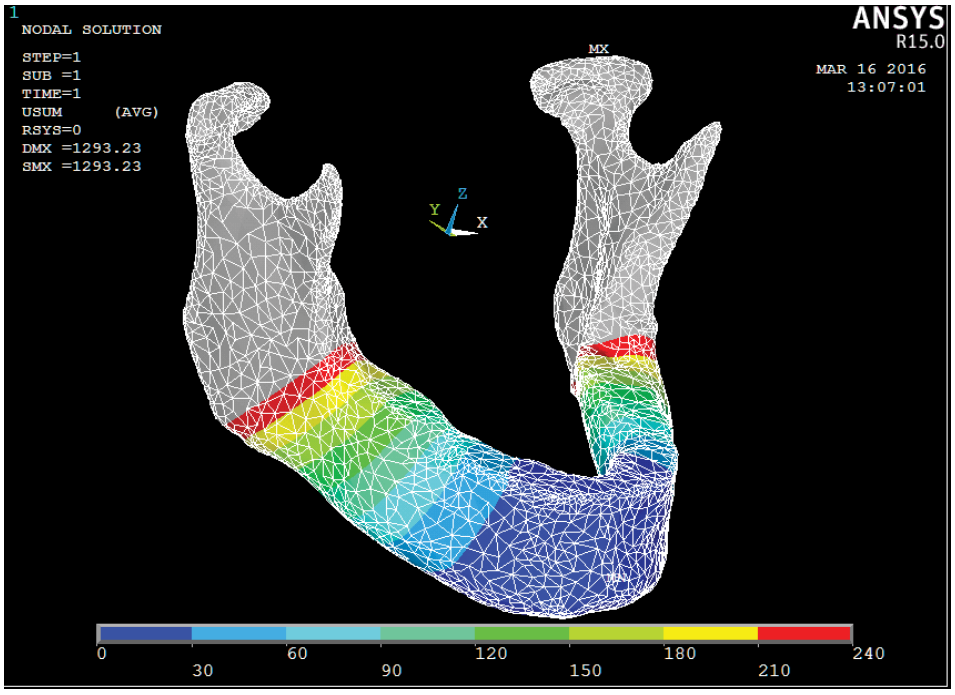

Figure 6.14 Colour bands corresponding to deformation during wide opening (values are in micrometers) (modified from Taraschi, 2016)

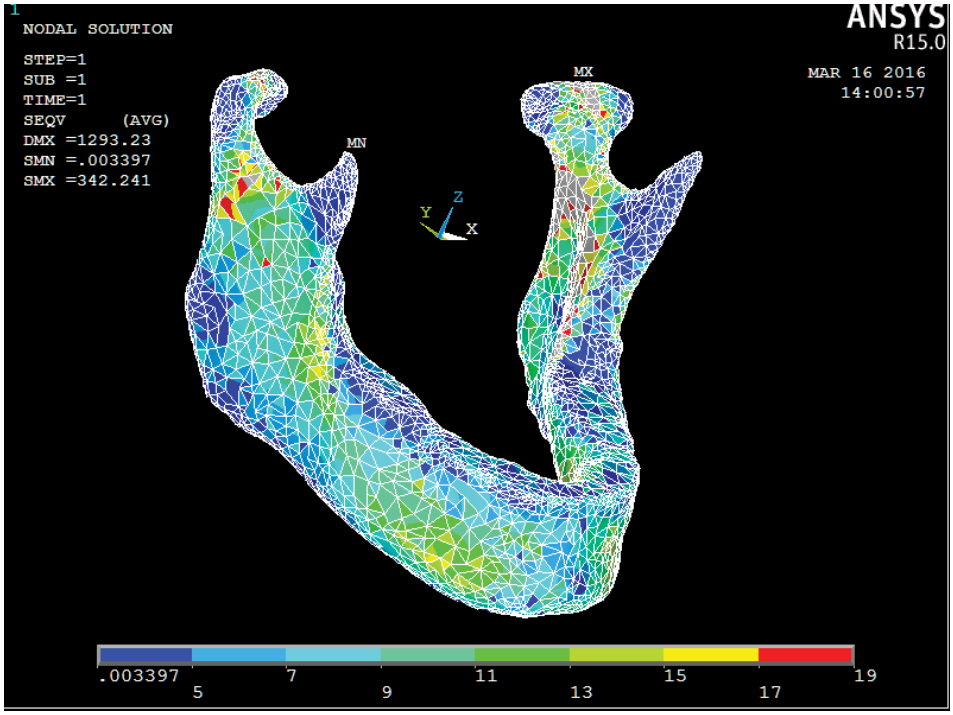

Figure 6.15 von Mises stress during wide opening (units are Pa) (results post-processed in ANSYS APDL; modified from Taraschi, 2016)

In summary, the results in Tables 6.2 to 6.5, correlated with Figures 6.12 to 6.19, best illustrate how the performance of the GEN and PS models are matched to previously published and well established models, such as those of Choi (2005) and Ben-Nissan (1987), and in doing so, validate the subsequent data produced, explain the occurrence of erroneous peak stress in the PS model and do not distract from the accuracy of the remaining results.

CHAPTER 7:
THIRD OUTPUT – MANDIBULAR FRACTURE AND REPAIR MODELLING METHOD

7.1 Introduction

In this chapter, the methods related to the collection of data results will be explained, specifically, additional modelling carried out to design a simple linear fracture of the right edentulous mandibular body with analysis related to the insertion of several fracture fixation systems and the related stress strain analyses. The following sections are covered:

7.2 Fracture model of the mandible

7.3 Constants within the various analyses

- 7.3.1 Linear plate dimensions
- 7.3.2 Placement of fracture plates
- 7.3.3 Material properties data

7.4 Design of the fixation systems to be analysed

- 7.4.1 Linear plate varying screw hole diameter
- 7.4.2 Linear plate varying thickness
- 7.4.3 Linear plate varying material (Ti-6Al-4V, PLA and ZrO_2)
- 7.4.4 Linear composite laminated plate (Ti-6Al-4V and PLA)
- 7.4.5 Mesh plate design
- 7.4.6 Patient specific plate

7.5 Description of each analysis for design variations

- 7.5.1 Variation in old versus new fracture sites for a 1.0mm thick Ti-6Al-4V plate with 2.25mm diameter screw holes under the functional movement of clenching (measuring von Mises stress)
- 7.5.2 Variation in functional movements of clenching, opening and protrusion for a 1.0mm thick Ti-6Al-4V plate with 2.25mm diameter screw holes (measuring von Mises stress and distortion)

7.5.3 Variation in screw hole diameter of a Ti-6Al-4V linear fracture plate under the functional movements of opening, protrusion and clenching (measuring von Mises stress and distortion)

7.5.4 Variation of a Ti-6Al-4V plate with thicknesses of 0.5mm, 1.0mm and 2.0mm respectively under the functional movement of clenching with screw hole diameter constant at 2.25mm (measuring von Mises stress and distortion)

7.5.6 Results for von Mises stress with variation in plate material, Ti-6Al-4V, PLA and ZrO_2 under the functional movement of clenching with plate thickness and screw hole diameter constant at 1.0mm and 2.25mm respectively (measuring von Mises stress and distortion)

7.5.7 Variation in a linear laminated fracture plate (measuring von Mises stress and distortion)

7.5.8 Variation in mesh fracture plate (measuring von Mises stress and distortion)

7.6 Application of linear design plate across a fracture in the PS model (measuring von Mises stress and distortion)

7.7 Measurement criteria for data collection and presentation of date

7.2 Fracture model of the mandible

The fracture model of the edentulous mandible was carried out using the first model by STRAND and consists of 1635 nodes and 258 brick elements (Figure 7.1). The mandible was cross-sectioned vertically into 28 sections. Each cross-section of the bone was divided into five sections, the outer four representing the cortical bone and the inner one representing the cancellous bone.

To improve the accuracy of the model and introduce the fracture (in the premolar region), a section was taken from right hemimandible that extended from the first molar to the third molar region and was reconstructed as this would be the position for generating the fracture site and later an interface for the fracture fixation systems (Figures 7.2, 7.3 & 7.4). For higher output and accuracy, smaller and finer solid elements (Hexa20) were generated for both the cortical and cancellous bone in this section.

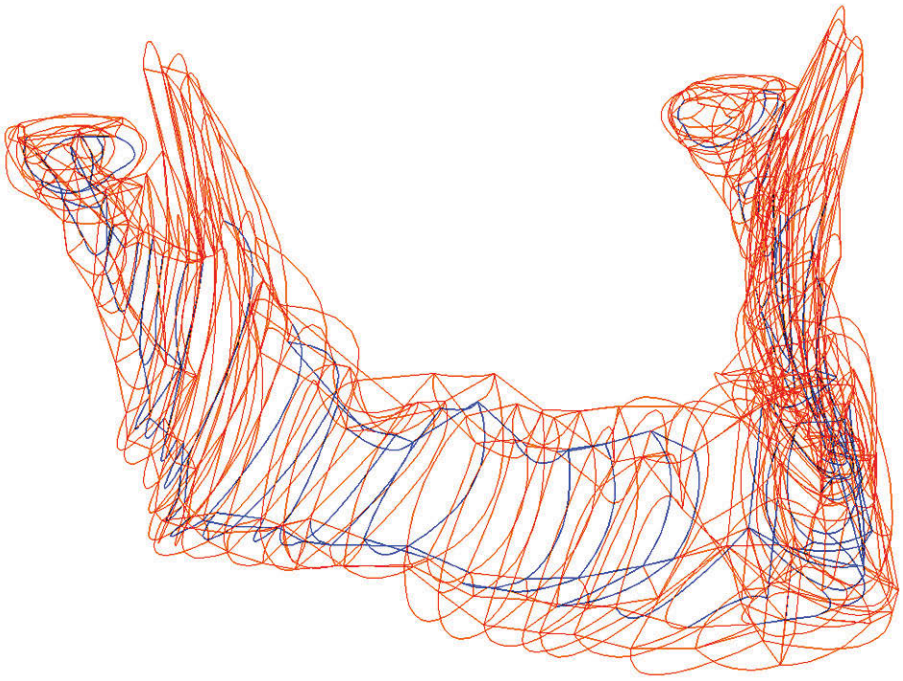

The cortical bone outline is represented in orange and the cancellous bone inner layer is represented in blue.

Figure 7.1 Finite element wire frame mandible model (produced in STRAND7) (modified from Choi, 2005)

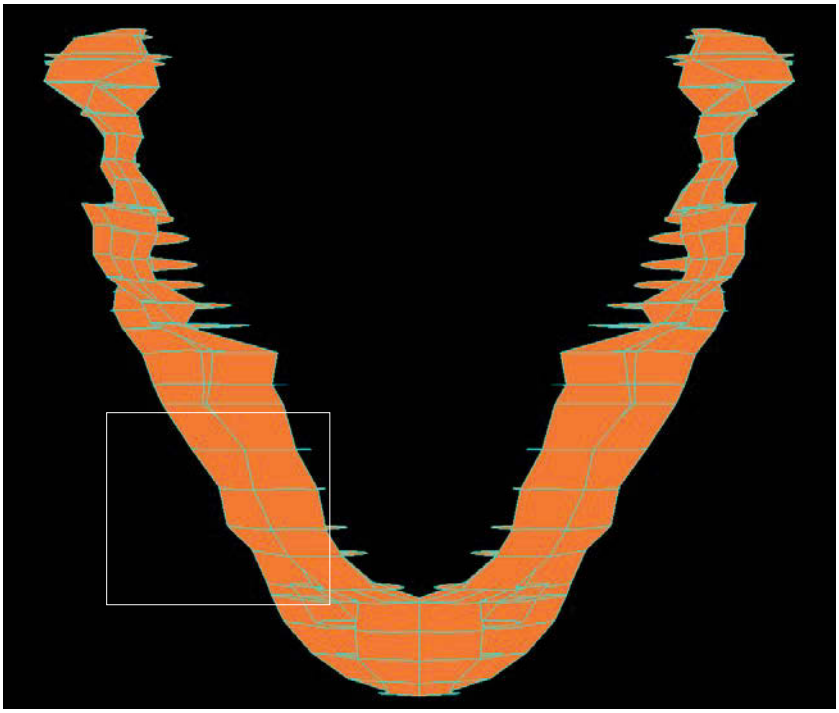

Figure 7.2 Location of the original section before reconstruction on the mandible model (modified from Choi, 2005)

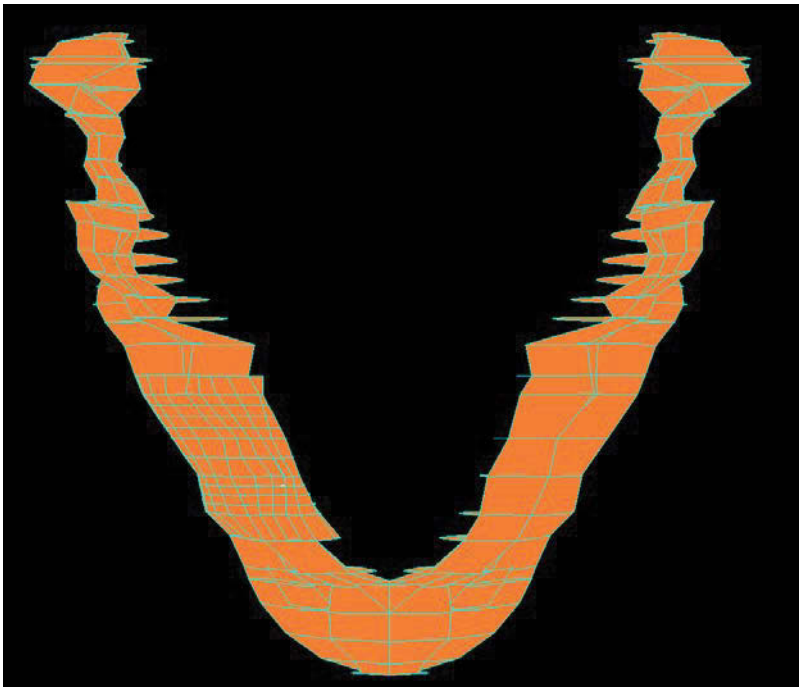

Figure 7.3 Location of the original section after reconstruction on the mandible model (modified from Choi, 2005)

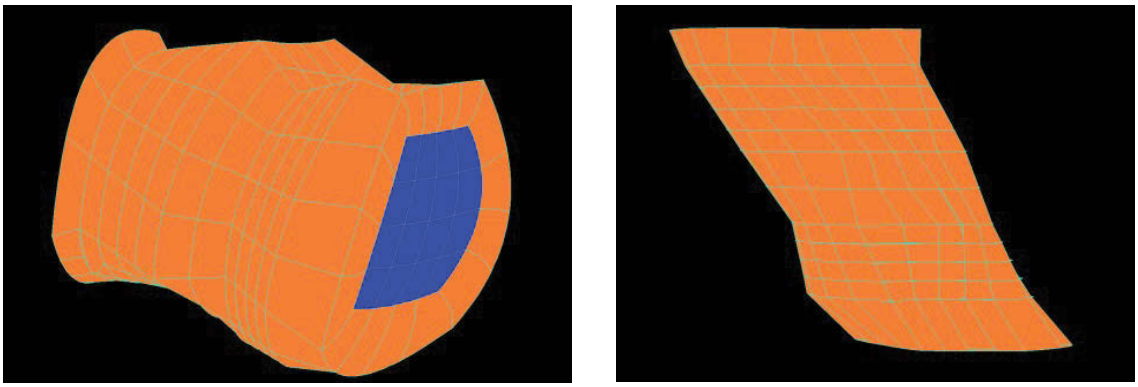

(A) (B)

Figure 7.4 Section after reconstruction: (A) three-dimensional view; (B) top view (produced in STRAND7 modified from Choi, 2005)

As previously mentioned, a fracture was introduced on the right side of the hemimandible between the second premolar and the first molar. A homogeneous layer of callus 0.01mm thick was used to simulate the process of fracture healing (Figure 7.5). The immature callus tissue was assumed to behave in a homogeneous and linearly elastic manner, with an elastic modulus of 3MPa and a Poisson's ratio of 0.4 (Claes & Heigele, 1999; Vajgel et al., 2013; Murakami et al., 2015).

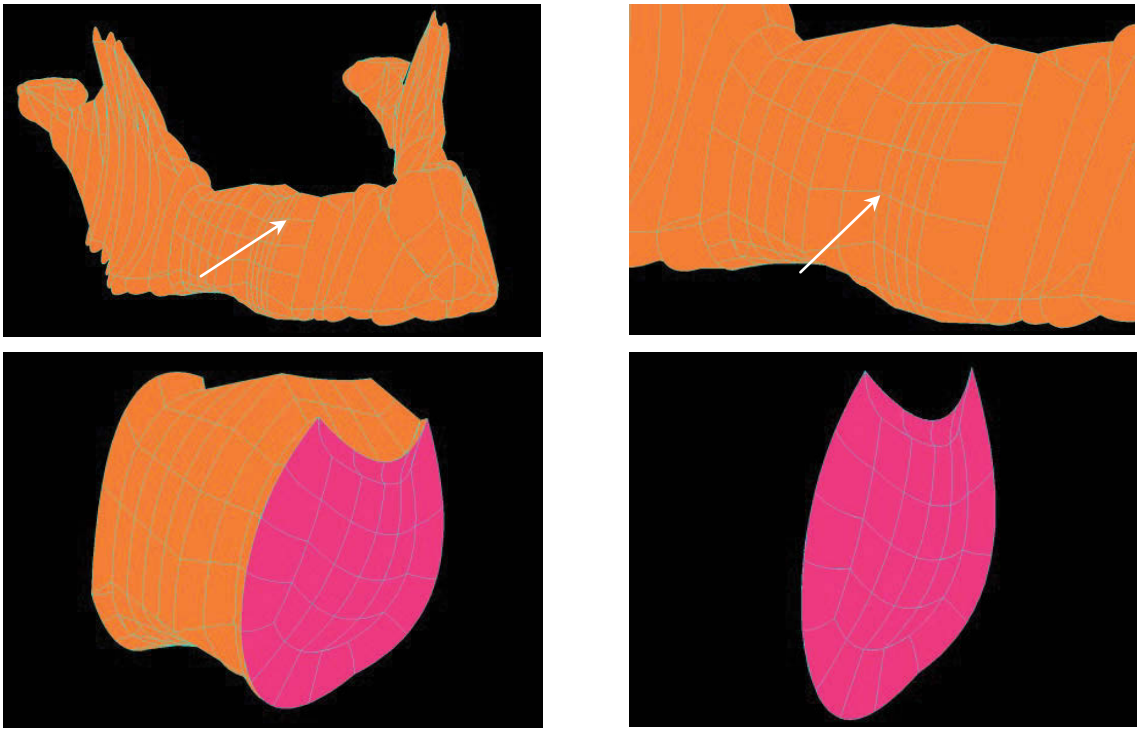

Figure 7.5 Location and modelling of the fracture site is shown by the arrows (modified from Choi 2005)

For finite element analysis (FEA), the mesh on the reconstructed section is difficult to interconnect with mesh on the mandible model. In order to overcome the connectivity problem, coupling links were used. For this analysis, eight coupling links were used to reconnect the cortical and cancellous bone on the reconstructed section to the mandible model. After connecting the fracture fixation system to the surrounding bone structure, the three-dimensional FEM was completed. For this analysis, three nodes on the symmetry plane were fixed in space through the utilisation of spring elements.

Once constructed, the model was modified by adding the various fracture fixation systems. These systems varied based on six parameters:

1. Variation in screw hole diameter
2. Variation in plate thickness
3. Variation in plate material
4. Composite laminate plate
5. Mesh plate
6. Patient specific plate

With each modification, analysis was performed and recorded for von Mises stress and distortion. The analysis consisted of distortion and von Mises stress with each measured and reported in two directions. For comparison throughout Chapter 7, Figure 7.6 shows the final stresses on the mandible during clenching and the distortions recorded prior to the addition of any fracture fixation system fracture.

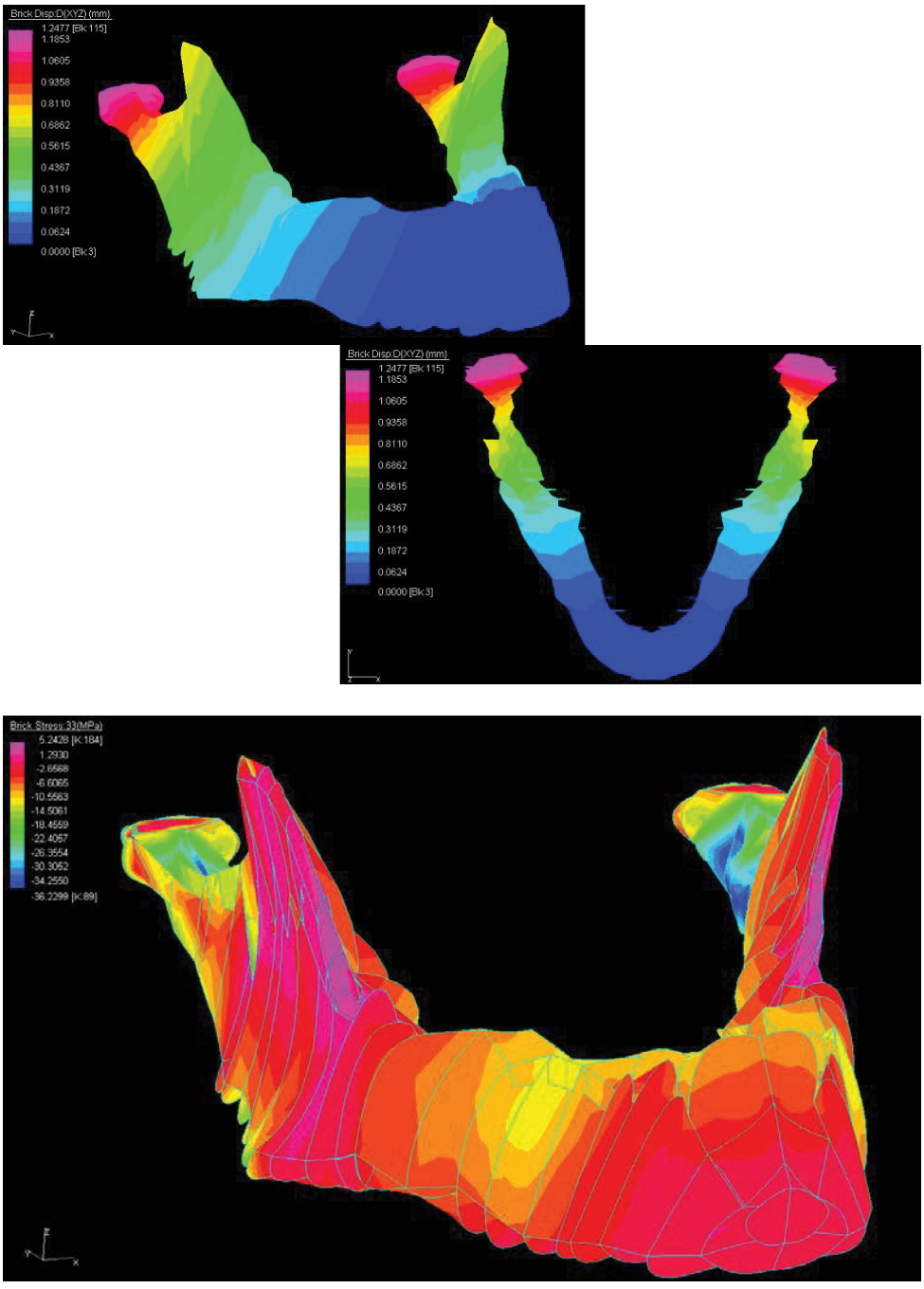

Figure 7.6 Three-dimensional FEM and analysis showing the distortion (top and middle) and compressive stresses (bottom figure) of the mandible under biting conditions (modified from Choi, 2005)

As explained previously, the premolar region of the horizontal mandibular body was chosen for fracture positioning because it is one of the most common sites for fracture in the edentulous mandible. As fracture fixation system most commonly use a linear 'plate' design, this configuration was also adopted for this thesis and then compared to several novel designs that were utilised.

7.3 Constants within the various analyses

7.3.1 Linear plate dimensions

Firstly, all linear plates were designed using the STRAND7 FEA (G+D Computing, Australia) package. All the fracture plates have an overall length of 19.5mm and a width of 3.0mm. The only systems analysed that fell outside of these constants were the mesh plate design and PS plate design for which specifics of each is discussed later.

7.3.2 Placement of fracture plates

Secondly, placement of the fracture plates required the plates to be modelled in such a way that they sat on top of the cortical bone and across the fracture site. The fracture would lie in the mid-point of the fracture plate in the longitudinal direction. This resulted in an equal distribution of the fracture plate (in terms of length) between the two ends of the fracture (Figure 7.7).

The ends of the fracture plates are directly fixed to the cortical bone to eliminate any modelling error created by the application of mechanical fixations, such as screws and pins. This will give us a direct contact between the fracture plate and cortical bone, as well as a better indication with respect to stress transfer at the plate-bone interface.

7.3.3 Material properties data

The material properties of mandibular cortical and cancellous bone and Ti-6Al-4V, PLA and ZrO_2 were taken from published results. The maximal von Mises stress that would produce failure the material was 800MPa, 200MPa, 1000MPa for Ti-6Al-4V, PLA and ZrO_2 respectively. The material properties for bone were determined on small specimens obtained from the mandibles of cadavers by means of ultrasonic wave methods (Ashman & Van Buskirk, 1987; Dechow et al., 1993; Pithioux et al., 2002) and

other material testing techniques (Arendts & Sigolotto, 1989, 1990). The cortical and cancellous bone of the mandible can be considered to be transversely isotropic, with a higher elastic modulus in the longitudinal direction and a lower elastic modulus in all transverse directions. Therefore, all individual elements for both cortical and cancellous bone in our model were represented as transversely isotropic.

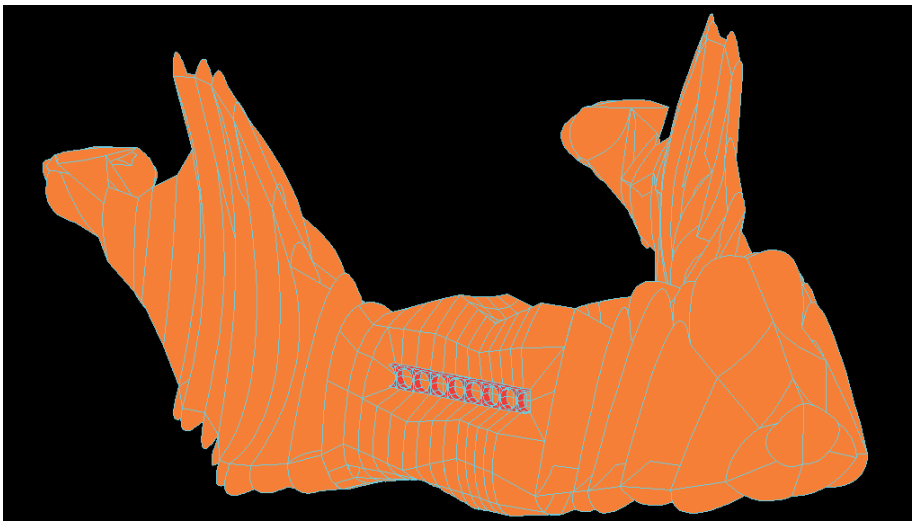

(A) Front view

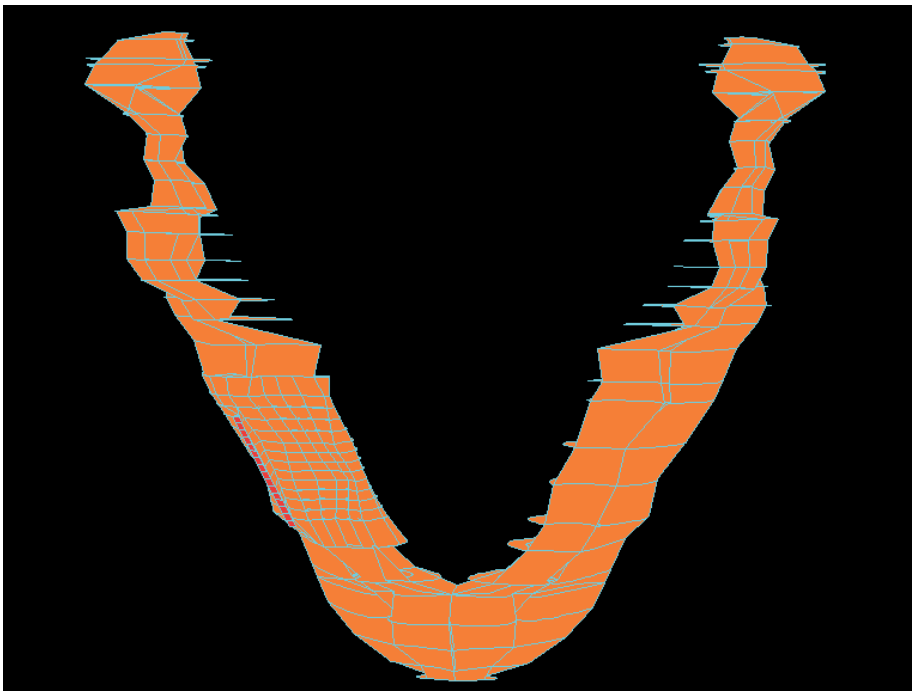

(B) Top view

Figure 7.7 FEM of the fractured mandible with fixation plate (produced in STRAND7)

In this analysis, the Young's modulus and Poisson's ratio for the cortical bone were obtained from Arendts and Sigolotto (1989, 1990) and cancellous bone were obtained from Turner et al. (1990). The material properties of the cortical and cancellous bone, Ti-6Al-4V, PLA and ZrO_2 used for the finite element computation are shown in Tables 7.1 and 7.2.

Table 7.1 Mechanical properties used in finite element computations

Material	Young's modulus (GPa)			Poisson's ratio		
	E1	E2	E3	ν12	ν23	ν13
Cortical Bone[1]	6.9	8.2	17.3	0.315	0.325	0.310
Cancellous Bone[2]	0.32	0.39	0.96	0.3	0.3	0.3

[1] Arendts & Sigolotto, 1989, 1990
[2] Turner et al., 1990

Table 7.2 Mechanical properties of the fracture plates used in this study

Materials	Young's modulus (GPa)	Compressive strength (MPa)	Tensile strength (MPa)	Poisson's ratio
Titanium alloy (Ti-6Al-4V)	114	450-1850	900-1172	0.34
PLA	3.5	80*	50	
ZrO_2	250	5200	711	0.32

* Flexure strength

7.4 Design of the fracture fixation systems to be analysed

As outlined above, the fracture fixation systems to be analysed varied in six categories: (i) screw hole diameter; (ii) plate thickness; (iii) plate material; (iv) mesh design; (v) composite plate; and (vi) PS plate.

As observed, stable but flexible fixation is the primary concern in the treatment of fractures as inadequate stability will result in non-union of the fracture sites. For this reason, the fracture plates used for fracture fixation have to provide fracture fixation in semi rigid capacity, as well as provide the ability to resist excessive torsional or bending

stresses generated by muscles during functional movements, such as clenching. By varying the fracture system design in six keys areas we are able to compare and judge each system simultaneously. In addition, the FEA system used gives us internal stresses and distributions, as well as distortions within the mandible, which is very difficult if not impossible to measure via any other method. To date, no other paper has so comprehensively analysed six systems in unison on two analytical models, GEN and PS.

7.4.1 Linear plate varying screw hole diameter

A relationship based on Young's modulus or stiffness of the plate material, along with the second moment of inertia, is utilised in the design of the fracture systems used in this thesis then it is accepted that the second moment of inertia is related to the cross-sectional area and the geometry. This assumption is reasonable due to the same cross sectional area used for the plate design The capacity of a particular plate design, therefore, can be examined by reducing the amount of plate material available, for example, by increasing the screw hole diameter to effect the bending stress.

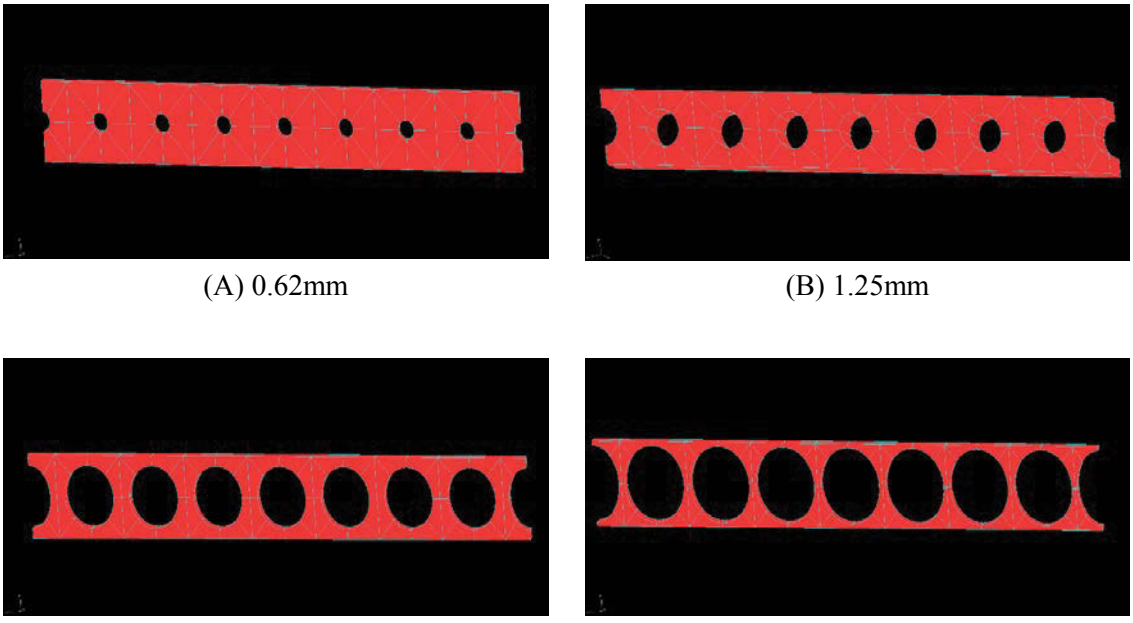

(A) 0.62mm (B) 1.25mm

(C) 1.88mm (D) 2.25mm

Figure 7.8 Modelling of the fracture plates with various screw hole diameters

Four different fracture plates with the dimensions of 19.5mm length, 3.0mm width and 1.0mm thickness each made of Ti-6Al-4V are constructed. The plates contain eight screw holes with diameters ranging from 0.62mm to 2.25mm. By increasing the diameter of the screw holes, the cross-sectional area of the plate is reduced. For example, the fracture plate with a screw hole diameter of 0.62mm has a cross-sectional area of 55.43mm^2 while the plate with a screw hole diameter of 2.25mm has a cross-sectional area of 21.22mm^2 (Figure 7.8).

7.4.2 Linear plate varying thickness

Based on the same assumptions used in Section 8.4.1, rather than varying the screw hole diameter to influence the amount of plate material, a Ti-6Al-4V plate was constructed with the following constants: 19.5mm length, 3.0mm width and a screw hole diameter of 2.25mm. The plate thickness was then varied from 0.5mm to 1.0mm and finally to 2.0mm.

7.4.3 Linear plate varying material (Ti-6Al-4V, PLA and ZrO_2)

A plate was designed with the following constant dimensions: 19.5mm length, 3.0mm width, 1.0mm thickness and 2.25mm screw hole diameter. The plates were then homogenously constructed of Ti-6Al-4V and PLA being two core materials used to manufacture fixation plates, both were compared. Additionally, a ZrO_2 plate was modelled as ZrO_2 is now emerging as a biocompatible alternative to the current Ti and PLA plates commercially available.

7.4.4 Linear composite laminated plate (Ti-6Al-4V and PLA)

Figure 7.9 shows the design of the plate, which consists of two laminates each of 0.5mm thickness and 2.25mm screw hole diameter. The combined plate thickness is 1.0mm, plate length is 19.5mm and 3.0mm width. The laminates were applied to each other and restrained to prevent movement between the laminates, then restrained at either end to simulate fixation with screws, and then allowed to freely deform during the functional movement of clenching. The plate was applied in two ways: (i) Ti-6Al-4V laminate facing outward; and (ii) PLA laminate facing outwards, that is, firstly with Ti-6Al-4V applied to the cortical bone surface across the fracture, and secondly with PLA

applied to the cortical bone surface. Each scenario was analysed and measured for maximum von Mises stress and distortion.

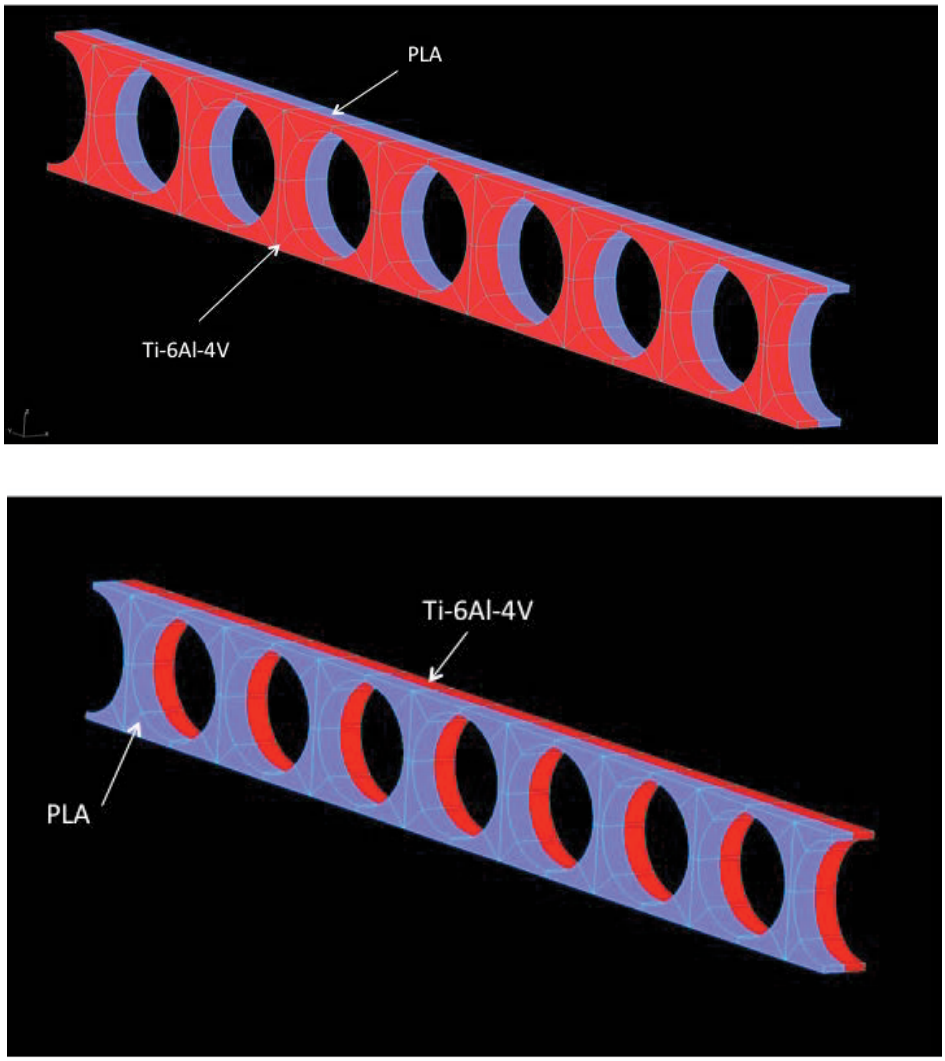

Figure 7.9 Composite laminate design with the Ti-6Al-4V side facing outwards followed by the reverse with the PLA laminate facing outwards

7.4.5 Mesh plate design

Taking into account the reduced weight, easy attachability and shaping advantages during surgery, a mesh design was considered. A rectangular mesh was constructed consisting of two sectional units in height and 20 sectional units in length. The mesh was restrained at each end to the bone and the rest was allowed to freely deform. The mesh plate has the following dimensions: length 19.5mm, width 3.0mm and thickness 1.0mm. For comparison, a linear plate of 19.5mm thickness, 3.0mm width, 1.0mm

depth and eight screw holes each of 2.25mm diameter has the same cross-sectional area as the mesh design (Figure 7.10).

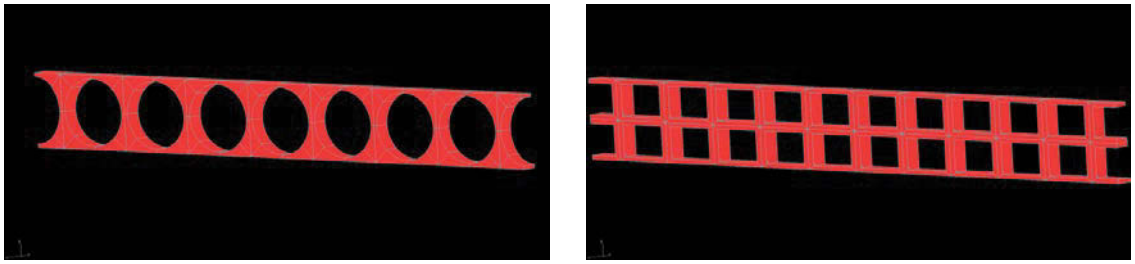

The cross-sectional area between these two plates were identical (20.91mm^2).

Figure 7.10 Comparison of mesh design to 'traditional' linear plate design

Figure 7.11 shows the meshed plate fixed at both ends either using screws or bone cement/PMMA. The rest of the plate is free to deform and is fixed to the bone itself.

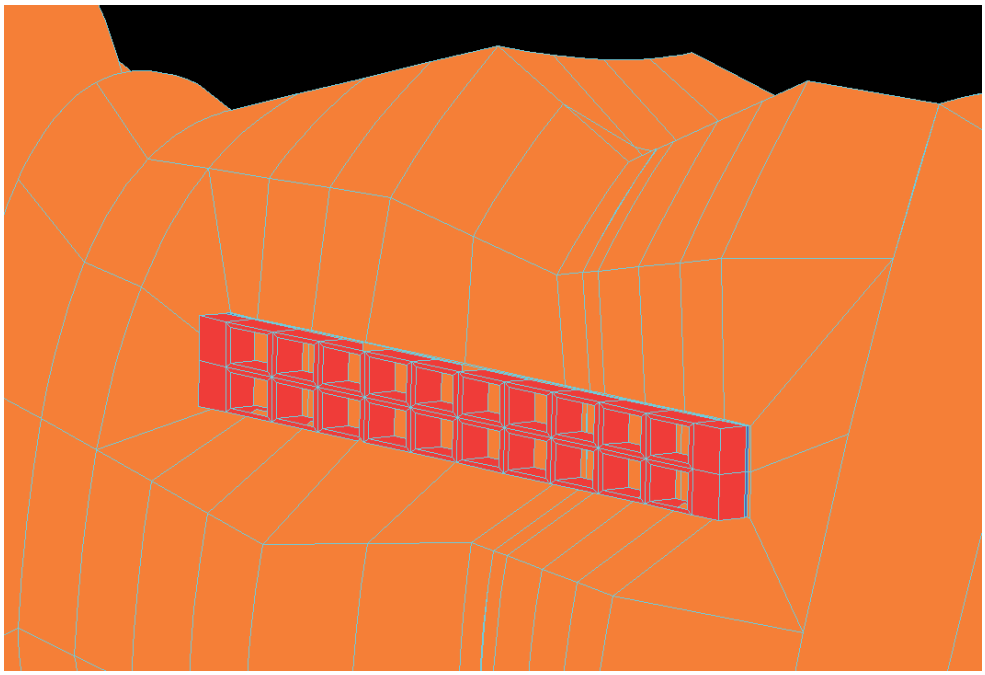

Figure 7.11 Model with a new design Ti-6Al-4V mesh plate applied across fracture at the angle of the mandible

7.5 Description of each analysis for design variations

7.5.1 Variation in old versus new fracture site for a 1.0mm thick Ti-6Al-4V plate with 2.25mm diameter screw holes under the functional movement of clenching (measuring von Mises stress)

A comparison in results from the original extensively validated model (termed ‘old fracture’) is presented alongside data from the modified model (termed ‘new fracture’), as described earlier in this chapter.

For the comparison, a 1.0mm thick Ti-6Al-4V with 2.25mm holes is applied across both models and functioned in clenching. The purpose of such a comparison is to quickly establish that data collected from the new fracture model is aligned with data from the validated old model.

7.5.2 Variation in functional movements of clenching, opening and protrusion for a 1.0mm thick Ti-6Al-4V linear plate with 2.25mm diameter holes (measuring von Mises stress and distortion)

Data is collected for a commonly applied fracture plate (1.0mm thick Ti-6Al-4V plate with 2.25mm diameter screw holes) used in the clinical management of fractures. In this section of data presentation, the ‘new’ fracture model is used only and analysed in clenching, opening and protrusion. In addition to von Mises stress, data for distortion is presented.

7.5.3 Variation in screw hole diameter of a Ti-6Al-4V linear fracture plate under the functional movements of opening, protrusion and clenching (measuring von Mises stress and distortion)

Data is collected for variation in a 1.0mm thick Ti-6Al-4V plate with screw hole diameters of 0.62mm, 1.25mm, 1.88mm and 2.25mm under the functional movement of clenching, measuring maximum von Mises stress and distortion. In this data set, we begin by looking at design scenarios outside of commonly used fixation plates in current surgical practice.

7.5.4 Variation of a Ti-6Al-4V plate with thicknesses of 0.5mm, 1.0mm and 2.0mm respectively under the functional movement of clenching, with screw hole diameter constant at 2.25mm (measuring von Mises stress and distortion)

Data is collected for von Mises stress and distortion in the variation of a Ti-6Al-4V plate with thicknesses of 0.5mm, 1.0mm and 2.0mm respectively under the functional movement of clenching with a screw hole diameter constant at 2.25mm. Again, in this data set we begin by looking at design scenarios outside of commonly used fixation plates in current surgical practice.

7.5.5 Variations in plate material, Ti-6Al-4V, PLA and ZrO_2 under the functional movement of clenching with plate thickness and screw hole diameter being constant at 1.0mm and 2.25mm respectively (measuring von Mises stress and distortion)

Data is collected for von Mises stress and distortion with variations in plate material, Ti-6Al-4V, PLA and ZrO_2 were utilised for the fracture fixation under the functional movement of clenching. Plate thickness and screw hole diameter are constant at 1.0mm and 2.25mm respectively. Again, in this data set we begin by looking at design scenarios outside of commonly used fixation plates in current surgical practice.

7.5.6 Variation in a linear laminated fracture plate (measuring von Mises stress and distortion)

Data is collected for von Mises stress and distortion with variation in a composite laminated plate (Ti-6Al-4V and PLA) under the functional movement of clenching. The plate consisted of two laminates each of 0.5mm thickness and 2.25mm screw hole diameter. The combined plate thickness was 1.0mm. The laminates were applied to each other and restrained to prevent movement between the laminates, restrained at either end to simulate fixation with screws and allowed to freely deform during the functional movement of clenching. The plate was applied in two ways: (i) with the Ti-6Al-4V laminate facing outward; and (ii) with the PLA laminate facing outwards. Each scenario was analysed and measured for von Mises stress and distortion.

7.5.7 Variation in a mesh fracture plate (measuring von Mises stress and distortion)

Data is collected for a linear mesh plate design using Ti-6Al-4V in clenching. The mesh was of the following dimensions, length 19.5mm, width 3.0mm and thickness 1.0mm. Data was collected for von Mises stress and distortion.

7.5.8 Application of linear design plate across a fracture in the patient specific model (measuring von Mises stress and distortion)

To briefly summarise the procedure, the mandibular model has been obtained from CT scan, as previously described in detail. The scan data is imported into a segmentation software (Materialise Mimics). With the use of segmentation marks, the outer body of the mandible is marked and exported as an STL file. The STL file is imported into Rhinoceros3D for mesh repair and generation of a polysurface, which is then exported into a CAD Modelling software (Autodesk Inventor).

A maxillofacial fracture plate is modelled in 3-Matic (Materialise) and then exported into Autodesk Inventor (Figure 7.12).

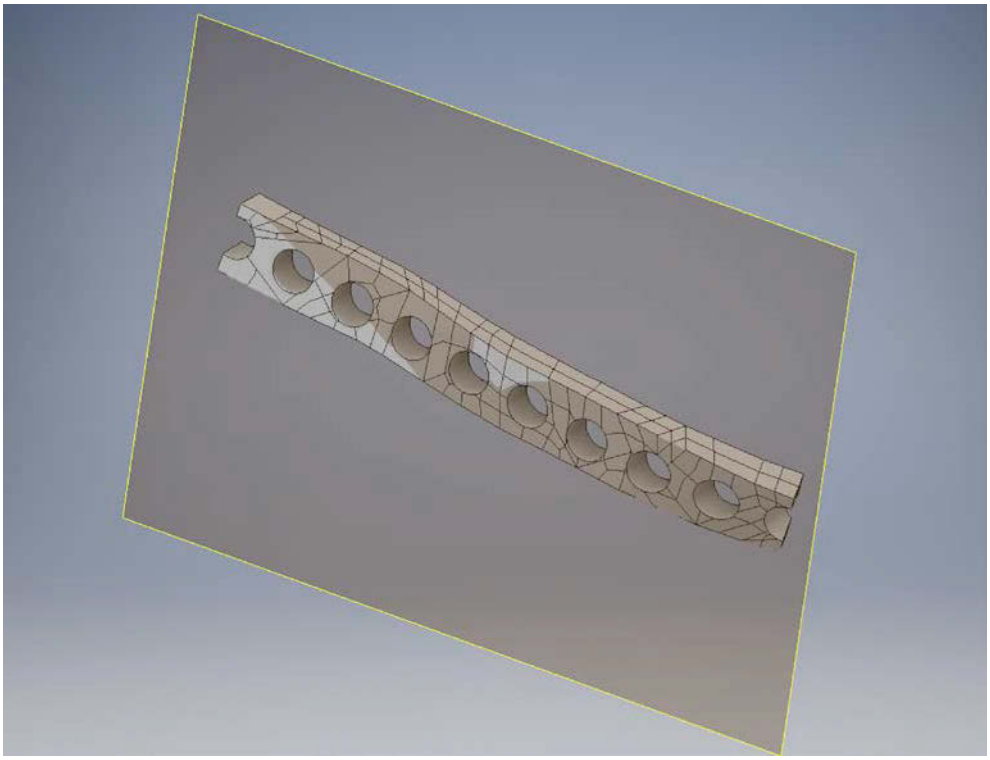

Figure 7.12 Linear fracture plate modelled in Autodesk inventor

Once the assembly has been validated, a fracture is created in the CAD software, and two mandible segments, together with the plate, are exported into Ansys Workbench for FEA pre-processing (Figure 7.13).

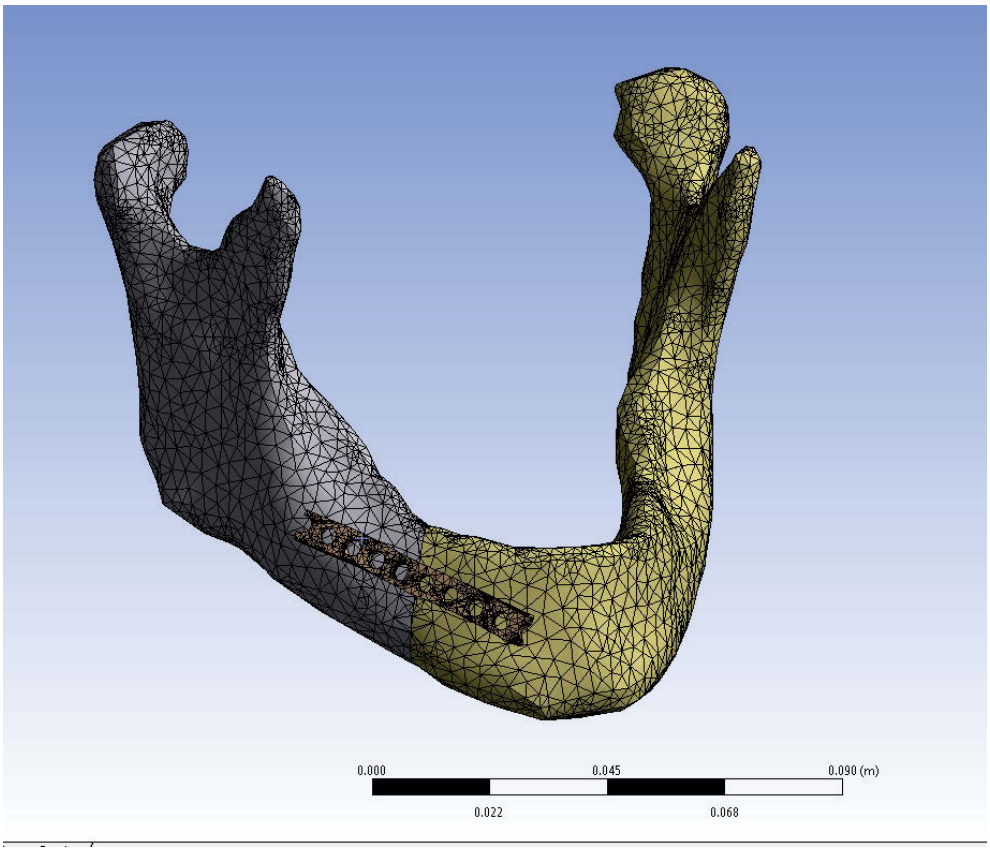

Figure 7.13 Assembled model ready for analysis with scale for reference to dimensions

Contact between the two bone segments is assumed to be frictional with a coefficient of 0.4 (Goffin et al., 2013) while the plate is supposed to be bonded to the mandible. This design assumption has been consistent with all models in this study.

Loads are assigned in accordance with Ben-Nissan's studies for clenching functional movement, as have been previously described and used for all of the models.

Bone tissue was assigned a Young's modulus of 10GPA and the fracture plate is made of TI-6Al-4V. With application of the plate to the model, results were obtained in clenching for stress and distortion.

7.7 Measurement criteria for data collection and presentation

For each analysis presented in Chapter 8, a standardised method of measurement was adopted termed the 'fracture segment' (FS) and 'isolated plate' (IP). Figure 7.14 (A, B) show the portion of the FS model with a plate in situ. The FS is the premolar region of the right mandible where a fracture was introduced into the model and the fixation system applied and tested. Measurement for the FS starts at the plate surface and progresses centrally into the medullary cavity of the mandible. The measurement was taken at the midpoint of the fixation plate and progressed perpendicular to the plate surface as shown by arrows in Figure 7.14 (A, B).

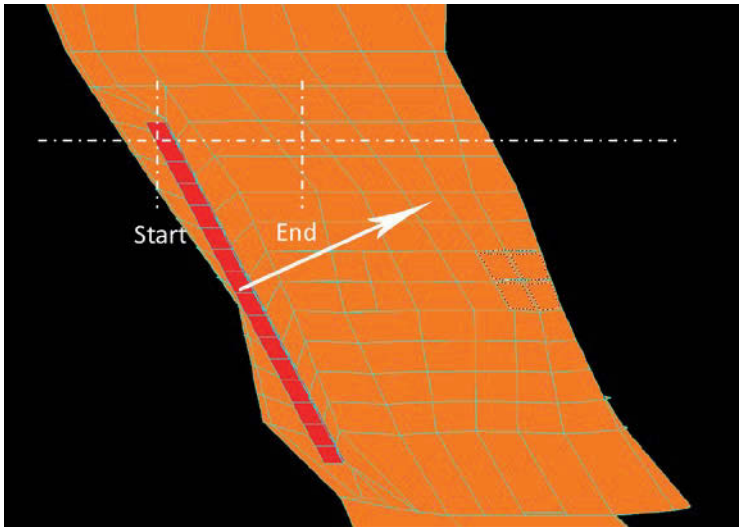

(A) Depth of data measurement starting from plate surface to 4.5mm centrally within the model

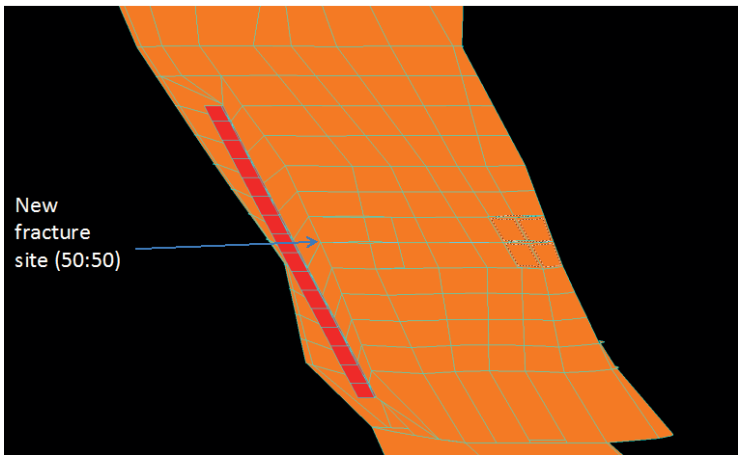

(B) Exact central location of measurement

Figure 7.14 Depth, direction and location of measurements perpendicular to plate surface

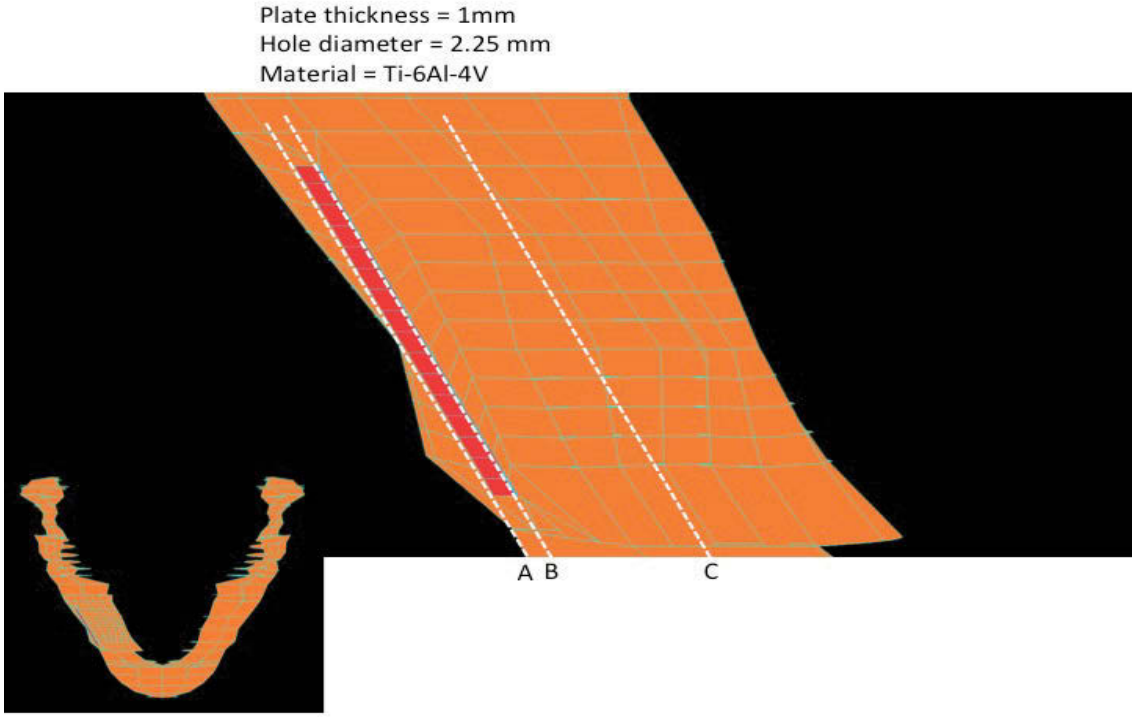

Point A being the plate surface, Point B being the interface between the plate and the cortical bone surface and Point C being the endpoint of measurement some 4.5mm within the medullary cavity of the mandible.

Figure 7.15 Three key points in data measurement for FS, starting from the outer surface of the plate to the centre of the medullary cavity

In Figure 7.15, it is further explained that Point A is the plate surface and Point B is the bone and plate interface. The distance between Points A and B varied from 0.5mm to 2.0mm depending on the thickness of the system being tested. Point C is within the cancellous bone or medullary cavity of the bone.

The thickness of the cortical bone, that is, the segment of bone that exists beyond Point B but before cancellous bone starts in vivo is highly variable ranging from 1.36mm to 2.06mm in the edentulous mandible (Katranji, 2007). For this study, a thickness of 1.5mm was chosen for the cortical bone thickness.

For each data set, an overall FEM was produced containing the FS with the fixation system in situ centred over the fracture site on the edentulous mandible, as shown in Figure 7.16. Models were constructed to analyse both von Mises stress and distortion.

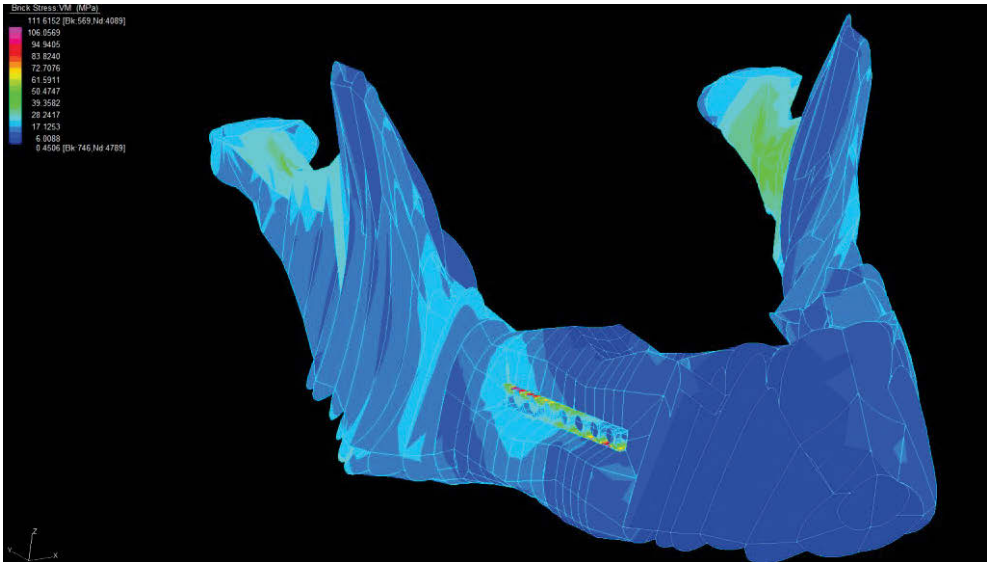

Figure 7.16 FEM Ti-6Al-4V linear plate in situ in the FS of the overall fixation system model (plate = 19.5mm long x 1.0mm thick x 3.0mm wide with 2.25mm diameter screw holes)

With the overall model constructed, the fixation system was then isolated and extracted from it, as shown in Figure 7.17 as an example. Each data set has the FS modelled with a fracture plate in situ. Data is presented showing the fracture plate in isolation only in combination with graphs to represent data collected from the FS. This illustrates the results better than reproducing the FS model as a figure in each data set.

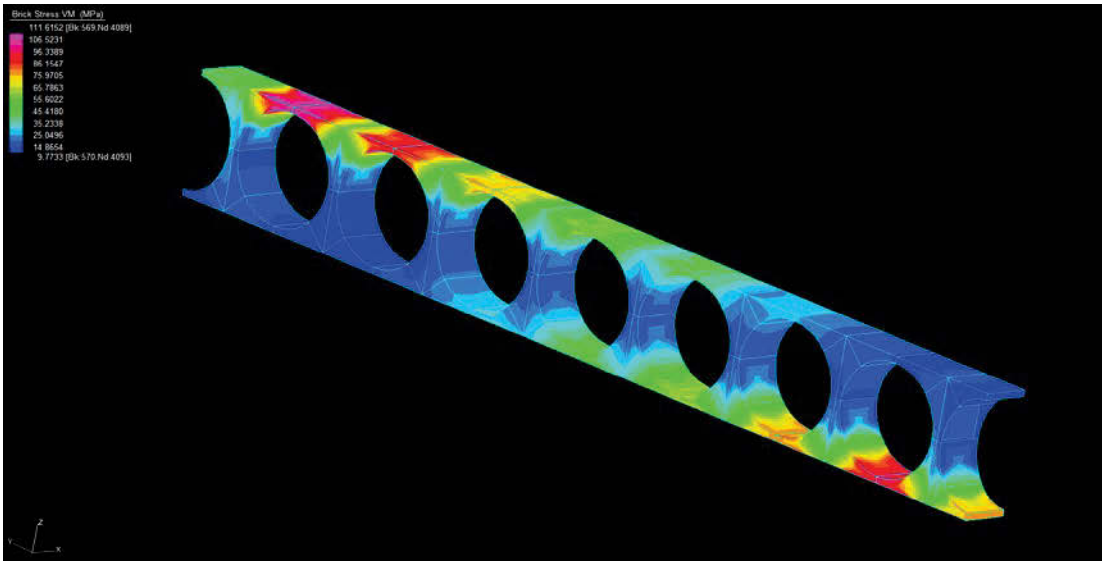

Figure 7.17 FEM plate extracted from the overall model and presented in isolation

Data from the models is presented in two ways. Firstly, peak values from the IP are presented as in the form of a model with varying colouration. Pink colouration denotes the area of highest stress or distortion depending on the model. Data from FS is also presented, as previously explained as a graph, to aid in comparative analysis and better representation of the results.

The purpose of doing this is to compare the performance of the plate alone in comparison to the performance of the fixation system in situ and more representing what occurs in vivo. To analyse one and not the other would not give the best overall picture of what is happening in the 'patient'.

Finally, in Chapter 8, data is summated in tabulated form and repeated in Chapter 9 for the purpose of summary and discussion of the results.

CHAPTER 8:
THIRD OUTPUT – MANDIBULAR FRACTURE AND REPAIR MODELLING RESULTS

8.1 Results for variation in old versus new fracture site for a 1.0mm thick Ti-6Al-4V plate with 2.25mm diameter screw holes in clenching

To begin the presentation of data, a comparison in results from the original extensively validated model (termed 'old fracture') is presented alongside data from the modified model (termed 'new fracture'), as described in Chapter 7. For comparison, a 1.0mm thick Ti-6Al-4V with 2.25mm screw holes is applied across both models and functioned in clenching (Figure 8.1A & B).

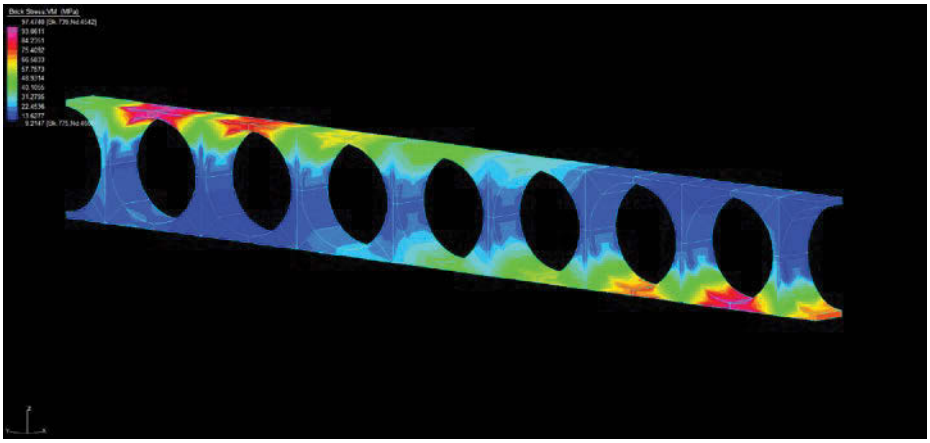

(A) FEM IP taken from the 'old' fracture model

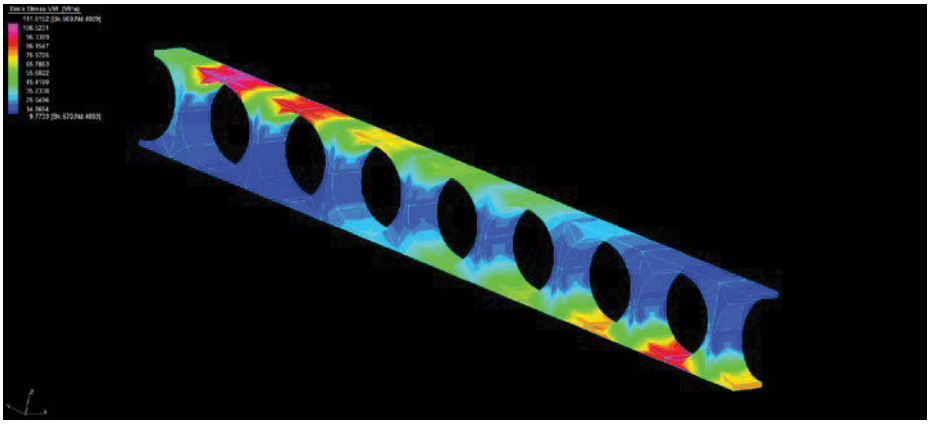

(B) FEM IP taken from the 'new' fracture model

Figure 8.1 (A & B) Stress analysis for 'old' and 'new' fractures

The difference in peak stress within the plate between ‘old’ and ‘new’ models is 97.74MPa and 111.61MPa respectively. As illustrated in Figure 8.2, maximum stresses were observed within the FS of the overall model at the cortical bone to metal plate interface, producing values of 117MPa and 122MPa respectively.

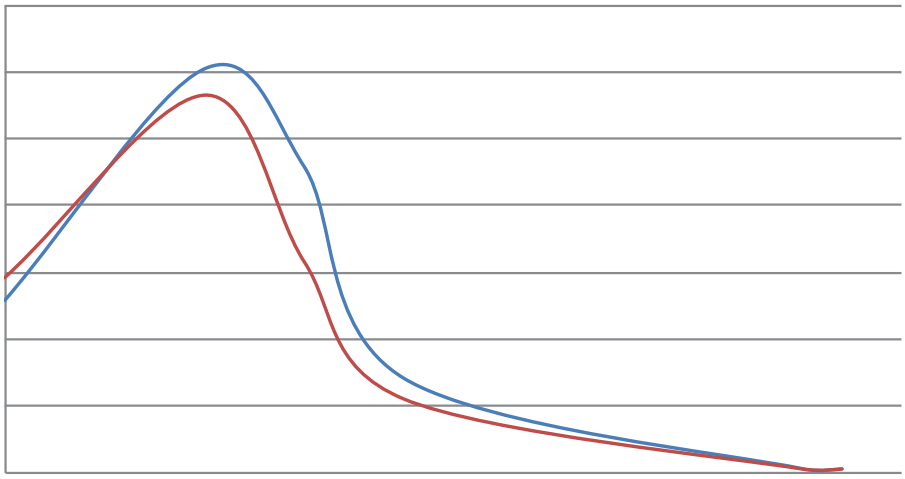

fracture sites

Note that peak stress for both occurs just within the cortical bone layer close to the plate/bone interface at 1.0mm.

Figure 8.2 von Mises stress curves for FS of ‘old’ and ‘new’ fractures

Of significance in these results are the following points:

1. The peak stress for ‘old’ and ‘new’ fractures coincides with the plate and bone interface falling just within the cortical bone.

2. Both stress curves are similarly shaped.

3. Both maximum stresses of 97.74MPa and 111.61MPa are well matched and fall well within the maximum stress at failure for Ti-6Al-4V (Table 7.2).

4. Values are also within the range for cortical bone maximum stress values.

5 The comparison has allowed us to establish that the ‘new’ fracture design performs predictably and is comparable to the ‘old’ design that had been previously extensively validated.

Following these important key points, the results obtained are not surprising given that the plate design applied across both fractures is derived from STL files for a KLS Martin plate that is commonly used in this type of fracture management and is not expected to fail. It is important to note that it has allowed us to compare both models and more importantly, allows us to assess other fracture management systems that certainly do fall outside of current usage and to compare them with the current clinical standard.

Given this demonstration of comparative validity between both fracture models, the following analyses are conducted using only the ‘new’ fracture model.

8.2 Results for variation in functional movements of clenching, opening and protrusion for a 1.0mm thick Ti-6Al-4V plate with 2.25mm diameter screw holes measuring for each scenario von Mises stress and distortion.

To further progress the research logically, data is collected for a commonly applied fracture plate (1.0mm thick Ti-6Al-4V plate with 2.25mm diameter screw holes) used in the clinical management of fractures. In this section of data presentation, the ‘new’ fracture model is used and analysed in clenching, opening and protrusion. In addition to von Mises stress, data for distortion is also presented.

8.2.1 Effects of functional movements on von Mises stress

Firstly, looking at clenching, the results in Figure 8.3 show a peak stress of 111.61MPa. Stress is concentrated at each end of the plate where the model has been restrained to simulate plate fixation with mono cortical screws. At the proximal end, stress is concentrated at the superior portion of the plate, compared with concentration on the inferior portion at the distal end of the plate. This correlates predictably with the biomechanical direction and orientation of forces in vivo when the mandible is clenched.

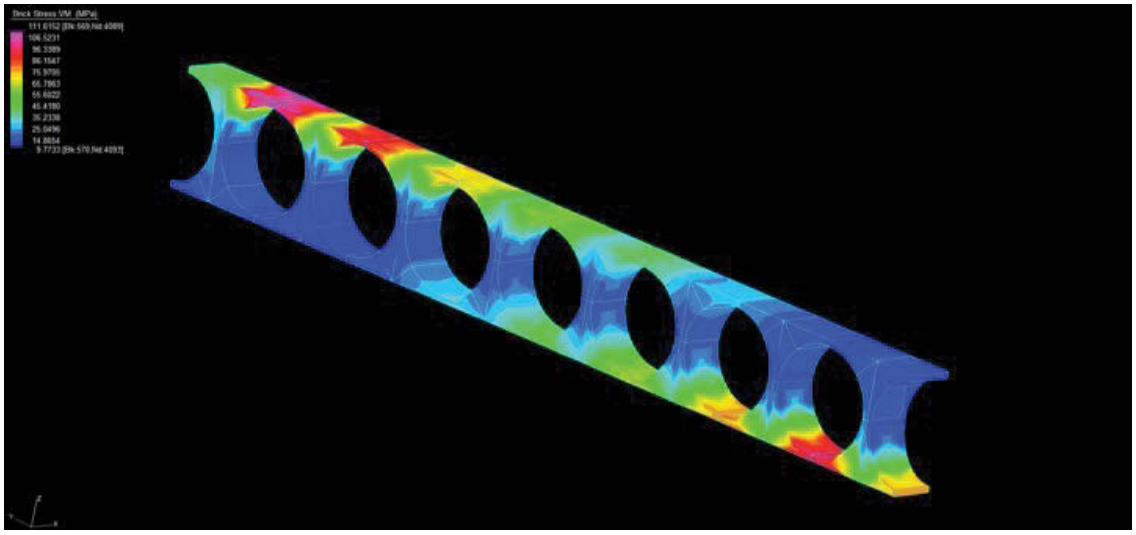

Figure 8.3 FEM of the IP showing areas of maximum stress concentration in pink during clenching

Following on from clenching, Figure 8.4 shows the stress distribution on opening. In comparison to a maximum of 111.61MPa on clenching, opening produces a maximum of 60.18MPa. The FEM models display this as pink highlighting and interestingly, are concentrated in the same areas as clenching but over a broader area.

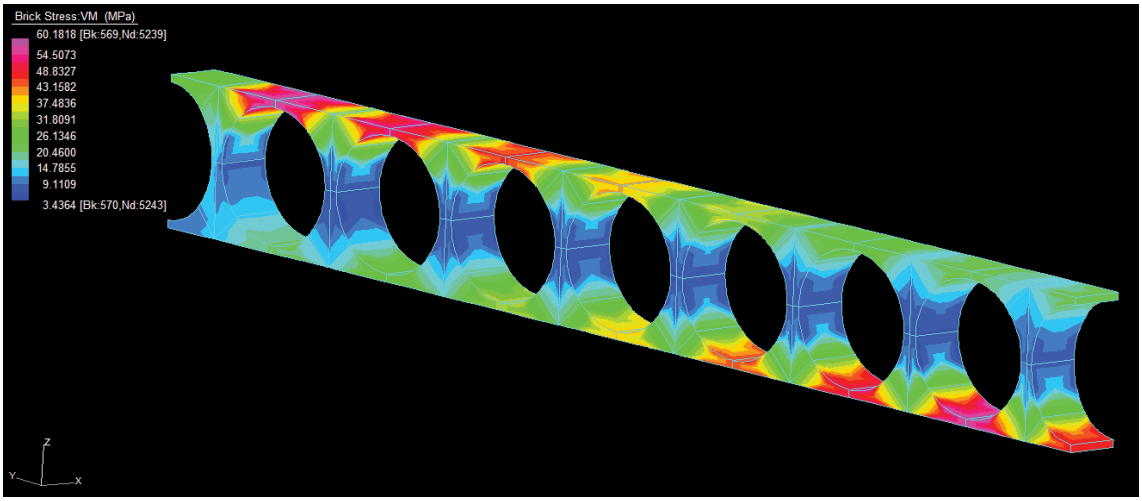

Figure 8.4 FEM of IP during the functional movement of opening (maximum stress reached is highlighted in FEM models as pink colouration)

Finally, protrusion is analysed (Figure 8.5), showing maximum stress of 77.36MPa being reached.

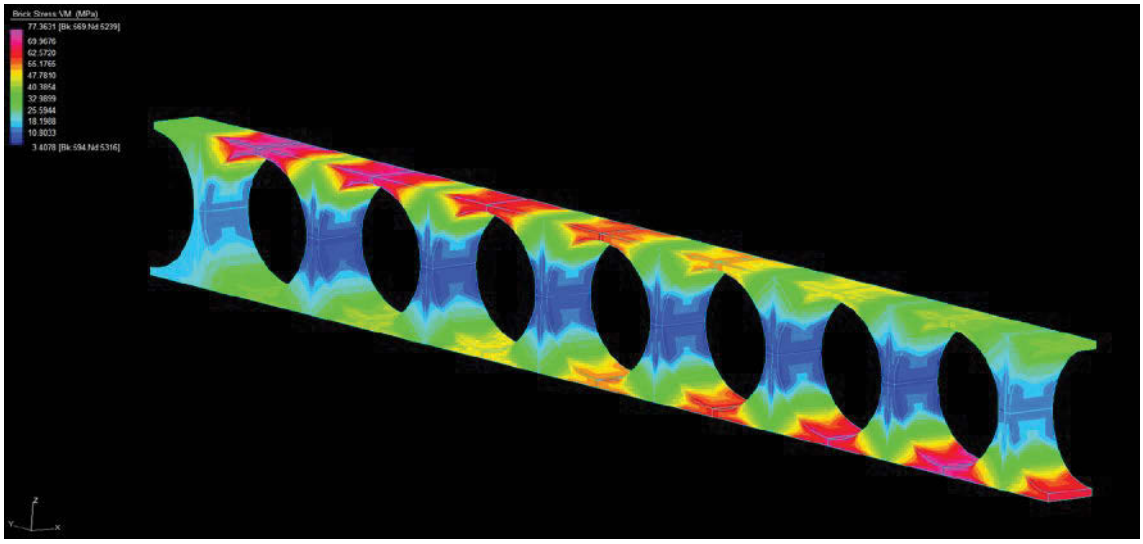

Figure 8.5 FEM of IP during the functional movement of protrusion (maximum stress is illustrated by pink colouration)

Figure 8.6 summarises the results for the FS for von Mises stress in graph form for clenching, opening and protrusion.

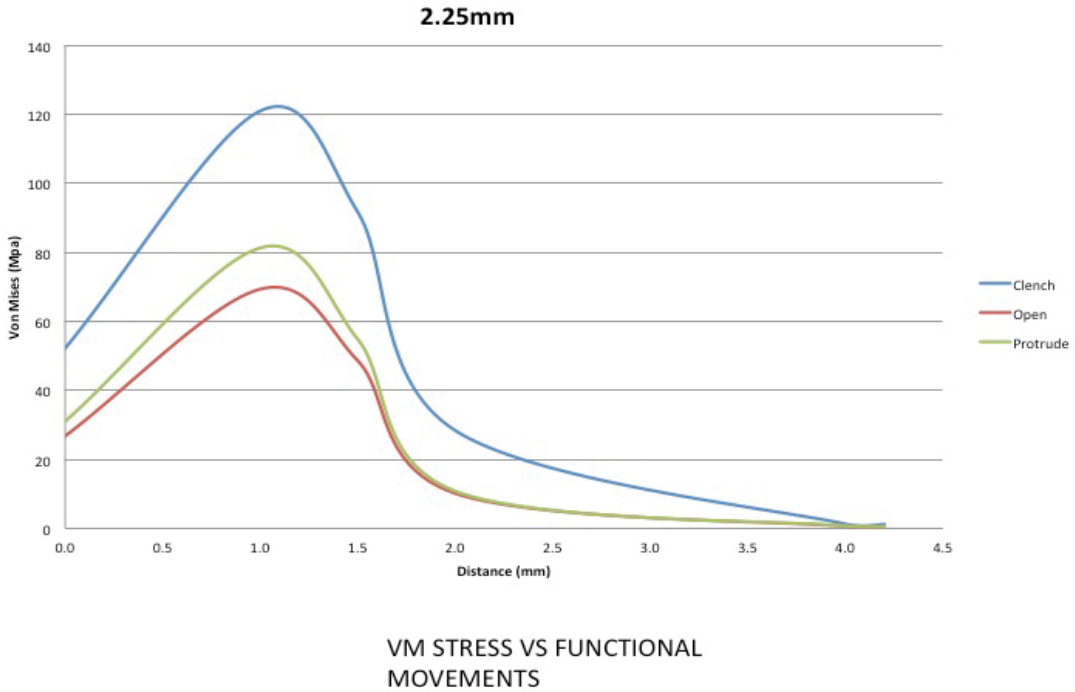

Figure 8.6 Graph plot for FS – comparison for clenching, opening and protrusion with peaks stress of 122MPa, 70MPa and 81MPa respectively

Of significance in these stress results are the following three points:

1. The results for clenching, opening and protrusion are what we would expect with clenching being significantly higher than opening and protrusion in both the IP and the FS analysis.

2. Stress concentration is toward the proximal and distal ends of the plate, oriented on the superior portion of the plate at the proximal end and inferior at the distal end.

3. Overall peak stress occurs at the plate cortical bone interface just within the cortical bone

Both observations are what we would see in the clinical application of such a plate. To further investigate these points, data is presented for clenching, opening and protrusion in the form of distortion, followed by combining the points of interest for stress and distortion data before moving to Section 8.3 where the relevance of Sections 8.1 and 8.2 to the subsequent results will be explained.

8.2.2 Effects of functional movements on distortion

Similar to Section 8.2.1, the results for clenching will be presented first. Figure 8.7 shows maximum distortion for the IP model of 0.086mm concentrated at its proximal end by pink colouration.

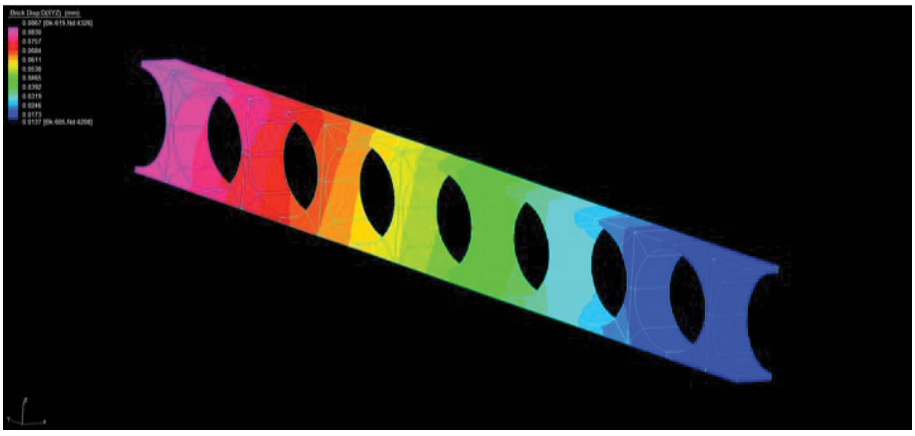

Figure 8.7 FEM of IP for distortion during functional movement of clenching

Moving onto data collected for opening, Figure 8.8 shows a maximal distortion of 0.126mm for the plate in isolation with maximum distortion occurring again at the proximal end of the plate.

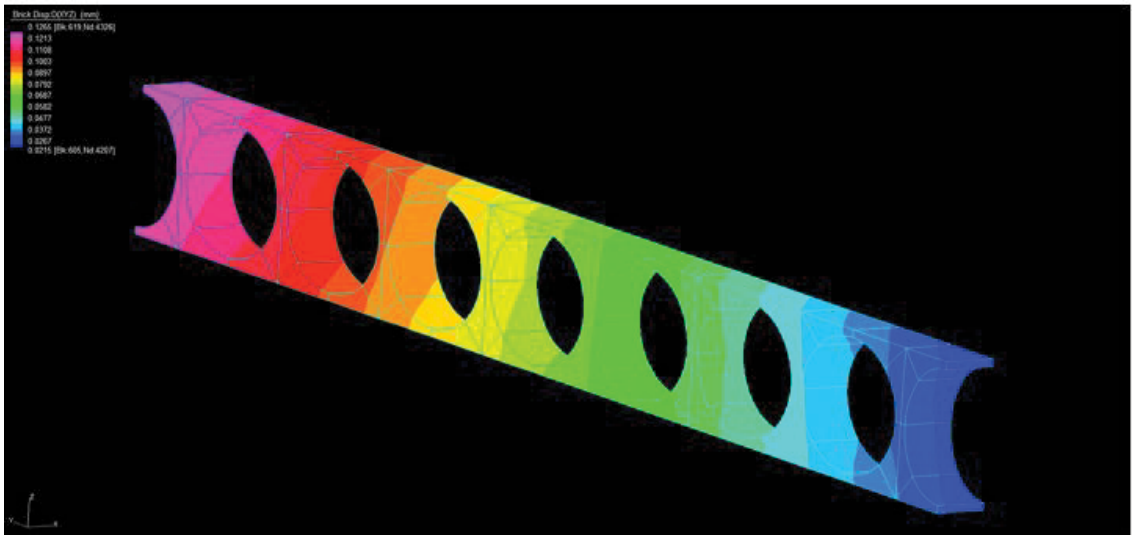

Figure 8.8 FEM of IP for distortion during functional movement of opening

Finally, data collected for protrusion is illustrated in Figure 8.9 shows the maximum distortion to be centred over the proximal portion of the plate with a value of 0.18mm.

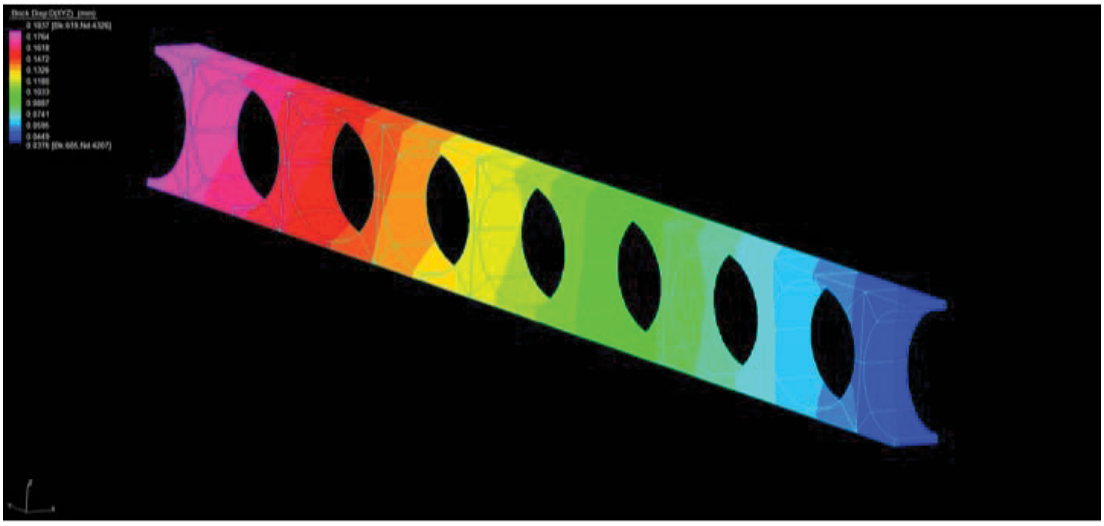

Figure 8.9 FEM of IP for distortion during functional movement of protrusion

Of significance in these distortion results are three points:

1. Maximum distortion of the plate occurs in protrusion with a value of 0.18mm compared with 0.126mm for opening and 0.086mm for clenching.

2. These values are within the range of distortions measured and/or calculated by various workers for mandibular distortions under functional movements.

3. For each scenario, maximum distortion occurs at the proximal end of the plate.

Interestingly, the results for maximum distortion during function occur inversely to the results for maximum stress. As illustrated in Table 8.1, clenching shows the highest stress across the plate but the least distortion, whereas in comparison, opening and protrusion show similar values but do the opposite to clenching regarding stress and distortion values.

Table 8.1 Comparison of highest stress and distortion values between clenching and protrusion/opening

	Maximal plate stress (MPa)		**Maximal plate distortion (mm)**	
Highest value	Clenching	111.61	Protrusion	0.180
	Protrusion	77.36	Opening	0.126
Lowest value	Opening	60.18	Clenching	0.086

These seemingly incongruous results make sense when it is considered that during clenching the process of the mandible closing against the stable maxilla acting as a bracing effect allows stress to manifest itself freely but limits distortion due to the splinting effect of biting against a stable maxilla that cannot deform freely.

The converse of opening and protrusion is true as with each of these functional movements when no such splinting or bracing effect occurs and hence distortion is not restrained as it is with clenching.

The points that have been extrapolated from the results in Sections 8.1, 8.2.1 and 8.2.2, whilst seemingly obvious, are critical to explain in the evolution of this research analysis. In Section 8.1, we established that the 'new' fracture model would be used due to its validity. We have now demonstrated that this model performs as predicted in three functional applications and that clenching produces the greatest stress. Distortion, however, performs differently as discussed.

The following sections looking at variances in plate configuration, dimensions and materials will be analysed using the 'new' fracture model in clenching only. Whilst until this point in Chapter 8 data has been presented that reflect a commonly used fixation plate, the following section will look at several novel alternatives, hence, making the data retrieved new to this setting of FE fracture analysis.

8.3 Results for variation in a 1.0mm thick Ti-6Al-4V plate with screw hole diameters of 0.62mm, 1.25mm, 1.88mm and 2.25mm under the functional movement of clenching measuring maximum von Mises stress and distortion

8.3.1 Results for 0.62mm hole diameter plate, maximum von Mises stress and distortion

Maximum von Mises stress was measured at 161MPa and occurred at 1.5mm, that is, within the cortical bone of the mandible (Figure 8.16). With the plate itself, maximum stress was 70.85MPa (Figure 8.10).

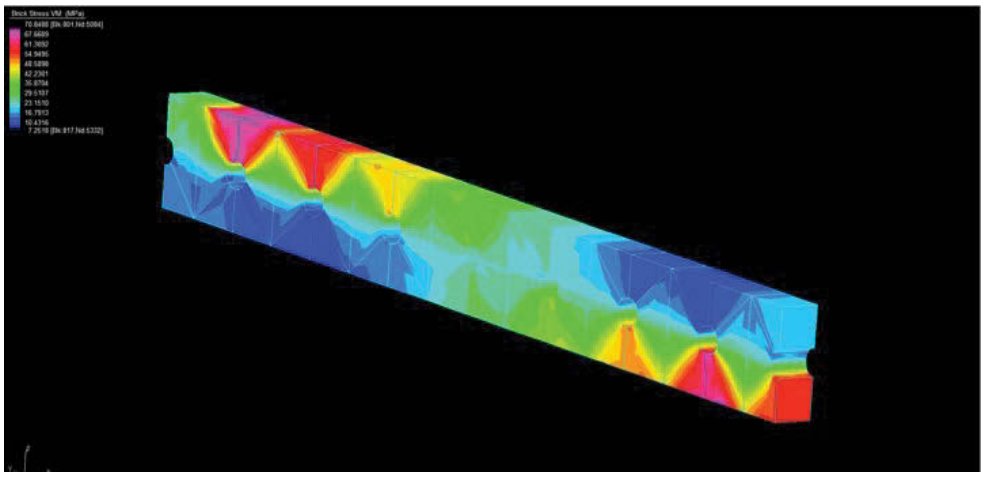

Figure 8.10 FEM of IP and concentration of point of maximum von Mises stress at ends of the plate (coloured pink)

Maximum distortion was measured at 0.085mm (Figure 8.11).

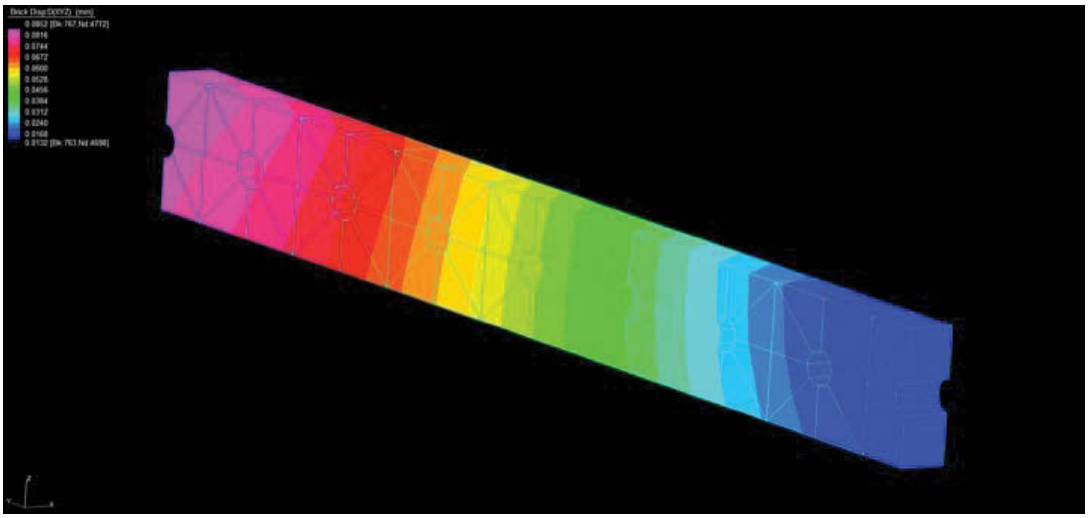

FEM plate in isolation

Figure 8.11 FEM of IP and concentration of point of maximum distortion at the proximal end of the plate (coloured pink)

8.3.2 Results for 1.25mm hole diameter plate, maximum von Mises stress and distortion

Maximum von Mises stress was measured at 158MPa at 1.4mm, again within the cortical bone of the model (Figure 8.16). In the plate alone, maximal stress was 85.17MPa (Figure 8.12).

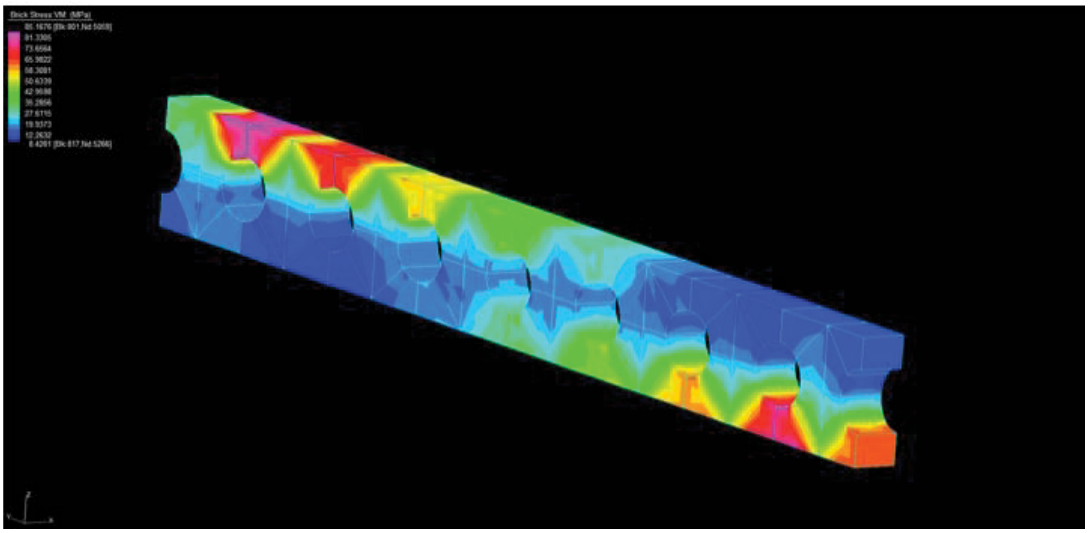

Figure 8.12 FEM of IP. Maximum stress concentrated at ends of the plate (coloured pink)

Maximum distortion was 0.08mm and occurred at the proximal end of the plate (Figure 8.13).

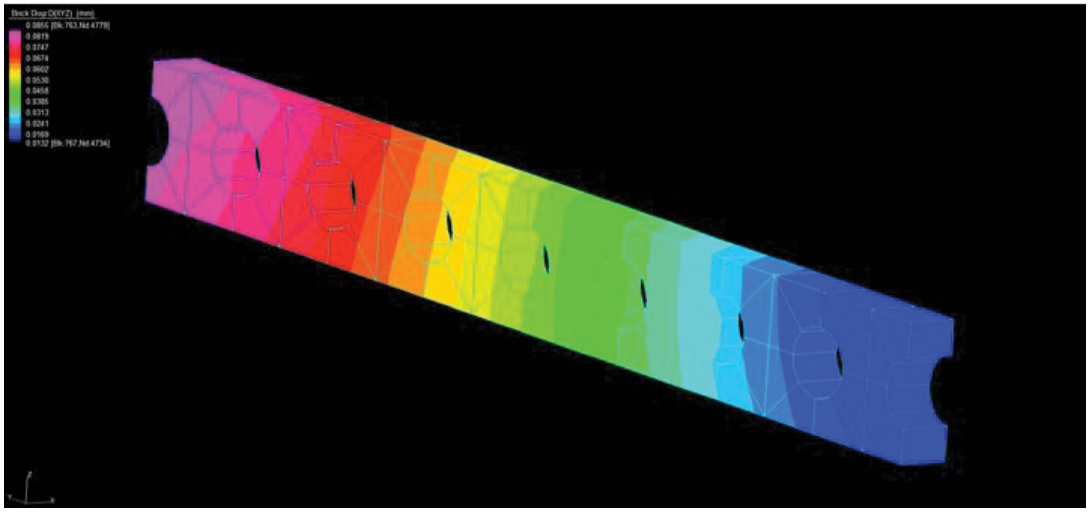

Figure 8.13 FEM of IP.Maximum distortion in the FEM (coloured pink)

8.3.3 Results for 1.88mm screw hole diameter plate, maximum von Mises stress and distortion during the functional movement of clenching

Maximum von Mises stress was measured at 151MPa at a depth of 1.15mm and is now much closer to the bone/plate interface (Figure 8.16). Within the plate itself, maximum stress was 101.04MPa (Figure 8.14).

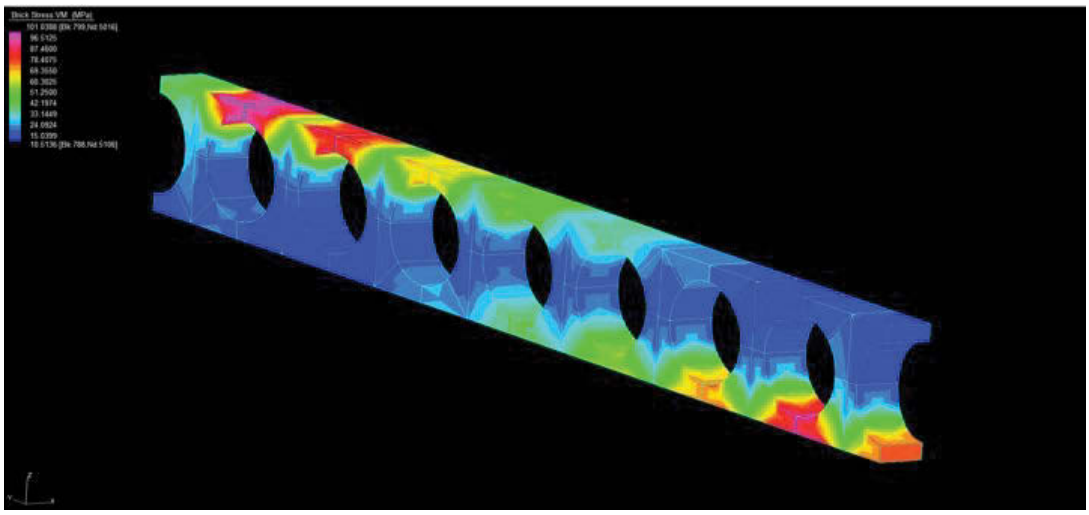

Figure 8.14 FEM of IP.Maximum von Mises stress (coloured pink)

Maximum distortion was measured at 0.086mm (Figure 8.15).

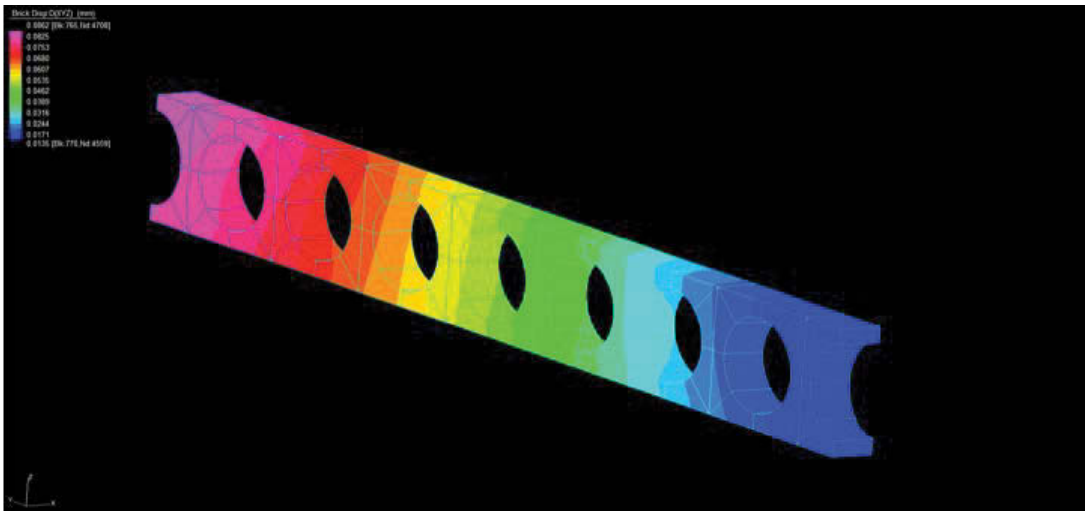

Figure 8.15 FEM of IP.Maximum distortion (coloured pink)

8.3.4 Results for 2.25mm screw hole diameter plate, maximum von Mises stress and distortion during the functional movement of clenching

The results for maximum stress and distortion are the same as those in Sections 8.1 and 8.2, and with the largest screw hole diameter, maximum stress has moved back towards the bone/plate interface (Figure 8.16).

8.3.5 Cumulative tabulation and graph plot of results

In Table 8.2, data collected in Section 8.3 is tabulated for better comparison. It illustrates a steady rise in maximum stress within the plate with increasing hole diameter, however, distortion remains relatively stable.

Table 8.2 Comparison of variation in results with increasing screw hole diameter during clenching

Screw hole diameter (mm)	Maximum von Mises stress fracture segment(MPa) and location (mm from plate surface)	Maximum von Mises stress plate isolated (MPa)	Maximum distortion of plate isolated (mm)
0.62	161 at 1.5mm	70.85	0.080
1.25	158 at 1.4mm	85.17	0.085
1.88	151 at 1.15mm	101.04	0.086
2.25	122 at 1.10mm	111.61	0.087

In Figure 8.16, the von Mises stress is presented as measured for the FS.

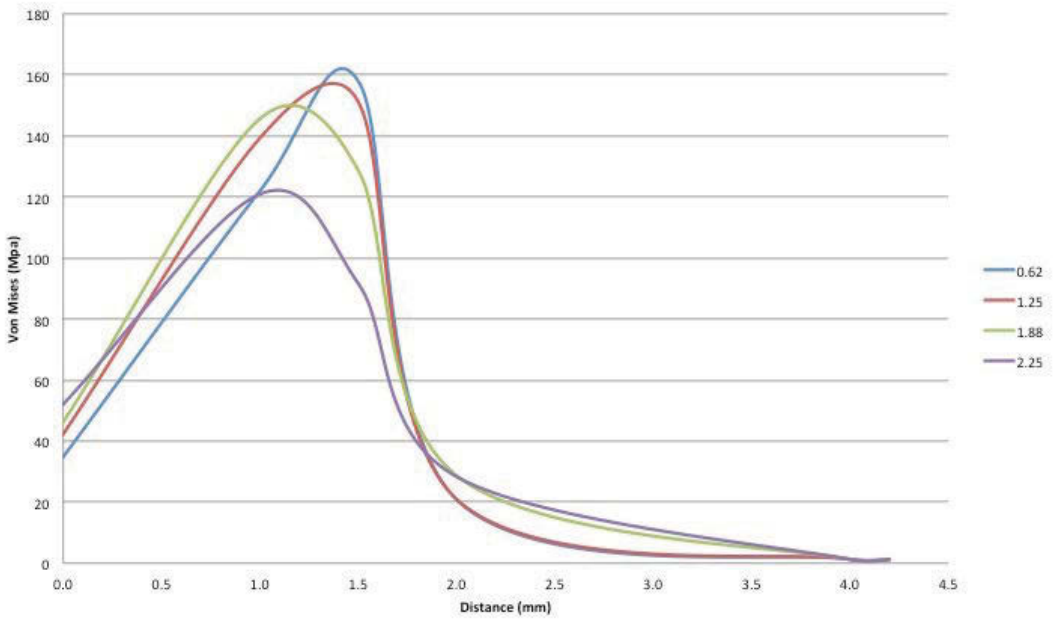

Figure 8.16 Graph plot of von Mises stress of FS from plate surface through to mandibular cortical and cancellous bone

The significance of this data is as follows

1. By increasing the screw hole diameter from 0.62mm to a maximum of 2.25mm, the plate surface area is decreased and shows a resultant decrease in maximal von Mises stress.

2. Plates with screw hole diameters of 2.25mm and 1.88mm have their maximal von Mises stress at the plate bone interface. With plate screw hole diameters of 1.25mm and 0.62mm, maximal von Mises stress is located in the cortical bone layer.

3. Plates with screw hole diameters of 2.25mm and 1.88mm most closely resemble currently available plate designs. These plates seem to perform better than plates with smaller screw hole diameters in terms of maximal von Mises stress and where this maximum is located, that is, at the plate bone interface. In addition,

whilst outside the scope of this thesis, plates with very small screw hole diameters may show inadequate plate stabilisation due to their small screw size.

8.4 Results for von Mises stress and distortion in the variation of a Ti-6Al-4V plate with thicknesses of 0.5mm, 1.0mm and 2.0mm respectively under the functional movement of clenching with screw hole diameter constant at 2.25mm

8.4.1 Results for 0.5mm thick plate

During clenching, the plate in isolation showed a maximum von Mises stress of 133.69MPa at its proximal and distal ends but centrally located over the position of the fracture had dropped significantly, shown by blue and green colouration (Figure 8.17).

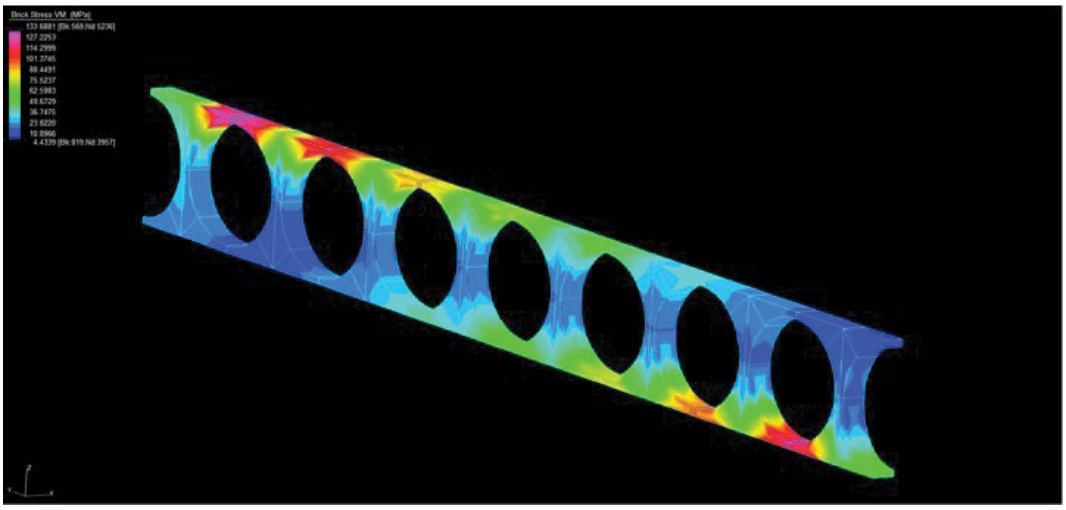

Figure 8.17 FEM of IP with thickness of 0.5mm (area of maximum stress concentration coloured pink)

8.4.2 Results for 1.0mm thick plate

During clenching, the plate showed a maximum von Mises stress of 111.61MPa at its proximal and distal ends but centrally located over the position of the fracture had dropped significantly, as shown by blue and green colouration (Figure 8.18).

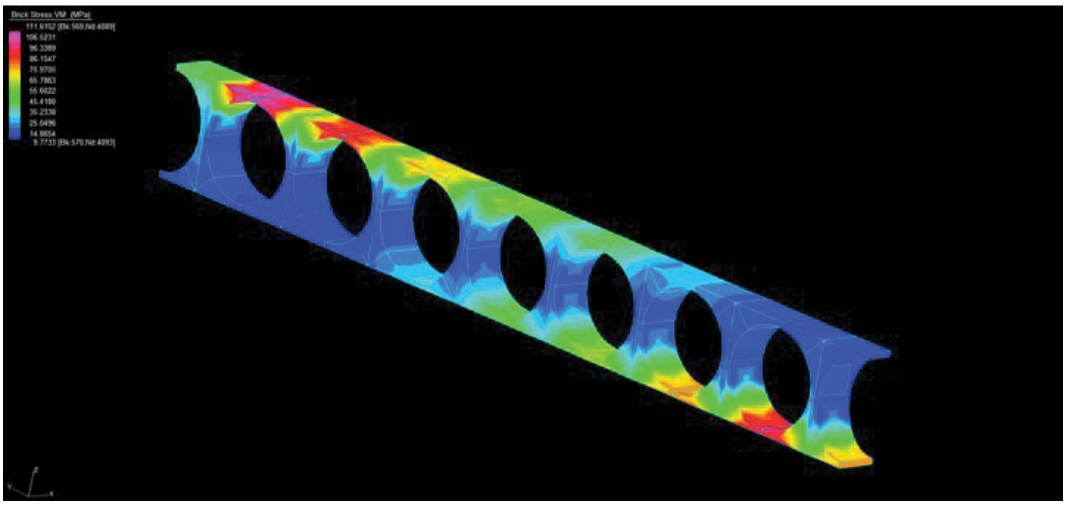

Figure 8.18 FEM of IP with thickness of 1.0mm (area of maximum stress concentration coloured pink)

8.4.3 Results for 2.0mm thick plate

During clenching, the plate showed a maximum von Mises stress of 116.12MPa at its proximal and distal ends, but centrally located over the position of the fracture, it had dropped significantly, as shown by blue and green colouration (Figure 8.19).

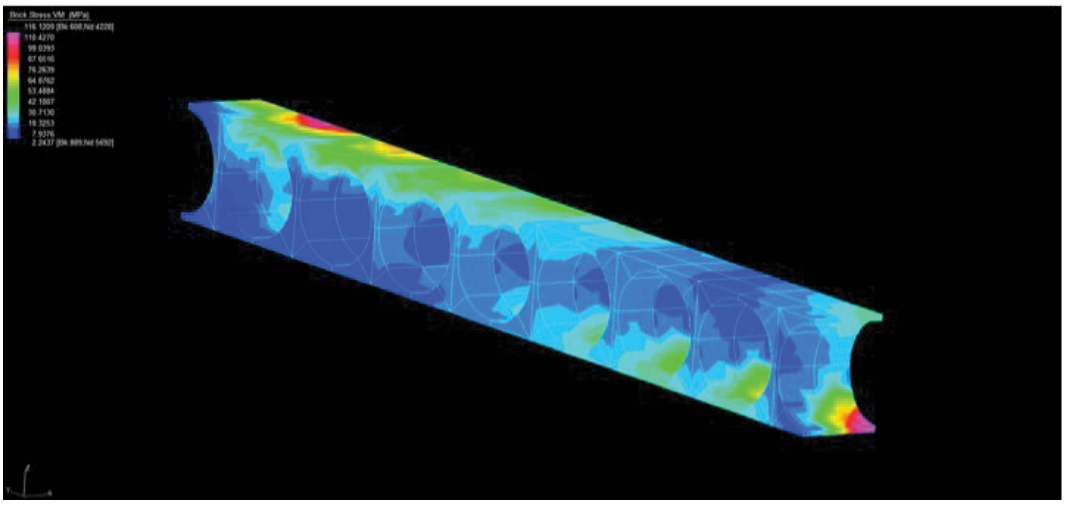

Figure 8.19 FEM of IP with thickness of 2.0mm (area of maximum stress concentration coloured pink)

8.4.4 Tabulation and graph plot of results from the fracture segment

Table 8.3 Comparison of variations in results with increasing plate thickness as maximum stress and distortion is affected within the fracture segment

Plate thickness (mm)	Maximum von Mises stress FS (MPa)	Maximum distortion of plate in FS (mm)
0.5mm	82MPa	0.086mm
1.0mm	122MPa	0.087mm
2.0mm	140.5MPa	0.090

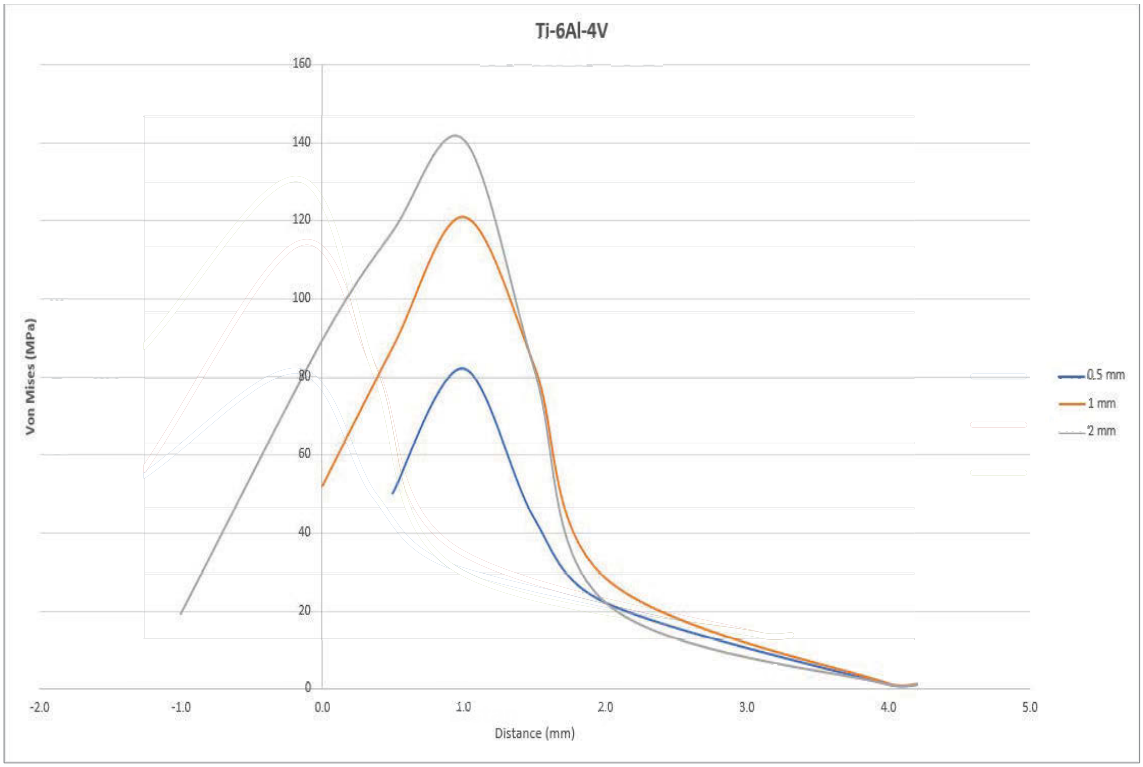

Figure 8.20 Graph plot showing FS variation in von Mises stress for plates with thicknesses of 0.5mm, 1.0mm and 2.0mm, measured from the plate surface through to mandibular cortical and cancellous bone

The results for distortion in the FS is graphically illustrated in Figure 8.21.

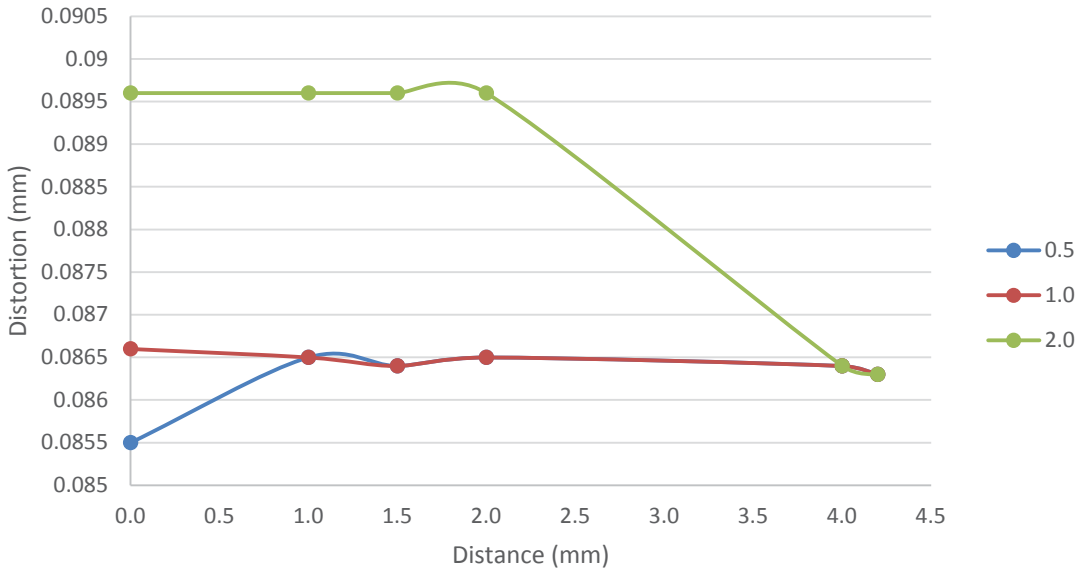

Figure 8.21 Graph plot showing FS variation of distortion

8.4.5 Significant points of the data results

Of significance in the stress and distortion results are the following four points:

1. Data collected in this section shows that the bulk of the plate is increased by varying only the thickness of the plate in isolation, resulting in least maximum stress but maximum fracture FS highest.

2. The maximal von Mises stress is located within the cortical bone for the 0.5mm and 1.0mm plate but within the plate for the 2.0mm thick design. This indicates that possible stress shielding on the bone is highest for the 2.0mm plate and least for the 0.5mm plate.

3. In comparison, the other data set where the plate bulk is altered is due to the variation in screw hole diameter. This is similar to changing the plate thickness by decreasing the screw hole diameter to increase the plate bulk to the maximal on von Mises stress, as presented in Section 8.3

4. Distortion results in Figure 8.21 for three variations in plate thickness are 0.086mm, 0.087mm and 0.090mm for the 0.5mm, 1.0mm and 2.0mm plate

thicknesses respectively. While some researchers would look at these values and query the significance of such minor variation, the important point is that for all three plate thicknesses limited distortion (micromotion) occurs.

With such data and literature available, it becomes clear that whilst it is agreed that controlled micromotion at a fracture site does promote healing, it is not agreed at which point micromotion becomes deleterious rather than advantageous. Einhorn (1995) stated that if there is any motion at the site of fracture then callous formation will occur, however, with excessive motion, a hypertrophic non-union may occur.

Perren (2002) postulates that pure fixation without compression produces flexible fixation, which is minimally invasive, enhances normal biological healing and returns patients to function with limited complications. All fixation systems designed and analysed in this thesis adhere to the principles outlined by Perren. However, Perren (2002) and Einhorn (1995) do not address the optimum micromotion allowed by flexible fixation in their research. When investigating this further, there appears to be a wide range of micromotion in the literature that is reported as being acceptable to healing. Szmukler-Moncler et al. (1998) claimed that 0.05mm to 0.15mm is the threshold for micromotion that positively contributes to healing associated with osseointegrated implants.

Yamaji et al. (2001) investigated micromotion of 0.3mm and 0.7mm and gaps between the fracture ends of 2.0mm and 6.0mm. They found that close fracture approximation with a larger value of 0.7mm micromotion produced uncomplicated healing. White et al. (1991) and Klein et al. (2002) investigated fracture micromotion of up to 1.0mm. In particular, White applied a force of 400N at a frequency of 0.5Hz over 500 cycles per day. Although not replicating the function of mastication, it was similar and the forced applied of 400N matched the force applied in this thesis during clenching. From data in this paper and comparing to the literature available, distortion values for each fixation system are valuable because they display the potential for safe micromotion that is acknowledged to promote favourable healing.

As outlined by Perren (2002), flexible fixation has many advantages over heavy rigid fixation that compresses the fracture ends. The advantages outlined by Perren have also been a pivotal aim of the research presented in this thesis. In the distortion data for variation in plate thickness and for the variations in plate design at no point does distortion become excessive to the point of detrimental fracture healing.

8.5 Results for von Mises stress and distortion with variation in plate material, Ti-6Al-4V, PLA and ZrO_2 under the functional movement of clenching.

Plate thickness and screw hole diameter is constant at 1.0mm and 2.25mm respectively.

8.5.1 Results for Ti-6Al-4V

The results for this configuration of plate are presented along with the FEM in Sections 8.1 and 8.2. To summarise, a maximum stress of 111.61MpA was recorded and concentrated at the plate ends.

8.5.2 Results for PLA

Maximum stress was measured at 4.87MPa. While significantly lower than the Ti-6Al-4V plate, stress was concentrated at the plate ends. The results are illustrated in Figures 8.22.

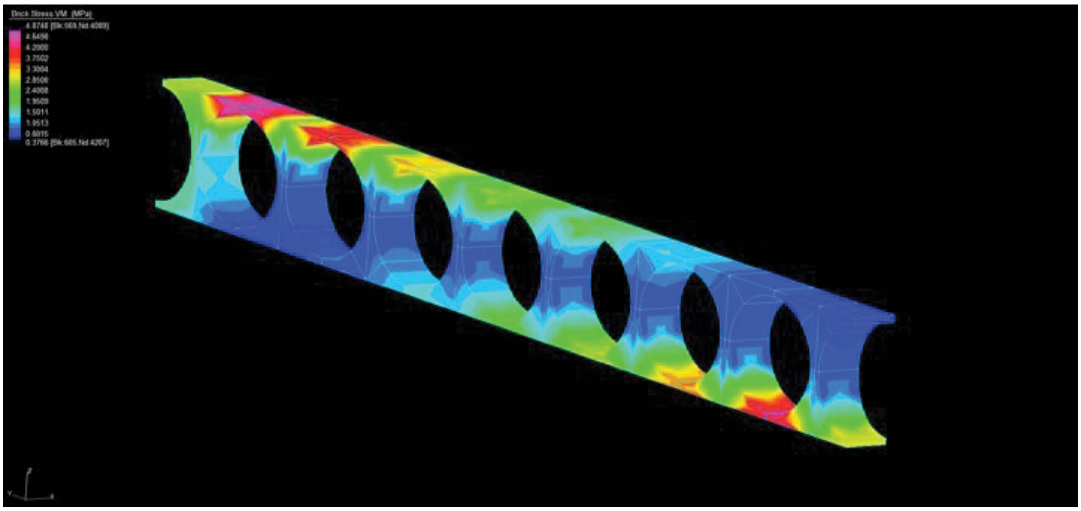

Figure 8.22 FEM of IP for PLA plate showing maximum stress concentration as illustrated by pink colouration

8.5.3 Results for ZrO_2

Maximum stress was measured at 172.21MPa and whilst one of the highest values obtained again, the stress was concentrated at the plate ends. The results are illustrated in Figures 8.23.

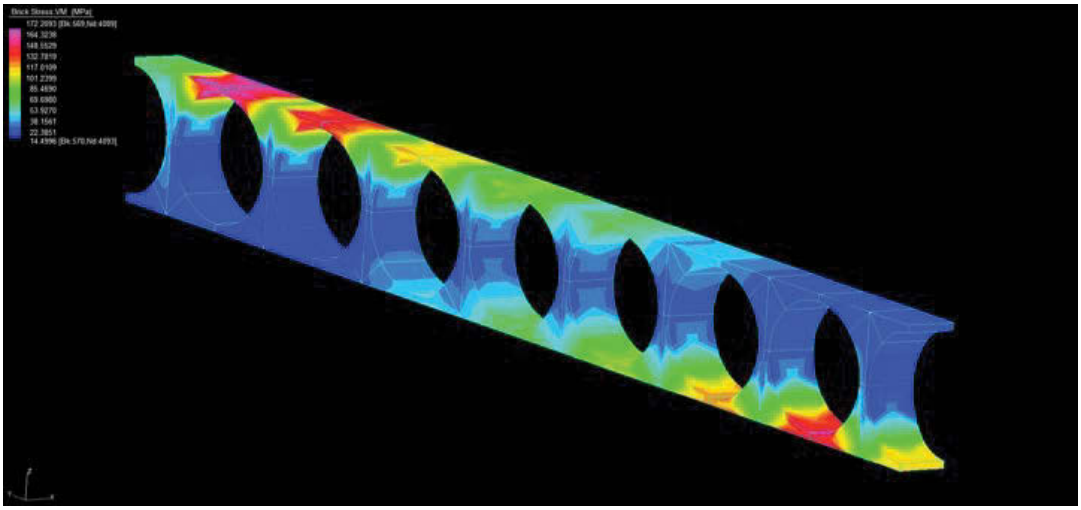

Figure 8.23 FEM of isolated plate for ZrO_2 plate showing maximum stress concentration as illustrated by pink colouration

The results for FS data for each plate are illustrated in Figure 8.24.

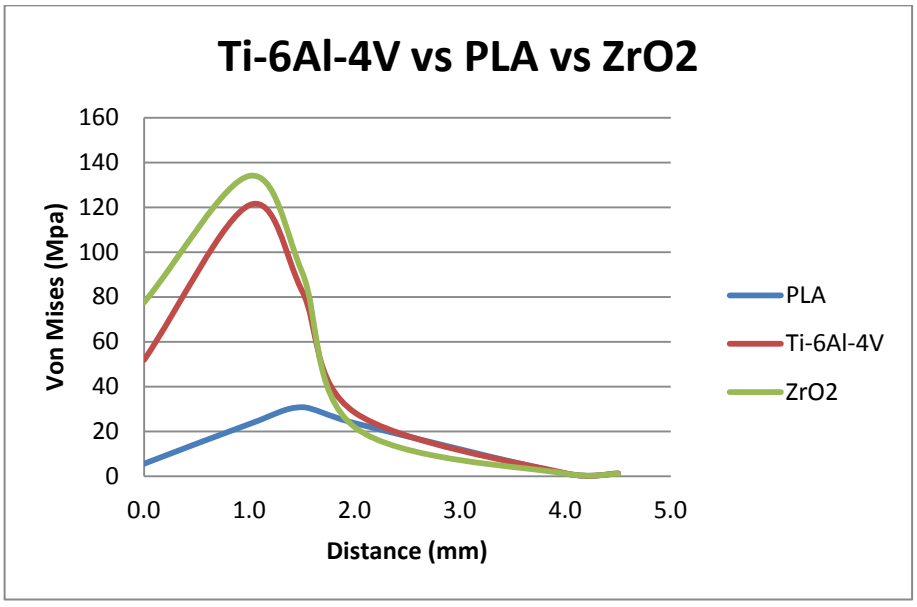

Figure 8.24 Graph plot of FS data for von Mises stress with Ti-6Al-4V, PLA and ZrO_2 plates

The results for distortion in the FS are illustrated in Figure 8.25.

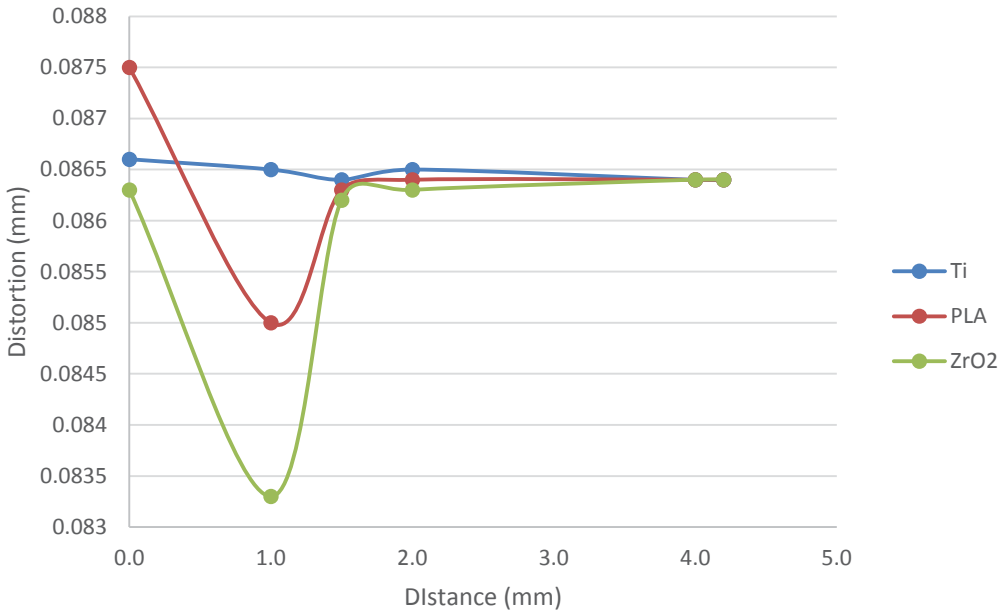

Figure 8.25 Graph plot of distortion within the FS

8.6 Results for von Mises stress and distortion with variation in a composite laminated plate (Ti-6Al-4V and PLA) under the functional movement of clenching

Figure 8.26 shows the design of the plate. The plate consisted of two laminates each of 0.5mm thickness and 2.25mm screw hole diameter. The combined plate thickness was 1.0mm. The laminates were applied to each other and restrained to prevent movement between the laminates, restrained at either end to simulate fixation with screws and allowed to freely deform during the functional movement of clenching.

The plate was applied in two ways: (i) the Ti-6Al-4V laminate facing outward; and (ii) the PLA laminate facing outwards. Each scenario was analysed and measured for maximum von Mises stress and distortion.

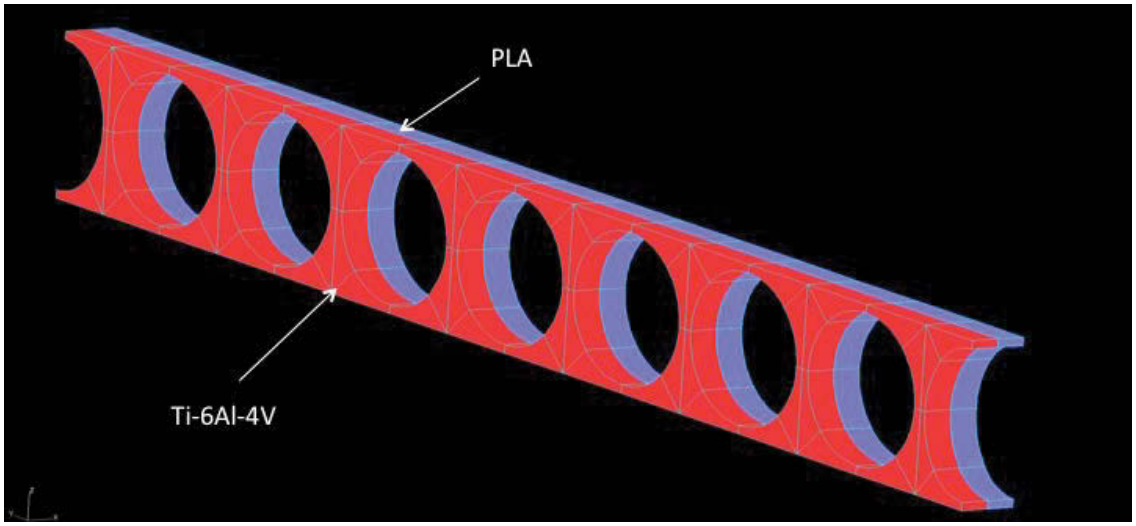

(A)

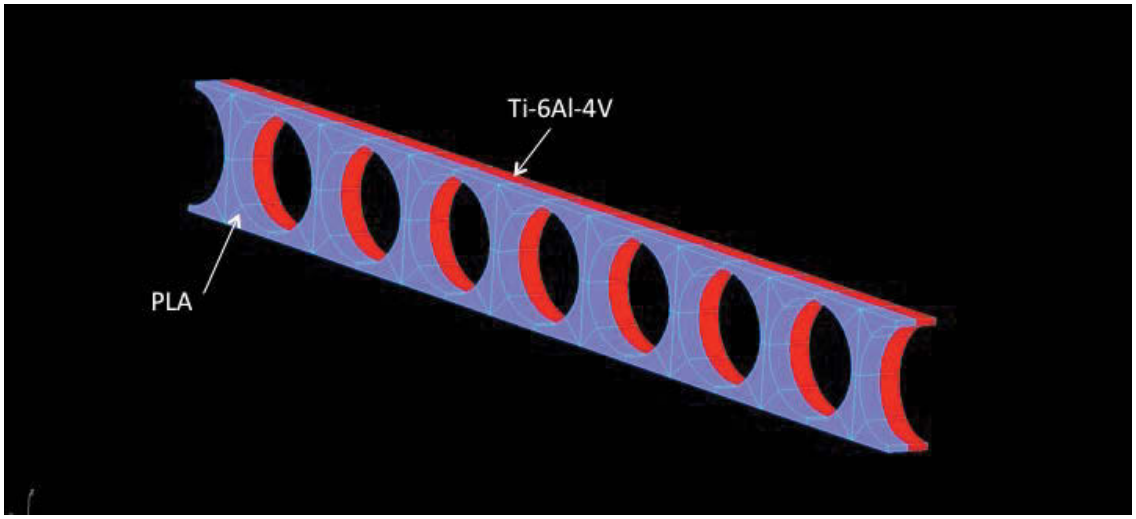

(B)

Figure 8.26 Composite laminate design with Ti-6Al-4V side facing outwards followed by the reverse with PLA laminate facing outwards

8.6.1 Results for PLA laminate facing outwards

A maximum stress of 133.64MPa was recorded within the composite plate. This stress was concentrated within the Ti-6Al-4V laminate and virtually reproduced the results in Section 9.4.1 where a 0.5mm thick, 2.25mm screw hole diameter Ti-6Al-4V was tested without the bonded PLA laminate. The results are illustrated in Figure 8.27.

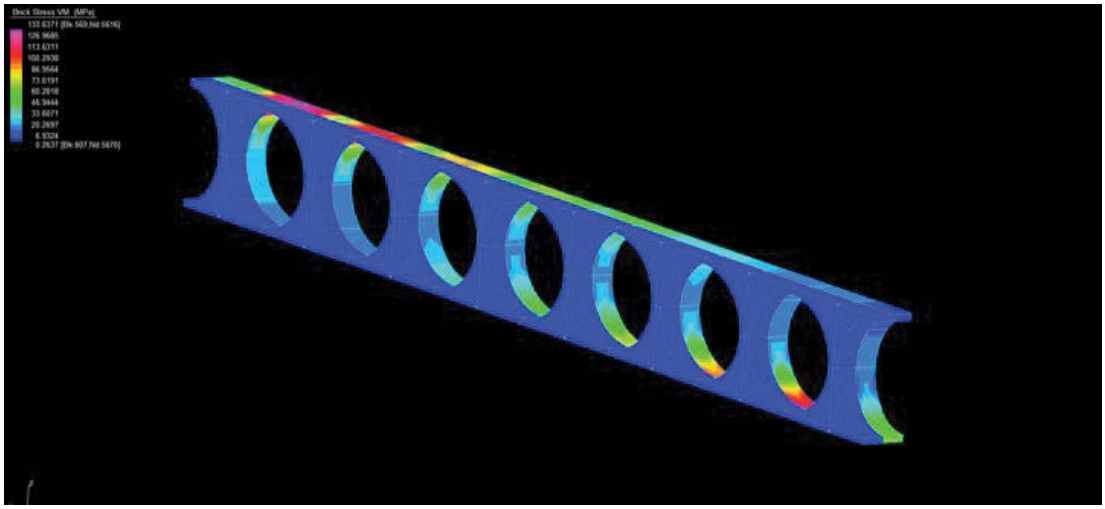

Figure 8.27 FEM of IP for composite laminated with PLA laminate facing outward

8.6.2 Results for Ti-6Al-4V laminate facing outwards

With Ti-6Al-4V laminate facing outwards, the interesting result of maximum stress being 56.20MPa is obtained. Whilst maximum stress is still concentrated in the Ti-6Al-4V laminate, the PLA laminate appears to have an increased stress in the vicinity of 31MPa, whereas in Section 9.6.1 where the plate is reversed, the PLA has a maximum stress in the vicinity of 7MPa and is homogenously distributed through the PLA laminate with no area of concentration. Results are illustrated in Figure 8.28.

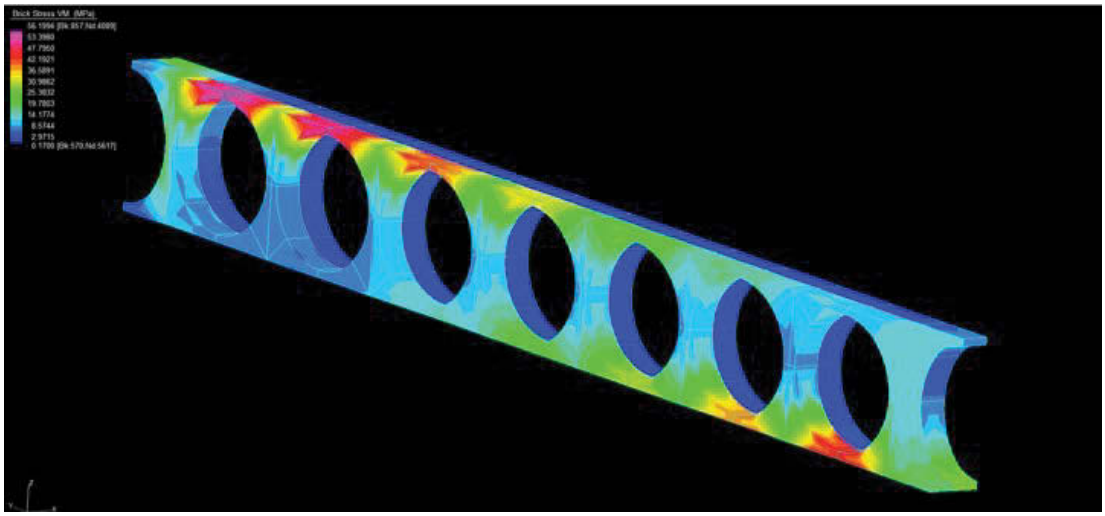

Figure 8.28 FEM of IP for composite laminated with Ti laminate facing outward

The results for von Mises stress in the FS with composite laminated plates in situ in both orientations are graphically illustrated in Figure 8.29.

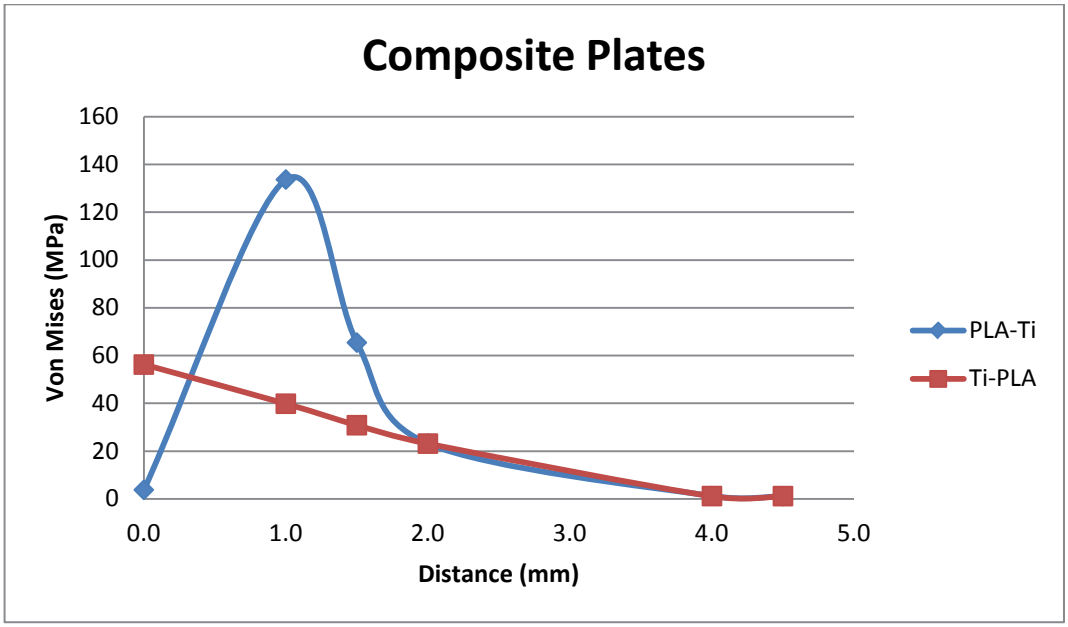

Figure 8.29 Graph plot of FS data for von Mises stress with composite laminate plates

The results for distortion in the FS with composite laminated plates in situ in both orientations are graphically illustrated in Figure 8.30.

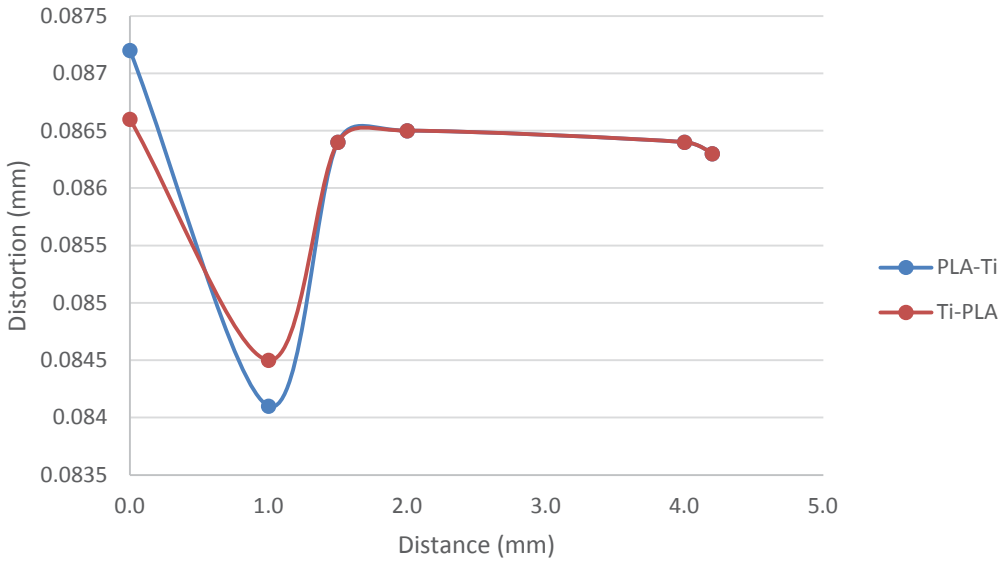

Figure 8.30 Graph plot of distortion of the FS

8.7 Results for variation in mesh fracture plate in clenching

Results for von Mises stress and distortion were collected for a new design linear mesh plate design using Ti-6Al-4V. The mesh was of the following dimensions: length 19.5mm, width 3.0mm and thickness 1.0mm. Data was collected for von Mises stress and distortion and compared to the linear Ti-6Al-4V plate design of thickness 1.0mm, length 19.5mm and width 3.0mm with 2.25mm diameter screw holes.

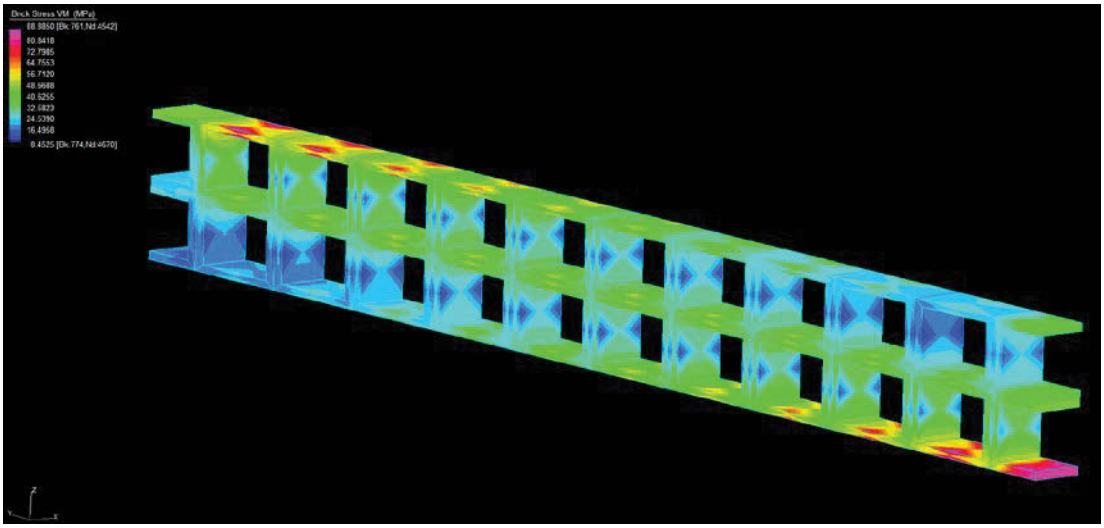

Figure 8.31 FEM of IP for Ti mesh showing maximal stress of 88.86MPa illustrated by areas of pink colouration

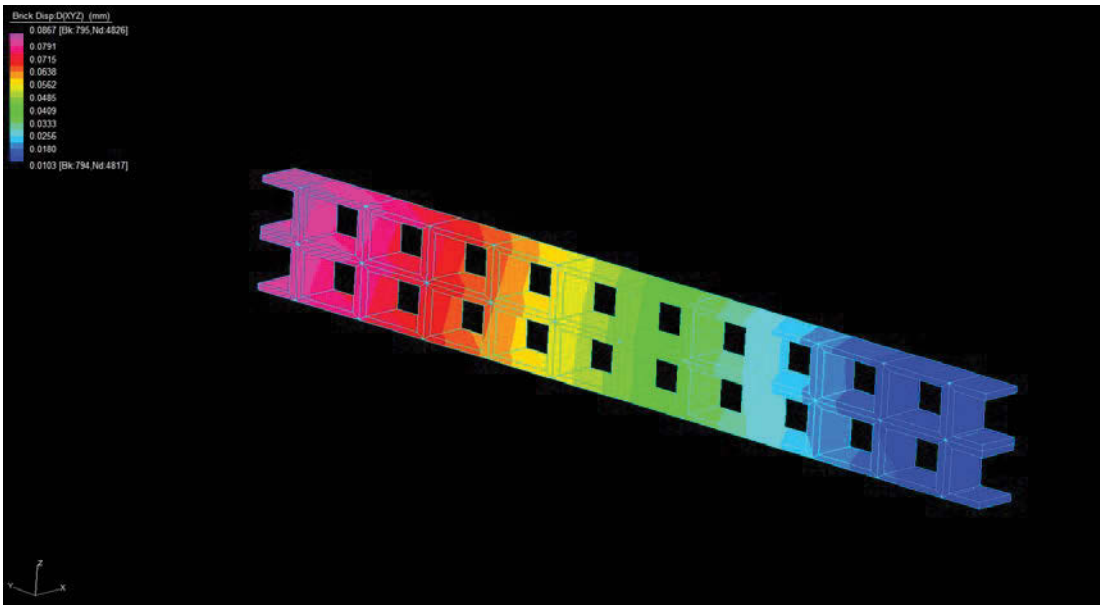

Figure 8.32 FEM of IP for Ti mesh showing maximal distortion of 0.0867mm.

Of importance was the comparison in surface area between the mesh plate design and the linear plate design. Figure 8.34 shows the linear plate design with the closest surface area compared with the mesh plate design and linear plate with 2.25mm diameter holes. This design had a surface are of 21.22mm^2 compared with 20.91mm^2 for the mesh plate.

In Figure 8.33, the comparison between the mesh plate design and linear plate design for von Mises stress is illustrated. The maximal von Mises stress in the FS for the mesh plate design is 143.7MPa and 122MPa for the plate design. Both have very similar distortion of 0.0867mm and 0.0865mm respectively.

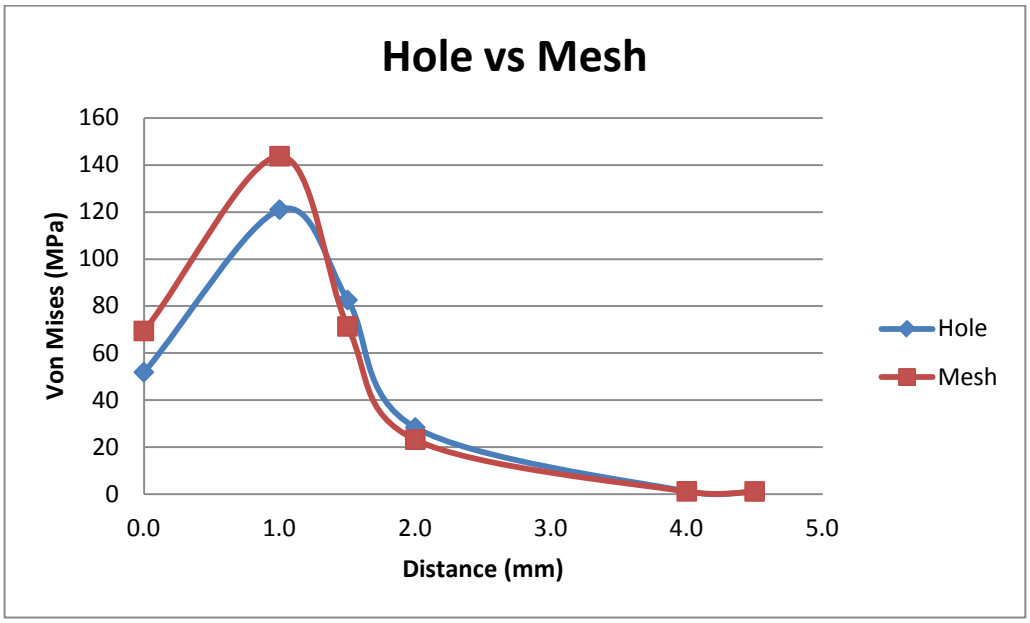

Figure 8.33 Comparison in performance between mesh plate and linear plate design (19.5mm x 3.0mm x 1.0mm with 2.25mm diameter holes) for von Mises stress in the FS

Table 8.4 Comparison of cross sectional area between mesh plate linear plate design (19.5mm x 3.0mm x 1.0mm) varying hole diameter from 2.25mm to 0.62mm

Model name	Surface area of plate (mm^2)
Mesh plate	20.91
Diameter 2.25mm	21.22
Diameter 1.88mm	32.56
Diameter 1.25mm	46.88
Diameter 0.62mm	55.43

8.8 Results from application of linear design plate across a fracture in the patient specific model during clenching

This model was designed as stated in previous chapters from PS CT data and then modelled and analysed using Materialise (Mimics and 3-Matic),Rhinoceros3D, Autodesk Inventor and finally Ansys Workbench for FEA processing. The muscle forces and the constraints are the same as the STRAND model, however, muscles of clenching were applied to an area rather than nodal insertion.

The results for maximum stress for clenching, as evidenced in Figure 8.34, shows an extremely high value of 1.1077e10 Pa. Considering this value and its apparent discrepancy to the rest of the model, the erroneous peak stress measurement is attributed to inaccuracy produced during the meshing process in the production of the model. Looking at the remainder of values indicated by blue, green and yellow colouration, the average value of 312.23MPa is reached. With regard to distortion, a value of 0.0758mm is reached in the plate adjacent to the fracture (Figure 8.35).

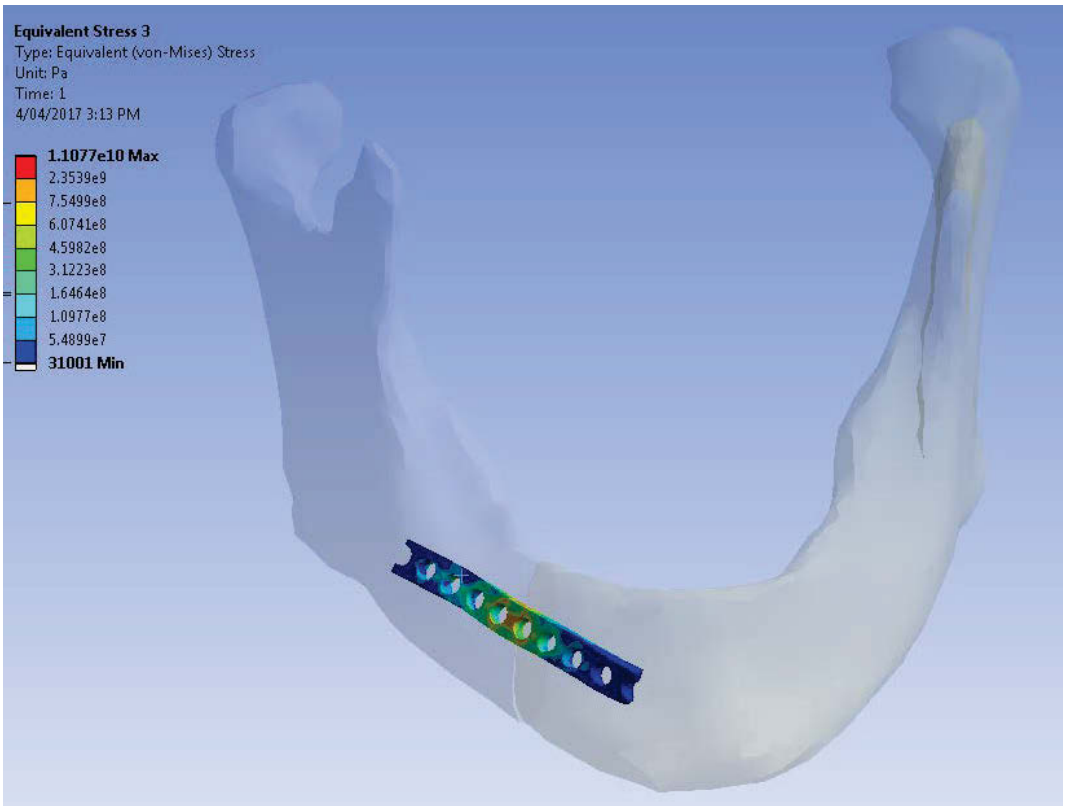

Figure 8.34 FEM of IP tested for von Mises stress during clenching (mandibular model is greyed out to emphasise the plate)

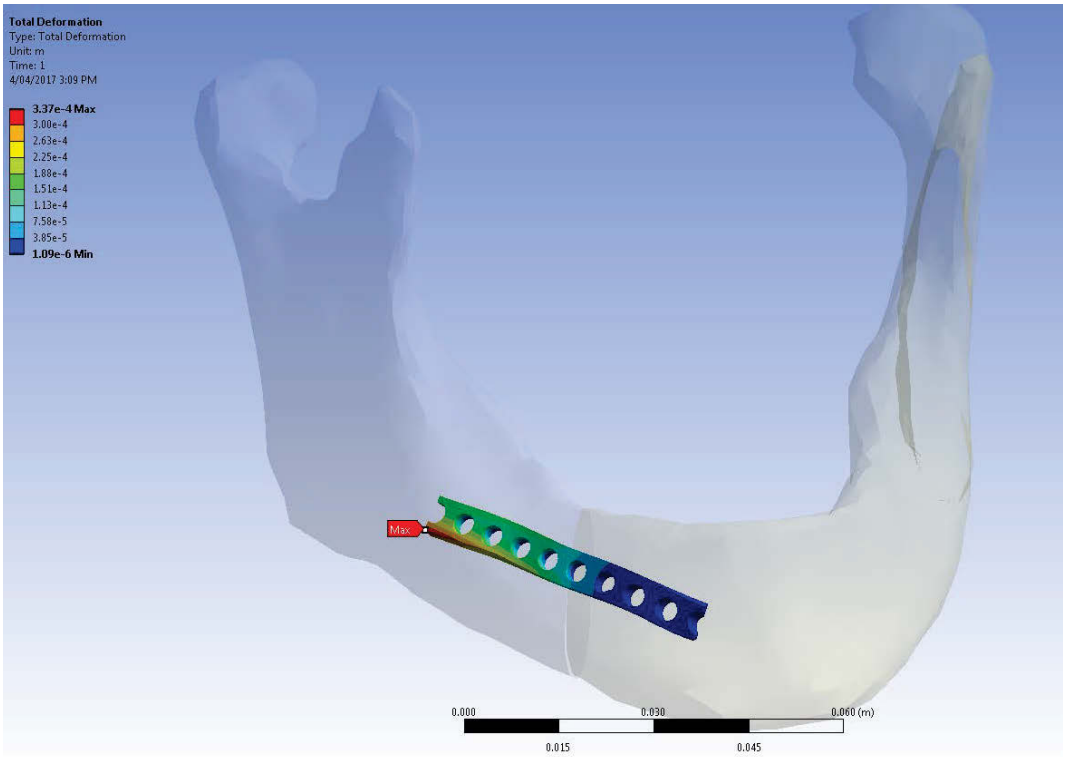

Figure 8.35 FEM of IP tested for distortion during clenching (mandibular model is greyed out to emphasize the plate and a scale is provided to reference for dimensions)

8.8 Summation and tabulation of all data set results

Table 8.5 shows data collected for comparison from seven data sets: (i) Validation; (ii) Variation in screw hole diameter; (iii) Variation in plate thickness; (iv) Variation in material; (v) Composite laminate plate; (vi) Mesh plate; and (vii) Patient specific.

Table 8.5 Summation of data set results

Fixation System	Isolated plate, maximum von Mises stress in clenching	Isolated plate, maximum von Mises stress in protrusion	Isolated plate, maximum von Mises stress in opening	Fracture segment, maximum von Mises stress and location in clenching	Fracture segment, maximum von Mises stress and location in protrusion	Fracture segment, maximum von Mises stress and location in opening	Isolated plate, maximum distortion in clenching	Isolated plate, maximum distortion in protrusion	Isolated plate, maximum distortion in opening
Validation data set									
Ti 1.0 x 19.5 x 3.0mm HD 2.25mm	111.61MPa	77.36MPa	60.18MPa	122MPa in cx bone	81MPa in cx bone	70MPa in cx bone	0.0865mm	0.18mm	0.126mm
Variation in hole diameter data set									
Ti 1.0 x 19.5 x 3.0mm HD 2.25mm	111.61MPa	_	_	122MPa in cx bone	_	_	0.0865mm	_	_
Ti 1.0 x 19.5 x 3.0mm HD 1.88mm	101.04MPa	_	_	151MPa in cx bone	_	_	0.086mm	_	_
Ti 1.0 x 19.5 x 3.0mm HD 1.25mm	85.17MPa	_	_	158MPa in cx bone	_	_	0.085mm	_	_
Ti 1.0 x 19.5 x 3.0mm HD 0.62mm	70.85MPa	_	_	161MPa in cx bone	_	_	0.08mm	_	_
Variation in plate thickness data set									
Ti 0.5 x 19.5 x 3.0mm HD 2.25mm	133.64MPa	_	_	82MPa in cx bone	_	_	0.0865mm	_	_
Ti 1.0 x 19.5 x 3.0mm HD 2.25mm	111.61MPa	_	_	113MPa in cx bone	_	_	0.0865mm	_	_
Ti 2.0 x 19.5 x 3.0mm HD 2.25mm	116.12MPa	_	_	140.5MPa in plate	_	_	0.0896mm	_	_

Fixation System	Isolated plate, maximum von Mises stress in clenching	Isolated plate, maximum von Mises stress in protrusion	Isolated plate, maximum von Mises stress in opening	Fracture segment, maximum von Mises stress and location in clenching	Fracture segment, maximum von Mises stress and location in protrusion	Fracture segment, maximum von Mises stress and location in opening	Isolated plate, maximum distortion in clenching	Isolated plate, maximum distortion in protrusion	Isolated plate, maximum distortion in opening
Variation in plate material data set									
Ti 1.0 x 19.5 x 3.0mm HD 2.25mm	111.61MPa	_	_	113MPa in cx bone	_	_	0.0865mm	_	_
PLA 1.0 x 19.5 x 3.0mm HD 2.25mm	4.87MPa	_	_	30MPa in cx bone	_	_	0.0875mm	_	_
ZrO_2 1.0 x 19.5 x 3.0mm HD 2.25mm	172.21MPa	_	_	133MPa in cx bone	_	_	0.0863.0mm		
Composite laminate plate data set									
CLP 1.0 x 19.5 x 3.0mm PLA/TI	133.64MPa	_	_	133.64MPa at bone plate interface	_	_	0.0872mm	_	_
CLP 1.0 x 19.5 x 3.0mm Ti/PLA	56.20MPa	_	_	56.20MPa at plate surface	_	_	0.0866mm		
Mesh plate data set									
Ti Mesh	88.86MPa	_	_	?	_	_	0.0867mm	_	_
Patient specific data set									
	312.23MPa						0.0758mm		

CHAPTER 9:
SUMMARY AND CONCLUSIONS

In practice, a significant chasm can exist between science and its application to patients and their clinical presentations. Where this gap is addressed successfully, it significantly serves to benefit healthcare, and it has been this aim that has driven this thesis. Failure to combine science with clinical application leads to disastrous outcomes, as illustrated in Figure 9.1.

Figure 9.1 Shows inadequate fracture fixation leading to fixation system failure resulting in fracture non-union in an elderly female with osteoporosis and an atrophic mandible

The purpose of this thesis is to initially look at the entity of facial trauma, its aetiology, prevalence, pathophysiology, process of uncomplicated and complicated healing, as well as difficulties in management and its associated socioeconomic cost. With this understanding, further areas of investigation in this thesis take on significance. Namely, the complexity of the anatomy and biomechanics, not only of the dentate mandible, but also the edentulous mandible. Fracture management systems that are currently in clinical use and their shortcomings, the use of finite element modelling and specifically how it can be used to study and improve fracture management, and finally the area of PS design are also investigated

In this discussion, it is worthwhile to focus on these elements, and then address the specific findings of the research and their implications to surgical management.

The dentate and edentulous mandible in the setting of trauma are points of significance worth noting. Amongst these are the number of incidents of facial skeletal trauma. Of the facial bones, the mandible sits second behind nasal bones fractures in terms of incidence but surges ahead to being the facial bone most often requiring surgical intervention to treat the fracture (Figures 9.2 & 9.3).

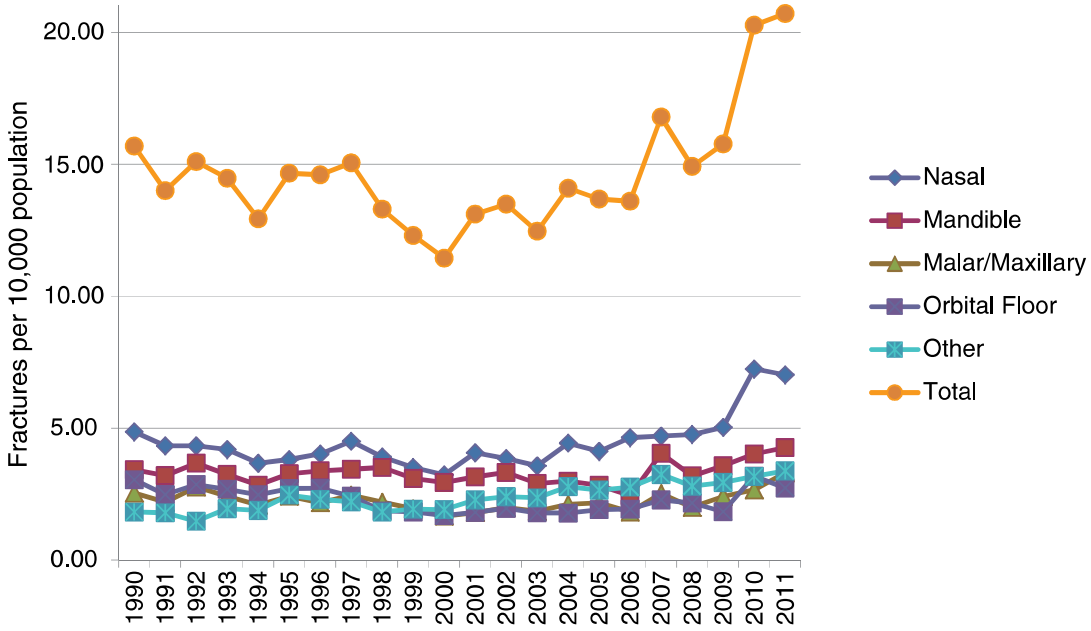

Figure 9.2 Incidence of facial bone fractures (VandeGriend, 2015)

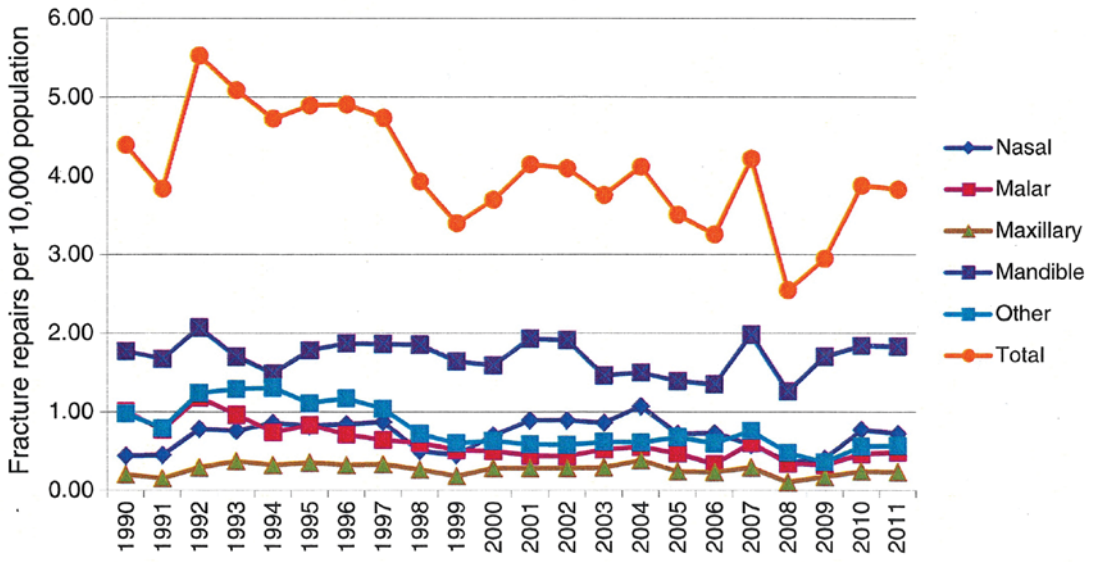

Figure 9.3 Facial bone fractures requiring surgical repair (VandeGriend, 2015)

In looking at VandeGriend's data in 2011, there was an incidence of 4.5 mandibular fractures per 10.000 population. Of these, 3.9 required repair or 87% of mandibular fractures. This is a very high figure that requires repair, and sits among the highest for all areas of skeletal trauma. To repair mandibular trauma is difficult and accounts for many millions in healthcare dollars each year. In the USA, the cost to repair each episode of mandibular trauma averages at US$49,892.00 per case (Allareddy, 2011). The reason for the high cost is that the mandible has a key and important anatomical location and function. In the facial form, it is prominent and not protected by other surrounding structures, therefore, blunt trauma in its vicinity is likely to produce injury.

In function, the mandible plays keys roles in facial expression, speech, mastication, deglutition and airway maintenance, to name a few key points. If trauma occurs that results in mandibular fracture, then any one of these key functions, if affected, leads to significant morbidity and possible mortality. Although mortality from isolated mandibular fractures is rare, mortality from mandibular fractures, combined with other forms of trauma, can be as high as 8.1% (Fischer 2001).

Not only is the mandible of significant location anatomically in itself, it is possibly the most complicated and unique bone in the entire human skeleton. From its embryonic intramembranous ossification to its blood supply, which varies from endosteal in the dentate mandible to periosteal in the edentulous mandible, its complex morphology involves multiple vertical and horizontal rami and angles along with the bilateral temporomandibular joints.

Being common and of anatomical significance, mandibular trauma often necessitates operative intervention to ensure a patient's full recovery (Figure 9.3). In providing treatment, a significant monetary cost is funded by the community and often the individual concerned. However, such cost is not only monetary but often physiological. Furthermore, if treatment is not appropriate, significant long-term morbidities can result.

To further complicate the issue of trauma leading to fracture of the atrophic mandible, which usually occurs in the older age group, this cohort carries with it significant

comorbidities such as poor cardiac health, diabetes, long-term effects of smoking and osteoporosis. As such, particularly in the older generation, it is important that treatment is successful, quick, uncomplicated and as uninvasive as possible. The aim of any fracture fixation system is to fulfil these criteria. To date, the easiest way to do this is with a fixation system that enhances the body's natural process of fracture repair, that is, haematoma formation, bone callous formation and bone remodelling. The system needs to be able to provide fixation and immobilization to a degree (we will discuss micromovement later in this chapter) and thus allow the body's natural repair to occur (Figure 9.4).

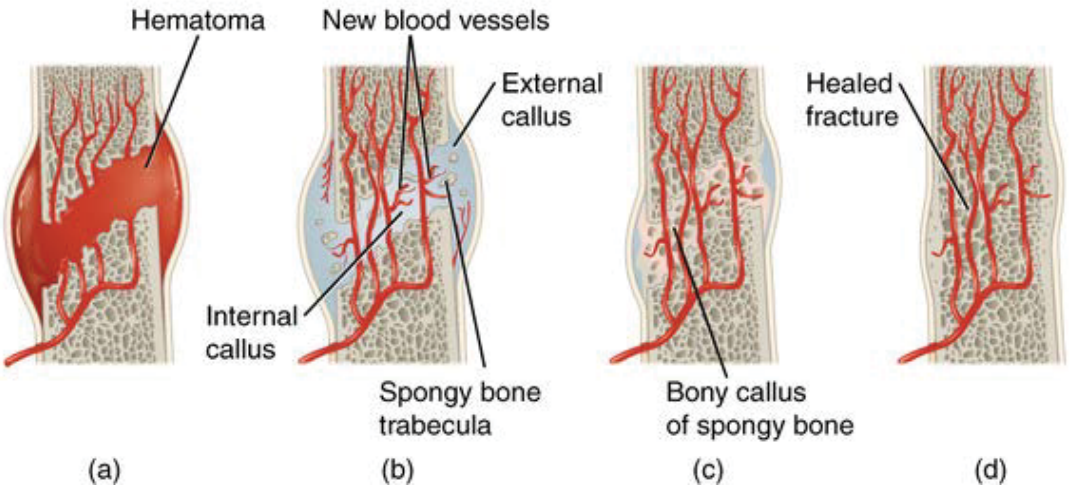

Figure 9.4 Four stages of fracture healing: (i) haematoma formation; (ii) bone regeneration; (iii) bony callous formation; and (iv) bone remodelling (courtesy of Boundless)

Current mandibular fracture repair systems show healthy degrees of success but still suffer from several flaws, including difficulty in adaptation to the patient and continued stress in vivo leading to hardware failure due to breakage. The process of plate bending and manipulation to fit a generic plate to the patient begins the process of work hardening (Figure 9.5) and continued stress on the plate, particularly if it is not correctly adapted to the patient, therefore, resulting in failure (Figures 9.6 & 9.7). An additional problem in shaping Ti-6Al-4V fixation devices is the notch effect created if unintensional deep scratches are created. Notch areas fail approximately at 80% of the maximum stress during in vitro testing.

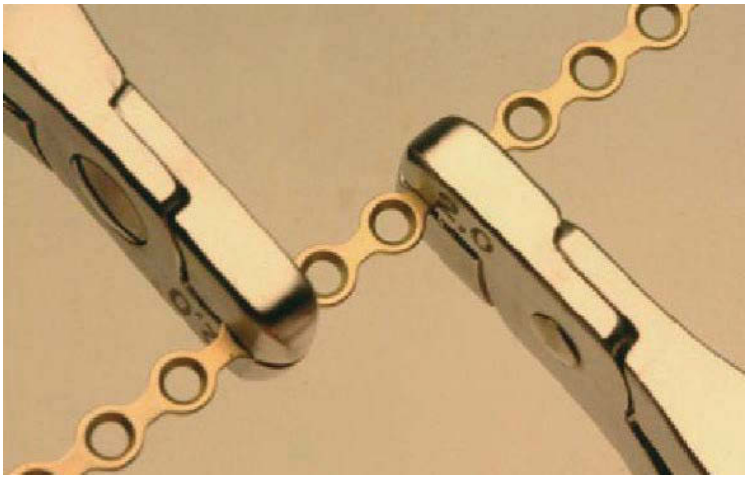

Figure 9.5 Plate benders being applied to manipulate and shape a Ti plate prior to insertion onto the fracture site, producing material distortion at the site where plate failure is most likely to occur (courtesy of AO Foundation)

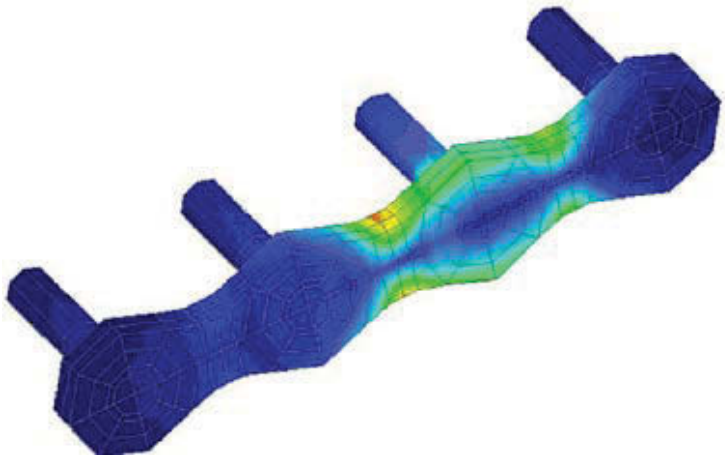

Figure 9.6 FEM of four screw hole miniplate showing the location of highest von Mises stress (Sugiura, 2009)

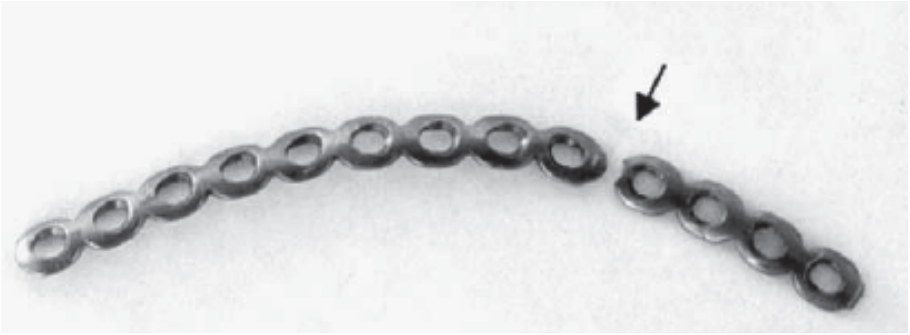

Figure 9.7 Failed commercially pure Ti plate for osteosynthesis (Azevedo, 2003)

With the knowledge of hurdles to be faced in successful fracture repair of the edentulous mandible, this thesis aimed to study a more PS FEM and the design of various fracture fixation systems, as well as to assess their degree of utility to the application of fracture repair.

To understand the requirements of a successful model, an understanding of mandibular anatomy and biomechanics is essential. As such, a detailed investigation of the relevant anatomy and biomechanics is undertaken in Chapter 2. From this analysis, key points taken into the design of the FEM are explained.

The mandible in function for the purpose of the FEM used in this research was assumed to behave as a Class III lever action, however, the debate between those in favour of the Class III lever versus non-lever hypothesis has been discussed.

The maximum bite force varies considerably, depending on age, sex, race and dentate versus edentulous. The maximum bite force occurs in males at the end of adolescence. The bite force is at its maximum in the dentate mandible during clenching when measured at the first molars in dentate subjects. Values up to 90kg have been reported (Howell, 1948). In comparison, Triparthi measured the bite force in the edentulous mandible at the first molar site during clenching to be only 4.43kg. The greatest force that can be generated during mandibular movement occurs during clenching. The mandibular movements of opening and protrusion produce far less force.

To test various fixation systems to maximal force, clenching was chosen as the primary function tested and the bite force was set at 400N applied bilaterally at the premolar/molar junction. Whilst this is greater than normally generated in the edentulous mandible, it is possible that such a force could be generated with training, for example, the force applied to the FEM during clenching in order that the fixation systems being analysed were subject to the maximum stress possible.

On this background of understanding that has been summarised above this thesis took FEA and used it as tool to try and address the complexities in mandibular fracture by analysing current plate design, comparing it to several novel designs and a PS design.

The models used were based on the preparatory work of my University co-workers Professor Ben-Nissan, Drs Choi and Taraschi. Without their guidance and help this

The FEM concept of a non-specific edentulous mandibular model with appropriate anatomy and musculature developed by Ben-Nissan, and later further modified by Choi, was used to conduct the analysis of a typical fracture plate used in current practice in the setting of the 'new' FEM. This plate was designed in Ti-6Al-4V with dimensions of length 19.5mm, width 3.0mm, depth 1.0mm and a screw hole diameter of 2.25mm. It was compared with a variety of novel designs as described and presented in Chapters 8 and 9. The concept of Dr Taraschi's CT based PS model was modified and used to analyse a typical fracture plate used in current practice and compare with previously published data using a non-specific model, that is, that based on works of Ben-Nissan and Choi.

However, before discussing the results from surgeon's perspective, what was observed in the belief that any computational analysis is only as good as the data entered certainly holds true for finite element modelling. For example, where a FEM is used to analyse a beam, the model is relatively simple (Figure 9.8). That is, the dimension and morphology of the beam are easily established, the material of construction is homogenous and loads and points of application are also well known. Hence, constructing a FEM in this scenario is relatively easy compared with that of the human mandible.

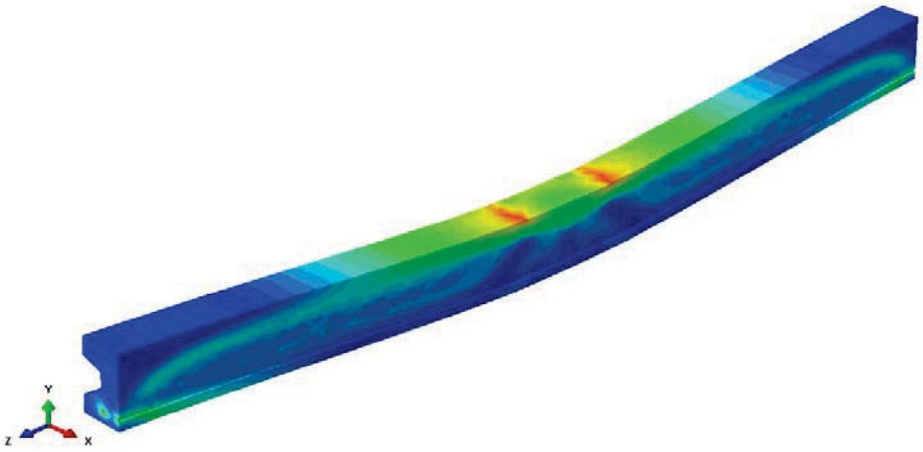

Figure 9.8 FEM of bridge C section beam (courtesy of Vanderbilt University School of Engineering)

In the human mandible, the reverse of the above description of the steel beam is true. A model that represents the heterogynous nature of human tissue and anatomy is very difficult, the application of force is complex, and finally, the individual variation between human subjects is vast.

Taking this into account, this thesis presents a chronological evolution in the development of mandibular FEMs. Firstly, the work pioneered by Ben-Nissan and illustrated in Figure 9.9(A) show the infancy of mandibular finite element modelling, as well as show its simplicity of anatomical representation.

In the work of Choi, the building block from Ben-Nissan's work was expanded (Figure 9.9(B)), particularly work done to improve modelling the fracture area when comparing the 'old' with the 'new' model.

Finally, the PS model was further developed from Ben-Nissan and Choi's work by Taraschi, as illustrated in Figure 9.9(C). Across all three variances, the muscle forces and applications were similar, however, muscle insertions and origins were applied on areas rather than points. The major difference was the improvement in the anatomical and PS representations of their anatomy.

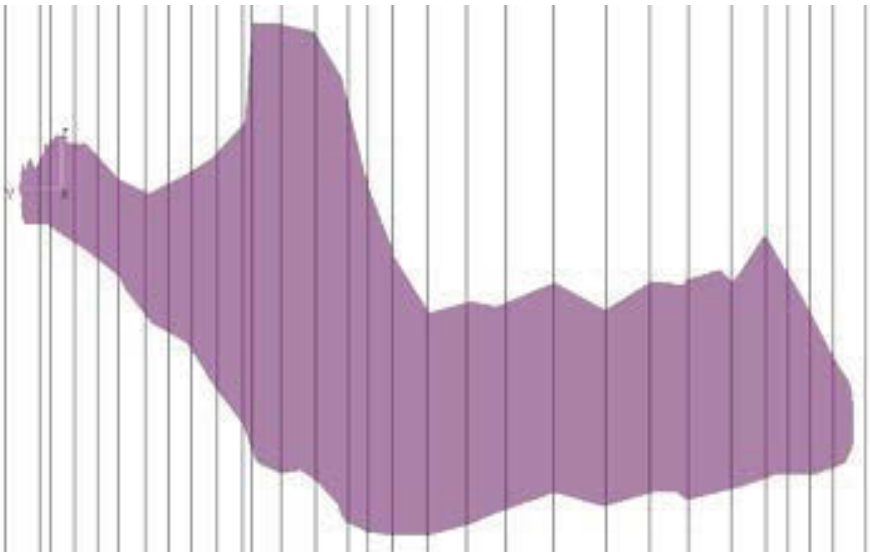

(A) Example of Ben-Nissan's segmentation of the mandible.

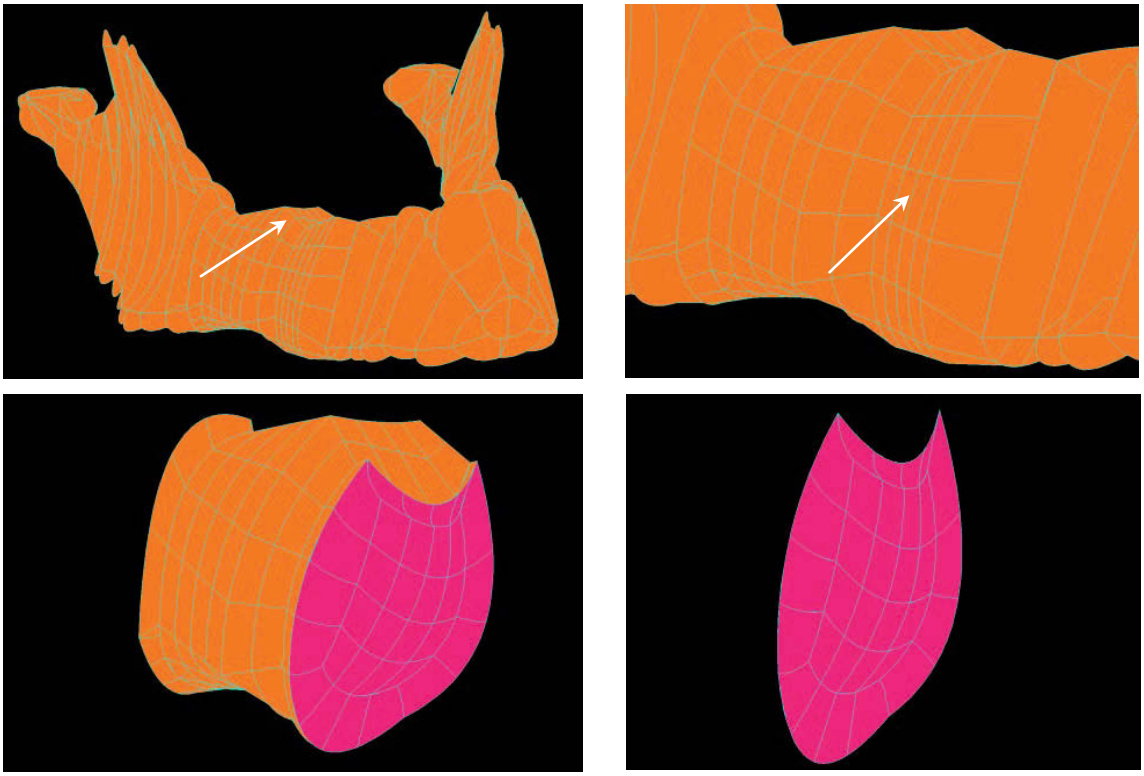

(B) Progress of Choi's work to produce a more anatomically accurate model but one that is not patient specific.

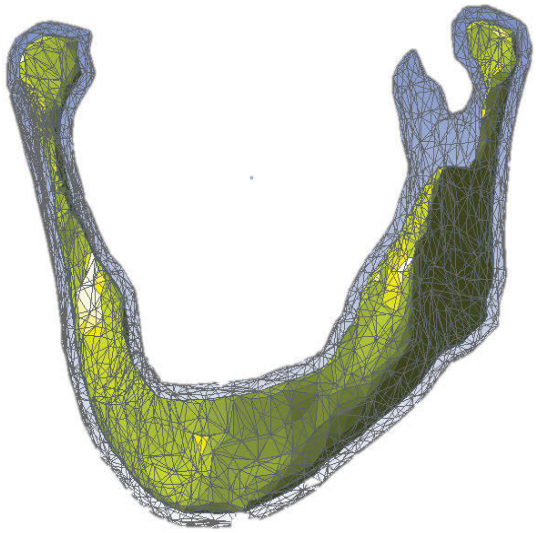

(C) Culmination to the most recent model of Taraschi (2016) being patient specific from CT data and hence most anatomically accurate to an individual.

Figure 9.9 Summary of six data set results

To aid in presenting the results from this work, data is presented in Table 9.1.

Table 9.1 Results for seven data sets

Fixation System	Isolated plate, maximum von Mises stress in clenching	Isolated plate, maximum von Mises stress in protrusion	Isolated plate, maximum von Mises stress in opening	Fracture segment, maximum von Mises stress and location in clenching	Fracture segment, maximum von Mises stress and location in protrusion	Fracture segment, maximum von Mises stress and location in opening	Isolated plate, maximum distortion in clenching	Isolated plate, maximum distortion in protrusion	Isolated plate, maximum distortion in opening
1. Validation data set									
Ti 1.0 x 19.5 x 3.0mm HD 2.25mm	111.61MPa	77.36MPa	60.18MPa	122MPa in cx bone	81MPa in cx bone	70MPa in cx bone	0.0865mm	0.18mm	0.126mm
2. Hole diameter data set									
Ti 1.0 x 19.5 x 3.0mm HD 2.25mm	111.61MPa	–	–	122MPa in cx bone	–	–	0.0865mm	–	–
Ti 1.0 x 19.5 x 3.0mm HD 1.88mm	101.04MPa	–	–	151MPa in cx bone	–	–	0.086mm	–	–
Ti 1.0 x 19.5 x 3.0mm HD 1.25mm	85.17MPa	–	–	158MPa in cx bone	–	–	0.085mm	–	–
Ti 1.0 x 19.5 x 3.0mm HD 0.62mm	70.85MPa	–	–	161MPa in cx bone	–	–	0.08mm	–	–
3. Plate thickness data set									
Ti 0.5 x 19.5 x 3.0mm HD 2.25mm	133.64MPa	–	–	82MPa in cx bone	–	–	0.0865mm	–	–
Ti 1.0 x 19.5 x 3.0mm HD 2.25mm	111.61MPa	–	–	122MPa in cx bone	–	–	0.0865mm	–	–
Ti 2.0 x 19.5 x 3.0mm HD 2.25mm	116.12MPa	–	–	140.5MPa in plate	–	–	0.0896mm	–	–

Fixation System	Isolated plate, maximum von Mises stress in clenching	Isolated plate, maximum von Mises stress in protrusion	Isolated plate, maximum von Mises stress in opening	Fracture segment, maximum von Mises stress and location in clenching	Fracture segment, maximum von Mises stress and location in protrusion	Fracture segment, maximum von Mises stress and location in opening	Isolated plate, maximum distortion in clenching	Isolated plate, maximum distortion in protrusion	Isolated plate, maximum distortion in opening
4. Plate material data set									
Ti 1.0 x 19.5 x 3.0mm HD 2.25mm	111.61MPa	–	–	122MPa in cx bone	–	–	0.0865mm	–	–
PLA 1.0 x 19.5 x 3.0mm HD 2.25mm	4.87MPa	–	–	30MPa in cx bone	–	–	0.0875mm	–	–
ZrO_2 1.0 x 19.5 x 3.0mm HD 2.25mm	172.21MPa	–	–	133MPa in cx bone	–	–	0.0863.0mm	–	–
5. Composite laminate plate data set									
CLP 1.0 x 19.5 x 3.0mm PLA/TI	133.64MPa	–	–	133.64MPa at bone plate interface	–	–	0.0872mm	–	–
CLP 1.0 x 19.5 x 3.0mm Ti/PLA	56.20MPa	–	–	56.20MPa at plate surface	–	–	0.0866mm	–	–
6. Mesh plate data set									
Ti Mesh	88.86MPa	–	–	–	–	–	0.0867mm	–	–
7. Patient specific data set									
	312.23MPA	–	–	–	–	–	0.0758mm	–	–

From the data sets, conclusions from surgical analysis are as follows.

1. From the validation data set, the analysis using the 'new' more accurate generic model of a Ti-6Al-4V linear fracture plate of design currently used in surgical practice shows that data collected compares similarly with data for older models as summarised in Figure 9.10.

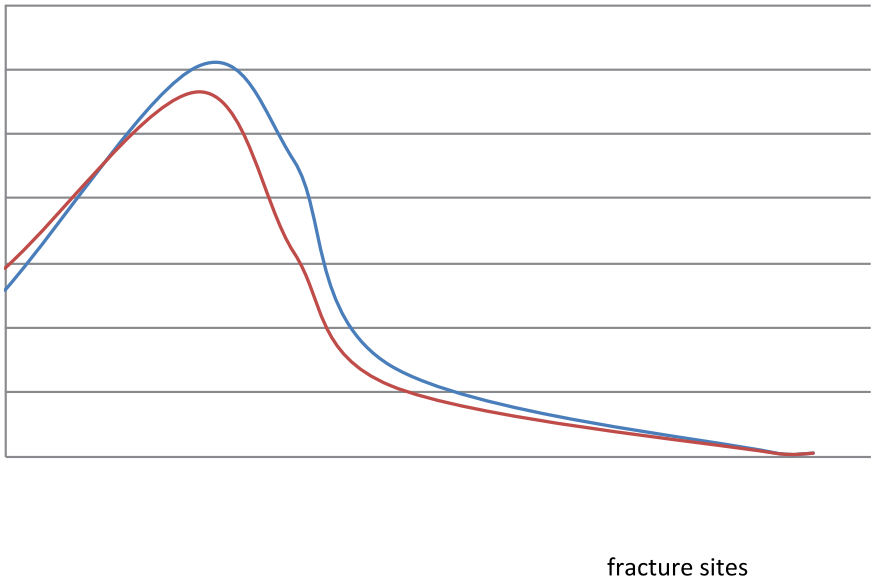

Figure 9.10 Showing comparison in stress curve for 'old' generic model and 'new: generic model

Maximum peak stress values are similar and both fall well within the margin of safety beyond which plate failure can occur. Both show that peak stress is just within the cortical bone layer and drops away rapidly as the cancellous bone layer is entered in clenching. A micromotion of 0.0865mm is allowed in clenching which would protect against potential stress shielding in the surrounding bone as it tries to remodel during healing. Interestingly, distortion in opening and protrusion are higher at values of 0.126mm and 0.18mm respectively, some 200% higher than with clenching. This can be accounted for by clenching the occluding surface, whether it be teeth, dentures or mucosa acting as a brace and minimising distortion, whereas with protrusion and opening no such 'bracing effect' occurs. This leads to the postulation that with stress a maximum obviously occurs in clenching where the force delivered to the

mandible is above that delivered in opening and protrusion, however, despite the force disparity due to the 'bracing effect', distortion is worse with opening and protrusion. How much stress is tolerable beyond which failure occurs has been well documented in the literature for Ti and bone, however, for distortion this is not as clear. Joos (2001) looked at the role of movement in fracture management and suggested that excessive micromovement at the 'gap tissue' (fracture site) was a significant factor in the clinical outcome of fracture treatment leading to success or failure. However, it is difficult to determine how much movement is acceptable as the balance between micromovement necessary to facilitate healing and prevent stress shielding versus movement that is detrimental to fracture healing is not known and certainly would have variance based on differences between individuals. What is clear, however, is that clenching produces maximal stress opening and protrusion produces maximal distortion, and these movements may play a bigger role in the failure of fracture healing than expected, either within the fixation system or the bone itself, or both.

The following data sets are presented for clenching only, as per the original design and intention of the study, however, opening and protrusion are obvious areas of interest that should be addressed in future research because the results of a PS model would be interesting and valuable to our knowledge.

2. The variation in the screw hole diameter data set showed that clenching by decreasing the screw hole diameter from 2.25mm to 1.88mm, 1.25mm and 0.62mm created a gradual decrease in plate stress from 111.61MPA down to 70.85MPa and a converse increase of stress within bone from 122MPa to 161MPa (Figure 9.11). Distortion changed from 0.0865mm to 0.08mm. All of these values fit inside clinical margins of safety that would prevent fixation system failure.

   Of most interest is changing the plate hole diameter from 2.25mm to 0.62mm, which produces a difference in surface from 21.22mm^2 to 55.43.0mm^2, a difference of 261%, however, stress has a maximum change of 157% and a distortion change of 101%. Compared with the significant difference in surface,

there are resultant differences in peak stress and distortion, particularly rare less acute. Following on from this, another point of note is by altering the screw hole diameter from 2.25mm down to 0.62mm, maximal stress is driven further within the body of the mandible, as evidenced by the shift in peaks in Figure 9.11.

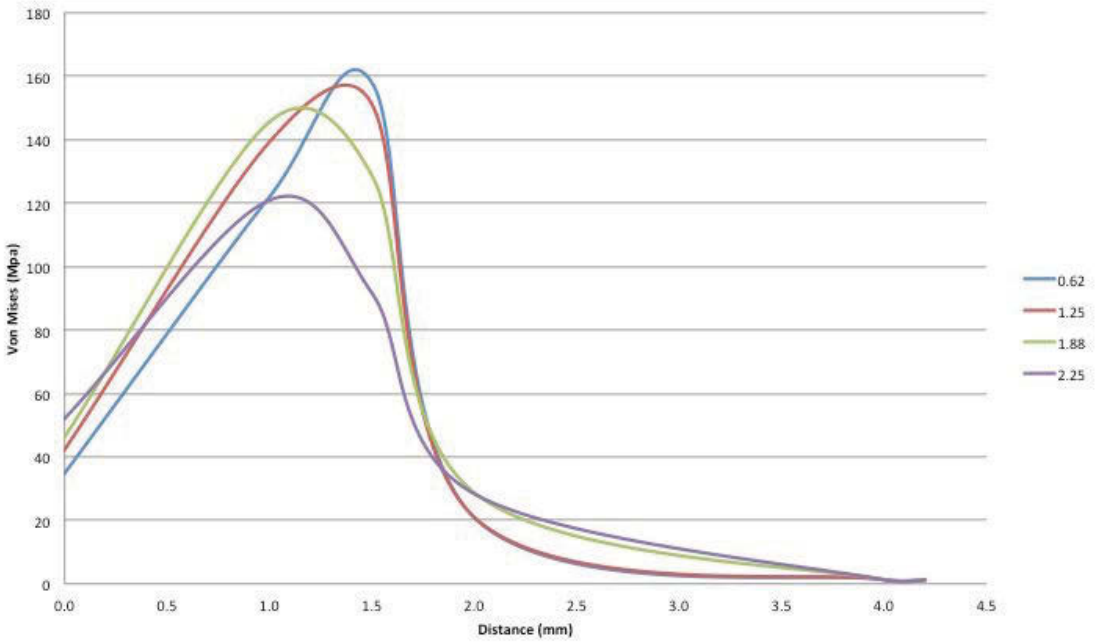

Figure 9.11 Graph plot of von Mises stress from plate surface through to mandibular cortical and cancellous bone

From a surgical perspective, altering the screw hole diameter produces little change in plate performance, however, it must be remembered that in vivo these fixation systems are secured with monocortical screws that do not affect plate performance in isolation, Decreasing the screw diameter to 0.62mm could have a significant effect on performance, either requiring a greater number or longer screws to ensure retention of the plate. Whilst this research has concentrated on fixation system performance, the analysis of the retention system, whether with the use of screws or another form such as bone cement would be an excellent point for future study.

3. The variation in plate thickness data set did not show the same results for stress and distortion as the screw hole, however, the diameter data set did show the same trends. To consider changing the plate thickness is another way of altering

plate surface area, the similarity in stress and distortion tends are understandable, as evidenced in Figure 9.12 for stress. Values for distortion in clenching varied from 0.0865mm for the 0.5mm thick plate to 0.0896mm for the 2.0mm thick plate.

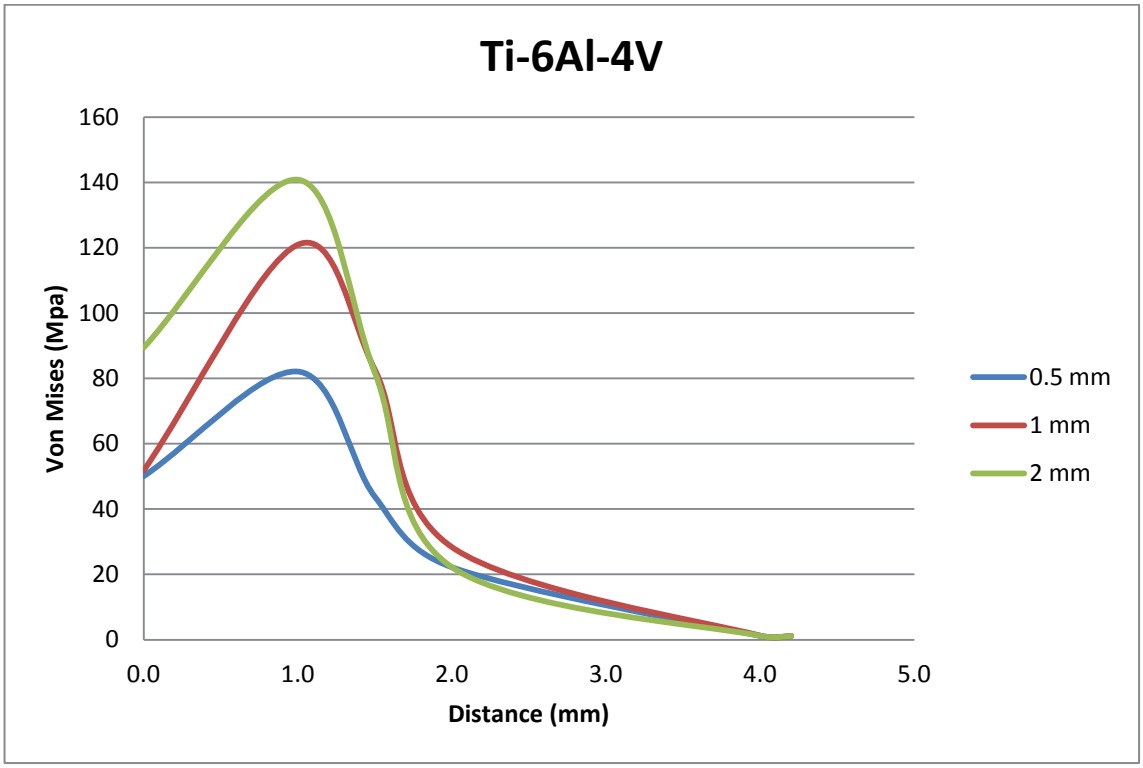

Figure 9.12 Graph plot showing variation in von Mises stress for plates with thicknesses of 0.5mm, 1.0mm and 2.0mm measured from the plate surface through to mandibular cortical and cancellous bone

When combining the screw hole diameter with plate thickness, it can be simply extrapolated for a Ti-6Al-4V plate in clenching, as applied to an edentulous mandible. There is no significant mechanical advantage in increasing the plate surface area either by decreasing the screw hole diameter or increasing plate thickness. However, it is important for future analysis that surgically in the myriad of literature on edentulous mandibular fixation, particularly the atrophic mandible that such a simplistic approach can lead to fixation system failure and, therefore, further research is required to categorise exactly where breakdown occurs.

4. Variation in plate material data is significant for its discrepancy in variation for stress data versus the variation for distortion data. As Figure 9.13 shows, the variation in stress data varies widely with it being highest for ZrO_2 intermediate for Ti-6Al-4V and significantly lower for PLA.

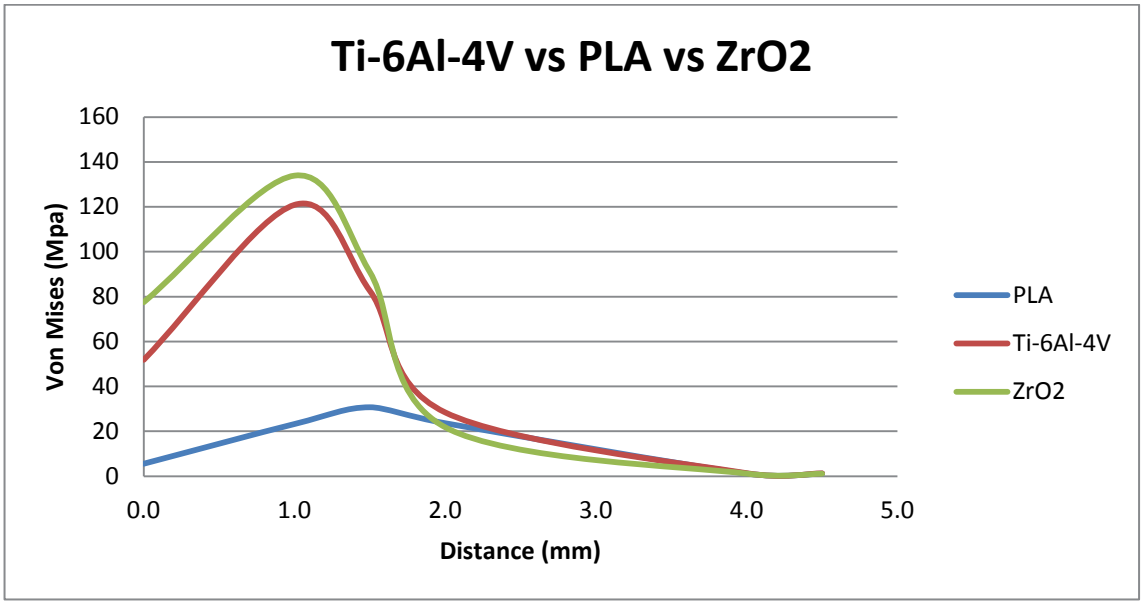

Figure 9.13 Graph plot of FS data for von Mises stress with Ti-6Al-4V, PLA and ZrO_2 plates

In comparison for distortion, the values were as follows: Ti-6Al-4V 0.0865mm, PLA 0.0875mm and ZrO_2 0.0863mm. The conclusion drawn is that PLA has a significantly lower stress curve and its distortion is almost the same as that of Ti-6Al-4V. Surgical interpretation would lead us to conclude that in terms of performance there are other materials that are bio compatible and have several advantages over Ti-6Al-4V, which is the most common material used to manufacture fracture fixation plates. PLA on its own has the significant advantage of being resorbable, which means that once the role of the plate is redundant, that is, fracture healing has occurred, the plate 'resorbs' away. This is of particular importance because the plate does not require future removal, particularly in a growing patient whose normal growth pattern will not be interfered with.

5. The laminate composite plate data set was adopted to determine if a combination of two materials could improve the performance of the plate over the use of each material separately. The first scenario where Ti-6Al-4V laminate is applied to the bone surface to allow the outer PLA laminate to resorb over time would be used in vivo. However, if the reverse was to occur, that is, PLA being applied to the bone when PLA resorbs, it would leave behind an unattached Ti-6Al-4V laminate. Whilst osseointegration of the residual Ti-6Al-4V laminate is possible, it has not been studied and hence for the purpose of this study is assumed not to occur. With the Ti-6Al-4V laminate is applied to the bone, a peak of stress is found at the Ti-6Al-4V laminate and bone interface of 133.64MPa, which is the same as the peak stress data for the Ti-6Al-4V: 0.5mm x 3.0mm x 19.5mm, 2.25mm screw hole diameter plate without the additional PLA laminate (Figure 9.14). Therefore, it can be concluded that including PLA in this orientation of the laminate plate does not add mechanical benefit compared to the 0.5mm thick Ti-6Al-4V plate.

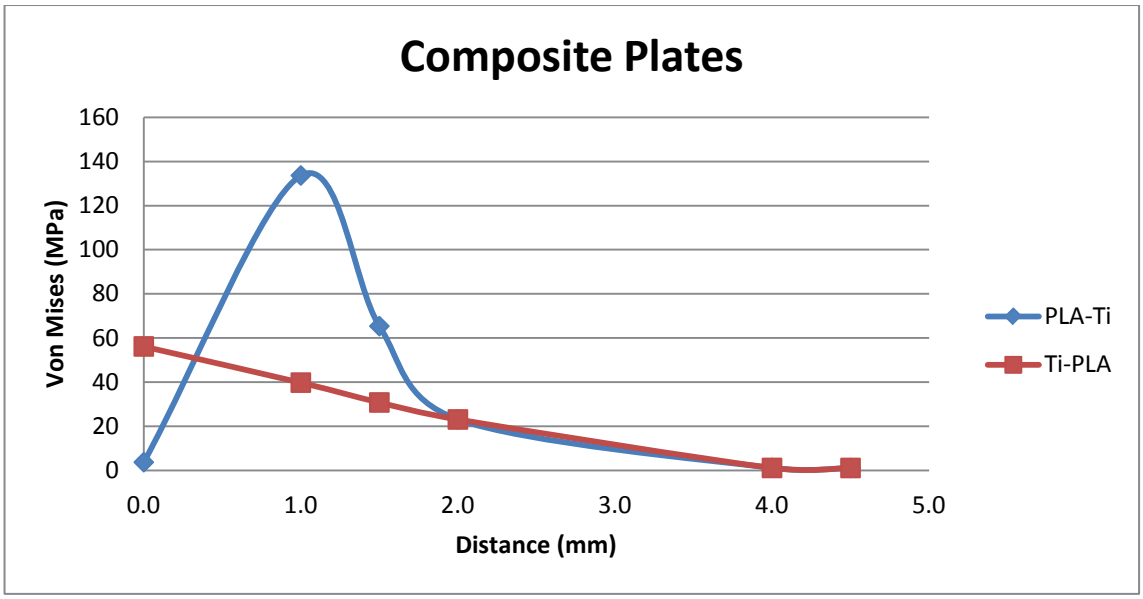

Figure 9.14 Graph plot of FS data for von Mises stress with composite laminate plates

Looking at the reverse with PLA now applied to the bone surface shows a stress analysis where stress values are much lower, however, distortion is similar at 0.0866mm compared with the alternate orientation of laminates at 0.0872mm.

Surgically, the concept of laminating a non-resorbable material with a resorbable material to produce a composite plate did not seem to produce any significant mechanical or clinical advantage over using either a pure Ti-6Al-4V or PLA plate. When the Ti-6Al-4V laminate was applied to bone, it acted similar to a non-laminate Ti-6Al-4V plate, and when the PLA laminate was applied to the bone surface, it acted similar to a non-laminate PLA plate.

6. The mesh plate data set was designed to provide the surgeon with choices in which screw holes to use as any of the 20 frames in the mesh could be used as a screw hole compared with seven available in the linear plate design (Figure 9.15).

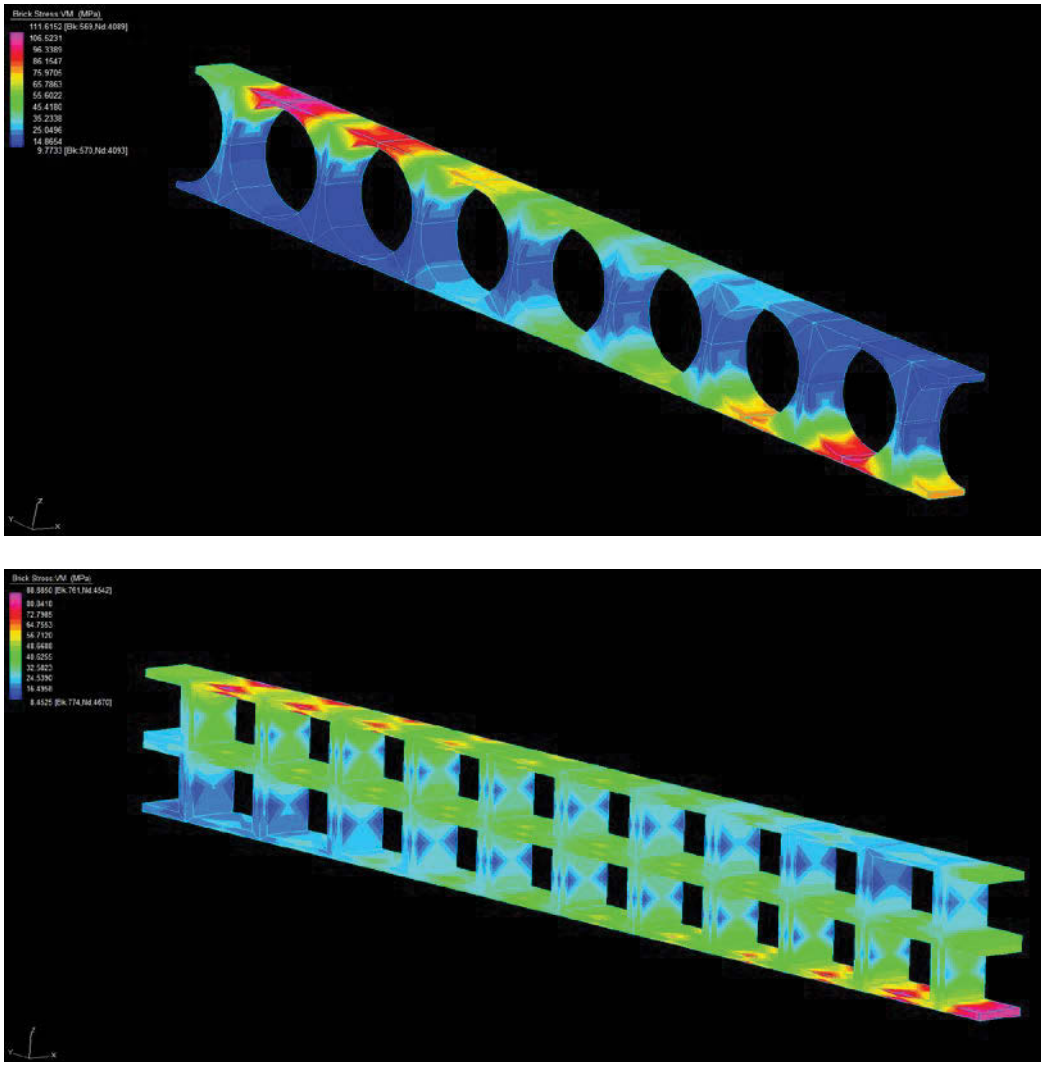

Figure 9.15 Comparison of the seven available screw hole in the linear plate design versus the twenty available in the mesh plate design

To a surgeon, such an advantage can be valuable because it allows the plate retention screws to be optimally placed in the best quality and thickest bone, as well as being able to be positioned away from the bone of the fracture site, which is often damaged and unsuitable due to the trauma sustained during the fracture.

The mesh plate design was also produced to be similar in surface area to a typical linear fixation plate that is currently used in surgical practice. Subsequently, the mesh plate design has a surface of 20.91mm^2 compared with 21.22mm^2 for a 1.0mm x 19.5mm x 3.0mm Ti-6Al-4V plate with 2.25mm diameter screw holes.

The comparison in performance is illustrated in Figure 9.16.

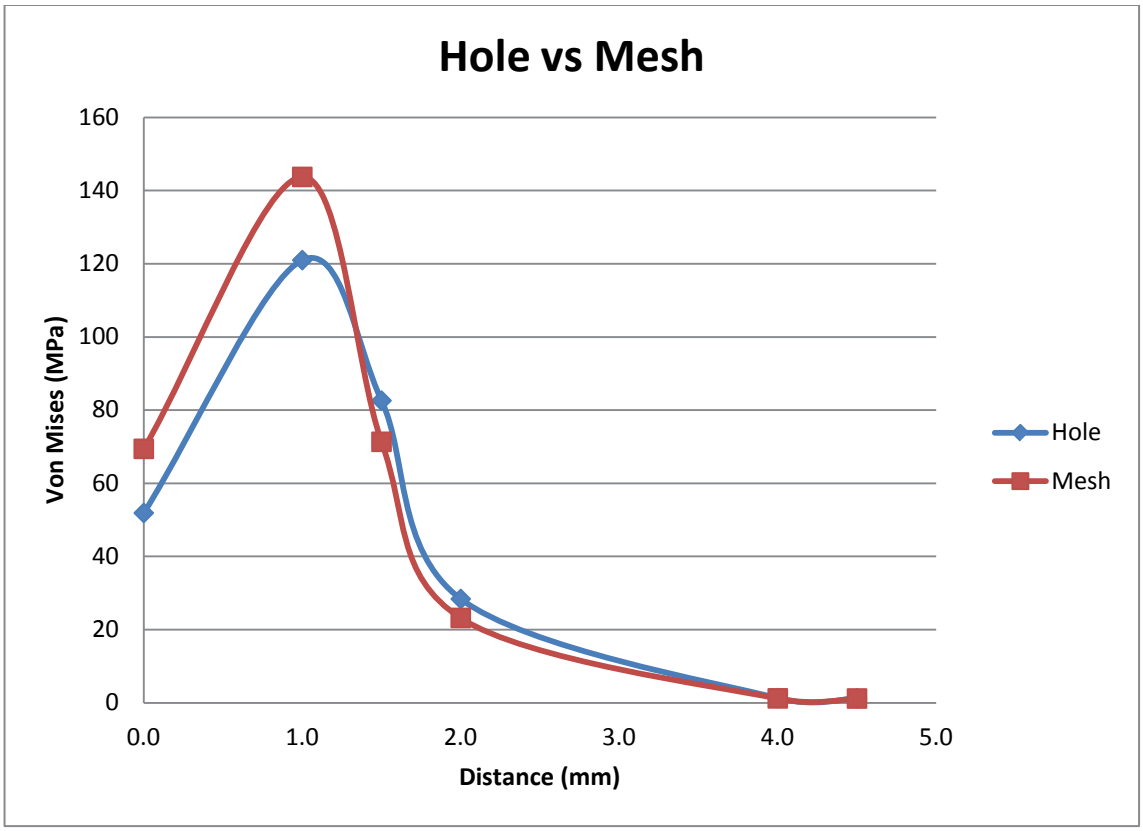

Figure 9.16 Comparison in performance between mesh plate and linear plate design (19.5mm x 3.0mm x 1.0mm with 2.25mm diameter screw holes) for von Mises stress

The values for mesh versus linear plate were 0.0867mm versus 0.0865mm.

From this data, if applied surgically the mesh palate has four advantages: (i) shows similar stress and distortion performance data compared to the linear plate design; (ii) allows better modification intra operatively due to increased choice of available screw holes; (iii) allows better positioning of retention screws in to the best available bone; and (iv) if required, can be shaped easily to anatomical configurations during surgery due to its configuration.

7. Patient specific data set. By constructing and adapting a Ti-6Al-4V linear Ti fixation plate to a PS derived FEM, the values of 312.23MPa for plate stress and 0.0758mm for distortion were obtained at the fracture site. These compare favourably with data from the generic model with values of 111.61MPa (plate stress) and 0.0865mm (distortion) being obtained for a similarly designed plate. Whilst stress is higher, it can be accounted for due to the PS linear plate being longer than the generic linear plate.

From the body of research presented in this thesis, the following conclusions can be drawn.

1. Trauma resulting in mandibular fractures, especially of the edentulous mandible, is a significant and complex problem that warrants the investment in time and funds to research and improve management.

2. On the area of research is the use of finite element modelling to better understand the biomechanics of the mandible, which will result in a better understanding of engineer appropriate fracture fixation systems.

3. To date, finite element modelling has been a useful tool, however, it has several disadvantages, mainly its reliance on reference data to be utilised in the construction of the model. By its nature, such data can be widely variable and hence any generic model designed, whilst useful, can lack specific data related to the individual patient at hand. As a surgeon, such a generic model can act as a useful research tool and guide, but it lacks patient specificity that surgeons must employ in treatment.

4. For example, the insertion of muscle force reference data to produce a FEM does not take into account the individual's age, sex, race or body stature, all of which when combined, produce significant variances that make any one generic model limited in the results it produce.

5. One method of producing a better model is to use a PS CT to assign anatomical accuracy and better delineation between cortical and cancellous bone.

Under this circumstance, the PS model represents the external and internal morphology of the mandible more accurately than previous models. By doing this, an accurate representation of the cortical and cancellous bone regions was produced in the model. This is in contrast to previous models that assigned an arbitrary thickness to the cortical bone which has significant influence on the overall distribution of stresses in the mandible and hence, accuracy of the model.

It is envisaged that this model could be used by surgeons on a variety of maxillofacial problems, not only limited to mandibular fractures, but branching into dental implantology and maxillofacial reconstruction due to trauma, oncology or congenital defects. The model and FEA could aid in diagnosis, as well as determine the best treatment sequence prior to performing a procedure.

Data collected from the generic 'new' for clenching suggest that a variety of fixation system designs are suitable to be used for clinical applications. It also raises the question: To what extent does protrusion and opening affect the performance of any fracture fixation system? In addition, the scope of this research was to look at the plate, whether it be linear or mesh, and not to research the integral nature of the system's retention, whether screw fixation or other methods.

Overall, the mesh plate design offered the best combination of biomechanical performance with ease and flexibility in its clinical application. In analysing the PS data set, it is clear that the more comprehensive the model and resultant FE analysis can be then greater confidence is gained in the results being applicable to the patient at hand.

CHAPTER 10:
PROPOSED FUTURE WORK

For future works to further our knowledge of fracture management and improve the concept of PS FE modelling and analysis, the four directives are proposed, as follows:

1. Research PS FE modelling and analysis of an entire fracture management system that is not just limited to the 'plate' but to include modelling and analysis of plate retention systems. For example, screws versus bone cement to secure a fixation system in situ (Figures 10.1 & 10.2).

2. Investigate PS FE modelling and analysis of the entire system to include all functional movements, not just clenching.

3. Refine the PS model by adding a method of ascertaining accurate muscle force mapping that is subject specific.

4. Use an accurate subject specific FEM to analyse and manufacture customised prostheses and conduct clinical trials.

In producing this thesis, the infancy of finite element modelling and analysis of the facial skeleton to achieving an accurate PS model has been researched. This does not diminish the value of previous works but serves as an obvious improvement and scope for future research. As illustrated in Figures 10.1 and 10.2, the current 'gold' standard of where this research has been reached.

As Figures 10.1 and 10.2 clearly show, the model produced by the culmination of research in this thesis is unique in that it is PS, detailed for cortical and cancellous bone representation and shows muscle insertion as an area more realistically representing the anatomy and biomechanics of the mandible. The product is exciting as a tool for future research, and as illustrated, data is already being collected (although not presented in this thesis) for the fixation of a bar plate to the cortical bone with bone cement rather than screw fixation.

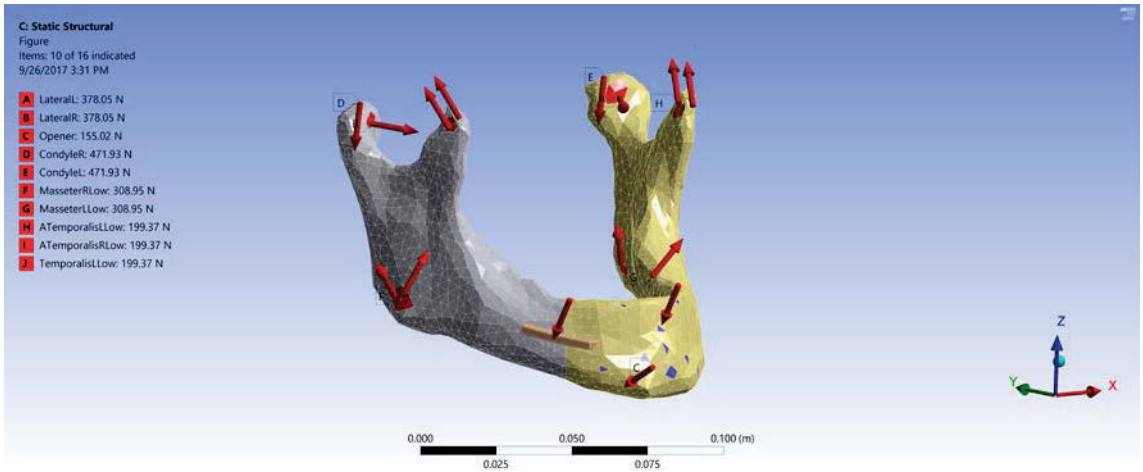

Figure 10.1 Mandibular FEM with muscle forces, fracture and fixation bar

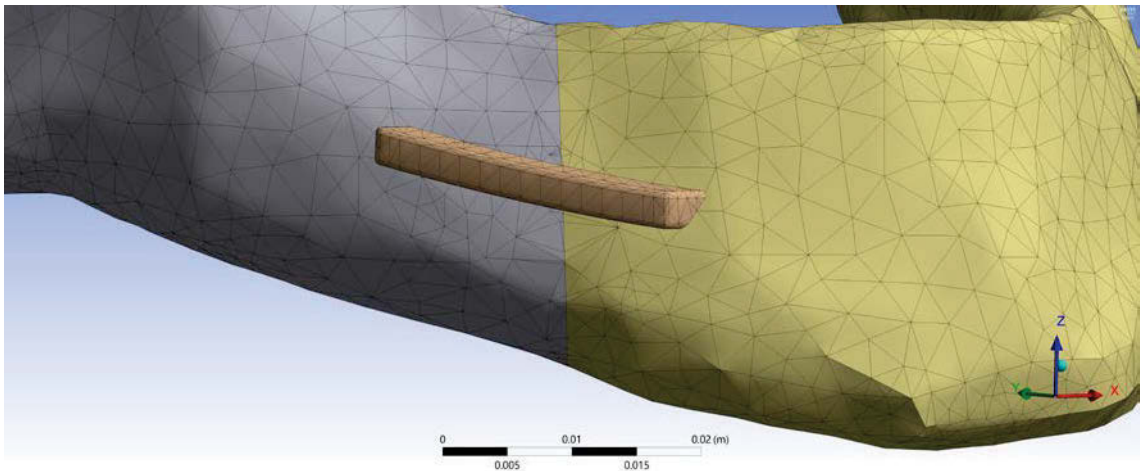

Figure 10.2 Showing close up of fracture and fixation bar

It is envisaged that with further areas being addressed, we would be approaching an era of clinical practice where a FEM is created that accurately reproduces detailed biomechanical functions that are unique to each patient, similar to fingerprint or DNA identification. Following on, all clinicians would be able to access this type of analysis on personal computers to design the prosthetic device required with the knowledge that it is perfectly tailored to the patient's specific requirements and not just an 'off the shelf' generic product.

APPENDIX A:
TRANSLATION OF CT DENSITY (HOUNSFIELD UNITS) INTO A FINITE ELEMENT MODEL

1 Introduction

In the production of models to date, the use of CT scan for imaging the mandible saw a representation of a solid bone, or a dry cadaveric specimen was reversed engineered through a contour extraction procedure.

In this research, mechanical properties of the mandible were determined in two stages:

1. The apparent specific density of each element of the model mesh was calculated by a linear association with the Hounsfield unit of the voxels enclosed in that element.

2. The elastic modulus was correlated to the apparent bone density according to experimental results found in the literature.

As a result, after aligning the mesh with the tomographic scan, a finite element model (FEM) was prepared in which local material properties were assigned to every single element of the mesh. Such a model represents an alternative to corticocancellous bone model approximations and offers the benefit of combining an accurate mesh of the external surface of the bone, easily segmented via a high contrast between cortical and surrounding soft tissue, with a density-based mapping of local stiffness.

2 Why chose an edentulous model?

An edentulous model was chosen on two grounds:

1. From the angle of the model construction and analysis, it was felt that the edentulous mandible removed confounding factors, such as teeth, dental restorations and periodontal ligament structures. The biomechanics of each alone

being highly complex and hence in these early stages simplification of the model was thought judicious.

2. From the viewpoint of the clinician, the edentulous mandible has always presented significant difficulties in the treatment, as already discussed in detail in previous chapters. The edentulous model analysed in this thesis is novel and is expected to contribute, not only to pure science, but considerably in its application clinically to benefit patients and to do this more so than repeat analyses, as have already been done on the dentate mandible (Korioth et al., 1995; Marinescu et al., 2005; Ding et al., 2015).

3 Relation between the Hounsfield unit and density

In 1995, Rho undertook significant research and published his findings on the correlation between apparent bone density and Hounsfield units. He described how a preliminary correction to raw tomographic scalars was made so that Hounsfield units relative to a specific scan could be calculated, as follows:

$$HU = 1000\ \frac{CT - CT_{water}}{CT_{water} - CT_{air}} \quad (1)$$

where CT_{water} and CT_{air} are the raw CT values of respectively a water sample contained in the field of view and air as averaged in a small volume of the scan.

To derive data used for this study, we used the results from Taraschi (2016) who instructed a voluntary patient to keep a small water balloon in his mouth during the CT scan (Figure A.1). Before the segmentation process, the values of CT numbers in 10 locations within the balloon were averaged to calculate CT_{water}.

For the present study, it was found that:

$$CT_{water} = 54$$

$$CT_{air} = -1024$$

Which generates the following correction law:

$$HU = 0.93\ CT - 0.05 \quad (2)$$

Figure A.1 CT numbers correspondent to water are averaged over the scanned volume of a little water balloon (here circled in yellow) kept in the patient's mouth (modified from Taraschi, 2016)

Since taking into account different bone types on a large number of samples, Rho's study (1995) is considered to have a high relevance in establishing a relationship between the Hounsfield unit and density. The relationship for density ρ ($\frac{Kg}{m^3}$) found by Rho are summarised in Table A.1 according to the location of the specimen.

Table A.1 Relationship between Hounsfield units (CT units) and density ρ ($\frac{Kg}{m^3}$) for specimens from cancellous bone from different anatomical locations (Rho, 1995)

Proximal tibia cancellous bone	$\rho = 0.916\ CT + 114$
Proximal femur cancellous bone	$\rho = 1.067\ CT + 131$
Distal femur cancellous bone	$\rho = 1.205\ CT + 139$
Proximal humerus cancellous bone	$\rho = 0.624\ CT + 173$
Lumbar spine cancellous bone	$\rho = 1.122\ CT + 47$

Rho also theorised that Hounsfield units are a function of the porosity of the bone rather than the density of mineralisation. This thesis works from the hypothesis of Rho in that cortical bone is primarily a less porous and denser version of cancellous bone.

In line with the relationship found by Rho (1995), Bujtar (2010) uses Equation (3) to correlate bone density with Hounsfield unit values from the CBCT image in case of mandibular bone:

$$\rho\left(\frac{Kg}{m^3}\right) = 1.14\,HU + 309 \quad (3)$$

After a dedicated review of studies published on the correlation between elasticity and density for cancellous and cortical bone (summarised in Table A.2), this research adopted Carter and Hayes's law (1977). This law is a highly referenced work in subject-specific finite element models (FEM) (Schileo et al., 2007), including ones by Bitsakos et al., (2005), Keyak et al., (1993), Ota et al., (1999), Perillo-Marcone et al., (2004), Taddei et al., (2004), Wagner et al., (2002), Weinans et al., (2000) and Wong et al., (2005).

Assuming that the cancellous bone is a two-phase porous material, Carter and Hayes (1977) determined experimentally the constants *A* and *B* in the following equation:

$$Y = A(\rho)^B \quad (4)$$

where *Y* is a mechanical property (strength or Young's modulus) and ρ is the apparent dry density, calculated as the dry weight divided by the specimen volume (Keller et al. 1994, Keyak et al. 1994).

In the case of compressive Young's modulus, they found the following relationship:

$$E = E_c \varepsilon^{0.06} \left(\frac{\rho}{\rho_c}\right)^3 \quad (5)$$

With *E* = compressive Young's modulus in MPa, E_c = compressive Young's modulus of compact bone with apparent density ρ_c tested at strain rate 1.0 Hz.

Table A.2 Modulus-density relationships according to studies published in literature (Helgason et al., 2008)

Study	Site	Type of bone	Densitometric measure	ρ-range (g/cm^3)	E (GPa)	Test condition	Geometry $B \times W \times L$ or $D \times L$ (mm)	Strain rate (s^{-1})	n	R^2
Carter and Hayes (1977)	Pooled	Cortical and trabecular	ρ_{app}	0.07–2.0	$E = 3.79\dot{\varepsilon}^{0.06}\rho_{app}^{3}$	Confined compression	20.6 × 5	0.001–10.0	124	NR
Lotz et al. (1990)	Human femoral neck	Trabecular	ρ_{app}	0.18–0.95[RFG]	$E = 1.310\rho_{app}^{1.40}$	Platen	9 × 5	0.03	49	0.91
Lotz et al. (1991)	Human femoral metaphysis	Cortical	ρ_{app}	1.20–1.85[RFG]	$E = -13.43 + 14.261\rho_{app}$	3-Point bending	7 × 5 × 0.4	0.05	123	0.67
Snyder and Schneider (1991)	Human tibial diaphysis	Cortical	ρ_{app}	1.748–1.952	$E = 3.891\rho_{app}^{2.39}$	3-Point bending	2 × 2 × 40	0.001	45	$r = 0.75$[a]
Hodgskinson and Currey (1992)	Pooled	Trabecular	ρ_{dry}	0.094–1.111	$E = 3.98\rho_{dry}^{1.78}$	Platen	NR	0.0011–0.0033	57	0.91
Linde et al. (1992)[b]	Human proximal tibia	Trabecular	ρ_{app}	0.273[c]	$E = 4.778\rho_{app}^{1.99}$	Platen	7.5 × 7.5	0.01	31	$r = 0.89$[a]
Anderson et al. (1992)	Human proximal tibia	Trabecular	ρ_{dry}	0.14–0.48[RFG]	$E = 3.890\rho_{dry}^{2.0}$	Platen	10 × 10 × 20	0.01	31	NR
Dalstra et al. (1993)	Human pelvis	Trabecular	ρ_{app}	0.109–0.959	$E = 2.0173\rho_{app}^{2.46}$	Platen	6.5 × 6.5 × 6.5	0.001	57	0.58
Keller (1994)	Human spine	Trabecular	ρ_{ash}	0.028–0.182	$E = 1.89\rho_{ash}^{1.92}$	Platen	10 × 10 × 10	0.01	199	0.702
Keller (1994)	Human femur	Cortical and trabecular	ρ_{ash}	0.092–1.221	$E = 10.5\rho_{ash}^{2.29}$	Platen	8 × 8 × 8	0.01	297	0.849
Keller (1994)	Pooled	Cortical and trabecular	ρ_{ash}	0.028–1.221	$E = 10.5\rho_{ash}^{2.57}$	Platen	8 × 8 × 8 10 × 10 × 10	0.01	496	0.965
Keyak et al. (1994)	Human proximal tibia	Trabecular	ρ_{ash}	0.06–0.27	$E = 33.9\rho_{ash}^{2.20}$	Platen	15 × 15 × 15	0.01	36	$r = 0.916$[a]
Goulet et al. (1994)	Pooled	Trabecular	BV/TV	0.06–0.36	$E = 6.310(\mathrm{BV/TV})^{2.10}$	Platen	8 × 8 × 8	0.01	104	0.88
Keaveny et al. (1997)	Human lumbar spine	Trabecular	ρ_{app}	0.09–0.28	$E = 1.540\rho_{app} - 0.058$	End-caps[d]	8 × 16	0.005	9	0.64
Li and Aspden (1997)	Human femoral head	Trabecular	ρ_{app}	0.14–1.4	$E = 0.573\rho_{app} - 0.0094$	Platen	9 × 7.7	0.0033	49	0.59
Ouyang et al. (1997)	Human vertebra	Trabecular	ρ_{app}	0.46–0.71	$E = 2.3828\dot{\varepsilon}^{0.07}\rho_{app}^{1.88}$	Platen	10 × 10 × 24	0.00001–0.001	36	NR
Kopperdahl and Keaveny (1998)	Human vertebra	Trabecular	ρ_{app}	0.11–0.27	$E = 2.1\rho_{app} - 0.08$	End-caps[d]	8 × 16	0.005	44	0.61
Ciarelli et al. (2000)	Human proximal femur	Trabecular	BV/TV	0.15–0.40[RFG]	$E = 7.541(\mathrm{BV/TV}) - 0.637$	Platen	8 × 8 × 8	0.01	32	0.88
Morgan et al. (2003)	Human vertebrae	Trabecular	ρ_{app}	0.11–0. 35	$E = 4.730\rho_{app}^{1.56}$	End-caps[d]	8 × 16	0.005	61	0.73
Morgan et al. (2003)	Human proximal tibia	Trabecular	ρ_{app}	0.09–0. 41	$E = 15.520\rho_{app}^{1.93}$	End-caps[d]	8 × 16	0.005	31	0.84
Morgan et al. (2003)	Greater trochanter	Trabecular	ρ_{app}	0.14–0. 28	$E = 15.010\rho_{app}^{2.18}$	End-caps[d]	8 × 16	0.005	23	0.82
Morgan et al. (2003)	Human femoral neck	Trabecular	ρ_{app}	0.26–0. 75	$E = 6.850\rho_{app}^{1.49}$	End-caps and platens[d,e]	8 × 16	0.005	27	0.85
Morgan et al. (2003)	Pooled	Trabecular	ρ_{app}	0.09–0. 75	$E = 8.920\rho_{app}^{1.83}$	End-caps and platens[d,e]	8 × 16	0.005	142	0.88
Kaneko et al. (2004)	Human distal femur	Trabecular	ρ_{ash}	0.102–0.331	$E = 10.88\rho_{ash}^{1.61}$	Platens	15 × 15 × 15	0.01	49	0.775

Young's modulus (E) in GPa and density in g/cm^3. NR = not reported. RGF = read from graph. R^2 = determination coefficient.

[a] Pearson correlation coefficient, as reported in the original work.

[b] Reported results are for cylindrical specimens with diameter of 7.5 mm and a height of 7.5 mm. These specimens gave the highest correlation. In addition, mineral oil was used to eliminate frictional effects on the specimen–anvils interface.

[c] Average value. Range not reported.

[d] The free length of the bone specimen between the end-caps was reported.

[e] Fourteen specimens were tested in compression with platen end-conditions due to experimental difficulties.

Using E_c = 22.1GPa for compact bone with $\rho = 1.8\ \frac{g}{cm^3}$ the expression becomes:

$$E(GPa) = a\rho^3(\frac{d\varepsilon}{dt})^{0.6} \quad (6)$$

With:

$$a = 3.790$$

ρ: density

$\varepsilon = \frac{d\varepsilon}{dt}$: strain rate

Since this relationship will be used in a static structural FEM, the influence of strain rate is considered negligible as the mandible will deform in quasi-static conditions.

Table 3 shows the results for Equation 6 at different strain rates:

Table A.3 Experimental relationships between elastic modulus and strain rates

E	a
0.001	2.504
0.01	2.875
0.1	3.301
1	3.970

Brown (2010) applied an important correction to the apparent elastic modulus related to the Poisson ratio. The reason for this correction is that Carter and Hayes (1977) used the classic strain in the *E* formula but did not taken into account the plane stress. Their original mechanical compression tests were conducted under uniaxial strain conditions, not uniaxial stress.

Brown believed that Carter and Hayes's study was not correct for the plane strain condition when calculating Young's modulus from the experimental results. Therefore, for an apparent Young's modulus measured in the plane strain condition, E_{app}, the true Young's modulus E measured in the plane stress condition was given by:

$$E = E_{app} \frac{(1+\nu)(1-2\nu)}{(1-\nu)} \quad (7)$$

Given the difference of ranges for the Poisson ratio for denser cortical bone and two-phase cancellous bone, the author uses the following two laws for deriving Young's modulus from local density for cortical and cancellous bone:

$$E = 0.74\, E_{app} \ (\nu = 0.3)$$

$$E = 0.47\, E_{app} \ (\nu = 0.4)$$

The possibility of applying an analytical correction for plane stress testing conditions is another reason why the author has chosen to use Carter and Hayes' law over relations found in other comprehensive studies.

Keller (1994), by way of example, found a similar law for femoral specimens:

$$E(GPa) = 10.5(\rho)^{2.57} \quad (8)$$

where ρ is the apparent dry density.

In that experimental setup, Keller used oil in the interface between the specimen and compression testing jaws, which would make the correction for plain stress above not applicable. Moreover, Keller tested the specimens alongside their primary load axis only, which does not reflect the loading conditions the mandible is subject to during functional movements.

On this topic, Morgan et al. (2003) acknowledged how the anatomical site is significantly related to the bone tissue properties and their relationship with density. Using a testing protocol which minimises random error, it is found that:

$$E(GPa) = 6.950(\rho)^{1.49} \quad (9)$$

Although Morgan's study was robust, the author has decided not to adopt this law since it obtained testing specimens with densities in the limited range $0.25 - 0.75\ \frac{g}{cm^3}$.

On the contrary, mandibular cortical bone has been measured to reach densities of at least:

$$\rho = 1.8\ \frac{g}{cm^3}$$

The author believes that Carter and Hayes's work (1977) should be used only after considering which bone type it applies to. In this case, the association between density and elastic modulus (Lewis & Reid et al., 2013) needs to suit a whole mandibular bone.

Because of the naturally curved shape of the human jaw, it is not possible to obtain straight specimens of cancellous and cortical bone which can then be tested via a traditional four point bend test. This is why the pulse ultrasonic technique has been used to measure elastic properties of cortical and cancellous bone (Rho, 1995; Nomura, 2001), allowing smaller samples to be tested. Because of its reduced size, the average measurement of density would also be more relevant.

Using this method, Rho (1995) confirmed that mechanical properties of both cortical and cancellous bone depend on porosity, architecture and bone mineral density. In addition, he found that there is a difference in slope for the axial modulus versus the density for cortical bone from different parts of the body. Given that this behaviour is not present in the cancellous bone, it becomes evident how important it is to adopt different relationships for different bone types to derive elastic modulus from bone density.

According to the description of cancellous bone given at the beginning of this appendix and in previous chapters, the author proposes to support Carter and Hayes's assumption for which cortical bone is simply denser cancellous bone and that CT scalars must be considered as a function of the porosity of the bone rather than a variation of the mineralisation in the bone matrix. This would explain the higher correlation found by Rho between density and elastic modulus in the case of porous cancellous bone with respect to cortical bone.

4 Mapping density and elasticity

In order to map material properties of the mandibular model, this study used a software application called *Bonemat*.

Bonemat was developed for computational bone biomechanics by Institute Ortopedico Rizzoli in Bologna, Italy, as a tool for mapping elastic properties derived from CT data on a meshed bone model.

CT images and the finite element mesh were imported into the software and fused into a coherent representation. The product was exported as an updated finite element mesh once bone properties had been mapped.

A 'VMEmesh' (Taddei 2002), which is a volumetric data structure able to store scalars for each voxel in the volume, was created directly from an ANSYS ASCII archive (.cdb file) as prepared in ANSYS software. The importer module correctly interprets data relative to nodes, linear and quadratic solid elements and material cards. For each element, information regarding its static, mechanical, thermal or electrical properties is stored into a dedicated data structure.

Average material properties derived from the Hounsfield unit of the tissue in that region were assigned to the finite elements of the bone mesh. This finite element pre-processing operation resulted in a heterogeneous model based on the density information derived from the CT scan data set.

From the Hounsfield unit-derived bone density, the elastic modulus was calculated after a densitometric calibration. Up to three density-elasticity relationships corresponding to different density ranges and potentially different bone types were specified. The skeleton of the *Bonemat* algorithm is the numerical integration that maps the voxel-wise properties of the CT grid to element-wise properties of an unstructured mesh grid. The input data was a von Mises volume derived from DICOM data of a mandibular CT scan and a VMEmesh.

The output of the operation was an updated VMEmesh in which each element was assigned an elastic modulus value. Generated elements were grouped by their material card and could be classified by stiffness or density. An additional output was given in terms of a frequency file which listed how many elements shared the same elastic modulus.

The *Bonemat* application is non-dimensional, therefore, the user is responsible for setting coherent measurement units to the variables. Using the discussed relationship between density from CT numbers and elastic modulus from density, two units were used: (i) Input: density = G; and (ii) Output: Young's/Elastic modulus = MPa.

A minimum gap between two material cards was set. For example, given a typical elastic modulus range in the order of 50MPa to 20,000MPa, the user may want to avoid defining 19950 different materials but rather group them each, for example, 500MPa, resulting in maximum 40 material cards.

By default, elastic moduli bins were assigned by *Bonemat*, starting with the highest modulus among each element and then grouping to that value to all elements within the specified 'gap value'. Then the algorithm searched again for the highest value among the remaining elements and looped them until they were assigned an elastic modulus. This means that the distance from two consecutive elastic moduli bins was not necessarily the gap value.

Once material properties were assigned according to CT values, the mesh was exported back to ANSYS for the remaining finite element pre-processing operations, including assigning boundary conditions, loads, solver type, inertia relief and non-linear deformation controls (Figure A.2).

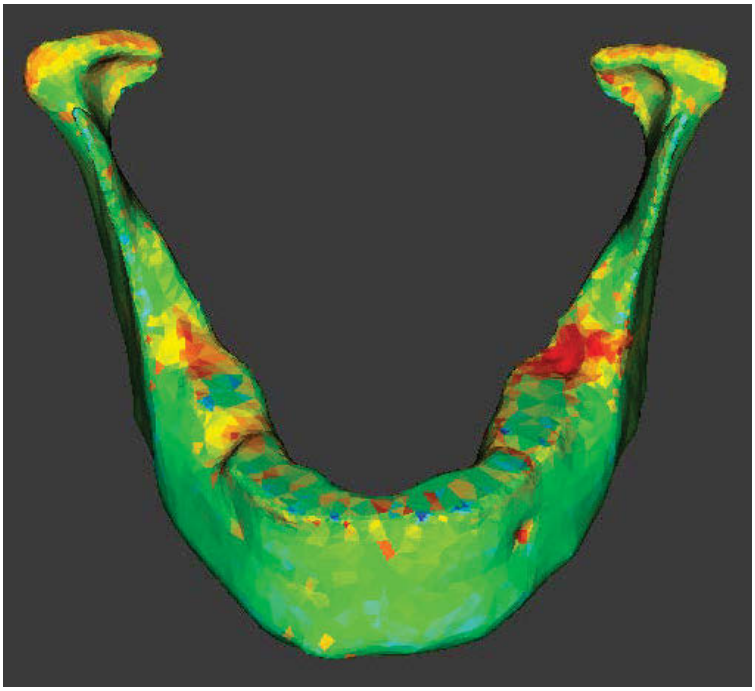

Representation of the mesh in *Bonemat* after material properties were assigned and mapped via Young's modulus. The different colours correspond to different material cards.

Figure A.2 Mesh in Bonemat Young's modulus (modified from Taraschi, 2016)

In literature, explicit guidelines do not exist for interpreting the results of stress analysis on the human bone, whether to use principal stresses (tensile or compressive) or equivalent stresses (Choi, 2005; 2013). One of the reasons is that ultimate stress depends on the direction of loading, other than age, sex and healthiness of the subject. According to Reilly and Burnstein (1975), the ultimate tensile stress of human cortical bone can range from 121MPa to 135MPa and the ultimate compressive stress ranges from 167MPa to 205MPa.

Other investigations into stresses for the mandibular bone under loading recorded values for the cortical bone between 21MPa and 150MPa include studies by Korioth et al. (1992), Lin et al. (2000), Menicucci et al. (2001), Hirabayashi et al. (2002) and Eskitascioglu et al. (2004), and ultimate stress values for cancellous bone vary between 1MPa and 20MPa.

APPENDIX B:
CT NUMBERS DENSITY, E FREQUENCY AND DISTRIBUTION IN MODEL MII

The choice of material properties in the FEM relative to this model relies entirely on the relations used to convert CT numbers into density and then Young's modulus. The distribution of CT numbers, as averaged inside each finite element and calculated for the entire mandible mesh, indicated two peaks of maximum concentration. Given the anatomy of the mandible, it is reasonable to assume that these two peaks correspond respectively to CT numbers relative to cancellous and cortical bone types. Also, in line with the definition of cortical bone given in this work, for which it is considered a denser form of the same porous structure which the cancellous bone is made of, we expected to see a continuous trend representing the progressive concentration of trabeculae reaching the most compact bone configuration. This behaviour is illustrated in Figure B.1, which reports the frequency of CT numbers for the present study.

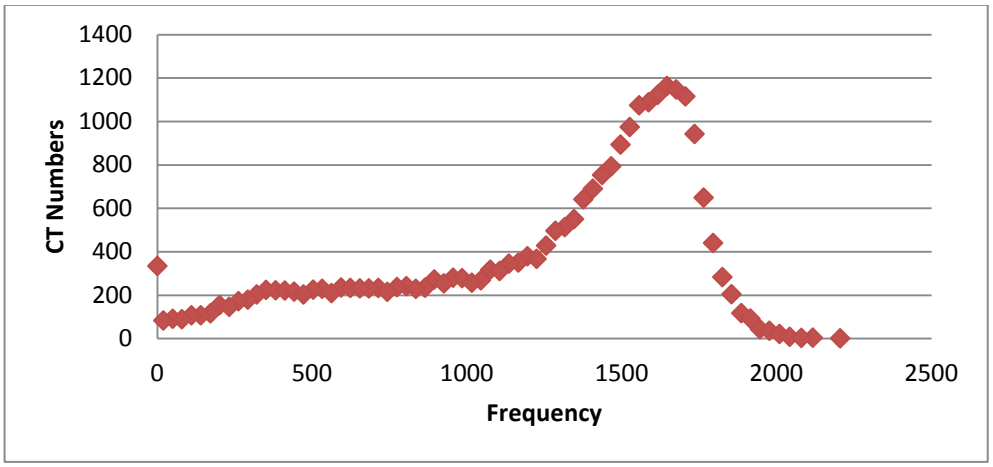

Figure B.1 CT numbers frequency showing distribution of CT numbers in the patient selective mandibular mesh (modified from Taraschi, 2016)

During the segmentation process, volumes of the solid models corresponding respectively to hard and soft bone were estimated to be:

$$V_{can}/V_{cor} = \frac{23140\ mm^3}{67331\ mm^3} = 0.34$$

For this reason, it is rational to suppose that the highest concentration of cancellous bone should have a count of:

$$N_{can} = 0.34\, N_{cor} = 560$$

Applying Carter and Hayes's relation (1977) for converting density to Young's modulus, inclusive of Brown's (2010) correction,

$$E(GPa) = 2.80\rho^3 \quad (13)$$

Using Bujtar's empirical law (2010) for deriving densities from Hounsfield units (obtained from normalising CT numbers for air and water),

$$\rho\left(\frac{Kg}{m^3}\right) = 1.14\, HU + 309 \quad (14)$$

The resulting frequency of Young's modulus (in gaps of 30MPa) in the mesh (Figure B.2) shows that the peak corresponding to denser bone is between 20GPa and 30GPa. Because this value is not aligned with the most significant works published in literature (as reviewed by Helgason in 2008), the author has decided to reject this finding and its associated workflow.

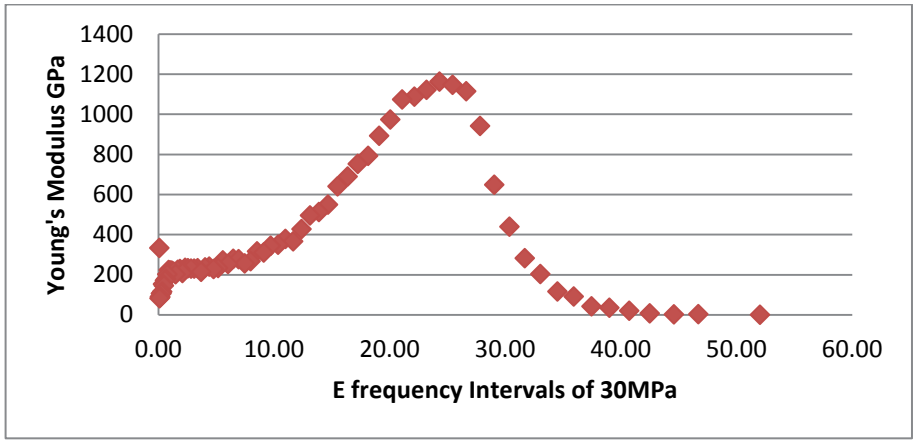

Figure B.2 Frequency of Young's modulus in the mandibular mesh (modified from Taraschi, 2016)

Alternatively, this study uses an inverse approach to determine the stiffness of the mandible from the distribution of CT scan numbers. The method uses the following hypotheses:

1. The right peak for high CT numbers corresponds to cortical bone in the volume mesh with the CT number:

$$CT_{cor} = 1616$$

2. The relationship that correlates CT numbers to density is linear.

3. Average Young's modulus for cortical and cancellous bone (as used by Ben-Nissan (1987) whose load set is being used in this study) are:

$$E_{cor} = 17.2\ GPa \quad (15)$$

$$E_{can} = 1.3\ GPa \quad (16)$$

4. The law for converting density to Young's modulus is Carter and Hayes (1977) (corrected by Brown (2010)):

$$E(GPa) = 2.80\rho^3 \quad (17)$$

5. Using (15) and (16) into (17) we obtained:

$$\rho_{cor} = 1.83\ g/cm^3$$

$$\rho_{can} = 0.76\ g/cm^3$$

6. When associated to the CT numbers for cortical and cancellous bones on the frequency peaks, and considering that:

$$\rho_{air} = 1225 g/m^3$$

The following plot (Figure B.3) is obtained for the relationship between CT numbers and density, where the CT numbers corresponding to cortical and cancellous bone have been assumed to be the ones corresponding to the frequency peaks associated to the two bone types.

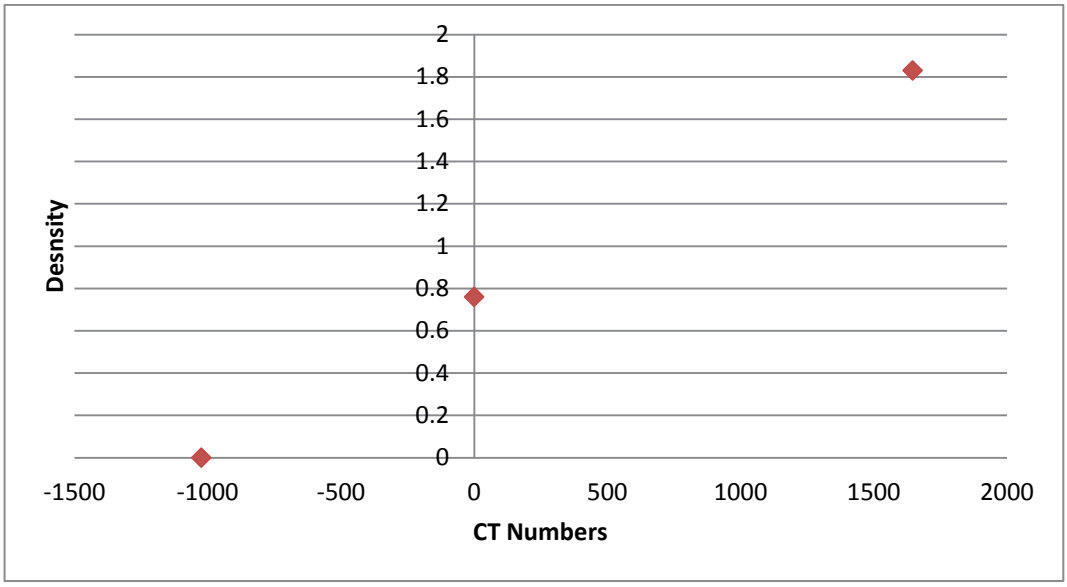

Figure B.3 Relation between CT numbers and density (modified from Taraschi, 2016)

Data have been interpolated with a linear law using *Gnuplot* (www.gnuplot.info) for calculating *a* and *b* in the equation:

$$\rho(g/cm^3) = a\,CT + b$$

resulting in the inverse approach linear relation:

$$\rho(g/cm^3) = 6.82 \times 10^{-4}\,CT + 0.722 \quad (18)$$

Using (17) and (18) in the *Bonemat* graphical user interface, this study has determined the frequency plot for respectively Young's modulus and density of the mandible and the values obtained that were used as material properties in the FEM pre-processor (Figures B.4, B.5 & B.6).

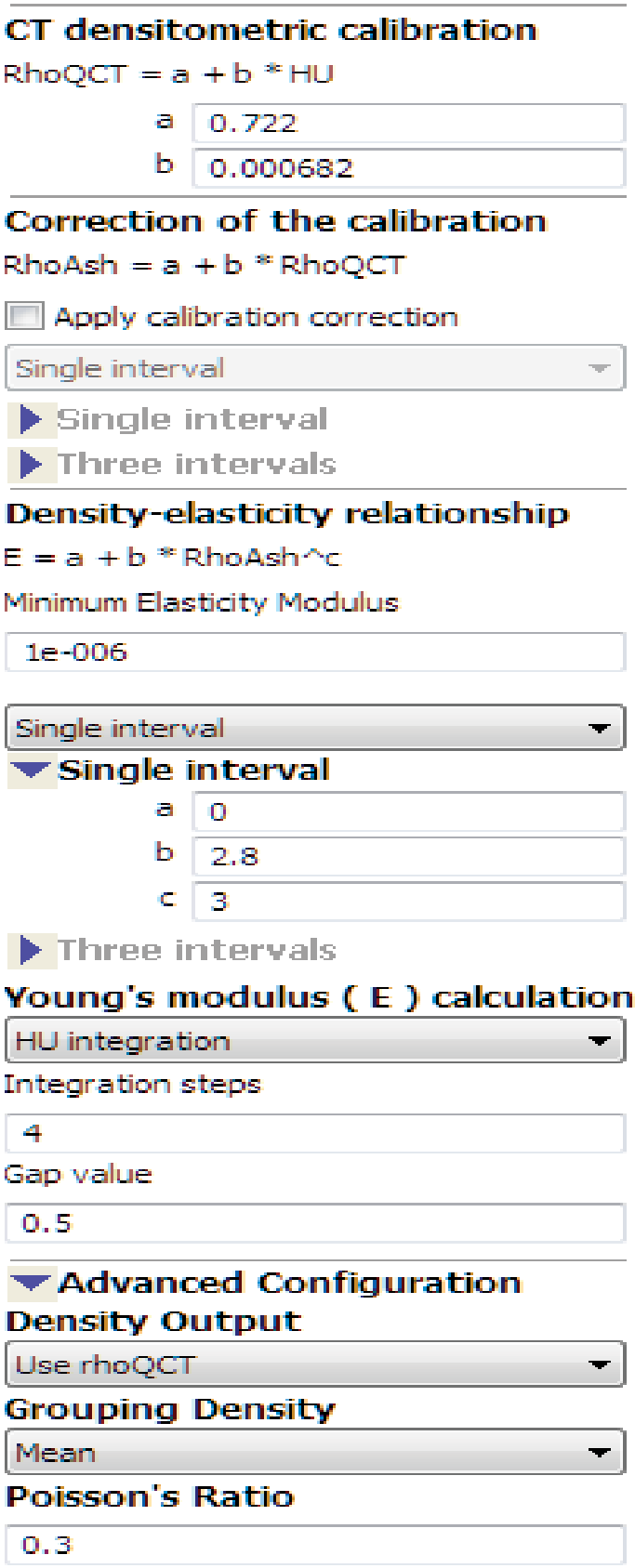

Figure B.4 ***Bonemat*** **graphical user interface showing all the parameters used to generate the conversion from CT numbers to Young's modulus for a specific finite element mesh (modified from Taraschi, 2016)**

The calculation of local material properties for the finite element mesh generates the distributions for E and ρ, as shown in Figure 7.20.

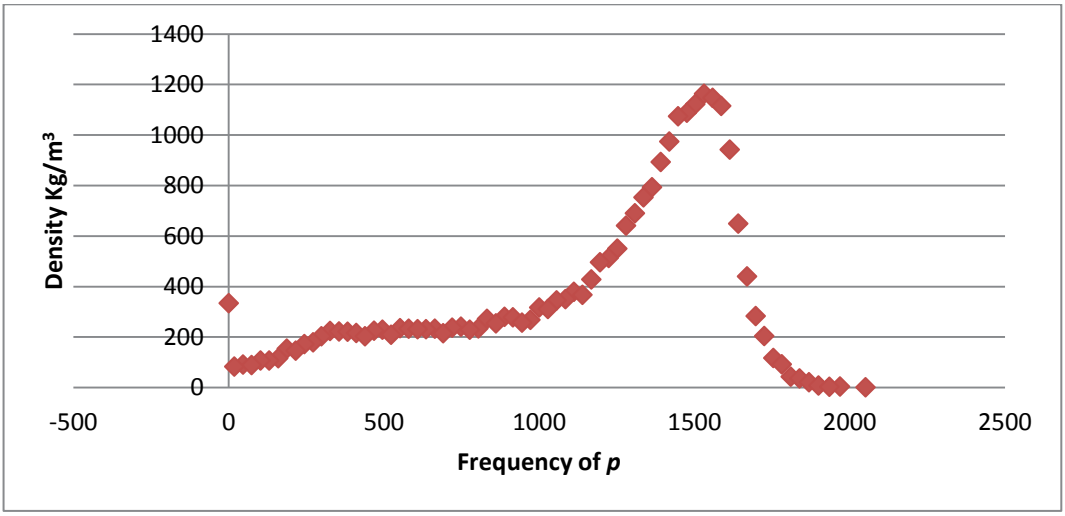

Figure B.5 Density distribution showing frequency of calculated densities in the mandibular mesh (modified from Taraschi, 2016)

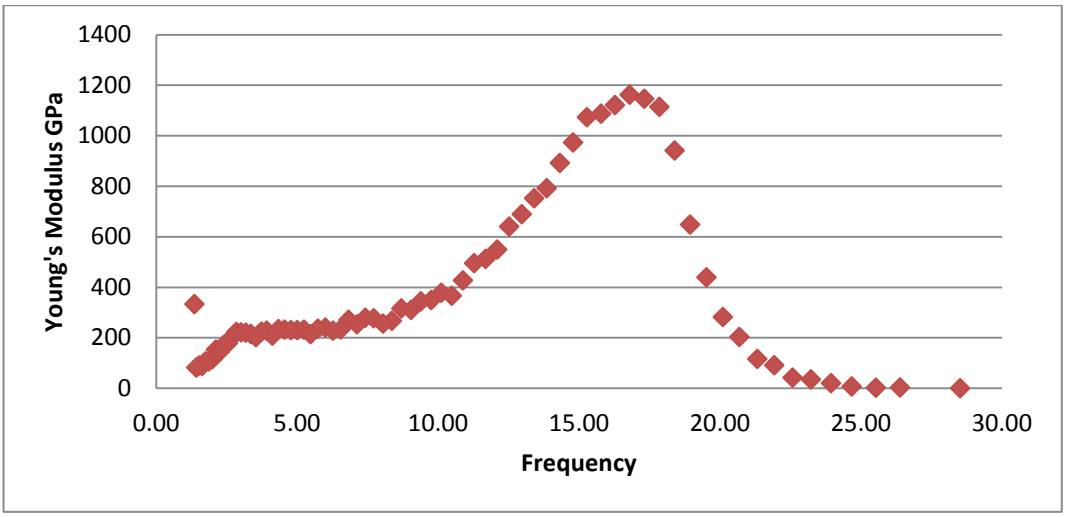

Figure B.6 Distribution of Young's modulus in the finite element mesh calculated using an inverse approach (modified from Taraschi, 2016)

Maximum principal stresses in cancellous and cortical bone were compared to the published values for ultimate tensile strength. From Keller et al. (1994), the ultimate stress *S* is estimated by the following law:

$$MPa) = 117(\rho)^{1.93} \quad (19)$$

Assuming that densities for the cortical bone are within the range specified in Table B.1 calculations show how generated stresses are below the values predicted when using Keller's empirical law.

Table B.1 Comparison of stress values obtained for cortical and cancellous bone respectively when using Keller's empirical law and the finite element simulation object of this study

	ρ	*S* (Keller et al., 1994)	M1a	M2	M3
Cortical bone	1.00	117	79	58	149
	1.25	180			
	1.50	255			

Density values are in g/cm^3 while stress is calculated as principal stress. Values are in MPa.

BIBLIOGRAPHY

Adams, S. H., & Zander, H. A. (1964). Functional tooth contacts in lateral and centric occlusion. *Journal of the American Dental Association*, *69*(10), 465.

Allareddy, V., Allareddy, V., & Nalliah, R. P. (2011). Epidemiology of facial fracture injuries. *Journal of Oral and Maxillofacial Surgery*, *69*(10), 2613-18.

Alpert, B. (1998). Management of the complications of mandibular fracture treatment. *Operative Techniques in Plastic and Reconstructive Surgery*, *5*, 325-33.

Al-Sukhun, J., Kelleway, J., & Helenius, M. (2007). Development of a three-dimensional finite element model of a human mandible containing endosseous dental implants. I. Mathematical validation and experimental verification. *Journal of Biomedical Materials Research*, *80*(1), 234-46.

Amis, A. A., Dowson, D., & Wright, V. (1980). Elbow joint force predictions for some strenuousisometric actions. *Journal of Biomechanics*, *13*(9), 765-75.

Arendts, F. J., & Sigolotto, C. (1989). Standard measurements, elastic values and tensile strength behavior of the human mandible, a contribution to the biomechanics of the mandible – I. *Biomedizinische Technik.*, *34*(10), 248-55.

Arendts, F. J., Sigolotto, C. (1990). Mechanical characteristics of the human mandible and study of in vivo behavior of compact bone tissue, a contribution to the description of biomechanics of the mandible – II. *Biomedizinische Technik.*, *35*, 123-30.

Ashman, R. B., Van Buskirk, W. C. (1987). The elastic properties of a human mandible. *Advances in Dental Research*, *1*(1), 64-67.

Australian Institute of Health and Welfare (AIHW). (2003), Australian hospital statistics 2001-2002. Canberra: AIHW.

Azevedo C.R.F. (2003). Failure analysis of a commercially pure titanium plate for osteosynthesis. *Engineering Failure Analysis*, *10*(2), 153-64

Badoux, D. M. (1966). Statics of the mandible. *Acta. Morph. Neerl. Scand.*, *6*(3), 251-56.

Baragar, F. A., & Osborn, J. W. (1984). A model relating patterns of human jaw movement to biomechanical constraints. *Journal of Biomechanics*, *17*(10), 757-67.

Barao, V. A., Assuncao, W. G., Tabata, L. F. Delben, J. A. Gomes, E. A. de Sousa, E. A. & Rocha, E. P. (2009). Finite element analysis to compare complete denture and implant-retained overdentures with different attachment systems. *Journal of Craniofacial Surgery*, *20*(4), 1066-71.

Barbenel, J. C. (1972). The biomechanics of the temporomandibular joint: A theoretical study. *Journal of Biomechanics*, *5*(3), 251-56.

Barbenel, J. C. (1974). The mechanics of the temporomandibular joint: A theoretical and electromyographical study. *Journal of Oral Rehabilitation*, *1*(1), 19-27.

Bayraktar, H. H., Morgan, E. F., Niebur, G. L., Morris, G. E., Wong, E. K., & Keaveny, T. M. (2004). Comparison of the elastic and yield properties of human femoral trabecular and cortical bone tissue. *Journal of Biomechanics*, *37*(1), 27-35.

Bechtol, C. O., Fergusson, A. B., & Laing, P. E. (1959). *Metals and engineering in bone and joint surgery* (p. 20). Baltimore: Williams Wilkins.

Begg, S., Vos, T., Barker, B., Stevenson, C., Stanley, L., & Lopez, A. (2007). *The burden of disease and injury in Australia, 2003*. PHE 82. Canberra: Australian Institute of Health and Welfare.

Ben-Nissan, B. (1987). *Three-dimensional modelling and finite element distortion analysis of the mandible* (PhD Dissertation). University of New South Wales, Australia.

Ben-Nissan, B., Svensson, N. L., Kelly, D. W., & Vajda, T. T. (1987) Computer aided three-dimensional modelling and finite element analysis of the mandible. In J. F. Williams, & L. Stevens (Eds), *Finite element methods in engineering* (pp. 290-294). University of Melbourne, Australia.

Berndt, R. M., & Berndt, C. H. (1994). *The speaking land: Myth and story in Aboriginal Australia*. Vermont: Inner Traditions.

Bisson, J. I., Shepherd, J. P., Joy, D., Probert, R., Newcombe, R. G. (2004). Early cognitive-behavioural therapy for post-traumatic stress symptoms after physical injury. Randomised controlled trial. *British Journal of Psychiatry*, *184*(1), 63-69.

Bitsakos, C., Kerner, J., Fisher, I. & Amis, A. A. (2005). The effect of muscle loading on the simulation of bone remodelling in the proximal femur. *Journal of Biomechanics*, *38*(1), 133-39.

Bock, W. J. (1966). An approach to the functional analysis of bill shape. *The Auk*, 83(1), 10-51.

Bock, W. J., & Kummer, B. (1968). The avian mandible as a structural grinder. *Journal of Biomechanics*, *1*, 89-96.

Bradley, J. C. (1975). A radiological investigation into the age changes of the inferior alveolar artery. *British Journal of Oral and Maxillofacial Surgery*, *13*, 82-90.

Brekhus, P. H., Armstrong, W. D., & Simon, W. J. (1941). Stimulation of the muscles of mastication. *Journal of Dental Research*, 20(2), 87-92.

Brown, T., Kohan, L. & Ben-Nissan, B. (2010). Hp15: Finite element analysis and surgical considerations of the impact of osteoporosis and osteoarthritis on hip resurfacing. *Orthopaedic Proceedings*, 92-B, SUPP I, 184.

Brudevold, F. (1951). A basic study of the chewing forces of a denture wearer. *Journal of the American Dental Association*, *43*(1), 45-51.

Bujtar, P., Sandor, G. K., Bojtos, A., Szucs, A., & Barabas, J. (2010). Finite element analysis of the human mandible at 3 different stages of life. *Oral Surgery, Oral Medicine, Oral Pathology, Oral Radiology and Endodontology*, *110*(3), 301-9.

Bujtar, P., Simonovics, J., Zombori, G., Fejer, Z., Szucs, A., Bojtos, A., Batista, W. O., Varadi, K., & Sandor, G. K. (2014). Internal or in-scan validation: A method to sssess Cbct and Msct gray scales using a human cadaver. *Oral Surgery, Oral Medicine, Oral Pathology, Oral Radiology and Endodontology*, *117*(6) ,768-79.

Burstein, A. H., Reilly, D. T., & Martens, M. (1976). Aging of bone tissue: mechanical properties. *Journal of Bone and Joint Surgery. American*, *58*(1), 82-86.

Cameron, P., Dziukas, L., Hadj, A., Clark, P., & Hooper, S. (1995). Patterns of injury from major trauma in Victoria. *ANZ Journal of Surgery*, *65*(12), 848-52.

Caputo, A. A., & Standlee, J. P. (1987). *Biomechanics in clinical dentistry*. Chicago: Quintessence.

Carlsoo, S. (1952). Nervous coordination and mechanical function of the mandibular elevators. An EMG study of the activity, and an anatomic analysis of the mechanics of muscles. *Acta Odontologica Scandandinavica*, *10*(11), 1-132.

Carlsoo, S. (1958). Motor units and action potentials in masticatory muscles. *Acta Morph Neel Scand*, *2*(1), 13-19.

Carter, D. R., & Hayes, W. C. (1977). The compressive behavior of bone as a two-phase porous structure. Journal of Bone and Joint Surgery, American Volume, 59(7), 954-62.

Carter, D. R., & Spengler, D. M. (1978). Mechanical properties and composition of cortical bone. *Clinical Orthopaedics and Related Research*, Sep(135), 192-217.

Champy, M., Lodde, J. P., & Schmidt, R. (1978). Mandibular osteosynthesis by miniature screwed plates via a buccal approach. Journal of Maxillofacial Surgery, 6(1), 14-21. doi:10.1016/S0301-0503(78)80062-9

Champy, M., Pape, H. D., Gerlach, K. L., & Lodde, V. P. (1986). The Strasbourg miniplate osteosynthesis. Oral and Maxillofacial Trauma, vol II. Chicago: Quintessence.

Chen, X., Lin, Y., Wang, C., Shen, G., Zhang, S. & Wang, X. (2011). A surgical navigation system for oral and maxillofacial surgery and its application in the treatment of old Zygomatic fractures. *International Journal of Medical Robotics*, *7*(1), 42-50.

Chen, X., Wu, Y. & Wang, C. (2011). Application of a surgical navigation system in the rehabilitation of maxillary defects using Zygoma implants: Report of one case. *International Journal of Oral and Maxillofacial Implants*, *26*(5), 29-34.

Choi, A. H., Ben-Nissan, B., & Conway, R. C. (2005). Three-dimensional modelling and finite element analysis of the human mandible during clenching. *Australian Dental Journal*, *50*(1), 42-48.

Choi, A. H., Conway, R. C., & Ben-Nissan, B. (2014). Finite-element modeling and analysis in nanomedicine and dentistry. *Nanomedicine (London)*, *9*(11) 1681-95.

Choi, A. H., Matinlinna, J. & Ben-Nissan, B. (2013). Effects of micromovement on the changes in stress distribution of partially stabilized zirconia (Ps-Zro2) dental implants and bridge during clenching: A three-dimensional finite element analysis. *Acta Odontologica Scandinavica*, *71*(1), 72-81.

Choi, A. H., Matinlinna, J. P., & Ben-Nissan, B. (2012). Finite element stress analysis of Ti-6al-4v and partially stabilized zirconia dental implant during clenching. *Acta Odontologica Scandinavica*, *70*(5), 353-61.

Choi, B. H., Zhu, J. S., & Kim, H. Y. (2005). A clinical evaluation of titanium miniplates as anchors for orthodontic treatment. *American Journal of Orthodontics and Dentofacial Orthopedics*, *128*(3), 382-84.

Claes, L. E., & Heigele, C. A. (1999). Magnitudes of local stress and strain along bony surfaces predict the course and type of fracture healing. *Journal of Biomechanics*, *32*(3), 255-66.

Cody, D. D., McCubbrey, D. A., Divine, G. W., Gross, G. J. & Goldstein, S. A. (1996). Predictive value of proximal femoral bone densitometry in determining local orthogonal material properties. *Journal of Biomechanics*, *29*(6), 753-61.

Croll, B. M. (2017). Mechanical principles applied to removable prosthetic occlusion. *Inside Dental Technology* (online), *8*(1).

Crowningshield, R. D., Johnson, R. D., Andrews, J. G., & Brand, R. A. (1978). Use of optimization techniques to predict muscle forces. *Journal of Biomechanics*, *100*(2), 88-92.

Currey, J. (2004). Incompatible mechanical properties in compact bone. *Journal of Theoretical Biology*, *231*(4), 569-80.

Currey, J. D. (2004). Tensile yield in compact bone is determined by strain, post-yield behaviour by mineral content. *Journal of Biomechanics*, *37*(4), 549-56.

Curtis, K. A., Mitchell, R. J., Chong, S. S., Balogh, Z. J., Reed, D. J., Clark, P. T., D'Amours, S., Black, D. A., Langcake, M. E., Taylor, Colman, B., McDougall, P., & Cameron, P. A. (2012). Injury trends and mortality in adult patients with major trauma in New South Wales. *Medical Journal of Australia*, *197*(4), 233-237. doi:10.5694/mja11.11351

De Vos, W. (2009). Cone-beam computerized tomography (CBCT) imaging of the oral and maxillofacial region: A systematic review of the literature. *International Journal of Oral and Maxillofacial Surgery*, *38*(6), 609-25.

Dechow, P. C., Nail, G. A., Schwartz-Dabney, C. L., & Ashman, R. B. (1993). Elastic properties of human supraorbital and mandibular bone. *American Journal of Physical Anthropology*, *90*(3), 291-306.

Ding, X., Zhu, X. H., Liao, S. H., Zhang X. H., & Chen, H. (2009). Implant-bone interface stress distribution in immediately loaded implants of different diameters: A three-dimensional finite element analysis. *Journal of Prosthodontics*, *18*(5), 393-402.

Einhorn, T. A. (1995). Current concepts review: Enhancement of fracture healing. *Journal of Bone and Joint Surgery*, *77-A*(6), 940-56.

Ellis, E. (1996). Complications of rigid internal fixation for mandibular fractures. *Journal of Cranio-maxillofacial Trauma*, *2*(2), 32-39.

Eskitascioglu, G., Usumez, A., Sevimay, M., Soykan, E., & Unsal, E. (2004). The influence of occlusal loading location on stresses transferred to implant-supported prostheses and supporting bone: A three-dimensional finite element study. *Journal of Prosthetic Dentistry*, *91*(2), 144-50.

Ferre, J. C., Legous, R., Helary, J. L., Albugues, F., Le Floc'h, C., Bouteyre, J., Lumineau, J. P., Chevalier, C., Le Cloarec, A. Y., Orio, E., Marquet, F., & Barbin, J. Y. (1985). Study of the deformations of the isolated mandible under static constraints by simulation on a physicomathematical model. *Anatomia Clinica*, *7*(3), 183-92.

Fick, H. (1904). *Handbuch der Anatomie und Mechanik der Gelenke*. Jena: Gustav Fisher.

Fischer, K., Zhang, F., Angel, M. F., & Lineaweaver, W. C. (2001). Injuries associated with mandible fractures sustained in motor vehicle collisions. *Plastic and Reconstructive Surgery*, *108*(2), 328-31.

Frank, L. (1950). Muscular influence on occlusion as shown by x-ray of the condyle. *Dental Digest*, *56*, 484-88.

Futterling, S., Klein, R., Straber, W., & Weber, H. (1998). Automated finite element modelling of a human mandible with dental implants. In *Proceedings of the sixth international conference in Central Europe on computer graphics and visualization, Sixth international conference in Central Europe on computer graphics and visualisation*. University of West Bohemia, Plzen, Czech Republic, February 9-13.

Garner, L. D., & Kotwal, N. S. (1973). Correlation study of incisive biting forces with age, sex and anterior occlusion. *Journal of Dental Research*, *52*(4), 698.

Gates, G. N., & Nicholls, J. L. (1981). Evaluation of mandibular arch width dhange. *Journal of Prosthetic Dentistry*, *46*(4), 385-92.

Ghanem, W. A., Elhayes, K. A., & Saad, K. (2011). The management of unstable oblique infected mandibular fractures with a 2.3mm mandibular osteosynthesis reconstruction bone plate. *Journal of Cranio-Maxillo-Facial Surgery*, *39*(8), 600-605.

Gibbs, C. H., Reswick, J. B., & Messerman, T. (1969). Investigation of functional mandibular movement. *Dental Clinics of North America*, *13*, 629.

Giesen, E. B., & Van Eijden, T. M. (2000). The three-dimensional cancellous bone architecture of the human mandibular condyle. *Journal of Dental Research*, *79*(4), 957-63.

Gingerich, P. D. (1971). Functional significance of mandibular translation in vertebrate jaw mechanics. *Postilla*, *152*, 1-10.

Glickman, I., Pameijer, J.H.N., Roeber, F. W., & Brion, M.A.M. (1969). Functional occlusion as revealed by miniaturized radio transmitters. *Dental Clinics of North America*, *13*(3), 667-79.

Goffin, J. M., Pankaj, P., & Simpson, A. H. (2014). A computational study on the effect of fracture intrusion distance in three- and four-part trochanteric fractures treated with Gamma nail and sliding hip screw. *Journal of Orthopaedic Research*, *32*(1), 39-45.

Grant, P. G. (1973). Biomechanical significance of the instantaneous center of rotation: the human temporomandibular joint. *Journal of Biomechanics*, *6*(2), 109-13.

Grant, P. G. (1973). Biomechanical significance of the instantaneous center of rotation: The human temporomandibular joint. *Journal of Biomechanics*, *6*(3), 109-13.

Guan, H.,van Staden, R., Loo, Y. C., Johnson, N., Ivanovski, S., & Meredith, N. (2009). Influence of bone and dental implant parameters on stress distribution in the mandible: A finite element study. *International Journal of Oral and Maxillofacial Implants*, *24*(5), 866-76.

Gysi, A. (1921). Studies on the leverage problem of the mandible. *Dental Digest*, *27*, 74-84, 184-190, 203-208.

Haagsma, J. A., Polinder, S., Toet, T., Panneman, M., Havelar, A. H., Bonsel, G. J., & van Beeck, E. F. (2010). Beyond the neglect of psychological consequences: post-traumatic stress disorder increases the non-fatal burden of injury by more than 50%. *Injury Prevention*, *17*(1), 21-26.

Hansson, S., & Halldin, A. (2012). Alveolar ridge resorption after tooth extraction: A consequence of a fundamental principle of bone physiology. *Journal of Dental Biomechanics*, *3*. doi:10.1177/1758736012456543

Hart, R. T., Hennebel, V.V., Thongpreda, N., Van Buskirk, W. C., & Anderson, R. C. (1992). Modeling the biomechanics of the mandible: a three-dimensional finite element study. *Journal of Biomechanics*, *25*(3), 261-86.

Haskell, B., Day, M., & Tetz, J. (1986). Computer-aided modeling in the assessment of the biomechanical determinants of diverse skeletal patterns. *American Journal of Orthodontics and Dentofacial Orthopedics*, *89*(5), 363-82.

Hawthorne, R. (1969). *Microscopic anatomy of the temporomandibular joint* (Dissertation). University of Sydney, Australia.

Helgason, B., Perilli, E., Schileo, E., Taddei, F., Brynjolfsson, S., & Viceconti, M. (2008). Mathematical relationships between bone density and mechanical properties: A literature review. *Clinical Biomechanics*, *23*(2), 135-46.

Henley, G., & Harrison, J. E. (2009). Injury deaths, Australia 2004-05. *Injury Research and Statistics Series*, No. 51 (Cat. no. INJCAT 127). Canberra: Australian Institute of Health & Welfare.

Hettinger, T. (1961). *Physiology of strength*. Illinois: Charles C. Thomas.

Hildebrand, G. Y. (1931). *Studies in the masticatory movements of the lower jaw*, Berlin: Walter De Gruyter.

Hirabayashi, M., Motoyoshi, M., Ishimaru, T., Kasai, K., & Namura, S. (2002). Stresses in mandibular cortical bone during mastication: Biomechanical considerations using a three-dimensional finite element method. *Journal of Oral Science*, *44*(1), 1-6.

Howell, A. H., & Manly, R. S. (1948). An electronic strain gauge for measuring oral forces. *Journal of Dental Research*, *27*(6), 705-12.

Hujoel, P. P. (1994). A meta-analysis of normal ranges for root surface areas of the permanent dentition. *Journal of Clinical Periodontology*, *21*(4), 225-29.

Hussein, M. O., & M. E. Rabie, M. E. (2015). Three-dimensional nonlinear contact finite element analysis of mandibular all-on-4 design. *Journal of Oral Implantology*, *41*(2), e12-8.

Hylander, W. L. (1975). The human mandible: Lever or link? *American Journal of Physical Anthropology*, *43*(2), 227-42.

Hylander, W. L. (1977). In vivo bone strain in the mandible of Galago crassicaudatus. *American Journal of Physical Anthropology*, *46*(2), 309-26.

Hylander, W. L. (1978). Incisal bite force direction in humans and the functional significance of mammalian mandibular translation. *American Journal of Physical Anthropology*, *48*(1), 1-7.

Hylander, W. L. (1979). An experimental analysis of temporomandibular joint reaction force in macaques. *American Journal of Physical Anthropology*, *51*(3), 433-56.

Hylander, W. L. (1984). Stress and strain in the mandibular symphysis of primates: a test of competing hypotheses. *American Journal of Physical Anthropology*, *64*(1), 1-46.

Hylander, W. L. (1985). Mandibular function and biomechanical stress and scaling. *American Zoologist*, *25*(2), 315-30.

Hylander, W. L., Johnson, K. R., & Crompton, A. W. (1987). Loading patterns and jaw movements during mastication in Macaca fascicularis: A bone-strain, electromyographic, and cineradiographic analysis. *American Journal of Physical Anthropology*, *72*(3), 287-314.

Ikai, M., & Fukunaga, T. (1968). Calculation of muscle strength per unit cross-sectional area of human muscle by means of ultrasonic measurement. *Internationale Zeitschrift Fur Angewandte Physiologie*, *26*(1), 26-32.

Jainkittivong, A., Aneksuk, V., & Langlais, R. P. (2010). Oral mucosal lesions in denture wearers. *Gerodontology*, *27*(1), 26-32.

Jarabak, J. R. (1957). An electromyographic analysis of muscular behaviour in mandibular movements from rest position. *Journal of Prosthetic Dentistry*, *7*(5), 682-710.

Jemt, T. (1981). Chewing patterns in dentate and complete denture wearers – recorded by light-emitting diodes. *Swedish Dental Journal*, *5*(5-6). 199-205.

Jiroušek, O. (2012). Nanoindentation of human trabecular bone – Tissue mechanical properties compared to standard engineering test methods. In J. Nemecek (Ed.). *Manoindentation in materials science* (Chapter 11). CC BY 3.0 license.

Jonasson, G., Lindberg, F., Jorge, A., Alstad, T., & Kashani, H. (2014). Mandibular trabecular bone structure in adults with Crohn's Disease. *Clinical Oral Investigations*, *18*(2), 423-28.

Joos, U., Piffko, J., & Meyer, U. (2001). New aspects in managing mandibular fractures. *Mund- Kiefer- und Gesichtschirurgie*, *5*(1), 2-16.

Kaneko, T. S., Pejcic, M. R., Tehranzadeh, J., & Keyak, J. H. (2003). Relationships between material properties and CT scan data of cortical bone with and without metastatic lesions. *Medical Engineering and Physics*, *25*(6), 445-54.

Katranji, A., Misch, K., & Wang, H. L. (2007). Cortical bone thickness in dentate and edentulous human cadavers. *Journal of Periodontology*, *78*(5), 874-78.

Kavanagh, E. P., Frawley, C., Kearns, G., Wallis, F., McGloughlin, T., & Jarvis, J. (2008). Use of finite element analysis in presurgical planning: treatment of mandibular fractures. *Irish Journal of Medical Science*, *177*(4), 325-31.

Kawamura, Y., Majima, T., Kato, I. (1967). Physiologic role of deep mechanoreceptor in temporomandibular joint capsule. *Journal of Osaka University Dental School*, *7*, 63-76.

Keaveny, T. M., & Hayes, W. C. (1993). A 20-year perspective on the mechanical properties of trabecular bone. *Journal of Biomechanics Engineering*, *115*(4B), 534-42.

Keller, T. S. (1994). Predicting the compressive mechanical behavior of bone. *Journal of Biomechanics*, *27*(9), 1159-68.

Kennady, M. C., Tucker, M. R., Lester, G. E., & Buckley, M. J. (1989). Stress shielding effect of rigid internal fixation plates on mandibular bone grafts. A photon absorption densitometry and quantitative computerized tomographic evaluation. *International Journal of Oral and Maxillofacial Surgery*, *18*(5), 307-10.

Keyak, J. H., Fourkas, M. G., Meagher, J. M., & Skinner, H. B. (1993). Validation of an automated method of three-dimensional finite element modelling of bone. *Journal of Biomedical Engineering*, *15*(6), 505-9.

Kirkup, J. (2003). Foundation lecture. Fracture care of friend and foe during World War I. *ANZ Journal of Surgery*, *73*(6), 453-59.

Kitagawa, T., Tanimoto, Y., Nemoto K., & Aida, M. (2005). Influence of cortical bone quality on stress distribution in bone around dental implant. *Dental Materials Journal*, *24*(2), 219-24.

Klein, P., Schell, H., Streitparth, F., Heller, M., Kassi, J., Kandziora, F., Bragulla, H., Haas, N. P., & Duda, G. N. (2002). The initial phase of fracture healing is specifically sensitive to mechanical conditions. *Journal of Orthopaedic Research*, *21*(4), 662-69.

Knoell, A. C. (1977). A mathematical model of an in vitro mandible. *Journal of Biomechanics*, *10*(3), 159-66.

Kollner, H. J. (1978). The registration of the retrusive closing phase and its effect on the mandible. *Zahn Mund Kieferheilkd Zentralbl*, *66*(8), 792-96.

Koolstra, J. H., & Van Eijen, T. M. (2005). Combined finite-element and rigid-body analysis of human jaw joint dynamics. *Journal of Biomechanics*, *38*(12), 2431-39.

Korioth, T. W., Romilly, D. P., & Hannam, A. G. (1992). Three-dimensional finite element stress analysis of the dentate human mandible. *American Journal of Physical Anthropology*, *88*(1), 69-96.

Koshy, J. C., Chike-Obi, C. J., Feldman, E. M., & Bullocks, J. M. (2010). Pearls of mandibular trauma management. *Seminars in Plastic Surgery*, *24*(4), 357-74.

Kreisfeld, R., Newson, R., & Harrison, J. (2004). Injury death, Australia 2002. *Injury Research and Statistics Series, No. 23*. Adelaide: Australian Institute of Health and Welfare.

Lane, W. A. (1895). Some remarks on the treatment of fractures. *BMJ*, *1*, 861-63. doi:10.1136/bmj.1.1790.861

Lehman, M. L. (1968). Stress-distribution in the alveolar bone. *Journal of Biomechanics*, *1*(2), 139-45.

Lehr, R. P., Blanton, P. L., & Biggs, N. L. (1971). An electromyographic study of the mylohyoid muscle. *Anatomical Record*, *169*(4), 651-59.

Lewis, M., Reid, K., & Toms, A. P. (2013). Reducing the effects of metal artefact using high keV monoenergetic reconstruction of dual energy CT (DECT) in hip replacements. *Skeletal Radiology*, *42*(2), 275-82.

Li, P., Tang, Y., Li, J., Shen, L., Tian, W., & Tang, W. (2013). Establishment of sequential software processing for a biomechanical model of mandibular reconstruction with custom-made plate. *Computer Methods & Programs in Biomedicine*, *111*(3), 642-49.

Li, T., Kong, L., Wang, Y., Hu, K., Song, L., Liu, B., Li, D., Shao, J., & Ding, Y. (2009). Selection of optimal dental implant diameter and length in type IV bone: A three-dimensional finite element analysis. *International Journal of Oral & Maxillofacial Surgery*, *38*(10), 1077-83.

Li, W., Swain, M. V., Li, Q., & Steven, G. P. (2005). Towards automated 3D finite element modeling of direct fiber reinforced composite dental bridge. *Journal of Biomedical Materials Research Part B: Applied Biomaterials*, *74*(1), 520-28.

Lin, S., Shi, S., LeGeros, R. Z., & LeGeros, J. P. (2000). Three-dimensional finite element analyses of four designs of a high-strength silicon nitride implant. *Implant Dentistry*, *9*(1), 53-60.

Liu, S. J., Wang, L. J., Gu, W. M., Wu, W., Xu, P., & Chen, Z. W. (2010). Clinical study of stress shielding after mini-plate internal fixation for mandibular fractures. *Zhonghua Kou Qiang Yi Xue Za Zhi*, *45*(8), 474-76.

Luhr, H. G. (1985). Basic research, surgical technique and results of fracture treatment with the Luhr-Mandibular compression screw system. *Proceedings from the Eight International Conferences on Oral and Maxillofacial Surgery.* Quintessence (pp 124-32). Chicago.

Luhr, H. G. (1992). Specification, indications and clinical application of the luhr vitallium. Maxillofacial systems. In M. J. Yarenchuk, J. S. Gruss, P. N. Manson & H. C. Vasconez (Eds.). *Rigid fixation of the craniomaxillofacial skeleton*. Oxford: Butterworth-Heinemann (pp. 79-115).

Luhr, H. G., Reidick, T., & Merten, H. A. (1996). Results of treatment of fractures of the atrophic edentulous mandible by compression plating: A retrospective

evaluation of 84 consecutive cases. *Journal of Oral and Maxillofacial Surgery*, *54*(3), 250-55.

Lund, P., Nishiyama, T., & Moller, E. (1970). Postural activity in the muscles of mastication with the subject upright, inclined and supine. *Scandinavian Journal of Dental Research*, *78*(5), 417-24.

Mainland, D., & Hiltz, E. J (1934). Forces exerted on the human mandible by the muscles of mastication. *Journal of Dental Research*, *14*, 107-24.

Marcian, P., Borak, L., Valasek, J., Kaiser, J., Florian, Z., & Wolff, J. (2014). Finite element analysis of dental implant loading on atrophic and non-atrophic cancellous and cortical mandibular bone: A feasibility study. *Journal of Biomechanics*, *47*(16), 3830-36.

Marciani, R. D. (2001). Invasive management of the fractured atrophic edentulous mandible. *Journal of Oral and Maxillofacial Surgery*, *59*(7), 792–95

Marinescu, R., Daegling, D. J., Rapoff, A. J. (2005). Finite-element modeling of the anthropoid mandible: The effects of altered boundary conditions. *Anatomical Record. Part A, Discoveries in Molecular, Cellular and Evolution Biology*, *283*(2), 300-9.

Marsh, D. R., & Li, G. (1999). The biology of fracture healing: optimising outcome. *British Medical Bulletin*, *55*(4), 856-69.

McCalden, R. W., McGeough, J. A., Barker, M. B., & Court-Brown, C. M. (1993). Age-related changes in the tensile properties of cortical bone. The relative importance of changes in porosity, mineralization, and microstructure. *Journal of Bone and Joint Surgery*, *75*(8), 1193-205.

Meijer, H. J., Starmans, F. J., Steen, W. H., & Bosman, F. (1993). A three-dimensional, finite element analysis of bone around dental implants in an edentulous human mandible. *Archives of Oral Biology*, *38*(6), 491-96.

Menicucci, G., Mossolov, A., Mozzati, M., Lorenzetti, M., & Preti, G. (2002). Tooth-implant connection: Some biomechanical aspects based on finite element analyses. *Clinical Oral Implants Research*, *13*(3), 334-41.

Michelet, F. X., Deymes, J., & Dersus, B. (1973). Osteosynthesis with miniatured screwed plates in maxillofacial surgery. *Journal of Oral and Maxillofacial Surgery*, *1*(2), 79-84.

Mishellany-Dutour, A., Renaud, J., Peyron, M. A., Rimek, F., & Woda, A. (2007). Is the goal of mastication reached in young dentates, aged dentates and aged denture wearers? *British Journal of Nutrition*, *99*(1), 121-28.

Moller, E. (1966). The chewing apparatus: an EMG study of the action of the muscles of mastication and its correlation to facial morphology. *Acta Physiologica Scandinavica*, *69*(280), 1-229.

Mommaerts, M. Y., Michiels, E., & De Pauw, G. (2005). A 2-year outcome audit of a versatile orthodontic bone anchor. *Journal of Orthodontics*, *32*(3), 175-81.

Mongini, F., Calderale, P. M., & Barberi, G. (1979). Relationship between structure and the stress pattern in the human mandible. *Journal of Dental Research*, *58*(12), 2334-37.

Morais, E.C.C., Ornaghi, B. P., Sponchiado, A. P., Zielak, J. C., da Costa, R. G., Bindo, M.J.F., de Campos, E. A. (2015). Determination of final occlusal vertical dimension by cephalometric analysis, *RSBO* (online), *12*(2).

Morgan, E. F., Bayraktar, H. H., Yeh, O. C., Majumdar, S., Burghardt, A., & Keaveny, T. M. (2004). Contribution of inter-site variations in architecture to trabecular bone apparent yield strains. *Journal of Biomechanics*, *37*(9), 1413-20.

Morris, C. B. (1948). The measurement of the strength of muscle relative to the cross-section. *Research Quarterly. American Association for Health Physical Education and Recreation*, *19*(4), 295-303.

Morrison, J. B. (1967). *The forces transmitted by the human knee joint during activity* (Dissertation). Glasgow: University of Strathclyde.

Moyers, R. E. (1950). EMG analysis of certain muscles involved in a temporomandibular movement. *American Journal of Orthodontics*, *36*, 481-515.

Munro, R. R., & Basmajian, J. V. (1971). The jaw opening reflex in man. *Electromyography*, *11*(2), 191-206.

Murakami, K., Yamamoto, K., Sugiura, T., Kawakami, M., Horita, S., & Kirita, T. (2015). Biomechanical analysis of poly-L-lactic acid and titanium plates fixated for mandibular symphyseal fracture with a conservatively treated unilateral condylar fracture using the three-dimensional finite element method. Dental Traumatology, *31*(5), 396-402.

Neumann, D. A. (2016). *Kinesiology of the musculoskeletal system: Foundations for Rehabilitation* (3rd ed.). Mosby Elsevier Press.

Nickenig, H. J., Wichmann, M., Eitner, S., Zoller, J. E., & Kreppel, M. (2015). Lingual concavities in the mandible: A morphological study using cross-sectional analysis determined by CBCT. *Journal of Cranio-Maxillo-Facial Surgery*, *43*(2), 254-59.

Nomura, T., Gold, E., Powers, M. P., Shingaki, S., & Katz, J. L. (2003). Micromechanics/structure relationships in the human mandible. *Dental Materials*, *19*(3), 167-73.

Novelli, G., Sconza, C., Ardito, E., & Bozzetti, A. (2012). Surgical treatment of the atrophic mandibular fractures by locked plates systems: Our experience and a literature review. *Craniomaxillofac Trauma Reconstruction*, *5*(2), 65-74.

Novelli, G., Sconza, C., Ardito, E., & Bozzetti, A. (2012). Surgical treatment of the atrophic mandibular fractures by locked plates systems: Our experience and a literature review, *Craniomaxillofacial Trauma and Reconstruction*, *5*(2), 65-74.

Oberdan, W., & Finn, B. (2007). Mandibular fractures in Far North Queensland: An ethnic comparison. *ANZ Journal of Surgery*, *77*(1-2), 73-79.

Okeson, J. P. (1985). *Fundamentals of occlusion and temporomandibular disorders*. St Louis: CV Mosby.

Okumura, N., Stegaroiu, R., Kitamura, E., Kurokawa K., & Nomura, S. (2010). Influence of maxillary cortical bone thickness, implant design and implant diameter on stress around implants: A three-dimensional finite element analysis. *Journal of Prosthodontics*, *54*(3), 133-42.

Osborn, J. W., & Baragar, F. A. (1985). Predicted pattern of human muscle activity during clenching derived from a computer assisted model: symmetric vertical bite forces. *Journal of Biomechanics*, *18*(8), 599-612.

Ota, T., Yamamoto, I., & Morita, R. (1999). Fracture simulation of the femoral bone using the finite-element method: How a fracture initiates and proceeds. *Journal of Bone and Mineral Metabolism*, *17*(2), 108-12.

Parrington, F. R. (1934). On the Cynodont genus Galesaurus, with a note on the functional significance of the changes in the evolution of the Theriodont skull. *Annals and Magazine of Natural History*, *13*, 38-67.

Paul, J. P. (1966). Forces transmitted by joints in the human body. *Proceedings of the Institution of Mechanical Engineers*, *181*, 8-15.

Paulson, J. (1973). *Biomechanics of the leg* (Dissertation). Glasgow: University of Strathclyde.

Perillo-Marcone, A., Ryd, L., Johnsson, K., & M. Taylor, M. (2004). A combined RSA and FE study of the implanted proximal tibia: Correlation of the post-operative mechanical environment with implant migration. *Journal of Biomechanics*, *37*(8), 1205-13.

Perren, S. M. (2002). Evolution of the internal fixation of long bone fractures. *Journal of Bone and Joint Surgery*, *84-B*(8), 1093-10.

Pithioux, M., Lasaygues, P., & Chabrand, P. (2002). An alternative ultrasonic method for measuring the elastic properties of cortical bone. *Journal of Biomechanics*, *35*(7), 961-68.

Posselt, U. (1962). *Physiology of occlusion and rehabilitation*. Oxford: Blackwell Scientific Publication.

Pruim, G. J., De Jongh, H. J., Ten Bosch, J. J. (1980). Forces acting on the mandible during bilateral static bite at different bite force levels. *Journal of Biomechanics*, *13*(9), 755-63.

Pruim, G. J., Ten Bosch, J. J., & De Jongh, H. J. (1978). Jaw muscle EMG-activity and static loading of the mandible. *Journal of Biomechanics*, *11*(8-9), 389-95.

Qian, L., Todo, M., Matsushita, Y., & Koyano, K. (2009). Effects of implant diameter, insertion depth and loading angle on stress/strain fields in implant/jawbone systems: Finite element analysis. *International Journal of Oral and Maxillofacial Implants*, *24*(5), 877-86.

Queensland Institute of Medical Research (2017). *Facial expression as a non invasive diagnostic tool for mental health* (Current study).

Ralph, J. P., & Caputo, A. A. (1975). Analysis of stress patterns in the human mandible. *Journal of Dental Research*, *54*(4), 814-21.

Reilly, D. T., Burstein, S. H., & Frankel, V. H. (1974). The elastic modulus for bone. *Journal of Biomechanics*, *7*(3), 271-75.

Rho, J. Y., Hobatho, M. C., & Ashman, R. B. (1995). Relations of mechanical properties to density and CT numbers in human bone. *Medical Engineering and Physics*, *17*(5), 347-55. doi: 10.1016/1350-4533(95)97314-F

Roberts, D. (1974). The etiology of the temporomandibular joint dysfunction syndrome. *American Journal of Orthodontics*, *66*(5), 498-515.

Roberts, D., & Tattersall, I. (1974). Skull form and the mechanics of mandibular elevation in mammals. *American Museum Novitates*, *2356*, 1-9.

Roberts, D., & Tattersall, I. (1974). Skull form and the mechanics of mandibular evolution in mammals. *American Museum Novitates*, *2536*, 1-9.

Robinson, M. (1946). The temporomandibular joint: Theory of reflex controlled non-lever action of the mandible. *Journal of the American Dental Association*, *33*(19), 1260-71.

Schileo, E., Dall'ara, E., Taddei, F., Malandrino, A., Schotkamp, T., Baleani, M., & Viceconti, M. (2008). An accurate estimation of bone density improves the accuracy of subject-specific finite element models. *Journal of Biomechanics*, *41*(11), 2483-91.

Schileo, E., Taddei, F., Malandrino, A., Cristofolini, L., & Viceconti, M. (2007). Subject-specific finite element models can accurately predict strain levels in long bones. *Journal of Biomechanics*, *40*(13), 2982-89.

Schmitz, J. P., & Hollinger, J. O. (1986). Critical size defect as an experimental model for craniomaxillofacial non-union. *Clinical Orthopaedics and Related Research*, *205*, 299-308.

Schuller, S., Sawall, S., Stannigel, K., Hulsbusch, M., Ulrici, J., Hell, E., & Kachelriess, M. (2015). Segmentation-free empirical beam hardening correction for CT. *Medical Physics*, *42*(2), 794-803.

Schumacher, G. H. (1961). *Funktionelle Morphologie der Kinnmuskulatur*. Jena: Fisher.

Shetty, D., Urs, A., & Kaur, R. (2009). A radiographic technique for differentiating enamel and dentin in odontogenic tumors. *Internet Journal of Radiology*, *12*(1),

Sicher, H., Du Brul, E. L. (1975). *Oral Anatomy*. St Louis: CV Mosby.

Simpson, A.H.R.W., Mills, L., & Noble, B. (2006). The role of growth factors and related agents in accelerating fracture healing. *Journal of Bone and Joint Surgery, British*, *88*(6), 701-5.

Slagter, A. P., Bosman, F., van der Glas, H. W., van der Bilt, A. (1993). Human jaw-elevator muscle activity and food comminution in the dentate and edentulous state. *Archives of Oral Biology*, *38*(3), 195-205.

Smith, R. J. (1978). Mandibular biomechanics and temporomandibular joint function in primates. *American Journal of Physical Anthropology*, 49(3), 341-49.

Soule, W. C., & Chew, F. S. (2015). *Mandibular Fracture Imaging*. Medscape

Standlee, J. P., Caputo, A. A., & Ralph, J. P. (1977). Stress trajectories within the mandible under occlusal loads. *Journal of Dental Research*, *56*(11), 1297-1302.

Starr, A. J., Smith, W. R., Frawley, W. H., Borer, D. S., Morgan, S. J., Reinert, C. M., & Mendoza-Welch, M. (2004). Symptoms of post traumatic stress disorder after orthopaedic trauma. *Journal of Bone and Joint Surgery. American*, *86-A*(6), 1115-21.

Sugiura, T., Yamamoto, K., & Murakami, K. (2009). Biomechanical analysis of miniplate osteosynthesis for fractures of the atrophic mandible. *Journal of Oral and Maxillofacial Surgery*, *67*(11), 2397-403.

Suit, S. R., Gibbs, C. H., & Beng, S. T. (1975). Study of gliding tooth contacts during mastication. *Journal of Periodontology*, *47*(6), 331-34.

Szmukler-Moncler, S., Salama, H., Reingewirtz, Y., & Dubruille, J. H. (1998). Timing of loading and effect of micromotion on bone-dental implant interface: Review of experimental literature. *Journal of Biomedical Material Research*, *43*(2), 192-203.

Taddei, F., Pancanti, A. & Viceconti, M. (2004). An improved method for the automatic mapping of computed tomography numbers onto finite element models. *Medical Engineering & Physics*, *26*(1), 61-69.

Taraschi, V. (2016). *Patient specific 3D finite element modelling, analysis and verification of dental implant navigation and insertion system* (PhD dissertation). School of Mathematical and Physical Sciences, University of Technology, Sydney

Tattersall, I. (1973). Cranial anatomy of Archaeolmurinae (Lemuroidea Primates). *Anthropological Papers of the American Museum of Natural History*, *52*, 1-110.

Throckmorton, G. S. (1985). Quantitative calculations of temporomandibular joint reaction forces II. The importance of the direction of the jaw muscle forces. *Journal of Biomechanics*, *18*(6), 453-61.

Tohnak, S., Mehnert, A.J.H., Mahoney, M., & Crozier, S. (2011). Dental CT metal artefact reduction based on sequential substitution. *Dentomaxillofacial Radiology*, *40*(3), 184-90. https://doi.org/10.1259/dmfr/25260548

Tripathi, G., A.A.P., Ralwadha, N., Chhaparia, N., Sharma, A., & Anant, M. (2014). Comparative evaluation of maximum bite force in dentulous and edentulous individuals with different facial forms. *Journal of Clinical and Diagnostic Research*, *8*(9). doi:10.7860/JCDR/2014/8801.4837

Tsukrov, I., DeCew, J. C., Baldwin, K., Campbell-Malone, R., & Moore, M. J. (2009). Mechanics of the right whale mandible: Full scale testing and finite element analysis. *Journal of Experimental Marine Biology and Ecology*, *374*, 93-103.

Turner, C. H., Cowin, S. C., Rho, J. Y., Ashman, R. B., Rice, J. C. (1990). The fabric dependence of the orthotropic elastic constants of cancellous bone. *Journal of Biomechanics*, *23*(6), 549-61.

Uhthoff, H. K., Poitras, P., & Backman, D. S. (2006). Internal plate fixation of fractures: short history and recent developments. *Journal of Orthopaedic Science*, *11*(2), 118-26.

Vajgel, A., Camargo, I. B., Willmersdorf, R. B., de Melo, T. M., Laureano Filho, J. R., & Vasconcellos, R. J. (2013). Comparative finite element analysis of the biomechanical stability of 2.0 fixation plates in atrophic mandibular fractures. *Journal of Oral and Maxillofacial Surgery*, *71*(2), 335-42.

VandeGriend, V. P., Hashemi, A., & Shkoukani, M. (2015). Changing trends in adult facial trauma epidemiology. *Journal of Craniofacial Surgery*, *26*(1), 108-12.

Veyrune, J., Lassauzay, C., Nicolas, E., Peyron, M. A., & Woda, A. (2007). Mastication of model products in complete denture wearers. *Archives of Oral Biology*, *52*(12), 1180-85.

Vollmer, D., Meyer, U., Joos, U., Vegh, A., & Piffko, J. (2000). Experimental and finite element study of a human mandible. *Journal of Cranio-Maxillo-Facial Surgery*, *28*(2), 91-96.

Wagner, A., Wanschitz, F., Birkfellner, W., Zauza, K., Klug, C., Schicho, K., Kainberger, F., Czerny, C., Bergmann, H., & Ewers, R. (2003). Computer-aided placement of endosseous oral implants in patients after ablative tumour surgery: Assessment of accuracy. *Clinical Oral Implants Research*, *14*(3), 340-48.

Weinans, H., Sumner, D. R., Igloria, R., & Natarajan, R. N. (2000). Sensitivity of periprosthetic stress-shielding to load and the bone density-modulus relationship in subject-specific finite element models. *Journal of Biomechanics*, *33*(7), 809-17.

White, S. H., Cunningham, J. L., Richardson, J. B., Evans, M., Kenright, J., Adams, M. A., Goodship, A. E., Smith, E., & Newham, J. H. (1991). Improvement of fracture healing by applied axial micromovement: A clinical study. *Interfaces in Medicine and Mechanics – 2*. Amsterdam: Elsevier Science Publishers.

Wilson, G. H. (1921). The anatomy and physics of the temporomandibular joint. *Journal of the National Dental Association*, *8*(3), 236-41.

Woelfel, J. B. (1979). *Permar's outline for dental anatomy*. Philadelphia: Lea & Febiger.

Woelfel, J. B., Hickey, J. C., Stacy, R. W., & Rinear, L. L. (1960). Electromyographic analysis of jaw movements. *Journal of Prosthetic Dentistry*, *10*(4), 688-98.

Wong, A. S., New, A. M., Isaacs, G. & Taylor, M. (2005). Effect of bone material properties on the initial stability of a cementless hip stem: A finite element study. *Proceedings of the Institution of Mechanical Engineers*, *219*(4), 265-75.

Wood, W. W. (1986). Medial pterygoid muscle activity during chewing and clenching. *Journal of Prosthetic Dentistry*, *55*(5), 615-21.

World Health Organisation (2007). *World Health Organization global burden of disease study*. Geneva. Available from www.globalburden.org.

Worner, H. K. (1939). Gnathodynamics: The measurements of biting force with a new design of gnathodynamometer. *Australian Dental Journal*, *43*, 381.

Worner, H. K., & Anderson, M. N. (1944). Biting force measurements in children. *Australian Dental Journal*, *48*, 1.

Yamaji, T., Ando, K., Wolf, S., Augat, P., & Claes, L. (2001). The effect of micromovement on callus formation. *Journal of Orthopaedic Science*, *6*(6), 571-75.

Zarb, G., Hobkirk, J., Eckert, S., & Jacob. R. (2012). *Prosthodontic treatment for edentulous patients: Complete dentures and implant-supported prostheses* (13th ed.). Amsterdam: Mosby Elsevier.